DISS. ETH NO. 23577

TIMBER-CONCRETE COMPOSITE SLABS MADE OF BEECH LAMINATED VENEER LUMBER WITH NOTCHED CONNECTION

A thesis submitted to attain the degree of

DOCTOR OF SCIENCES of ETH ZURICH
(Dr. sc. ETH Zurich)

presented by

Lorenzo Boccadoro

MSc ETH Civil Eng

born on 22.09.1987
citizen of
Muralto TI

accepted on the recommendation of
Prof. Dr. Andrea Frangi (ETH Zurich, Examiner)
Prof. Dr. Walter Kaufmann (ETH Zurich, Co-examiner)
Prof. Dr. Jan-Willem van de Kuilen (TU Munich, Co-examiner)
Dr. René Steiger (EMPA, Dübendorf, Co-examiner)

2016

Preface

I wrote this doctoral thesis during my time as research assistant at the Chair of Timber Structures of the Institute of Structural Engineering (IBK) at ETH Zurich. Inspired by the elevated mechanical properties of beech wood, Prof. Andrea Frangi had the idea to create a very simple laminated veneer lumber (LVL)-concrete composite slab made of a thin LVL plate and a concrete layer, connected by means of notches. During this research project, we developed a design model for these composite members to ensure a ductile and predictable failure mechanism. This objective was fulfilled, and the model was validated by means of laboratory tests. The most challenging aspect was the modelling of the interaction between materials with completely different mechanical properties, including LVL, concrete and steel reinforcement. An important part of the work was the study of the load-carrying mechanism of notched connections, which is characterised by a complex stress state that may lead to brittle failure. This research allowed us to improve the knowledge about several structural problems with notched connections.

The *Swiss National Science Foundation SNSF* (NRP 66) and *Climate-KIC* are gratefully acknowledged for financing and supporting the project.

I would like to thank Prof. Andrea Frangi for giving me the opportunity to conduct this research work. He gave me the freedom to choose an approach to conduct the research, was always happy to discuss critical issues and gave very good suggestions. Constant motivation, belief, trust, support and understanding shown by him have made this work possible. I would also like to thank the co-examiners, Prof. Walter Kaufmann, Prof. Jan van de Kuilen and Dr. René Steiger. Jan van de Kuilen contributed his knowledge about LVL made of beech wood and timber-concrete composite members to this research project. Walter Kaufmann asked critical questions, in particular, regarding the structural behaviour of the concrete part of the composite members. I enjoyed my discussions with him about possible approaches to assess the minimal vertical reinforcement. I appreciated Steiger's comments on my research work because they were very helpful to improve the content and the readability of the dissertation. Furthermore, I would like to thank Prof. Mario Fontana for the suggestions on the topic of gap opening in composite structures.

I especially thank Dr. Simon Zweidler for his guidance and support. The successful results, presented in this thesis, would not have been possible without his input. He assisted me greatly to develop a consistent analytical model to assess the structural behaviour of composite members, and helped me to deepen several technical skills. He immediately recognised the influence that timber compressive deformations within the notches have on the crack propagation behaviour in concrete, and the issue of localised plastic zones (Section 3.3.9). Thus, it was possible to understand and justify the necessity of vertical reinforcement to prevent brittle failure (Sections 3.3.8 and 3.3.10). He also gave me very important suggestions about the design of the specimens, which validated the analytical model (Section 4.4.3).

Laboratory tests were important parts of this research work. My acknowledgements go to all the people who worked in the laboratory with me. First of all, I thank the students who wrote theses about project: Remo Villiger, Damian Lüthi and Andrea Moro. They helped me to conduct the tests and gave me very important inputs. I would also like to thank the technicians

in the laboratory: Patrick Morf, Thomas Jaggi, Christoph Gisler, Pius Herzog and Dominik Werne. I appreciate their professional and precise work and their suggestions. Then, I would like to thank the carpenter's workshop of ETH Zurich and the companies, Pollmeier GmbH, Balteschwiler AG and Tschirren Bau AG, for the fabrication of the specimens.

I sincerely thank help and support of my colleagues from ETH. I also thank Catherine Whyte for proofreading several important parts of this thesis.

Ringrazio di cuore la mia famiglia e i miei amici. In particolare ringrazio i miei genitori Marco e Raffaella e mia sorella Giulia per il sostegno e l'affetto. Un sentito ringraziamento va anche agli zii Flavia e Adrian che con la loro esperienza in campo accademico mi hanno dato preziosi consigli.

Abstract

This thesis focuses on the structural behaviour of timber-concrete composite slabs made of beech laminated veneer lumber (LVL) with notched connections. A timber-concrete composite member consists of a timber part in the tensile zone, a concrete layer in the compression zone, and a connection between the timber and the concrete. These slabs are usually made of spruce wood, and several connection systems have been developed (e.g. screws and notches). These composite members are interesting systems because they are able to offer several structural, economic and ecological advantages compared to traditional reinforced concrete slabs and timber slabs. Beech LVL is an efficient structural material because it is able to combine the high strength and stiffness of beech wood with the consistency of the mechanical properties of LVL. Moreover, in Europe, beech wood is available in large quantities. The composite slabs studied in this thesis have spans between 5 and 8 m and were developed at ETH Zurich in the framework of a project about innovative uses of beech LVL. In general, if the load-carrying capacity of the notched connection is governed by a compressive failure of the timber, ductility can be achieved. Thus, the design goal is to make sure that yielding of the notches governs the global structural behaviour. This is accomplished through the development and use of a clear and reliable model. At present, several structural aspects of notched connections are still unclear, and the benefit of notch yielding for improved global slab ductility is almost unknown.

This thesis presents both theoretical and experimental investigations. The theoretical studies include development of analytical models to predict the failures of notched timber-concrete connections, and to analyse the structural behaviour of timber-concrete composite members with a ductile connection. The models were able to predict the structural behaviour of several specimens tested during this work with good accuracy, and can be used as a basis to design timber-concrete composite members made of beech LVL.

This work shows that the use of LVL materials, instead of solid wood or glued laminated timber, markedly improves the predictability of the timber behaviour, and a ductile notch design becomes feasible. Notch yielding causes an increase of the curvature of the cross section, which improves global ductility of the composite member. However, the ductility of the slab predicted by the analytical model can be reached only if the composite member is provided with end-to-end vertical reinforcement, which holds the LVL and concrete together and keeps the concrete cracks closed. The composite member should be designed so that, after connection yielding, concrete crushing occurs in the upper part of the composite member. Thanks to this design approach, the load-carrying capacity of the composite member is governed by a series of ductile failures. In general, the deformations of the composite member are limited by the rotation capacity of the LVL part. Thus, to maximise ductility, the parts of the composite member should be designed so that a tensile-bending failure of LVL occurs as late as possible.

In conclusion, this thesis offers a straightforward method to analyse the structural behaviour of a timber-concrete composite member with a notched connection, and demonstrates that, if a ductile design approach is applied, beech LVL, as the tensile part, ensures a good structural performance and a predictable failure behaviour.

Riassunto

Questa tesi riguarda il comportamento strutturale di solette composite legno-calcestruzzo realizzate con multistrato impiallacciato di faggio (LVL), con connessione ad intaglio. Le solette composite legno-calcestruzzo sono costituite da un elemento in legno sotto trazione, che può fungere da cassero a perdere, da uno strato di calcestruzzo sotto compressione, e da una connessione legno-calcestruzzo. Queste strutture sono solitamente realizzate in abete, ed esistono diversi tipi di connessione (ad esempio viti e intagli). Il legno-calcestruzzo può rappresentare un'alternativa interessante alle solette in legno e in calcestruzzo armato, in quanto offre vantaggi di tipo economico, ecologico e strutturale. L'LVL di faggio è un materiale molto efficace dal punto di vista strutturale poiché combina le elevate resistenze e rigidità del faggio con la bassa varianza delle proprietà meccaniche tipica delle configurazioni LVL. Inoltre, in Europa, il faggio è una specie vegetale presente in quantità molto abbondanti. Le solette composite sviluppate in questo lavoro sono pensate per campate tra 5 e 8 m, e sono state ideate al Politecnico Federale di Zurigo (ETHZ) in seno ad uno studio sugli usi innovativi del faggio. In generale, se il comportamento dell'intaglio è governato da una rottura compressiva del legno, si ottiene duttilità, un'importante ed apprezzata caratteristica strutturale. L'idea di base è di fare in modo che le deformazioni plastiche degli intagli governino il comportamento globale della soletta ottenendo così una struttura duttile. Lo sviluppo di questa soletta composita richiede modelli chiari e affidabili per prevederne il comportamento strutturale. Diversi problemi statici delle connessioni a intaglio non sono ancora stati risolti con sufficiente chiarezza, e l'influsso della plastificazione degli intagli sul comportamento dell'intera struttura è pressoché sconosciuto.

Questa struttura composita è stata studiata sia sul fronte teorico sia su quello sperimentale. Gli studi teorici comprendono una serie di modelli analitici per la previsione delle rotture della connessione a intaglio, e un modello per quantificare il comportamento statico di strutture composite legno-calcestruzzo con connessione duttile. I risultati di una serie di test al taglio e alla flessione sono stati paragonati alle previsioni effettuate con i modelli analitici, convalidando gli studi teorici.

Questo lavoro dimostra che l'uso dell'LVL al posto del legno massiccio e del legno lamellare incollato migliora l'affidabilità delle previsioni delle rotture del legno, rendendo possibile un dimensionamento duttile basato sulla rottura compressiva del legno. La plastificazione degli intagli genera un aumento della curvatura delle componenti della sezione che si traduce in una deformazione plastica della soletta. Dagli studi condotti nell'ambito di questa tesi risulta che la duttilità può svilupparsi solo se la soletta è munita di rinforzi verticali in grado di impedire un'apertura della fuga tra le due parti e di tenere chiuse le crepe del calcestruzzo. La struttura composita dovrebbe essere dimensionata affinché la plastificazione degli intagli sia seguita da una rottura compressiva del calcestruzzo nella zona superiore della sezione, anch'essa dotata di duttilità. In questo modo la resistenza della soletta è determinata da una serie di rotture duttili. Tuttavia le deformazioni plastiche della soletta sono limitate dalla capacità di rotazione del legno. Per massimizzare la duttilità si consiglia quindi di progettare la struttura in modo che una rottura fragile del legno dovuta alla combinazione trazione-flessione avvenga il più tardi possibile.

In conclusione questa tesi offre un modello chiaro per l'analisi del comportamento strutturale di solette composite legno-calcestruzzo con connessione a intaglio, e dimostra che, seguendo un metodo di dimensionamento duttile, l'uso dell'LVL di faggio assicura un comportamento strutturale ottimale.

Zusammenfassung

Die vorliegende Dissertation konzentriert sich auf das Tragverhalten von Holz-Beton Verbunddecken aus Buchenfurnierschichtholz (LVL) mit Kerbenverbindung. Holz-Beton Verbundstrukturen bestehen aus einem Holzelement in der Zugzone, einer Betonschicht in der Druckzone und einer Schubverbindung zwischen Holz und Beton. Solche Verbundbauteile bestehen in der Regel aus Fichtenholz, und verschiedene Verbindungssysteme wurden entwickelt (zum Beispiel Schrauben und Kerben). Holz-Beton-Verbunddecken repräsentieren attraktive Systeme, weil sie verschiedene strukturelle, ökonomische und ökologische Vorteile im Vergleich zu konventionelle Stahlbetondecken und reine Holzdecken bieten können. Buchenfurnierschichtholz ist ein leistungsfähiger Baustoff, weil er die hohe Festigkeit und Steifigkeit des Buchenholzes mit der geringen Variabilität der mechanischen Eigenschaften des Furnierschichtholzes kombiniert. Darüber hinaus ist in Europa Buchenholz in grossen Mengen verfügbar. Die Verbunddecken, die in dieser Arbeit untersucht wurden, haben eine Spannweite zwischen 5 und 8 m und wurden an der ETH Zürich im Rahmen eines Forschungsprojektes über innovative Nutzungen von Buchenfurnierschichtholz entwickelt. Im Allgemeinen, wenn die massgebende Versagensart der Kerbe ein Druckversagen des Holzes ist, entstehen plastische Druckverformungen und es stellt sich ein duktiles Tragverhalten der Kerbenverbindung ein. Das Grundkonzept der in dieser Arbeit entwickelten Verbunddecke ist sicherzustellen, dass das Druckversagen des Furnierschichtholzes in den Kerben massgebend ist, und die Verbunddecke sich duktil verhält, was eine sehr wichtige Anforderung ist. Um diese Verbunddecken zu bemessen, sind klare und zuverlässige Modelle notwendig. Des Weiteren sind einige statische Aspekte der Kerbenverbindung noch unklar und der Einfluss plastischer Verformungen in den Kerben auf die globale Duktilität der Verbunddecke ist fast unbekannt.

Diese Arbeit enthält theoretische und experimentelle Untersuchungen. Die theoretische Studien umfassen analytische Modelle, mit denen die Versagensarten von Holz-Beton Kerbenverbindungen vorausgesagt werden können, sowie Modelle, die das Tragverhalten von Holz-Beton Verbundstrukturen mit duktiler Schubverbindung beschreiben. Die entwickelten Modelle wurden mit Laborversuchen validiert, und bilden die Basis zur Erarbeitung von Bemessungsverfahren für Holz-Beton Vebunddecken aus Buchenfurnierschichtholz.

Diese Arbeit zeigt, dass die Verwendung von Furnierschichtholz anstelle von Vollholz oder Brettschichtholz die Berechenbarkeit des Tragverhaltens der Holzkomponente deutlich verbessert, und eine duktile Bemessung der Kerbe somit sinnvoll wird. Die Auswirkung plastischer Druckverformungen des Furnierschichtholzes in den Kerben verursacht eine Zunahme der Krümmung der Querschnittsteile der Verbunddecke. Dadurch wird Duktilität erzeugt. Es wurde aber beobachtet, dass die mit dem Modell vorausgesagte Duktilität nur erreicht werden kann, wenn vertikale Verstärkungen eingebaut werden, die Holz und Beton zusammenhalten und die Vergrösserung der Schubrisse im Beton vermeiden. Die Verbunddecke sollte so dimensioniert werden, dass, nachdem die Fliessgrenze der Kerben erreicht wird, die Betondruckzone zu stauchen beginnt. Somit besteht der Bruchmechanismus der Decke aus einer Serie von duktilen Versagen, und die Decke versagt nach grossen Verformungen. Im Allgemeinen werden die Verformungen des Verbundbauteils durch die Rotationsfähigkeit des Holzquerschnittes begrenzt. Um die Duktilität

zu maximieren, sollten die Teile der Verbunddecke so bemessen werden, dass ein kombinierter Biegezugbruch des Holzes so spät wie möglich auftritt.

Diese Dissertation stellt ein klares und nachvollziehbares analytisches Modell zur Verfügung, um das Tragverhalten von Holz-Beton Verbunddecken mit Kerbenverbindung zu beschreiben, und zeigt, dass, wenn ein duktiler Bemessungsansatz angewendet wird, der Einsatz von Buchenfurnierschichtholz als Zugelement ein berechenbares und duktiles Tragverhalten der Verbunddecke gewährleistet.

Contents

Chapter 1

Introduction

1.1 Motivation

This thesis focuses on the development of timber-concrete composite slabs made of beech wood. Typically, a timber-concrete composite slab consists of a timber part in the tensile zone, a concrete layer in the compression zone, and a connection between the timber and concrete. These slabs are usually made of spruce wood (e.g. glulam beams), and since the nature of the timber-concrete connection determines the structural behaviour of the composite member, many connection systems have been developed (e.g. screws, dowels and notches). Composite timber-concrete systems offer several advantages over traditional timber floors, including increased strength and stiffness under gravity load, improved sound insulation, and higher fire resistance. Furthermore, timber-concrete composite slabs save time and materials in the fabrication process because the timber part acts as both the formwork and the tensile load-carrying component. However, a conventional reinforced concrete slab allows for more flexibility with regard to the geometrical shape of the slab.

Nowadays, in Europe, beech wood is available in large quantities but is typically used for non-structural applications. Currently, ETH Zurich is involved in a large, long-term research project focused on sustainable, innovative and reliable timber structures that use beech laminated veneer lumber (LVL). This thesis explores beech LVL for timber-concrete composite slabs. Beech LVL is advantageous due to its elevated and highly consistent mechanical properties and its improved form stability. Thus, the structural performance of the timber part of the composite member is improved.

The composite slab studied in this thesis has a simple and slender layout and consists of a beech LVL plate which acts as both the formwork and the tensile reinforcement and a concrete layer (Fig. 1.1). The total thickness of the composite slabs considered is about 200 mm. Notching is used to make the connection: the timber and concrete are connected with 15 mm deep notches cut in the LVL plate, which transfer the shear forces by means of compressive contact of the two materials at the edges of the notches. The composite slabs developed in this thesis carry the load only in one direction; consequently, the veneers of the beech LVL plate are oriented mostly in the longitudinal direction of the slab, and the composite member should

be linearly supported (for instance by a beam or a wall). This system can be used for slabs in office and residential buildings with spans between 5 and 8 m. Such slabs usually carry a permanent load of about 2 kN/m^2 and a live load of 2-3 kN/m^2 [1]. The composite slabs should be as stiff as possible at the service level, ductile at the ultimate limit state, and must have sufficient load-carrying capacity. Furthermore, vibration, sound insulation and fire resistance requirements should be fulfilled. In design of timber-concrete composite members, the long term effects on materials and connections should be considered. Also, the variation of the mechanical properties of timber and concrete should be taken into account.

This thesis concentrates on the failure mechanism of one-span composite members. To design timber-concrete composite slabs made of beech LVL with notched connections, a model to understand and calculate the structural behaviour is necessary. Whereas the elastic flexural behaviour of a timber-concrete composite cross-section during the elastic state is well-known and can be quantified with several calculation models (e.g. n- and γ-method), the load-carrying mechanisms of the notched connection are markedly more complex. A notched timber-concrete connection implies several multi-axial stress states in timber and concrete, which can generate different failure modes. The load-carrying mechanisms of the notches should be studied to prevent brittle failures (e.g. tensile and shear failures of the concrete part or shearing-off failures of the timber part), and a design procedure should be developed that guarantees a global ductile failure of the slab. According to previous research (e.g. [2]), a notch can fail in a ductile way if a compressive failure of timber is governing. The properties of LVL-based materials help in pursuing this objective. Whereas the high variability of the mechanical properties of solid wood and glued laminated timber makes the prediction of timber failures difficult, the consistency of the mechanical properties of LVL materials allows for predicting timber failures with higher certainty. This makes it possible to design the composite member so that a determinate timber failure is governing. Furthermore, a simplified model must be developed to determine whatever a composite member with a notched connection needs vertical steel reinforcement (e.g. screws) and which forces the reinforcement should be able to carry.

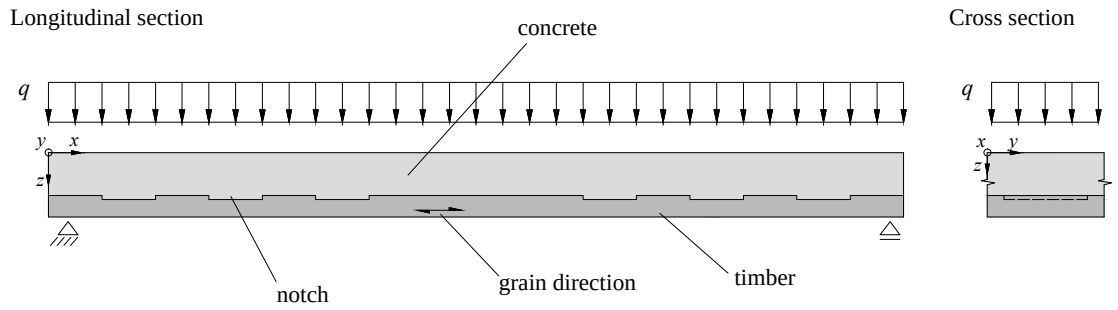

Figure 1.1: Timber-concrete composite slab with a notched connection

1.2 Objectives

The purpose of this thesis is to study the structural behaviour of a timber-concrete composite slab made of a beech LVL plate connected to a top layer of concrete by means of a notched connection. The following objectives are pursued:

- Understanding the load-carrying mechanisms of notched timber-concrete connections and developing simplified models to quantify the influence of geometric and material parameters on the failures.
- Investigating the possibility to design the composite member so that a ductile failure is governing, and developing a simplified model to describe the structural behaviour of a timber-concrete composite member after yielding of the connection.
- Clarifying whatever timber-concrete composite members with a notched connection need steel reinforcement and quantifying what load the reinforcement should be able to carry.
- Performing laboratory connection shear tests on timber-concrete composite members with notched connection made of beech LVL to analyse the notch behaviour.
- Performing full-scale bending tests to determine the structural behaviour of timber-concrete composite members made of beech LVL, and comparing the test results to calculations performed with the models developed.

1.3 Limitations

Since this thesis represents a first step to assess the failure mechanisms of the composite members, the serviceability and long-term behaviour analyses are not studied in detail. The influence of the variation of the mechanical properties of timber and concrete on the structural behaviour is not considered. All model calculations are performed using mean values of the mechanical properties from design codes and approvals (e.g. [3]). Furthermore, the dynamic behaviour, the fire resistance and the sound insulation properties are not discussed. The composite members studied in this thesis are simple beams, and the structural behaviour of a continuous beam is not addressed. The analytical models used to describe the structural behaviour of the composite members after connection yielding were developed with regard to connections designed proportional to the shear force generated by a uniformly distributed vertical load. The other cases are only discussed qualitatively. The causes of the gap opening phenomena observed in some experiments are discussed mostly in a qualitative way.

1.4 Overview of the thesis

The general structure of the thesis is illustrated in Fig. 1.2. Following the introduction, Chapter 2 discusses the current models that are available to estimate the structural behaviour of timber-concrete composite members, the existing theories to predict the failures of timber and concrete

with regard to notched connections, and the state-of-the-art in experimental investigations of timber-concrete composite members with notched connections.

At first, Chapter 3 illustrates an analytical model to describe the structural behaviour of a timber-concrete composite member with a ductile connection, which is an extension of the model developed by Frangi and Fontana [2], combined with the theories of ductile analysis of reinforced concrete members according to Marti [4], [5]. Then, a simplified method to understand the load-carrying mechanism of notched connections is presented, and several analytical models to study the different failure modes of the notches are discussed. This chapter also deals with the necessity of vertical reinforcement in timber-concrete composite members with notched connections, and presents a simplified model to design the reinforcement. Finally, the analytical models presented are applied to practical cases to perform a parametric study to understand the influence of several geometric and material parameters on the structural behaviour.

The experimental investigations are summarized in Chapter 4, beginning with the first preliminary bending test conducted at the beginning of this research project to examine the feasibility of the concept. Then, the connection shear tests are presented. Notches as timber-concrete connection systems are tested with a setup which reproduces the boundary conditions of the notch close to the support. The test results are compared to the estimates made with the analytical models. Finally, this chapter presents a series of bending tests performed to validate the analytical models of Chapter 3. A complete description of all experiments performed during this thesis can be found in a test report [6].

Chapters 5 and 6 include the most important conclusions and an outlook for further research on the subject.

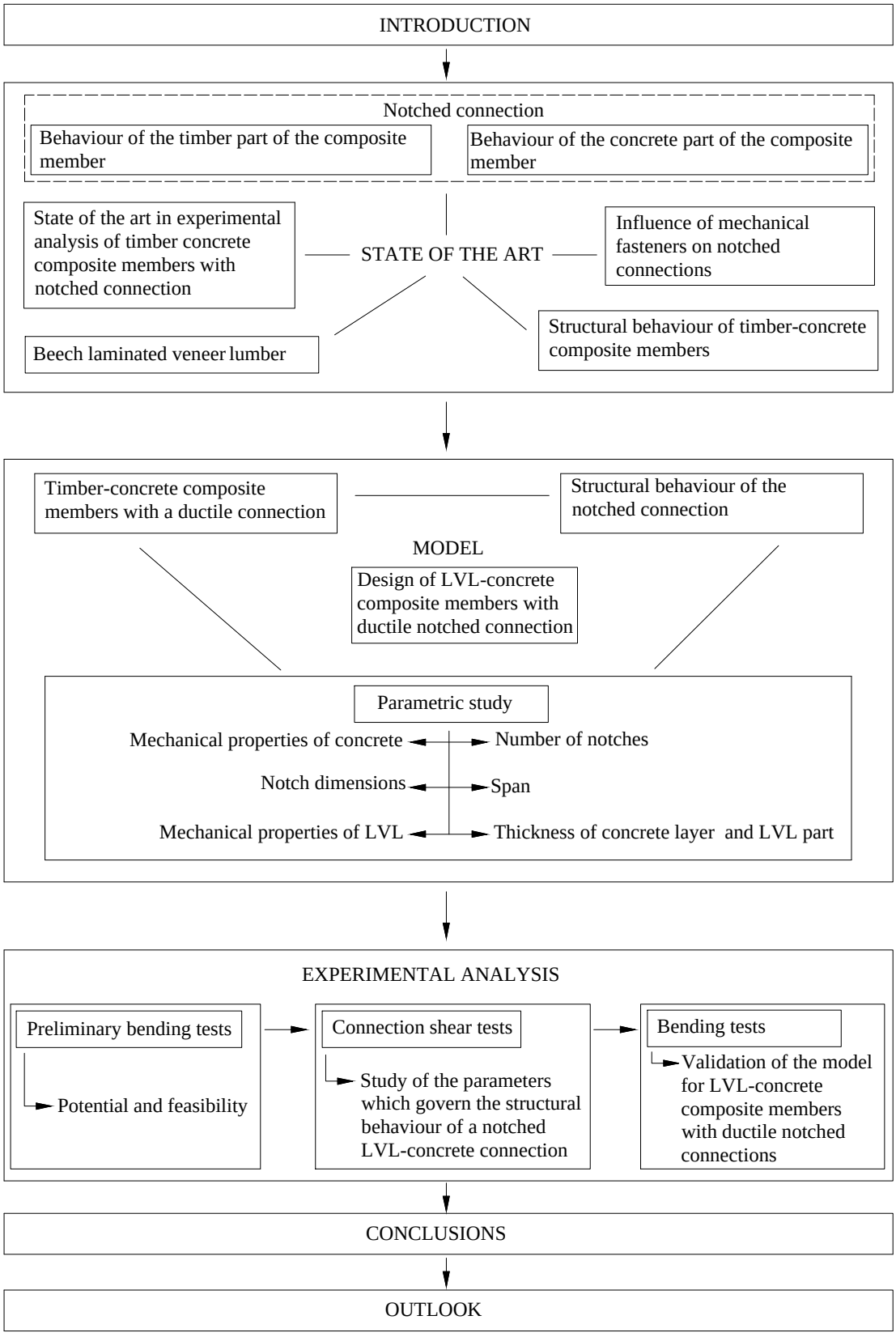

Figure 1.2: Overview of the thesis

Chapter 2

State of the art

2.1 Introduction

This thesis focuses on timber-concrete composite members made of beech laminated veneer lumber (LVL). Section 2.2 presents the most important mechanical properties and advantages of beech LVL. Then, Section 2.3 summarises the state-of-the-art in modelling of timber-concrete composite members. Since the connections are created by means of notches, different stress configurations are to be expected in the timber and concrete. Therefore, to be able to develop a model for the structural behaviour of the composite member, an in-depth study of the structural behaviour and the failure modelling of these two materials is needed. Section 2.4 explains the existing approaches to model failure of timber, and Section 2.5 presents several approaches to model the load-carrying behaviour of concrete. Finally, Section 2.7 summarises the most important outcomes of several previous experimental and numerical studies on notched timber-concrete connections.

2.2 Beech laminated veneer lumber

The higher strength and stiffness properties of beech wood (Fagus sylvatica L.), as compared to most softwood species, are well known [7], [8]. In Europe, beech wood is available in large quantities, but it is typically used for firewood or for non-structural applications (e.g. furniture) [9],[10]. Beech LVL offers improved consistency of mechanical properties and dimensional stability for structural elements [11]. The specimens tested in this research project were constructed using beech LVL produced by the company Pollmeier (Creuzburg, Germany), which made remarkable progress in the production of beech LVL structural elements [12], [13]. This structural material was tested by Van de Kuilen and Knorz at TU Munich [14], [15] and obtained a European Technical Approval [3]. Tab. 2.1 shows several mechanical properties of beech LVL significant for this research work, and Fig. 2.1 represents the corresponding veneer orientations.

Table 2.1: Mechanical properties of beech laminated veneer lumber (LVL) according to Fig. 2.1, determined by Van de Kuilen and Knorz [14],[15] in preparation of a European Technical Approval [3]. These mechanical properties were obtained with a moisture content of 8.1 % (mean value), and the mean value of the density was 730 kg/m^3.

Configuration	Property		Mean value [N/mm^2]	Characteristic value (5th percentile) [N/mm^2]	Coefficient of variation [%]
With $22-27$ % cross layers	Tensile strength parallel to the grain	$f_{t,0}$	58.5	43.3	15.5
	Bending strength parallel to the grain	$f_{m,0}$	77.9	66.8	7.9
	Compressive strength parallel to the grain	$f_{c,0}$	45.7	37.5	10.4
	Modulus of elasticity parallel to the grain	E	13800	12500	4.5
	Shear modulus parallel to the grain	G	433	376	7.4
	Compressive strength perpendicular to the grain	$f_{c,90}$	13.6	10	14.3
	Rolling shear strength of the cross layer	$f_{R,v}$	3.66	3.3	3.0
Without cross layers	Shear strength parallel to the grain	f_v	10.7	9	9.2
	Shear modulus parallel to the grain	G	853	763	5.9
	Tensile strength (load parallel to glue layers)	$f_{t,90}$	1.97	1.62	10.3

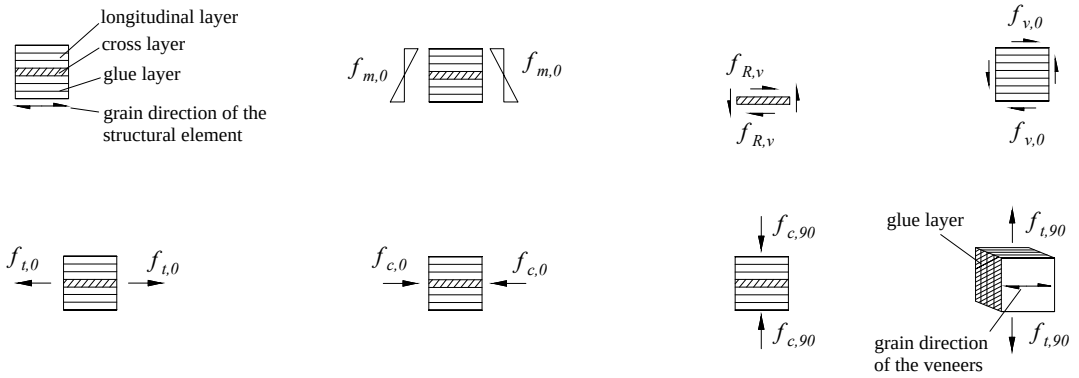

Figure 2.1: Mechanical properties of beech laminated veneer lumber (LVL)

2.3 Models for timber-concrete composite structures

2.3.1 Behaviour of the composite members in elastic conditions

Typically, timber-concrete composite slabs consist of a timber part in the tensile zone, a concrete part in the compression zone, and a connection between the timber and concrete to ensure composite action [16]–[18]. As a consequence of loading perpendicular to the plane q, the two parts of the composite member are subjected to axial forces N, bending moments M_i and shear forces V_i, which depend on the geometry and the mechanical properties of the parts and the connection (Fig. 2.2). At the interface between the two parts, theoretical horizontal shear forces t and vertical forces r occur, which are carried by the connection.

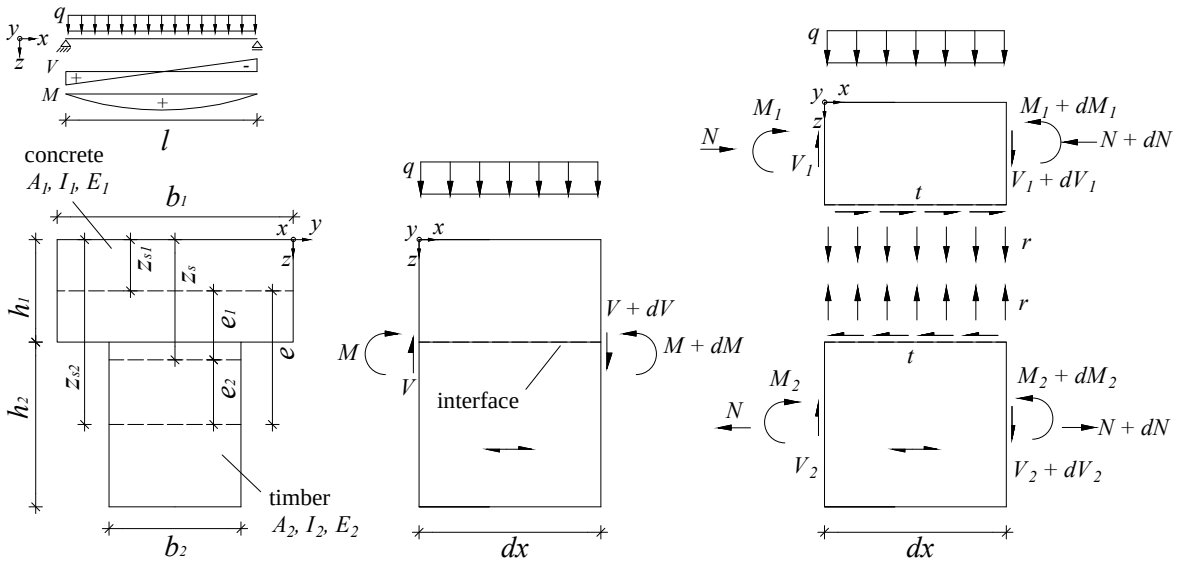

Figure 2.2: Composite member

Since the connection is subjected to shear stresses, its flexibility generates a horizontal relative displacement between the two parts which markedly influences the structural behaviour of the composite structure. A perfectly rigid shear connection would prevent horizontal slip

between the two materials. Such a system would be fully composite. However, almost all shear connection systems are flexible, at least to some extent. Therefore, a certain amount of relative slip between the two materials will occur. As a result, only partial composite action can be achieved, and any structural analysis of such a system requires consideration of the slip between the subcomponents.

In addition, when the elastic connection is flexible, the difference between the bending stiffness of the two parts of the composite member may cause differential deflections which result in uplift between the two elements [19].

Adekola [19] presented a theory of interaction, which accounts for both slip and uplift effects. The parameter k_s describes the shear connection modulus and k_t describes the uplift modulus. This theory differentiates between positive uplift (i.e. the tendency to have a gap opening, which causes tension in the connection) and negative uplift, which causes pressure at the interface and induces friction. For the zones with positive uplift, Adekola [19] derived the following differential equation:

$$\frac{\partial^2 N}{\partial x^2} - \kappa^2 \cdot k_s \cdot N(x) - \frac{k_s}{k_t} \cdot \left[\frac{\frac{h_2}{2} \cdot E_1 I_1 - \frac{h_1}{2} \cdot E_2 I_2}{E_1 I_1 + E_2 I_2} \right] \cdot \frac{\partial^2 r}{\partial x^2} = -\frac{k_s \cdot e}{E_1 I_1 + E_2 I_2} \cdot M(x) \tag{2.1}$$

where:

$$\kappa^2 = \frac{1}{E_1 A_1} + \frac{1}{E_2 A_2} + \frac{e^2}{E_1 I_1 + E_2 I_2} \tag{2.2}$$

Several simplified calculation methods for timber-concrete composite members (e.g. the n-method described in Section 2.3.2) are based on the assumption that no gap opening occurs. This assumption is valid if the composite member is provided with vertical reinforcement which prevents gap opening. The differential equation for composite members, derived by neglecting uplift and vertical stresses, is the following:

$$\frac{\partial^2 N}{\partial x^2} - \kappa^2 \cdot k_s \cdot N(x) = -\frac{k_s \cdot e}{E_1 I_1 + E_2 I_2} \cdot M(x) \tag{2.3}$$

As discussed by Frangi and Fontana [2], Stüssi [20], [21] was the first to derive the differential equation for the partial composite action. Analytical solutions to the differential equation for simply supported beams with constant slip stiffnesses, subjected to different load cases, are described by many authors (e.g. [22], [23], [24]).

As discussed by Frangi [25], another possibility to calculate the forces acting in timber-concrete composites are truss models. For instance Vierendeel-frame models with elastic cantilevers and truss models with elastic diagonals can be used.

2.3.2 Simplified models of the elastic behaviour

To calculate the stresses and the strains acting on the composite member in elastic conditions, simplified models were developed (Fig. 2.3). These models are based on the following assumptions: the two parts of the composite member bend with the same curvature, the distribution

of the axial strains ε is linear, and the behaviour of the materials is linear-elastic. When the connection is assumed to be fully rigid, the n-method can be used. Since a fully rigid connection is very difficult to achieve with timber, simplified models were developed to take into account the flexibility of the connection (e.g. the γ-method). The factor γ estimates the effect of the flexibility of the connection on the cross-section values. The n-method corresponds to the γ-method with $\gamma = 1$. As shown in Fig. 2.3, the shear deformations of the connection in x-direction cause a slip in the distribution of σ and ε at the level of the interface.

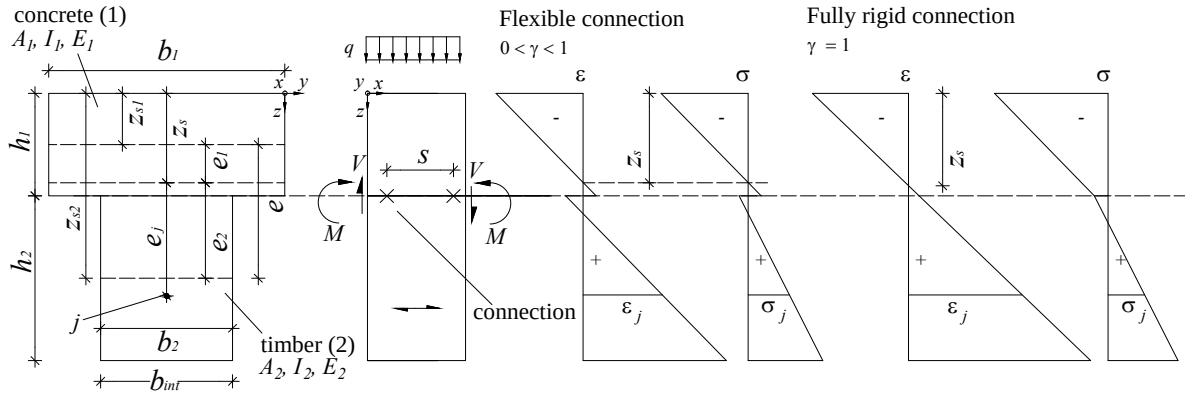

Figure 2.3: Axial stresses and strains acting on the composite member.

Rigid connection (n-method)

The n-method is a simplified model to determine the cross-sectional stresses σ and strains ε of a composite member with fully rigid connection (Fig. 2.3). The most important formulas of this method are presented, for instance, by Richter et al. [26].
The n-values take into account the different moduli of elasticity of the parts of the composite member and are defined as follows:

$$n_i = \frac{E_i}{E} \tag{2.4}$$

The z-coordinate value of the elastic centroid of the composite cross-section (which corresponds to the zero strain layer) is:

$$z_s = \frac{\sum n_i A_i z_{si}}{\sum n_i A_i} \tag{2.5}$$

The effective moment of inertia is:

$$I = \sum n_i I_i + \sum n_i A_i e_i^2 \tag{2.6}$$

The effective cross section is:

$$A = \sum n_i A_i \tag{2.7}$$

The static moment for the calculation of the shear stress acting at the interface is:

$$S_{i,i+1} = n_i A_i e_i \tag{2.8}$$

The axial stress at point j in part i of the composite member due to the bending moment M is:

$$\sigma_j = E_i \varepsilon_j = \frac{M}{EI} e_j E_i = \frac{M}{I} e_j n_i \tag{2.9}$$

The theoretical elastic shear stress at the interface between parts i and $i+1$ is:

$$\tau_{i,i+1} = \frac{V S_{i,i+1}}{I b_{int}} \tag{2.10}$$

Flexible connection (γ-method)

For design purposes, a method for mechanically jointed beams, based on the differential equation for the partial composite action, is widely used. The simplified design method, called γ-method, is closely related to Möhler's model [27] and was developed for simply supported beams with constant slip stiffnesses, subjected to loads that produce sinusoidally varying bending moments. For this case, the differential equation of the partial composite action has a simple analytical solution [2]. The γ-method can be expressed as a modification of the n-method, and it takes connection flexibility into account by means of a reduction of the members $n_i A_i e_i^2$ in the calculation of the bending stiffness. The most important formulas of this method are presented, for instance, by Richter et al. [26].

The γ-factor takes into account the geometry of the parts of the composite member, the shear stiffness of the connection k_s, the elasticity of the parts, the span l, and the distance between the connections s. For timber-concrete composite slabs, Blass et al. [28] formulated the γ-factor depending on the position of the centroid of the composite cross-section. If the timber part is thick and the concrete is thin and completely subjected to compression, the centroid is typically located in the timber. In this case, the γ-factors are:

$$\gamma_1 = \frac{1}{1 + \frac{\pi^2 E_1 A_1 s}{l^2 k_s}} \tag{2.11}$$

$$\gamma_2 = 1 \tag{2.12}$$

If the timber-concrete composite member is made of a thin timber plate and a thick concrete plate, the centroid is usually located in the concrete, and it can be assumed that the concrete area below the centroid cracks and does not carry tensile stresses. In this case, the γ-factors are:

$$\gamma_1 = 1 \tag{2.13}$$

$$\gamma_2 = \frac{1}{1 + \frac{\pi^2 E_2 A_2 s}{l^2 k_s}} \tag{2.14}$$

The position of the centroid of the composite cross-section can be calculated as follows:

$$z_s = \frac{\sum \gamma_i n_i A_i z_{si}}{\gamma_i n_i A_i} \tag{2.15}$$

The effective moment of inertia of the composite cross-section is:

$$I = \sum n_i I_i + \sum \gamma_i n_i A_i e_i^2 \tag{2.16}$$

The axial stress acting at the edge (top or bottom) of part i is:

$$\sigma_{i,t/b} = \frac{M}{EI} \left(\gamma_i e_i \pm \frac{h_i}{2} \right) E_i \tag{2.17}$$

The theoretic elastic shear stress at the interface between parts i and $i+1$ is:

$$\tau_{i,i+1} = \frac{V \gamma_i E_i A_i e_i}{EI b_{int}} \tag{2.18}$$

2.3.3 Timber-concrete connection systems

Figure 2.4 shows the typical behaviour of a timber-concrete connection. For simplified design purposes, the shear behaviour of the connection is described with three parameters: stiffness (K_{ser}), strength (T_u) and ductility (D) [2].

In the elastic range, a high shear connection stiffness is important to increase the bending stiffness of the composite member. The Swiss Standard SIA 265 [29] defines the stiffness at the service level as:

$$K_{ser} = \frac{0.4 \cdot T_u}{u\,(0.4 \cdot T_u)} \tag{2.19}$$

The connection stiffness K_u at the ultimate limit state can be estimated as follows [25]:

$$K_u = \frac{2}{3} K_{ser} \tag{2.20}$$

In the Swiss code SIA 265 [29], the ductility of the connection is defined as:

$$D = \frac{u_u}{u_y} \tag{2.21}$$

As shear connections markedly affect the behaviour of timber-concrete composite structures, several research projects have focused on developing and testing particular connection systems (e.g. [30]–[37]). As a result, many different connection systems with steel fasteners (e.g. screws, dowels and nail plates) and notches cut from the timber parts of the composite members have been explored. Fig. 2.5 illustrates several current timber-concrete connection systems. Dias [38] studied the mechanical behaviour of several timber-concrete connections by means of analytical models, finite element models and laboratory tests.

As discussed by Yeoh et al. [18], notches cut in the timber beam and reinforced with a mechanical fastener are often classified as the best type of connection system with respect to stiffness and load-carrying capacity. However, the advantage of mechanical fasteners (e.g. screws and nail plates) is that they do not require cutting the timber. On the other hand, they are less

efficient in strength and stiffness than a notched connection [18]. Connection systems made of metal plates and dowels typically achieve a ductile failure, thanks to the yielding of the steel.

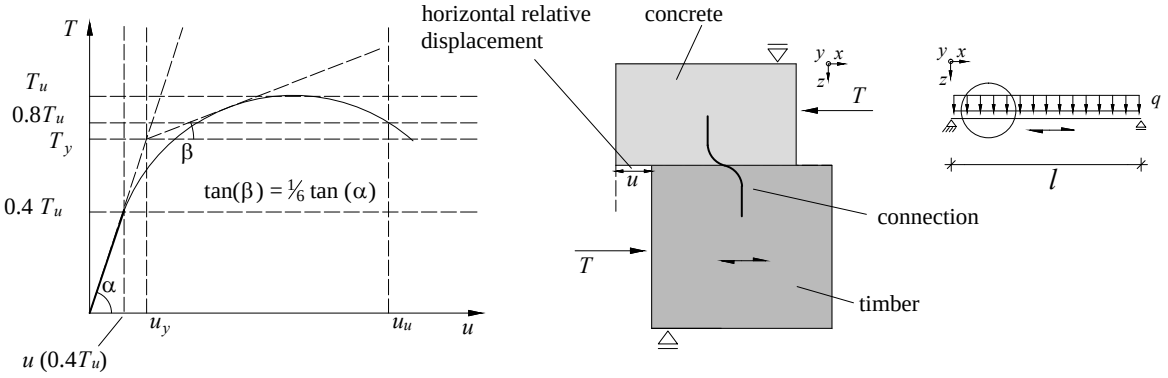

Figure 2.4: Stiffness, load-carrying capacity and ductility of timber-concrete connections [29],[25]

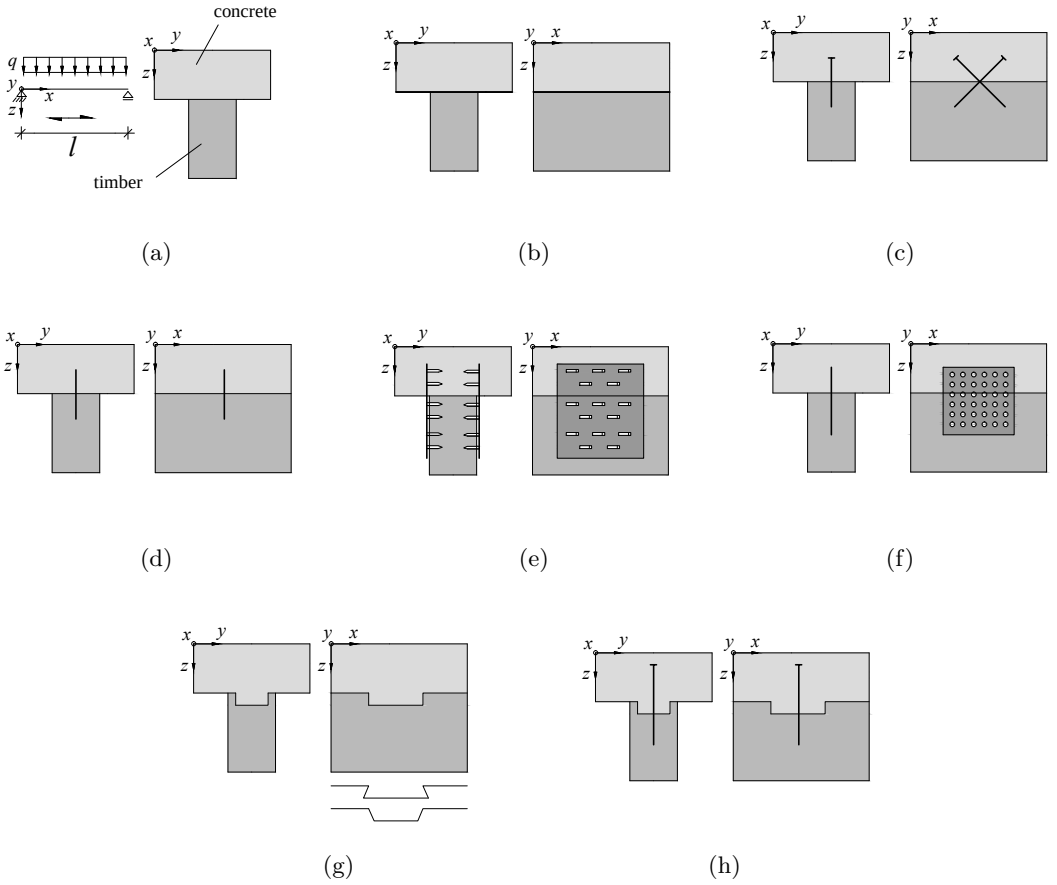

Figure 2.5: Examples of timber-concrete connections: (a) static system; (b) glued connection; (c) screws [39]; (d) glued-in steel rods [39]; (e) steel punched metal plates [28], [39]; (f) glued-in steel mesh [40]; (g) Notches cut in the timber part; (h) Notches cut in the timber part combined with mechanical fasteners [25]

2.3.4 Influence of the connection behaviour on the structural behaviour of the composite member

In a timber-concrete composite member, the timber-concrete connection influences the structural behaviour. In elastic conditions, the influence of the connection on the degree of composite action, the stiffness and the strength can be estimated with the γ-factor, as described in Section 2.3.2. In contrast, the influence of a connection, subjected to plastic deformations, on the structural behaviour of the composite member is more difficult to predict.

Ductile connection systems are advantageous because they are able to increase the load-carrying capacity and the ultimate deformation capacity of timber-concrete composite slabs [41]. On the other hand, the ductile behaviour of the connections does not necessarily mean that the behaviour of the composite slabs is ductile. As assessed by Ceccotti [39], if the connections are over-designed, linear elastic behaviour of the beam with brittle failure will be observed.

In general, in timber-concrete composite slabs, a ductile failure is more difficult to achieve than in reinforced concrete or steel-concrete composite slabs. This is due to the fact that, contrary to steel, the timber part fails in a brittle way when subjected to tension and bending. In timber-concrete composites, a ductile failure occurs if the connection is ductile, the ductile connection failure is governing, and the geometry and the material properties allow for plastic deformations.

Van der Linden [42] observed ductile behaviour of timber-concrete composite beams subjected to bending, in a research programme which analysed several types of timber-concrete connection systems (e.e. screws, nailplates and notches provided with reinforcement bars). The composite beams showed ductile behaviour before total collapse occurred. This behaviour was caused by plastic deformations of the connectors. The test results were compared with predictions made using three different approaches: an elastic analytical model, a frozen shear force approximation and finite elements calculations. The frozen shear force approximation is a calculation model which is used to determine the failure load of a timber-concrete composite beam once the first connectors have reached plasticity [42].

Frangi and Fontana [2] developed an elasto-plastic model for timber-concrete composite beams with ductile connections. The basic idea of this model has several commonalities with the frozen shear force approximation, presented by Van der Linden [42]. The model of Frangi and Fontana [2] considers the behaviour of the connections by assuming of a rigid, perfectly plastic load-slip relationship. This assumption is justified, for instance, in the case of notched connections with glued steel dowels because they usually show a very high slip stiffness at service load levels and large plastic deformations at failure. Because perfectly plastic behaviour of the connectors is assumed, full yielding of the interlayer is considered. In this way, the maximal shear force, which can be transferred between the two parts of the composite member, may be calculated from the shear resistance of the connection T_R and the number m of the connections between the support and the critical cross-section as:

$$N = m \cdot T_R \tag{2.22}$$

Consequently, the tensile stress in the timber cross section is calculated as:

$$\sigma_2 = \frac{m \cdot T_R}{A_2} \tag{2.23}$$

The bending stress $\sigma_{2,m}$ and σ_2 can be carried by the timber cross-section simultaneously. $\sigma_{2,m}$ is calculated from the linear elastic condition for timber subjected to combined bending and tension action:

$$\frac{\sigma_2}{f_{t,0,2}} + \frac{\sigma_{2,m}}{f_{m,0,2}} \leq 1 \tag{2.24}$$

The load-carrying capacity of the composite member after connection yielding is calculated using the stresses obtained with Eq. 2.23 and Eq. 2.24 [2].

The results of a series of bending tests of timber-concrete composite slabs made of glulam beams with notches and glued steel dowels showed that the elasto-plastic model presented by Frangi and Fontana gives a better prediction of the failure loads than the γ-method after plasticity has occurred [2]. Howewer, the model of Frangi and Fontana [2] does not predict the ultimate deflection after connection yielding.

Dias et al. [41] performed numerical simulations to assess the potential increase of the load-carrying capacity and the ultimate deformations of timber-concrete composite slabs due to the use of ductile connections. Furthermore, the maximum spacing for each type of connection, which is needed to maximise the load-carrying capacity and the ultimate deformation capacity, was identified by means of numerical simulations [41].

2.3.5 Gap opening

The opening of the gap between the tensile and the compressive parts, also known as uplift, is an important issue in composite structures. This phenomenon is difficult to quantify because it can be due to different reasons and is subjected to second-order phenomena.

Chapman [43] studied this phenomenon with steel-concrete composite structures. He discussed several possible causes, including the following:

- Due to the different geometry and material properties, the shear deflection of the lower part can greater than the shear deflection of the upper part. In this case, the two parts have a tendency to separate [43].

- In a composite structure made of two parts, each element is loaded eccentrically with respect to its own centroid by shear forces at the interface. Thus, there is a tendency for the elements to adopt different curvatures [43].

By solvin Eq. 2.1, Adekola [19] showed that differential deflections of the two parts can induce a tendency to uplift.

2.4 Models for the behaviour of the timber part

In a timber-concrete composite slab with a notched connection (Fig. 2.6(a)), depending on the zone, the timber part may be subjected to uniaxial or multi-axial stresses caused by tension, bending, compression or shear. Therefore, to predict the timber failures, the interaction between the different stresses must be studied and quantified. However, it is difficult to find failure criteria for timber because timber is orthotropic and not a homogeneous material. The first problem is that the mechanical properties of timber depend on the orientation as well as on the direction of loading; therefore, the development of failure criteria is challenging [44]. The second problem is described by Smith et al. [45]. Although several types of timber failures are classified as brittle by civil engineers, in reality, they are governed by complex mechanisms which cannot be explained with elastic strength theory or linear elastic fracture mechanics.

Sections 2.4.1 and 2.4.2 describe two different approaches for predicting the failure of a timber structural member:

- phenomenological strength criteria
- fracture mechanics

Sections 2.4.3, 2.4.4, and 2.4.5 summarise the state-of-the-art for predicting timber failures, which typically occur in timber-concrete composite slabs with notched connections:

- compressive failure in the notch (Fig. 2.6(b))
- shearing-off failure close to the notch (Fig. 2.6(c))
- combined tensile-bending failure (Fig. 2.6(d)).

2.4.1 Phenomenological strength criteria

A failure criterion is introduced to predict the failure of a structural timber member. If the stress in one direction is dominant, the stresses in the other directions can be neglected [44]. However, structural elements subjected to multi-axial stress states require the introduction of failure criteria to consider this effect. These multi-axial failure criteria are represented by mathematical expressions describing a strength surface [44]. Kasal and Leichti [44] presented and discussed the state-of-the-art multi-axial phenomenological strength criteria for wood members. Theses strength criteria are called phenomenological because they apply to the phenomenon of failure, but cannot explain the failure mechanism itself [44].

The simplest criterion in strength theory is the maximum stress criterion [46]. The failure occurs when the stress in one direction σ_x exceeds the strength X of the material in that same direction:

$$\frac{\sigma_x}{X} \geq 1 \tag{2.25}$$

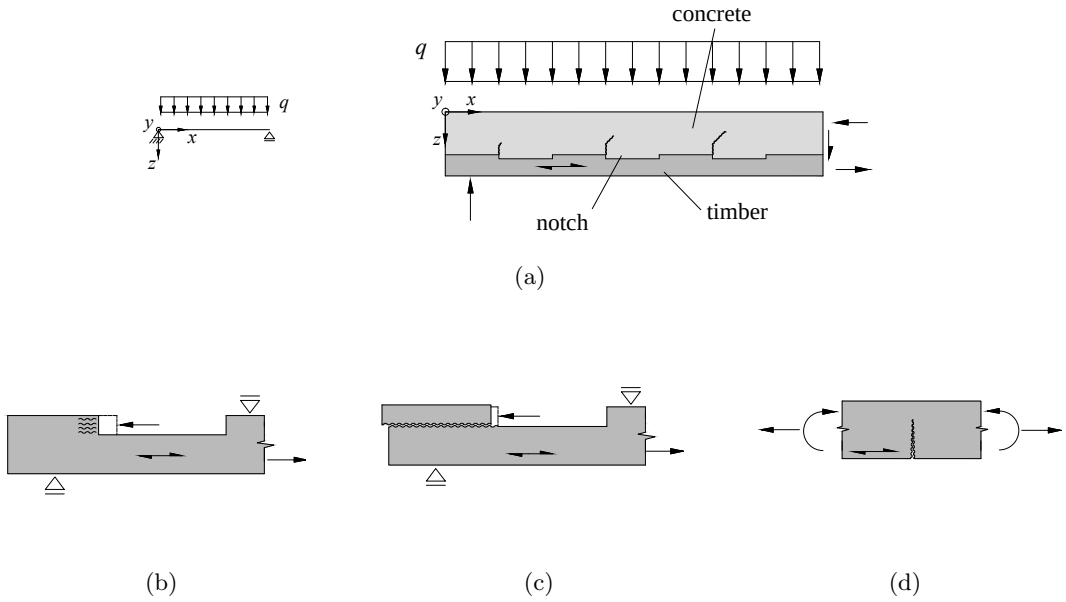

Figure 2.6: Examples of timber failures which typically occur in a timber-concrete composite member with notched connection: (a) static system; (b) compressive failure in the notch; (c) shearing-off failure; (d) combined tensile-bending failure

Another type of failure criteria is based on the strain energy. According to the van Mises-Hencky distorsion energy theory [47], a ductile solid yields if the energy of distortion reaches a critical value. In other words, failure is induced by the distortional energy, which is calculated by subtracting the hydrostatic strain energy from the total strain energy. Hill [48] extended the theory of von Mises-Hencky and developed a failure criterion under the assumption that when plastic deformation occurs, the material tends to become anisotropic [44]. In the von Mises-Hencky's theory, a hydrostatic pressure is assumed not to change the shape of a solid [44], and thus, the material is assumed to resist any hydrostatic pressure. However, as discussed by Kasal and Leichti [44], several experimental investigations proved that this assumption is not valid for wood.

Norris [49] proposed one of the first strength criteria for orthotropic materials. This failure criterion is based on van Mises-Hencky's distortion energy hypothesis, and for a two-dimensional stress state (Fig. 2.7), can be written as follows [44]:

$$\left(\frac{\sigma_x}{X}\right)^2 - \frac{\sigma_x \sigma_y}{XY} + \left(\frac{\sigma_y}{Y}\right)^2 + \left(\frac{\tau_{xy}}{S}\right)^2 = 1 \tag{2.26}$$

This failure criterion does not take into account the different compressive and tensile strengths of timber. In addition, Norris's criterion becomes too conservative for normal and shear stress combinations [44].

Hoffman [50] proposed an empirical expression for orthotropic brittle materials, where tensile and compressive strengths are assumed to be different [44]. The proposed failure criterion was developed using features of the van Mises-Schleicher isotropic yield condition and Hill's orthotropic yield condition [50]. The agreement with fibre-reinforced composite material exper-

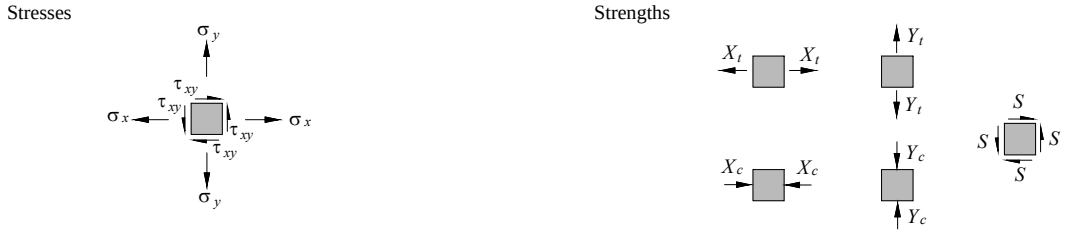

Figure 2.7: Two-dimensional stress state

imental data was good. Nevertheless, Hoffman found evidence that, despite formal similarities, yield conditions and brittle-fracture conditions pertain to unrelated physical phenomena [50]. The Hoffman failure criterion in a general state of plane stresses (Fig. 2.7) can be written as follows:

$$\left(\frac{1}{X_t}-\frac{1}{X_c}\right)\cdot\sigma_x+\left(\frac{1}{Y_t}-\frac{1}{Y_c}\right)\cdot\sigma_y+\frac{\sigma_x^2}{X_tX_c}+\frac{\sigma_y^2}{Y_tY_c}-\frac{\sigma_x\sigma_y}{X_cX_t}+\frac{\tau_{xy}^2}{S^2}=1 \tag{2.27}$$

As discussed by Kasal and Leichti [44], the main problem is a lack of constraints on the coefficients.

Tsai and Wu [51] presented a model of strength for anisotropic materials. This model was developed to estimate the load-carrying capacity of filamentary composites with an operationally simple criterion [51]. However, as discussed by Tsai and Wu [51], strength is an ambiguous term, and the fracture of a composite material is a complex mechanism. Thus, such an operationally simple criterion can be useful to estimate failures in engineering and for materials characterisation, but cannot possibly explain the mechanism of fracture [51]. Some authors denominated this approach the Tensor Polynomial theory [52]. The model of Tsai and Wu was developed from a scalar function of two strength tensors. The basic assumption of this strength criterion is that there exists a failure surface in the stress-space in the following scalar form [51]:

$$f(\sigma_k)=F_i\sigma_i+F_{ij}\sigma_i\sigma_j=1 \tag{2.28}$$

were $i,\ j,\ k$ = 1,2,...6; and F_i and F_{ij} are strength tensors of the second and fourth rank, respectively [51].

In a general state of plane stresses, according to Fig. 2.7, the Tensor Polynomial failure criterion of Eq. 2.28 can be written as follows:

$$F_1\sigma_x+F_2\sigma_y+F_{11}\sigma_x^2+2F_{12}\sigma_x\sigma_y+F_{22}\sigma_y^2+F_{66}\tau_{xy}^2=1 \tag{2.29}$$

where the coefficients are defined as follows:

$$F_1=\frac{1}{X_t}-\frac{1}{X_c} \tag{2.30}$$

$$F_2 = \frac{1}{Y_t} - \frac{1}{Y_c} \tag{2.31}$$

$$F_{11} = \frac{1}{X_c X_t} \tag{2.32}$$

$$F_{22} = \frac{1}{Y_c Y_t} \tag{2.33}$$

$$F_{66} = \frac{1}{S^2} \tag{2.34}$$

The coefficient F_{12} in Eq. 2.29 is an interaction term, and its calculation is challenging. As discussed by Kasal and Leichti [44], there is no agreement about the appropriate method to determine F_{12}. Narayanaswami and Adelman [52] proposed to set F_{12} to zero and showed by means of experimental analyses and numerical simulations that, with this approach, the failure of practical filamentary composite materials under general biaxial loading can be predicted with sufficient accuracy for engineering applications. Thus, Narayanaswami and Adelman [52] recommended to set F_{12} to zero as a preferred alternative to an experimental determination of F_{12}. The reason is that the strength envelope of the Tensor Polynomial theory is closed if the following inequality is respected:

$$F_{11}F_{22} - F_{12}^2 > 0 \tag{2.35}$$

Therefore, F_{12} must lie between $-\sqrt{F_{11}F_{22}}$ and $\sqrt{F_{11}F_{22}}$. Narayanaswami and Adelman [52] proposed that, if a value for F_{12} within this range does not introduce an unacceptable error, experiments are not necessary to determine F_{12}, and the most convenient value for F_{12} in this range is zero.

Since the two boundaries of F_{12} depend on F_{11} and F_{22} and, in other words, on the strengths of the materials, the consequences of neglecting F_{12} can be analytically estimated. Figure 2.8(a) illustrates the state of biaxial stress for beech LVL without shear. In Fig. 2.8(b), the Tensor Polynomial model (Eq. 2.29) is applied to a beech LVL element, loaded according to Fig. 2.8(a). The two boundaries of the interaction term F_{12}, as well as the no-interaction case, are considered, and are compared to the failure criterion of Hoffman (Eq. 2.27). For beech LVL, stressed according to Fig. 2.8(a), the interaction term has a particularly relevant influence if the member is subjected to compression perpendicular to the glue layers. The envelope of the Tensor Polynomial model without the interaction term is very similar to the curve of the Hoffman model, and is located between the two boundaries of Eq. 2.29.

With regard to the interaction term, the two approaches show an important difference. In the Tensor Polynomial model, the two boundaries of the interaction term of Eq. 2.29 are governed by the product $F_{11}F_{22}$, which depends on the strength in both x- and y-directions. In contrast, in the model of Hoffman, the coefficient which multiplies $\sigma_x\sigma_y$ depends only on the strengths in the x-direction.

It can be concluded that for beech LVL with biaxial loading, according to 2.8(a), the Tensor Polynomial model without the interaction term F_{12} should be applied carefully. Depending on the stress configuration, neglecting the interaction term can introduce relevant errors.

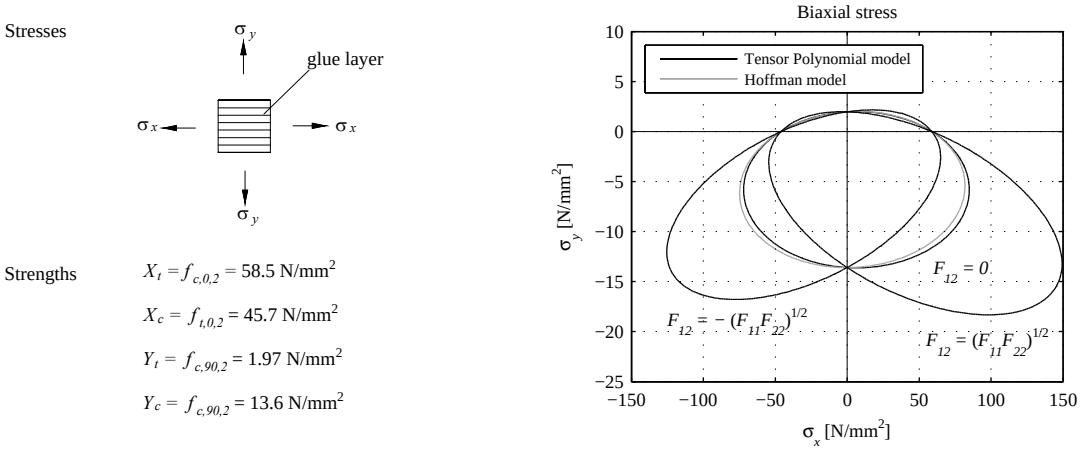

(a) (b)

Figure 2.8: Failure criteria for biaxial loading of beech LVL: (a) stress configuration and material parameters from Tab. 2.1; (b) comparison between the Tensor Polynomial model (Eq. 2.29) and the Hoffman model (Eq. 2.27)

With regard to a timber member subjected to a shear stress τ_{xy}, combined with a vertical stress perpendicular the shear plane σ_y, the Tensor Polynomial model of Eq. 2.29 can be applied without the interaction term F_{12} because σ_x is assumed to be zero. Therefore, in this case, a prediction of the failure using this criterion can be done with more certainty. Furthermore, with these stress conditions, the Tensor Polynomial model formula (Eq. 2.29) matches the Hoffman model (Eq. 2.27).

The Swiss Code SIA 265 [29] presents a criterion based on an elliptic interaction between the shear stress τ and the stress perpendicular to the shear plane σ_{90}:

$$\left(\frac{f_{c,90}+\sigma_{90}}{f_{c,90}+f_{t,90}}\right)^2+\left(\frac{\tau}{f_v}\right)^2\left[1-\left(\frac{f_{c,90}}{f_{c,90}+f_{t,90}}\right)^2\right]=1 \tag{2.36}$$

Eq. 2.36 is valid for $-f_{c,90} \leq \sigma_{90} \leq f_{t,90}$. As discussed by Jockwer [46], the benchmarking of Eq 2.36 with experimental data by Steiger and Gehri [53] shows a good representation of the interaction behaviour, especially with regard to the high variation observed in the experiments.

Figure 2.9 illustrates the influence of the vertical stress perpendicular to the glue layers of beech LVL on the shear strength estimated using the Tensor Polynomial model (Eq. 2.29), the Hoffman model (Eq. 2.27) and the formula suggested by the Swiss Code (Eq. 2.36). The mechanical properties of the timber member and the stress configuration are shown in Fig. 2.9(a). As presented in Fig. 2.9(b), if the timber member is subjected to tension perpendicular to the glue layers ($\sigma_y > 0$), the Tensor Polynomial model and Eq. 2.36 give the same result. In contrast, if compression perpendicular to the glue layers occurs, the envelope of the

Tensor Polynomial model reaches a peak and then decreases. According to Eq. 2.36, the shear strength should increase until the compressive strength is reached. The difference between the two methods becomes more significant with increasing compression perpendicular to the glue layers. However, it must be noted that the formula suggested by the Swiss Code (Eq. 2.36) has only been verified in the part of Fig. 2.9(b) where the plotted curve is solid.

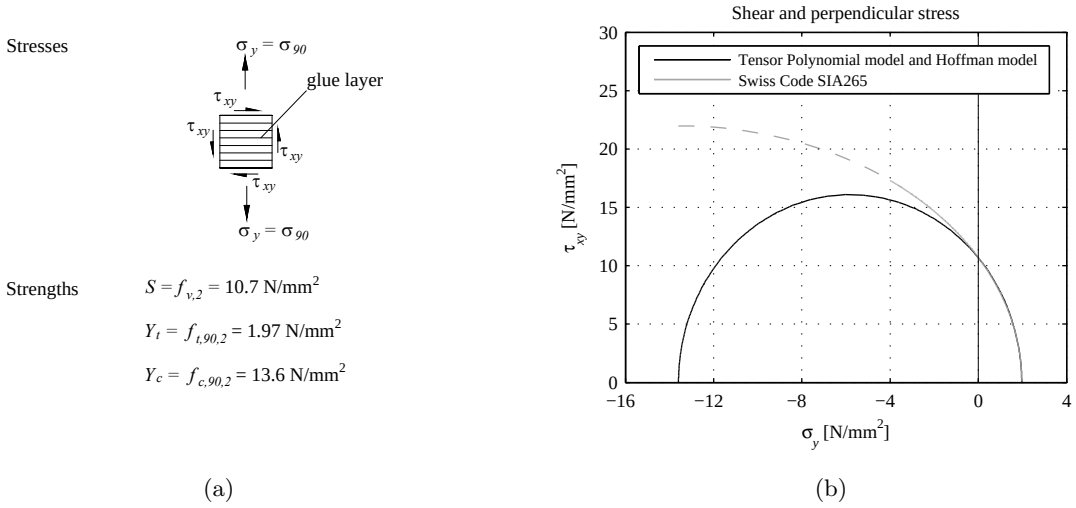

Figure 2.9: Failure criteria for the combination of shear and axial stress perpendicular to the glue layers: (a) stress configuration and material parameters from Tab. 2.1; (b) comparison between the failure criteria

In conclusion, the phenomenological strength criteria presented in this section help to understand the influence of multi-axial stresses on a failure. Since the failure criterion of Hoffman and the Tensor Polynomial model take into account the orthotropy of materials, it is possible to apply these criteria to estimate timber failures. However, the interpretation of the results can become challenging because such operationally simple criteria cannot explain the complex mechanisms of timber failures. In timber engineering, to analyse the outcomes of a failure prediction performed by means of these criteria, the stress situation should be simplified and the physical mechanisms of the failure should always be taken into account. Furthermore, depending on the timber material and the stress configuration, the influence of interaction terms can make the interpretation difficult.

2.4.2 Fracture mechanics

Another approach to study the failure of wood is the fracture mechanics theory [45]. Linear elastic fracture mechanics (LEFM) assumes that the material is linear or very nearly linear elastic right until fracture [45]. According to this theory, fracture occurs when the condition for crack propagation is satisfied. This condition is written in terms of a critical strain energy release rate, often called fracture energy. Since the theory of the strain energy release rate is often not practical for large systems, the concept of stress intensity factors has been introduced [45].

As discussed by Smith et al. [45], LEFM is appropriate for materials such as glass and cast iron. According to LEFM, all available strain energy goes into propagation of a crack. However, in nearly all materials, there are several other micro-structural mechanisms that are capable of dissipating strain energy (toughening mechanisms). Some examples of these toughening mechanisms are: micro-cracking around the main crack, crack bridging, or plastic deformation at a crack tip (2.10(a)). To describe such materials, the nonlinear fracture mechanics theory was developed. Wood is a typical example of material in which the toughening mechanisms play an important role in the fracture process [45].

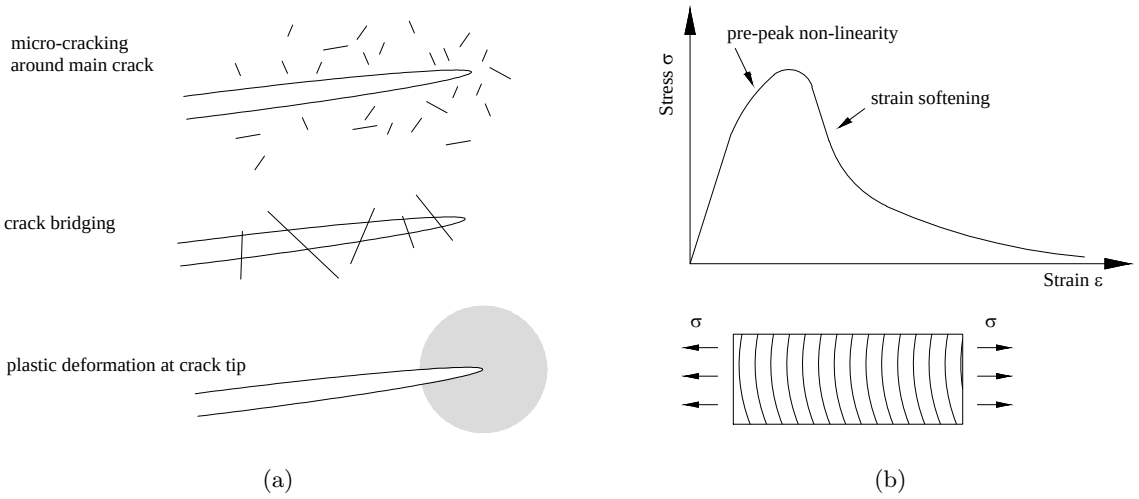

Figure 2.10: Non-linear fracture mechanics: (a) possible toughening mechanisms [45]; (b) quasi-brittle behaviour of wood in tension perpendicular to the grain [45]

Because of this deviation from the LEFM, Smith et al. [45] characterised wood as quasi-brittle material, and discussed the application of the nonlinear fracture mechanics to predict its behaviour. A quasi-brittle material is susceptible to some of the same types of failures as the brittle materials, but the behaviour is less dramatic. Fig. 2.10(b) shows a qualitative illustration of the quasi-brittle behaviour of wood subjected to tension perpendicular to the grain, according to Smith et al. [45]. However, it must be kept in mind that strain softening is not a material property, but depends on the entire system (including the test rig). As a timber member is loaded, small cracks begin to grow from microscopic imperfections. As these micro-cracks accumulate, the stiffness of the material decreases and the load-deformation curve becomes less steep (pre-peak non-linearity). As the peak is reached, a critical crack, accompanied by a fracture process zone, can occur. Because of the toughening mechanisms, energy is dissipated gradually, and strain softening occurs [45]. Nevertheless, the nature of energy dissipation in the fracture process zone in wood is still being discussed [54].

In conclusion, the fracture mechanics theory can be helpful to understand fracture processes of timber members and to interpret experimental results, which deviate from the outcomes of elastic calculations.

2.4.3 Compressive failure parallel to the grain

If timber and concrete are connected by means of notches, the horizontal forces, which ensure the composite action, are transferred from the concrete to the timber by compressive contact in the notch. This means that the timber part of the composite member is locally subjected to compression parallel to the grain. It is a well-known fact that a compressive failure of timber parallel to the grain can be classified as ductile. Thus, one possible way to achieve ductile behaviour of the composite structure is to design the slab so that a compressive failure in the timber parallel to the grain is governing.

Grosse [55] described the physical mechanisms which govern all types of wood failures. The compressive behaviour of timber parallel to the grain is highly complex. The failure mechanism is governed by buckling of fibres and formation of a kink band. After high axial strains, the material is subjected to hardening due to the fact that the hollows in the fibre tubes tend to close [55].

Estimate of ultimte strength

Frangi [25] and Michelfelder [33] used simple design formulas to determine the failure load, which did not account for multiaxial stresses. The failure load is obtained by multiplying the surface by the strength:

$$T_R = f_{c,0} \cdot b_N \cdot t_N \tag{2.37}$$

Schönborn [56] showed evidence of the problem of multi-axial stresses, which act close to inclined notch edges of timber-concrete composites. He proposed using failure criteria, and discussed the differences between the theories of Tsai and Wu, Hankinson, Norris and Ellund. Then, he decided to treat the situation as a compression problem with stresses acting at an angle to the grain using the approach given in the German Standard DIN 1052 [57]. The strength in the fibre direction was corrected using a correction factor, which depends on the compressive strengths parallel and perpendicular to the grain, the shear strength, and the angle of the stress due to the fibre direction. Schönborn [56] developed a design equation by adjusting this correction factor to fit the calculated values to his experimental results.

2.4.4 Shearing-off failure

In several experimental analyses of timber-concrete composite structures with notched connections, horizontal shearing-off failures of timber close to the notch were observed (e.g. [33]). In general, this failure is brittle and must be prevented. The first step to predict this type of failure using the strength theory is to determine the shear stress distribution.

The elastic shear stress distribution can be estimated using analytical models derived for composite problems. Marti [5] provided an analytical solution to several composite problems using the differential equations of the axial deformations of the members. Through use of similar analytical models, Kaiser [58] estimated the elastic shear stress and strain distributions due to pull out tests of a carbon fibre material glued to timber. These elastic calculations typically

showed non-linear distributions of the shear stress with peaks corresponding to the points where the loads were introduced. Fig. 2.11 shows a qualitative distribution of the elastic shear stress τ_{el} along the shear plane of a notched connection.

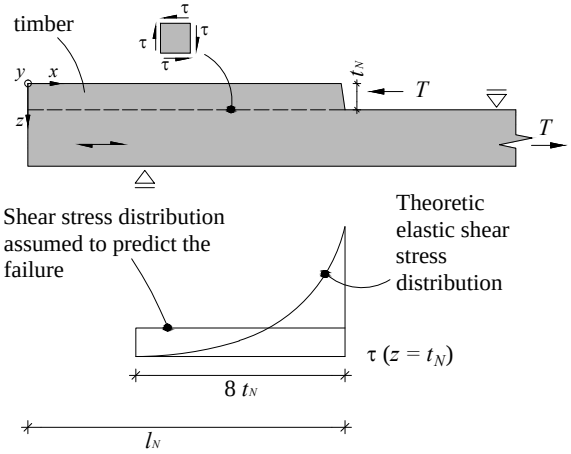

Figure 2.11: Shear stress distribution in timber close to the notch, according to Colling [59]

By means of numerical simulations, Michelfelder [33] verified the studies of Stephan [60] about the elastic shear stress distribution in timber notches. She found that the elastic shear stress distribution has a peak close to the notch edge, where the load is introduced, and that, from a determinate length of the timber next to the notch l_N, the shear stress distribution remains constant. Stephan [60] set a limit length, $8t_N$, as a function of the notch depth, and Michelfelder [33] verified this theory by means of numerical simulations. She also found that the elastic shear stress distribution is influenced by the notch depth: the deeper the notch, the lower the shear stress.

With regard to shear stress, a notched connection is similar to a step joint. For engineering applications, to prevent a horizontal shear failure of timber in a step joint, a rectangular shear stress distribution formula was developed [61]. Colling [59] explained, as also shown by Stephan [60] and Michelfelder [33], that the shear stress is distributed over a maximal effective length of about $8t_N$. For the prediction of the shear failure, Colling [59] suggested to distribute the notch force rectangularly over the length $8t_N$, even though the elastic shear stress distribution shows a peak close to the load transfer point (Fig. 2.11). The failure load is defined as:

$$T_R = 8 \cdot t_N \cdot b_N \cdot f_v \tag{2.38}$$

In the literature, it is difficult to find experimental research which shows measurements of the shear stresses and strains close to the shear failure surface of timber. Kaiser [58] performed pull-out tests on carbon-fiber-reinforced polymers glued to spruce wood with a 2-component epoxy glue, and measured the distribution of the shear stresses in the glue layer. One important outcome was that the structural behaviour of the connection showed a non-linear phase before the failure. For moderate loads, the shear stress distribution along the shear plane showed a peak close to the load introduction point. Then, the peak decreased and the shear stress tended to redistribute over the available length. In this case, the shear stress distribution at failure was

markedly different from the elastic distribution. This is an example of stress redistributions over the shear plane, even though the materials used are not ductile.

Another important issue is that a shearing-off failure can be facilitated or prevented by stresses perpendicular to the shear plane. These stresses occur because of the equilibrium of the timber member (Fig. 2.12). Heimeshoff and Köhler [62] analysed several timber-timber notched connections and developed a mechanical model to estimate the stresses perpendicular to the shear plane, generated by the eccentricity between the notch force and the shear surface. Steurer [63] presented a similar model and concluded that tensile stresses perpendicular to the shear plane facilitate a shear failure, whereas compression perpendicular to the shear plane increases the shear strength. Steurer [63] idealised this issue, as shown in Fig. 2.12, and suggested estimating the elastic stresses perpendicular to the shear plane σ_{90} as a function of the shear force T, the notch length l_N, and notch depth t_N as follows:

$$\sigma_{90} \approx \frac{M_{ecc}}{W_{notch}} \tag{2.39}$$

Here, the eccentricity moment is:

$$M_{ecc} = T \cdot \frac{t_N}{2} \tag{2.40}$$

and the section modulus of the shear plane of the notch is:

$$W_{notch} = \frac{b_N l_N^2}{6} \tag{2.41}$$

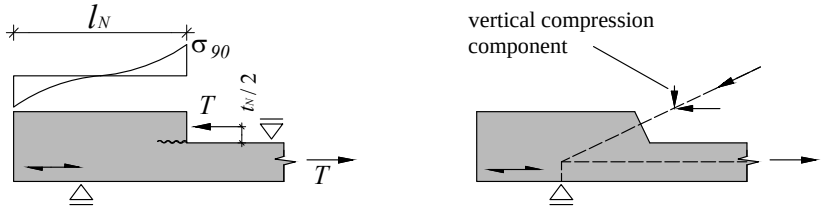

(a) (b)

Figure 2.12: Stresses perpendicular to the shear plane of a notched connection according to Steurer [63]: (a) stresses generated by the eccentricity between the notch force and the shear plane; (b) compression perpendicular to the shear plane.

Also, Michelfelder [33] showed evidence resulting from numerical simulations that tensile stresses perpendicular to the shear plane act in the notch, which facilitate a shear failure. She also took into account the positive influence of the vertical compression in the notch close to the support.

Through a series of experiments, Michelfelder [33] found that an increase of the notch depth causes a local increase of the shear strength of the timber. She stated that this happens because an increase of the notch depth causes a decrease of the eccentricity. However, this hypothesis

does not agree with the mechanical models presented by Heimeshoff and Köhler [62] and Steurer [63]. According to these models, the tension in the shear plane is due to the eccentricity of the horizontal load and hence, is directly proportional to the notch depth.

Estimate of ultimate strength in timber-concrete composite structures

Frangi [25] assumed a shear stress distribution over the full length of the timber before the notch l_N, and calculated the shear resistance with the following equation:

$$T_R = f_v \cdot b_N \cdot l_N \tag{2.42}$$

Michelfelder [33] reduced the value of the shear strength of timber using a reduction factor and distributed the shear stress along the entire length of the timber before the notch. She did not differentiate between the notch close to the support and the other notches. By means of numerical simulations, she showed that the tensile stresses perpendicular to the shear plane can be neglected. Michelfelder [33] compared the results of the formula with the shear failure loads measured during shear tests and observed that the formula underestimated the shear strengths.

Schönborn [56] adopted the formula of Fonrobert [61], presented in Eq. 2.38, but suggested that the length of the timber before the notch should be at least $l_{N,min} = 12 \cdot t_N$. The reason is that, even though the notch was designed according to Eq. 2.38, a horizontal shear failure of the timber occurred during some bending tests. This design approach did not take into account the tension and compression perpendicular to the shear plane.

2.4.5 Combined tensile-bending failure

In the timber layer of a timber-concrete composite member, tensile and bending stresses occur. Both tensile and bending failures of timber structures can be classified as brittle phenomena. However, a bending failure is more complex than a tensile failure because is partially governed by plastic mechanisms.

As shown in Fig. 2.13(a), in elastic conditions, the zero-stress layer of a timber member subjected to bending does not correspond to the centroid of the cross-section because the modulus of elasticity of timber in compression is smaller than that in tension. In contrast to the tensile failure of timber parallel to the grain, the compressive failure parallel to the grain is ductile. Furthermore, the compressive strength parallel to the grain is smaller than the tensile strength. Consequently, the bending failure mechanism begins when the compressive stress on top edge of the cross-section reaches the compressive strength. Then, the timber begins to develop plastic deformations in the compressive zone, and the compressive stress distribution becomes non-linear. The curvature of the cross section increases until the tensile stress on bottom edge of the cross section exceeds the tensile strength, and then a tensile crack propagates [63].

In practice, it is usually assumed that the tensile and compressive moduli of elasticity are identical and the cross-section remains plane. The difference between the tensile and compressive

strengths is neglected, and a virtual bending strength f_m is assumed (2.13(a)). The value of the bending strength f_m can be determined by means of laboratory tests [63].

As illustrated in Fig. 2.13(b), the timber layer of a timber-concrete composite member, subjected to positive bending moment, is usually subjected to a trapezoidal axial stress σ_x. This stress consists of a tensile component $\sigma_{t,0}$ and a bending component $\sigma_{m,y}$. Thus, two stress states act simultaneously on the timber layer. To estimate the strength of a member subjected to tension and bending, the Swiss Standard SIA 265 [29] recommends the following criterion:

$$\frac{\sigma_{t,0}}{f_{t,0}} + \frac{\sigma_{m,y}}{f_{m,y}} + \frac{\sigma_{m,z}}{f_{m,z}} \leq 1 \tag{2.43}$$

The load-carrying capacity of the timber part of a timber-concrete composite member is usually verified using this method [2].

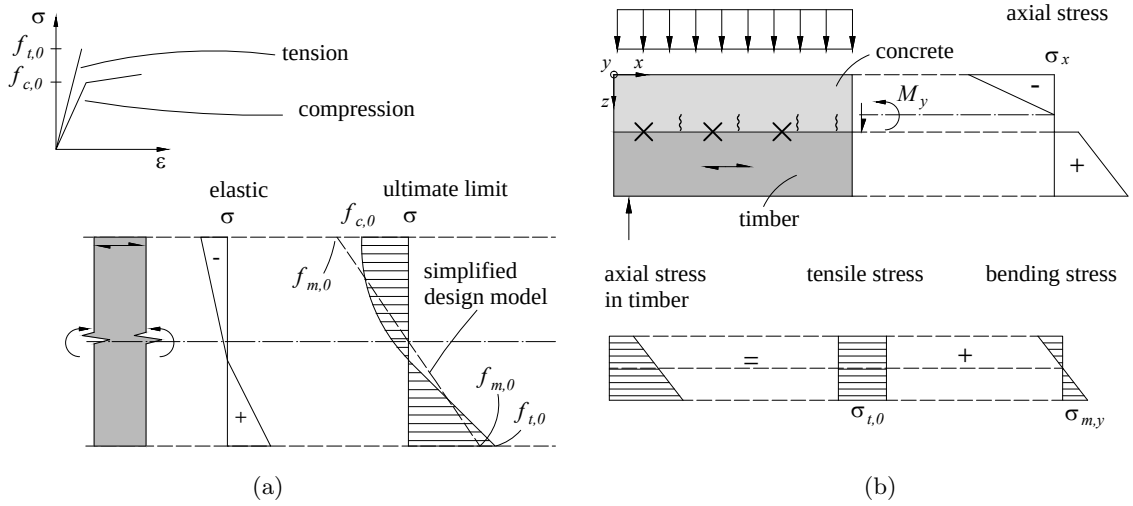

Figure 2.13: (a) bending stress in a timber cross section according to Steurer [63]; (b) division of the axial stress in the timber layer of a timber-concrete composite member

2.5 Models for the behaviour of the concrete part

In a timber-concrete composite member, the concrete part can be subjected to compression, shear and tension. Furthermore, the stress must be transferred from the concrete part, subjected to compression, to the timber part, subjected to tension. Therefore, shear and tensile stresses occur at the interface between the timber and the concrete. If no vertical steel reinforcement is included, the tensile and shear stresses are carried by the concrete. In contrast, if the structure is provided with vertical steel reinforcement, the steel carries vertical tension and the concrete carries compressive stresses after concrete cracking.

Depending on the geometry and the connection system, the load-carrying behaviour of timber-concrete composites can have similarities to the behaviour of conventional reinforced concrete structures (Fig. 2.14). However, the most important difference is that, in the reinforced concrete member, the force is usually transferred in a continuous way along the reinforcing bar,

whereas in the timber-concrete composite member with a notched connection, the load transfer occurs locally through the notch borders.

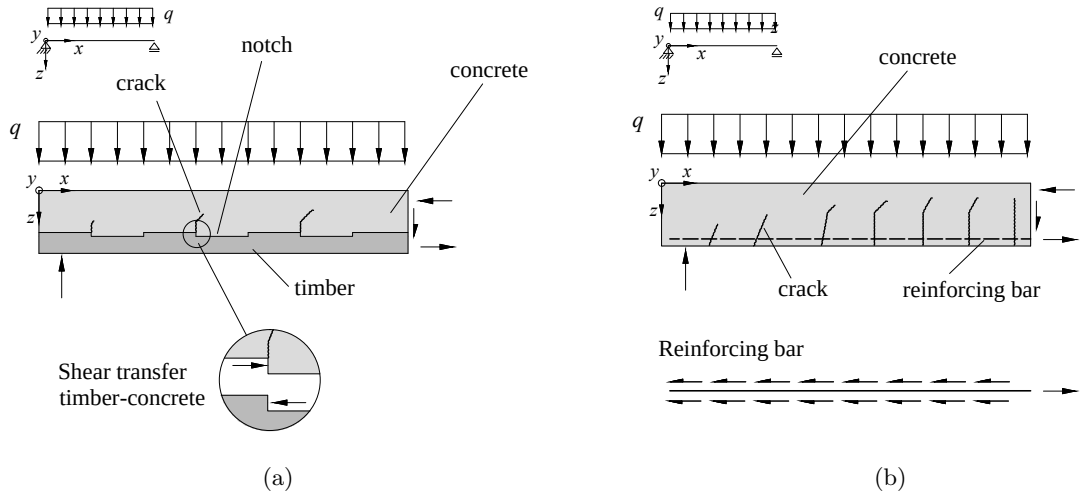

Figure 2.14: Comparison of the load-carrying mechanism in (a) a timber-concrete composite member with a notched connection and (b) a reinforced concrete member

Section 2.5.1 illustrates the existing analytical models which can be used to describe the failure of concrete in the compression zone of a structural member subjected to bending. Section 2.5.2 presents the failure criterion of Mohr-Coulomb, which can be used to predict the strength of a concrete member without steel reinforcement. In Section 2.5.3, the existing models for the shear resistance in structural concrete members are discussed. If the concrete does not contain vertical shear reinforcement, the shear stresses are carried by means of complex mechanisms which are challenging to model, and the shear strength is governed by the mechanical properties of concrete, the position of the cracks, and their widths. In contrast, a more favourable load-carrying mechanism is achieved if concrete contains vertical shear reinforcement. Finally, Section 2.5.4 presents the formulas which were developed for notches in timber-concrete composite members.

2.5.1 Behaviour of concrete in the compression zone

The upper part of a timber-concrete composite member subjected to bending is compressed. If the critical bending moment is achieved, the concrete may fail. The existing literature about this topic is related to the modelling of reinforced concrete structures.

The behaviour of concrete subjected to compression is influenced by several factors. First, plasticity can develop. According to Bachmann [64] and Kenel [65], commonly used analytical simplifications for the behaviour of concrete in the compression zone of a member subjected to bending assume that the relationship between the axial stress and strain is non-linear, as qualitatively illustrated in Fig. 2.15(a). The ultimate strain is represented by $\varepsilon_{c,u}$. The equations which govern the behaviour are given in [65].

According to the Swiss Code SIA 262 [66], when concrete reaches the compressive strength at the top of the cross-section, the stresses redistribute within the compression zone, and the strain can increase until $\varepsilon_{c,u} \approx 0.003$ (Fig. 2.15(b)). At this moment, the stress distribution is non-linear and can be approximated by means of a rectangle with a height of $0.85 \cdot x$ [66].

Ductile behaviour of steel and concrete determine whether ductility is achieved in reinforced concrete structures [67].

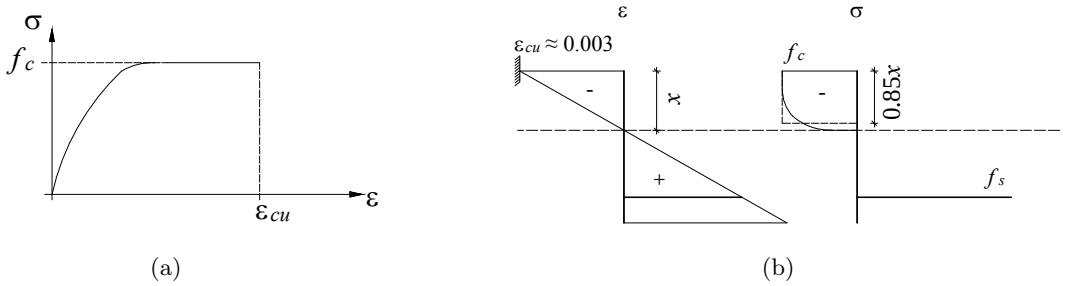

Figure 2.15: Model for the behaviour of the compression zone in reinforced concrete members subjected to bending; (a) qualitative illustration of the simplified stress-strain behaviour [64], [65]; (b) idealised stress-strain diagrams of the cross-section [66]

2.5.2 Mohr-Coulomb failure criterion

According to Marti [5], the failure criterion of Mohr-Coulomb can be used to describe the behaviour of concrete and is defined as:

$$Y = 0 = |\tau| + \sigma \cdot \tan(\varphi) - c \tag{2.44}$$

According to Fig. 2.16(a), the yielding limits of a concrete member subjected to un-axial loading are:

$$f_c = \frac{2 \cdot c \cdot \cos(\varphi)}{1 - \sin(\varphi)} = 2 \cdot c \cdot \tan\left(\frac{\pi}{4} + \frac{\varphi}{2}\right) \tag{2.45}$$

$$f_t = \frac{2 \cdot c \cdot \cos(\varphi)}{1 + \sin(\varphi)} = 2 \cdot c \cdot \tan\left(\frac{\pi}{4} - \frac{\varphi}{2}\right) \tag{2.46}$$

The values of f_c and φ are determined experimentally. For any concrete type, the angle of the internal friction has a constant value of $\tan(\varphi) = 3/4$. Thus, the cohesion becomes $c = f_c/4$.

This model predicts the behaviour of concrete subjected to compression in an accurate way. However, the value of the tensile strength of the concrete f_t is too high, and thus, unrealistic. Therefore, for materials with low tensile strengths like concrete, the modified Mohr-Coulomb failure criterion of Fig. 2.16(b) was developed [5]. This modification results from the condition that the tensile stress must be smaller than the tensile strength of concrete:

$$\sigma \leq f_{ct} \tag{2.47}$$

and:

$$f_{ct} < \frac{2 \cdot c \cdot \cos(\varphi)}{1 + \sin(\varphi)} \tag{2.48}$$

The resulting modification of the failure criterion is expressed with a circle BAC with diameter:

$$\oslash_{BAC} = f_c - \frac{2 \cdot \sin(\varphi) \cdot f_{ct}}{1 - \sin(\varphi)} \tag{2.49}$$

and the equation of the yielding line is:

$$\tau = -\frac{3}{4} \cdot \sigma + \frac{f_c}{4} \tag{2.50}$$

And the equation of the circle BAC is:

$$\left(\sigma + \frac{f_c}{2} - \frac{sin(\varphi) \cdot f_{ct}}{1 - sin(\varphi)} - f_{ct}\right)^2 + \tau^2 = \left(\frac{f_c}{2} - \frac{sin(\varphi) \cdot f_{ct}}{1 - sin(\varphi)}\right)^2 \tag{2.51}$$

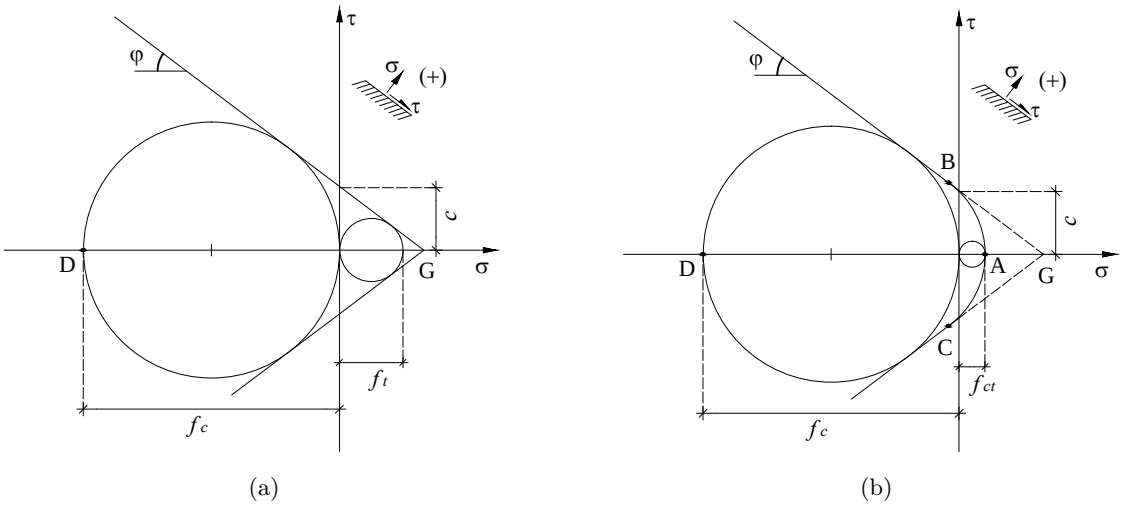

Figure 2.16: (a) Mohr-Coulomb failure criterion and (b) modified Mohr-Coulomb failure criterion applied to concrete according to Marti [5]

2.5.3 Models for carrying shear in concrete

In general, in a timber-concrete composite structure with a notched connection, depending on the geometry, some amount of shear has to be transferred through the concrete part. The limit case is a composite slab with a thin LVL plate and a thick concrete layer, where the timber part can be idealized as a tensile reinforcement. In this case, the LVL plate is mostly subjected to tension and the concrete carries almost the entire vertical shear, similar to a reinforced concrete member.

The shear transfer in concrete was studied in the context of the structural analysis of reinforced concrete. As discussed by Muttoni and Ruiz [68], several well-established theories based on equilibrium considerations (stress fields and truss models) can be applied when shear

reinforcement is provided. Although a significant effort has been made, currently there is no agreement about the modelling of members without shear reinforcement [68].

Structures without shear reinforcement

The failure modes of reinforced concrete structures without shear reinforcement were experimentally studied by Leonhardt and Walther [69] and Muttoni and Thürlimann [70]. It was observed that, in members without shear reinforcement, the flexural strength predicted by the theory of plasticity cannot be achieved because of the propagation of shear cracks in concrete [68].

Several authors (e.g. Fenwick and Pauley [71], Muttoni and Schwartz [72] and Muttoni and Ruiz [68]) analysed and modelled the various shear-carrying mechanisms in reinforced concrete structures without vertical shear reinforcement. After bending cracks develop, the load-carrying mechanism begins to change [72]. Cantilever action is a possible mechanism, which can occur. This mechanism was already recognized by Kani [73], who assessed that, due to the transverse cracks, the tension zone is divided into separate concrete elements. These can be visualized as cantilever beams fixed in the upper compression zone [72]. As explained by Zilch and Zehetmaier [74], these cantilever models are based on a strongly idealized crack geometry. Fig 2.17 shows an example of cantilever model in which the vertical shear force is carried by the compression zone (V_{cc}), by the aggregate-interlock action (V_{cr}) and by the dowel action from the longitudinal reinforcing bars (V_d). The cantilever is subjected to bending action, which can cause propagation of a horizontal shear crack [74].

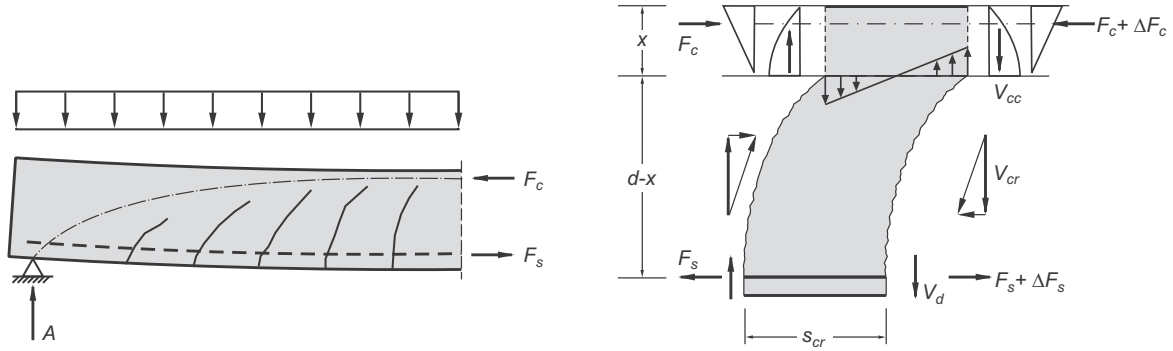

(a) (b)

Figure 2.17: Example of cantilever model according to Zilch and Zehetmaier [74]: (a) cantilever model; (b) single cantilever

The mechanisms which can cause the propagation of the critical shear crack can be classified as cantilever action, aggregate interlock action, and dowel action (Fig. 2.18(b)-(d)) [68]. These shear-carrying mechanisms cause tensile stresses in the concrete near the crack tip and close to the reinforcement (Fig. 2.18(e)). If these stresses reach the tensile strength of concrete, a shear crack can propagate and cancel the three previous mechanisms (Fig. 2.18(f)). Nevertheless, the propagation of the critical shear crack does not necessarily cause the failure of the structure because an arching action may be developed to carry the shear. According to Muttoni and Ruiz

[68], the arching action (and thus the shear strength of the member) is governed by the location of the critical shear crack, its width, and the aggregate size. Muttoni and Ruiz [68] proposed an analytical expression to evaluate the shear strength of a member as a function of the previous parameters. Based on this theory, the current Swiss Standard formula for structures without shear reinforcement was developed [66]. This theory shows a good agreement with experimental results.

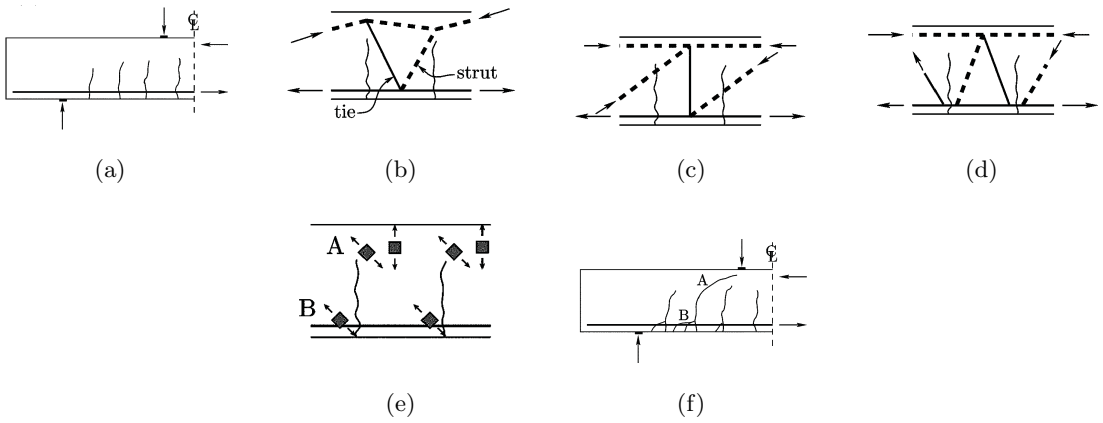

Figure 2.18: Development of the critical shear crack according to Muttoni and Ruiz [68]: (a) initial flexural cracks; (b) cantilever action; (c) aggregate-interlock action; (d) dowel action; (e) tensile stresses due to (b)-(d)); and (f) final crack pattern;

The load-carrying capacity of the concrete part of a timber-concrete composite member with a notched connection without shear reinforcement could also be analysed by means of the theories of plain concrete, as presented by Nielsen and Hoang [75].

Structures with shear reinforcement

The addition of vertical shear reinforcement to reinforced concrete members shows markedly improved behaviour because the vertical shear reinforcement carries vertical tension after the development of flexural-shear cracks. The load-carrying behaviour can be modelled with stress fields and truss models in which the shear reinforcement is represented by tension struts, according to Muttoni et al. [76], Marti [77] and Kaufmann [78]. The use of vertical reinforcement increases the shear strength of a structure considerably.

2.5.4 Estimate of ultimate strength in timber-concrete composite structures

Frangi [2] predicted the shear failure of the concrete along the notch by assuming a constant shear stress distribution over the entire notch length:

$$T_R = \tau_{R,c} \cdot b_N \cdot l_N \tag{2.52}$$

In numerical simulations, Michelfelder [33] observed that tensile concrete stresses occur close to the notch edge, and suggested that reinforcement of the notch provides a solution to the

risk of concrete failures (2.19(a)). She modelled the load-carrying behaviour with a truss model (2.19(b)) and defined three possible failures:

- compressive failure in the concrete notch (point 3 in Fig. 2.19(b))
- compressive failure in the strut (point 4 in Fig. 2.19(b))
- tensile failure in the tie (point 5 in Fig. 2.19(b))

(a) (b)

Figure 2.19: Model to predict the concrete failures in a timber-concrete composite slab with a notched connection according to Michelfelder [33]: (a) tensile stresses in concrete calculated with numerical simulations (b) truss model for the notch design;

To calculate the notch force which causes a tensile failure of concrete, Michelfelder [33] derived the depth x of the tie represented in Fig. 2.19(a) with numerical simulations. The resistance of the diagonal compressive strut was calculated by considering the notch depth and the angle between the diagonal strut and the vertical axis, which was assumed to be 60°. However, this assumption has not been verified.

Schönborn [56] developed design formulas under the assumption that, in the concrete member, a console failure or a horizontal shear failure may occur (Fig. 2.20). Schönborn [56] pointed out the problem of tensile stresses near the notch edge as a cause of the console failure. He wrote the tensile strength as a function of the compressive strength, used a formula developed by Zapfe [79] for steel-concrete composite members with concrete dowels, and used a correction factor to achieve a satisfying fit with the experimental results. The final expression to calculate the force which causes a console-failure of concrete was:

$$T_R = f_{model} \cdot f_{c,cube}^{2/3} \cdot t \cdot b \cdot \frac{l}{180} \tag{2.53}$$

Schönborn [56] assessed that the critical section for a horizontal shear failure in concrete corresponds to the surface delimited by the length and the width of the notch. For the prediction of the horizontal shear failure in concrete he assumed a constant distribution of the shear stress and used correction factors derived from experimental data.

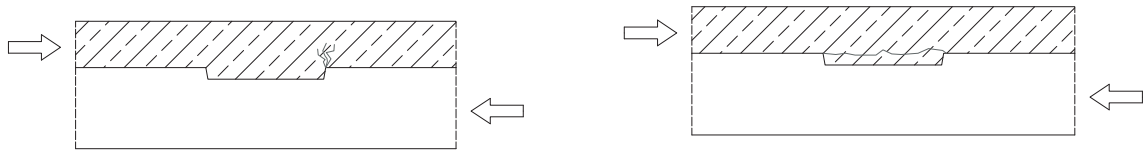

(a) (b)

Figure 2.20: Failures of concrete in a notched connection according to Schönborn [56]: (a) console failure of concrete; (b) horizontal shear failure of concrete

2.6 Modelling of the influence of mechanical fasteners on notched connections

Mechanical fasteners, such as screws and dowels fixed in the timber part of a timber-concrete composite member, are able to carry shear as well as tensile forces, and consequently are able to interact with the notches and to participate in the load-carrying mechanism.

Depending on the stiffness of a dowel and on the way it is fixed, the dowel carries a certain amount of horizontal shear. Furthermore, such a dowel, loaded perpendicular to its axis, can fail in a ductile way due to an embedment failure of the timber or a bending failure of the dowel. Frangi [25] developed an analytical model to estimate the amount of shear carried by a dowel in the case of combination notch-dowels. According to the theory of plasticity, he assessed that, if the behaviour of the notch without dowel is governed by a ductile compressive failure of the timber, the total shear failure load of the system is equal to the sum of the ductile failure load of the notch $T_{R,2C}$ and the dowels $T_{R,dowels,Ni}$:

$$T_R = T_{R,2C} + T_{R,dowels,Ni} \tag{2.54}$$

Frangi [25] calculated the ductile failure load of the dowel using the theory of Johansen [80]. He assumed that the dowel is fixed in the concrete, can bend in the timber, and is subjected to forces parallel to the interface between the timber and the concrete. He defined three different ductile failure modes of the dowel depending on the slenderness. For small slenderness, the dowel remains stiff and the failure load is governed by the embedment failure of timber. A higher slenderness implies an increase of the number of plastic hinges in the dowel and a higher failure load.

A mechanical fastener can also be activated in tension. If it is fixed perpendicular to the interface, it is able to carry vertical tensile forces. Several authors (e.g. Zöllig [81]) suggested installing vertical screws in timber-concrete composite members to carry the vertical tensile forces. A truss model can be used to design the reinforcement. The benefit of this reinforcement is that it helps to prevent gap opening and concrete failures. However, as discussed by Michelfelder [33], there is no agreement about the most appropriate method to determine whether such fasteners are necessary and how to design them.

2.7 Experimental analyses of timber-concrete composite structures with notched connections

This section summarises several experimental studies about the structural behaviour of timber-concrete composite members with notched connections. These studies are usually characterised by shear tests on the notched connections and bending tests on the composite members.

The performance of a notched connection is usually tested by means of a shear test. As explained by Steurer [63], an important issue regarding the investigation of the shear behaviour of a structural member is that a shear test, in addition to the shear stress, induces stresses perpendicular to the shear plane, generated by the eccentricity or by a reaction force (Fig. 2.12). Furthermore, Steurer [63] noted that the elastic shear stress distribution is influenced by the configuration of the external loads (Fig. 2.21). Thus, the experimental results are influenced by these phenomena [63]. Schönborn [56] summarised several possible setups to perform connection shear tests and emphasised the fact that each setup implies different stress distributions acting on the specimen.

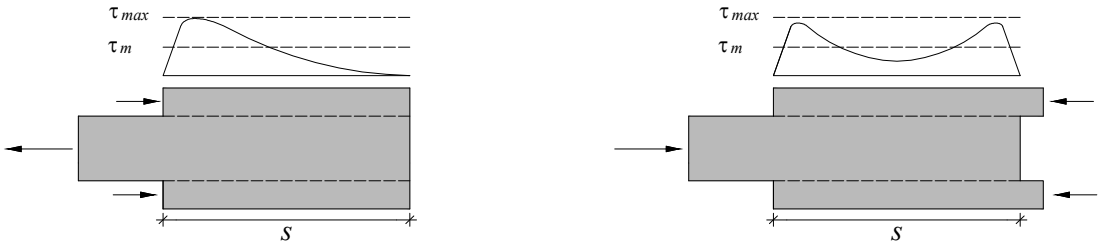

Figure 2.21: Influence of the load configuration on the elastic shear stress distribution according to Steurer [63]

Blass et al. [28] tested timber-concrete composite elements, each made of a 27-mm-thick Norway spruce LVL plate and a 70-mm-thick concrete layer, connected by 15-mm-deep round notches with a diameter of 115 mm. The concrete was reinforced with steel mat Q131 (steel bars with a diameter of 5 mm, spaced at a distance of 150 mm, in both directions). Seven different types of specimens with this notched connection were tested in shear to study the influence of the cross layers in the LVL plate, the reinforcement in the concrete notch, and a plastic film between the two materials. The first type of specimens had only longitudinal veneers and no plastic film. The borders of the timber plates of these specimen bent during concrete hardening and exhibited two different failure modes. The first tests showed a compressive failure in timber because the compressive strength of timber was negatively influenced by humidity, whereas the later tests showed a shear failure in concrete because the timber plate was less humid and the timber strength increased. In contrast, the specimens with 20% cross layers did not show significant timber deformations after concrete hardening. In the remaining tests, a plastic film was set between the timber and the concrete, and the influence of the reinforcement of the concrete notch was studied. Notches without brackets in the concrete failed in a brittle way due to the shear in the concrete. In contrast, notches with brackets in the concrete exhibited a ductile compressive failure in the timber, even though the timber plate was completely protected from

humidity. Blass et al. [28] also tested notches in glued laminated timber made of Norway spruce with steel dowels. These specimens showed a ductile behaviour. The timber part exhibited a local compressive failure and the dowel reached the plastic bending resistance. Furthermore, some specimens were tested with long-term loads and climate changes, and the time-dependent increase of the deformations was measured [28].

After that, Blass et al. [28] tested several specimens with notched connections in bending. The specimens, made of glued laminated timber beams with steel dowels in the notches, failed due to a splitting failure of the timber close to the dowels, or due to a horizontal shear failure of the timber near the notch closest to the support. The specimens made of spruce LVL plates with brackets in the notches failed due to exceeding the bending strength of the timber close to the notches. In these zones, the effective timber cross-section was reduced because of the notch. This experimental series also included long-term analyses with climate changes. Finally, Blass et al. [28] discussed the difficulty of predicting the long-term behaviours of timber-concrete composite structures because of the different creep behaviour of the two materials.

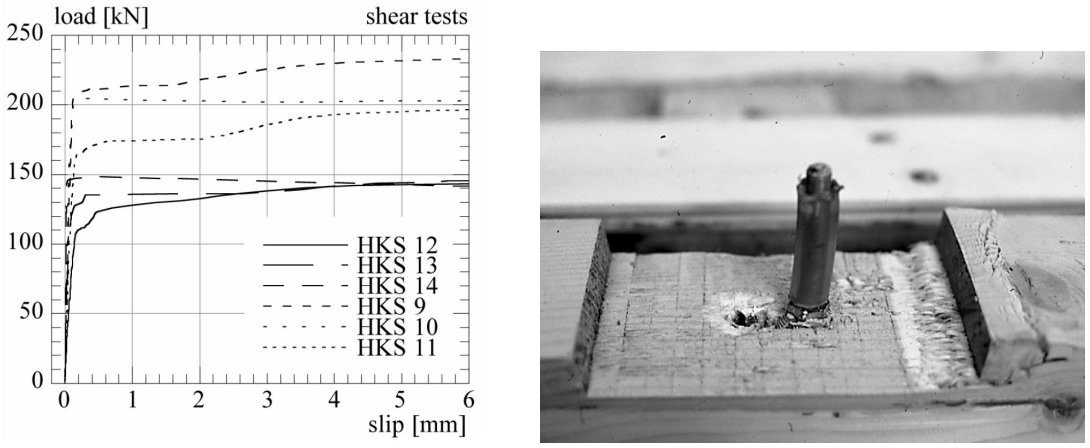

(a) (b)

Figure 2.22: Shear tests on timber-concrete composite specimens with notched connections performed by Frangi [25]: (a) horizontal load as a function of the horizontal relative displacement between the timber and the concrete ; (b) typical failure mode of a notched connection with a glued steel dowel

Frangi [25] performed a series of push-out tests with timber-concrete composite beams made of spruce timber. Each shear connection consisted of 20 mm deep and 150 mm long notches reinforced with glued steel dowels, and the length of the timber before the notch was 250 mm. The connections tested showed very high slip stiffnesses under service loads and large plastic deformations under failure loads, caused by local compressive failures of the timber near the notches and plastic deformations of the steel dowels (Fig. 2.22). The specimens without steel dowels showed smaller load-carrying capacities and shorter plastic deformations because the concrete plates tended to slide out of the notches [25].

Frangi [25] implemented the notched connections tests in timber-concrete composite beams, which were tested in four-point-bending. These tests showed ductile connection failures with plastic deformations of the notches and the dowels (Fig. 2.23(a)). This type of ductile connec-

tion failure caused a non-linearity in the load-deflection behaviour of the composite slab (Fig. 2.23(b)). The load could be increased until total collapse finally occurred, due to failure of the timber beams subjected to combined bending and tension. Frangi and Fontana [2] were able to predict this failure load using the model described in Section 2.3.4. Furthermore, an extensive theoretical and experimental research study was conducted about the fire behaviour of timber-concrete composite slabs [25].

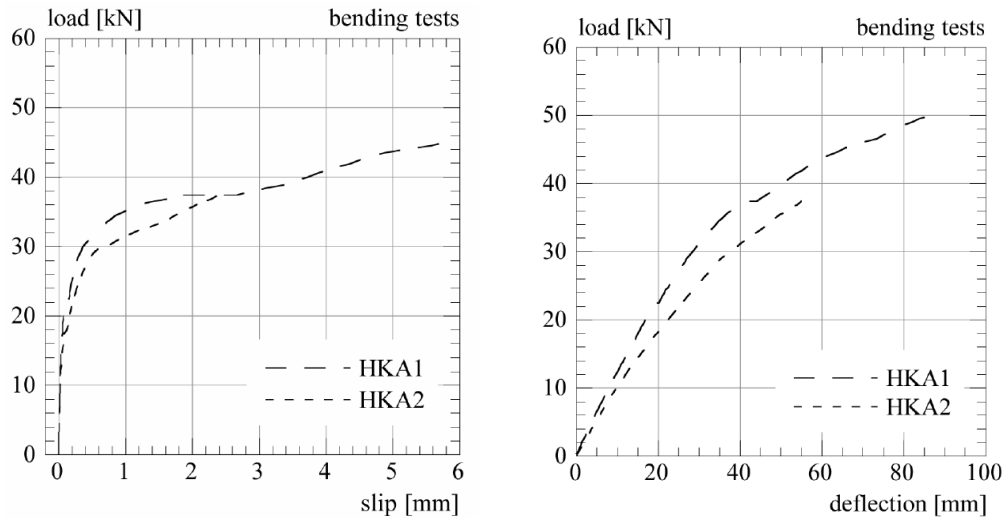

(a) (b)

Figure 2.23: Bending tests on timber-concrete composite beams with notched connections and glued steel dowels [25]: (a) relationship between the horizontal relative displacement and the vertical load; (b) relationship between the deflection at mid-span and the vertical load

Michelfelder [33] conducted an extensive experimental and numerical investigation using notches as the shear connections for timber-concrete composite slabs made of Norway spruce glued laminated timber. First, a series of shear tests was performed. These tests dealt with the influence of the notch inclination, the length of timber in front of the notch, the notch depth, the mechanical properties of the timber and the concrete, and the use of screws. In these experiments, four failure modes were observed: horizontal shearing-off failures in the timber, sliding of the concrete out of the notch, compressive failure of the concrete, and tensile failure of the concrete (Fig. 2.24). From the experimental results, the following conclusions were made [33]:

- A variation of the notch inclination from 90° to 45° had no positive influence on the structural behaviour of the notched connection.
- An increase of the timber length near the notch, as well as an increase of the notch depth, increased the shearing-off failure load of the timber.
- The screws used did not influence the failure load of the notch in a relevant way.

- Long-term shear tests, sustaining 30 % of the failure load (the failure load was determined from short-term shear tests), showed a creep effect. It was found that the use of screws tended to reduce the time-dependent deformations.

Since it was not possible to perform a statistical analysis of the test results, Michelfelder [33] derived design formulas to quantify the load-carrying capacity of notched connections from the outcomes of numerical simulations.

Michelfelder [33] tested the structural behaviour of timber-concrete composite elements with notched connections made of glued laminated timber in four-point-bending. The notches were 20 mm deep and contained screws. Two of the three specimens were tested with the loads located at distances from the supports of about one third of the span. The behaviour of these specimens was governed by a bending-tensile failure of the timber. The third specimen was loaded to reduce the bending moment, and a horizontal shear failure of the timber close to the notch was observed. During these tests, the load carried by the screws was measured by means of strain gauges. However, the results did not evaluate the influence of the screws. During the first two experiments, an uplift of the concrete of at most 1 mm was observed [33].

Michelfelder [33] conducted numerical simulations of the timber-concrete composite structures with notched connections and screws fixed into the notches. The outcomes of the simulations showed that about 80% of the shear force is carried by means of the compressive contact between the timber and the concrete, and the remaining 20% is carried by the screws. Michelfelder simulated composite slabs without screws too, and observed no gap opening occurring in the case with the screws or in the case without the screws. Therefore, she concluded that the screws are not necessary to prevent the gap opening. During the numerical simulations, she observed that tensile stresses in concrete occur close to the notch edges. Therefore, by means of the simulations, she optimised the geometry of the notches to minimise these tensile stresses and she derived construction rules [33].

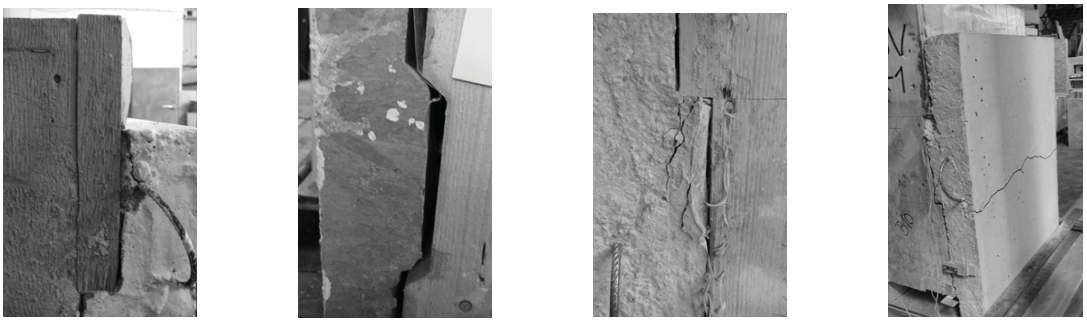

(a) (b) (c) (d)

Figure 2.24: Failure modes observed in short-term shear tests conducted by Michelfelder [33]: (a) shearing-off failure of timber; (b) sliding out of concrete; (c) compressive failure of concrete; (d) tensile failure of concrete

Schönborn [56] conducted a research study on timber-concrete composite slabs with notched connections, which gave important information about the influence of the connection on the structural behaviour of the composite member.

First, a series of short-term shear tests was performed. The timber part of the composite member consisted of glued laminated timber made of Norway spruce, and the interface between the two materials was covered with a PE-film. Several geometric parameters, including the length and the depth of the notch, the influence of the concrete quality and the effect of the screws were studied. Fig. 2.25 summarises the failure modes observed. The compressive failure of timber parallel to the grain occurred in several specimens and implied plastic deformations. During the shear tests, no relationship between the shear stiffness and the presence of screws was found. From the experimental results, Schönborn [56] created the design equations for notched connections provided in Sections 2.4 and 2.5.

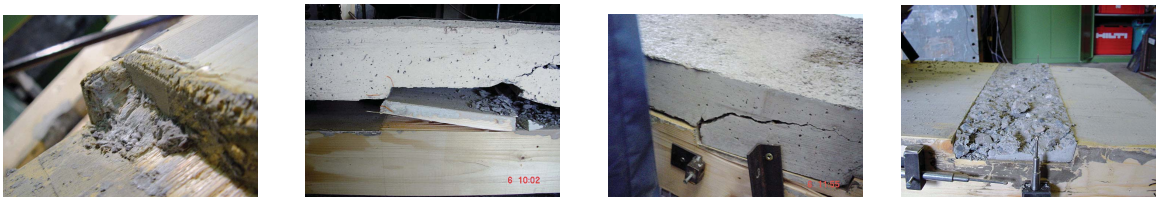

(a) (b) (c) (d)

Figure 2.25: Failure modes observed in short-term shear tests conducted by Schönborn [56]: (a) compressive failure of timber; (b) shear failure of timber; (c) consol failure of concrete; (d) shear failure of concrete

After the shear tests, Schönborn [56] conducted a series of four-point bending tests. He designed the notches in a way so that a ductile compressive failure in the timber parallel to the grain was governing and brittle connection failures were prevented. The length, the width and the depth of the specimens were kept constant. The notch length and the number of notches between the support and the load were varied (either four or five notches). Furthermore, some specimens were reinforced with screws. It was observed that the screws did not influence the bending stiffness but reduced the gap opening. In general, the results showed that the specimens could be divided into two groups [56]:

- In the specimens with five notches between the support and the load, a bending-tensile failure in timber occurred.
- In the specimens with four notches between support and load, plastic deformations in the interface were measured, which can be explained by a compressive failure of the timber. Then, a combined bending-tensile failure in the timber part occurred. Schönborn [56] assessed that this increase in relative displacement at the interface implied a decrease in bending stiffness of the specimen.

Kuhlmann and Aldi [82] performed a series of experimental investigations about notched connections without additional steel fasteners and presented a numerical model, based on finite

elements, to simulate the experimental results. All experimental investigations were performed using a symmetric push-out test, but there were several differences in the mechanical properties and the geometry. The test results exhibited different failure modes and a large scatter in the values of the load-carrying capacity and of the slip modulus. The variability of the mechanical properties was simulated with the Monte Carlo method, and the results of the FE simulation were in the range of the experimental data. In this paper, it was concluded that more experimental investigations are needed, with identical test conditions, to gain reliable values for the strength and stiffness of the notched connection [82].

2.8 Conclusion

The literature examined in this chapter represents a sound basis to develop a reliable design model for LVL-concrete composite members made of European beech wood with notched connections.

Published experimental studies revealed two important advantages of notched timber-concrete connections: high stiffness at service level, and the possibility of achieving a ductile compressive failure of timber. However, some aspects related to the shear-carrying mechanism, the estimation of the shear strength of the concrete part, the gap opening and the need for vertical reinforcement are still unclear. This thesis shall:

- develop models to understand the load-carrying mechanism in timber-concrete notched connections
- develop models to predict notch failure with the objective of reaching a ductile compressive failure in LVL in the notch
- quantify the influence of vertical reinforcement on the shear-carrying mechanism and the gap opening

According to published research (e.g. [2], [41], [42]), connection ductility (e.g. plastic timber deformations in the notch) has a positive influence on the structural behaviour of a composite member, thus enabling a ductile failure mode, provided that the structural element is suitably designed. The local plastic deformation of the timber in the notch may reach values larger than 10 mm [2], which may have a large influence on the global structural behaviour of the composite member. However, in contrast to the behaviour under elastic conditions, little research exists that addresses the estimate of the influence of connection ductility on the structural behaviour of the composite member. The current models for ductile design of reinforced concrete cross sections [66] and the models for timber-concrete composite members presented by Frangi and Fontana [2] shall be the basis to develop a model to quantify the impact of notch yielding on the structural behaviour of the composite member.

So far, research about beech LVL found elevated and consistent mechanical properties, which can represent an important advantage in design. The strength and stiffness of beech LVL [12] are higher than those of spruce LVL [83]. This is due to the properties of European beech

wood. The consistency of the mechanical properties, which is indicated by the coefficients of variation shown in Tab. 2.1, is enabled by the homogenisation obtained by the LVL configuration. A decrease in the variability of the mechanical properties helps to increase the safety margin between the compressive failure of timber in the notch and the undesired brittle failures. Thus, in this case, LVL materials have advantages over solid timber and glued laminated timber.

Chapter 3

Model

3.1 Introduction

The purpose of the analytical models presented in this chapter is to describe the structural behaviour of a timber-concrete composite slab made of a beech laminated veneer lumber (LVL) plate connected to a concrete layer by means of notches. Several theories presented in this chapter can be applied to notched connections in general or to other types of timber-concrete composite members. This chapter deals with:

- analytical strain-based models for the estimation of the structural behaviour of timber-concrete composite members with a ductile timber-concrete composite connection (Section 3.2)
- analytical models to describe the behaviour of notched timber-concrete connections (Section 3.3)
- parametric studies focused on timber-concrete composite slabs made of beech LVL (Section 3.4)

Fig. 3.1 and Tab. 3.1 provide an overview of the possible failure modes of a timber-concrete composite slab made of a beech LVL plate with a notched connection. Since the notches ensure the composite action, the LVL part is subjected to tension and bending, and the concrete part to compression and bending. Subsequently, the notches carry forces parallel to the interface. These connection forces are transferred from the concrete to the LVL by means of compressive contact in the notches. The only two ductile failure modes which can occur in such a composite slab are a compressive failure of the LVL in the contact area of the notch (2C) or a compressive failure in the upper part of the concrete layer (1C,c).

In the model calculations, the mechanical properties used to predict the structural behaviour of the composite member are mean values derived from codes and approvals. Any variation of the mechanical properties and the long term effects are neglected. However, both of these effects should be assessed in future studies in order to create a design model.

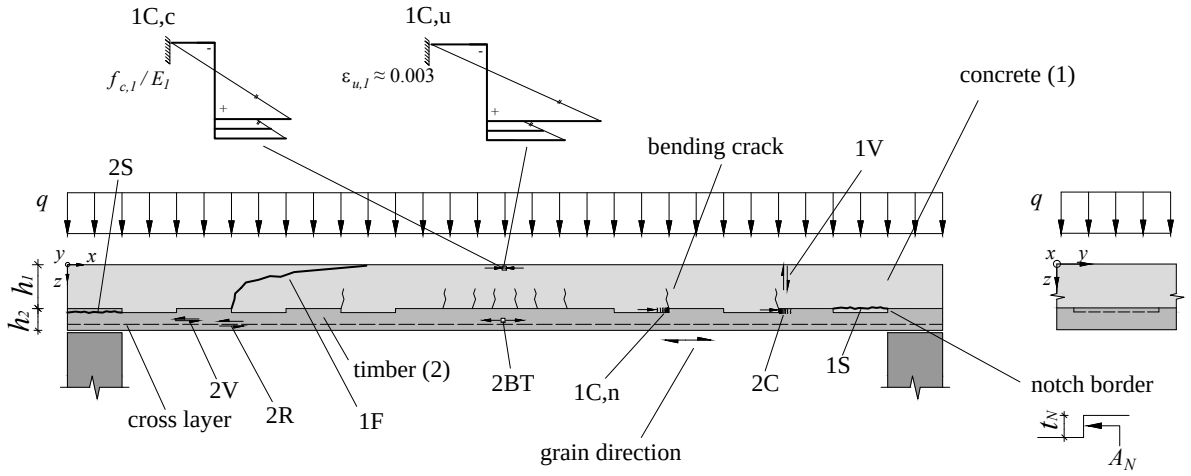

Figure 3.1: Overview of the failure modes of a timber-concrete composite slab made of a beech LVL plate with a notched connection devoid of vertical reinforcement

3.2 Timber-concrete composite members with ductile connections

3.2.1 Introduction

As shown in Fig. 3.2, the structural behaviour of a timber-concrete composite member is strongly influenced by the connection design. In general, a timber-concrete composite member can behave in three different ways depending on the design strategy:

- If the connection is over-designed, the composite member should fail in the cross-section, due, for instance, to a combined tensile-bending failure of the timber. As a consequence, the structural behaviour of the slab is elastic-brittle.

- If a brittle connection failure is governing, the composite member consequently fails in a brittle way.

- If a ductile connection failure is governing, the stiffness of the composite member decreases after yielding of the connection. Thus, the failure of the composite structure occurs after large deformations and the structural behaviour shows ductility. Sections 3.2.4 and 3.2.5 deal with the modelling of this mechanism. The ductile connection failure can be, for instance, a ductile compressive failure in the timber inside a notch or a ductile failure of a steel fastener.

Table 3.1: Failure modes of a timber-concrete composite slab made of a beech LVL plate with a notched connection devoid of vertical reinforcement

Material	Failure		Location	Failure type	Failure load
Concrete (1)	1C,n	compressive failure	contact area A_N of the notch Ni	depends on the configuration	$q_{R,1C,n,Ni}$
	1C,c	exceedance of the compressive strength $f_{c,1}$	top of the concrete cross section ($z = 0$)	ductile	$q_{R,1C,c}$
	1C,u	exceedance of the ultimate compressive strain $\varepsilon_{u,1}$ after 1C,c	top of the concrete cross section ($z = 0$)	ductile	$q_{R,1C,u}$
	1S	horizontal shear failure	close to the notch Ni ($z = h_1$)	brittle	$q_{R,1S,Ni}$
	1F	flexural-shear failure	close to the notch Ni ($z = x$)	brittle	$q_{R,1F,Ni}$
	1V	vertical shear failure	close to the notch Ni, in the compression zone	brittle	$q_{R,1V,Ni}$
Timber (2)	2BT	combined tensile-bending failure	timber cross section	brittle	$q_{R,2BT}$
	2V	shear failure	timber cross section	brittle	$q_{R,2V}$
	2R	rolling shear failure	cross layer	brittle	$q_{R,2R}$
	2C	compressive failure parallel to the grain	contact area A_N of the notch Ni	ductile	$q_{R,2C,Ni}$
	2S	shearing-off failure	close to the notch Ni ($z = h_1 + t_N$)	brittle	$q_{R,2S,Ni}$

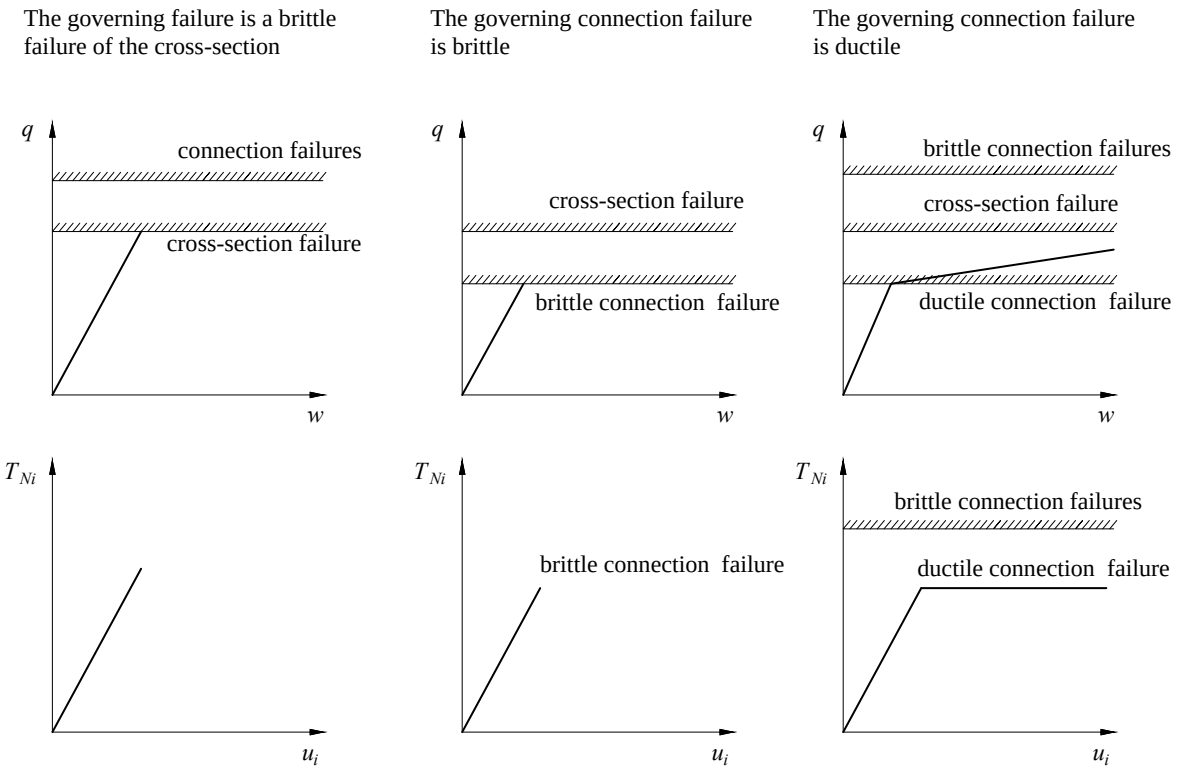

Figure 3.2: Strategies to design timber-concrete composite members (u_i is the horizontal relative displacement at the interface close to the notch Ni, and T_{Ni} is the force carried by the notch Ni)

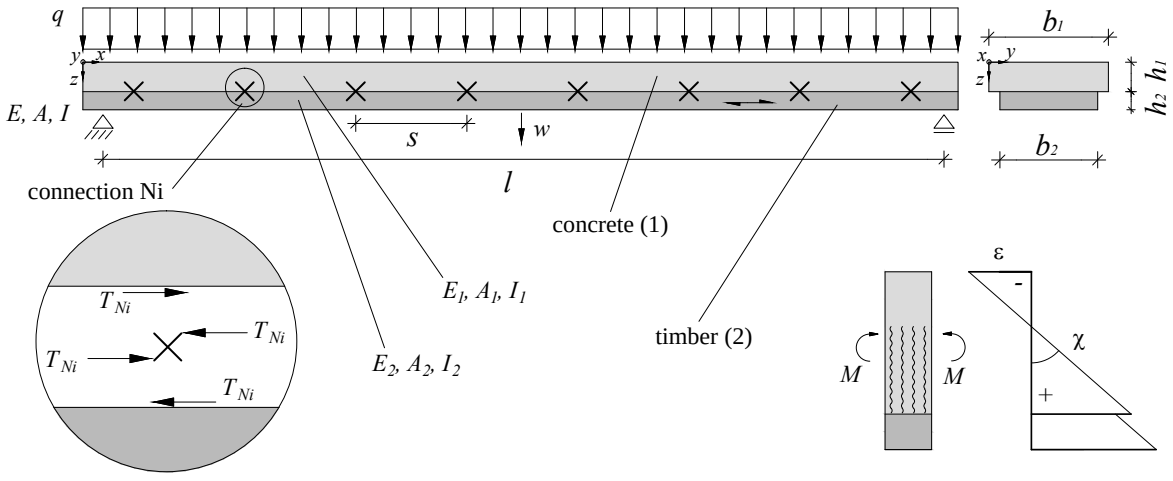

Figure 3.3: Timber-concrete composite slab

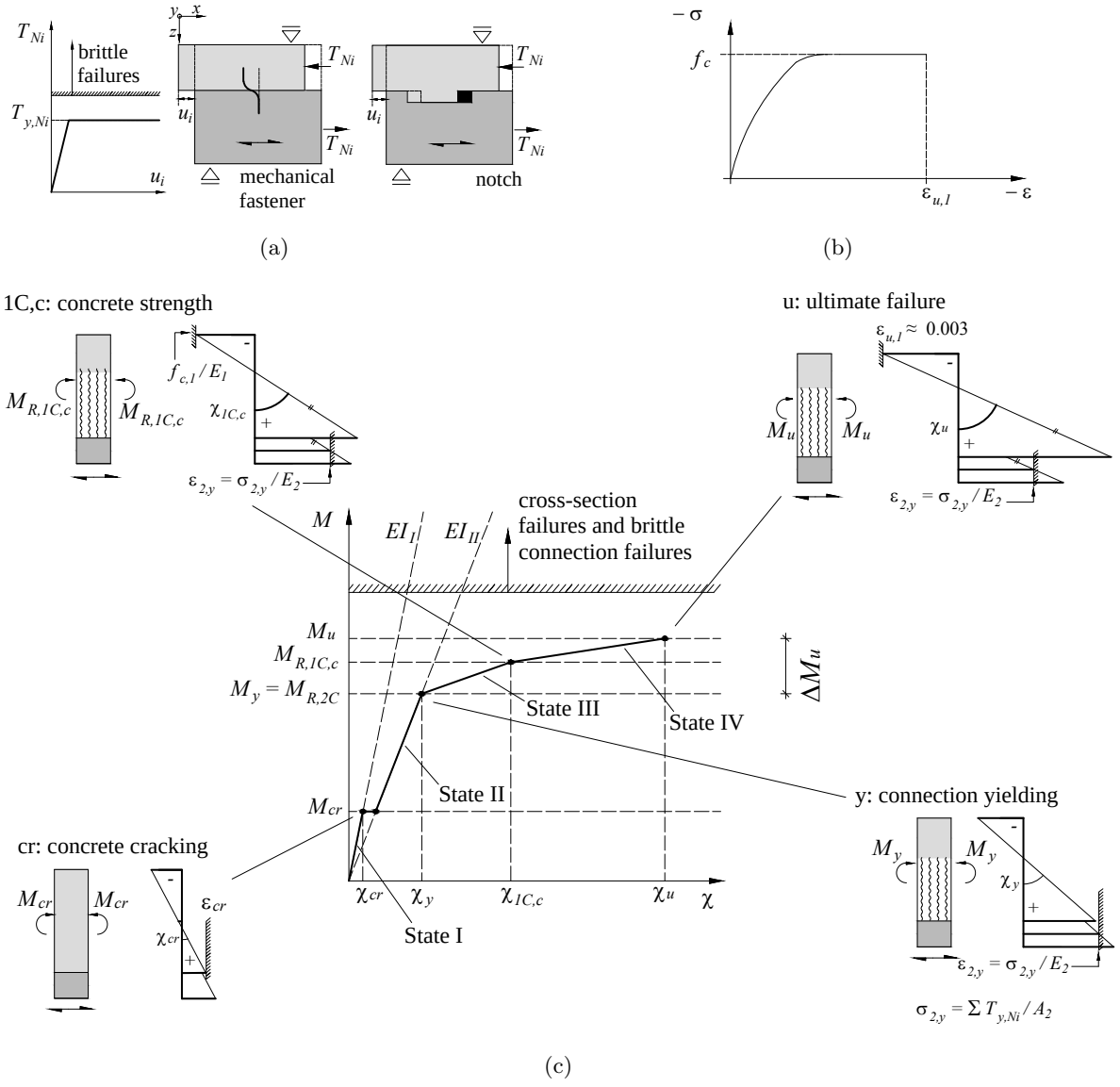

Figure 3.4: Model of the structural behaviour of timber-concrete composite members with ductile connections: (a) assumed structural behaviour of the timber-concrete connections; (b) assumed behaviour of concrete subjected to compression; (c) Moment-curvature behaviour of the composite member

The following model was developed to predict the structural behaviour of timber-concrete composite members with ductile connections subjected to uniformly distributed vertical loads (Fig. 3.3). As summarised in Fig. 3.4 and Tab. 3.2 , the analytical model presented in this section simplifies the structural behaviour of timber-concrete composite members with ductile connections using four states, similar to the models for reinforced concrete structures [84], [67]. The model presented was developed based on stress-strain relationships and on simple equilibrium models. First, the entire structure is assumed to be elastic and the concrete does not contain cracks (state I). Then, when the critical tensile stress in the concrete is reached, cracks occur, and the composite member enters state II. Since, the composite structure is assumed to be elastic during the first two states, the calculation method for composite members described in

Section 2.3.2 is used (γ-method) [26], [28]. Yielding of the connections indicates the beginning of the ductile behaviour, described by states III and IV. Ductility is due to the connection yielding and the ductile compression behaviour of concrete. The behaviour during states III and IV is idealised by means of an analogy to the reinforced concrete theories developed by Marti [4], [84] and implemented in the Swiss Code SIA 262 [66], combined with the model proposed by Frangi and Fontana [2].

Table 3.2: Structural behaviour of a timber-concrete composite member with a ductile connection

State	Connection	Concrete	Calculation method	Limit
I	elastic	uncracked/ elastic	γ-method [26],[28]	concrete cracking (cr.)
II	elastic	cracked/ elastic	γ-method [26],[28]	connection yielding (y.)
III	plastic	cracked/ elastic	analogy to reinforced concrete according to Marti et al. [84] and SIA 262 [66]	compressive strength of the concrete at the top of the cross-section (1C,c)
IV	plastic	cracked/ plastic	analogy to reinforced concrete according to Marti et al. [84] and SIA 262 [66] + model of Frangi and Fontana [2]	ultimate failure (u.): combined bending-tensile failure in the timber or achievement of the maximum compressive strain of the concrete on the top of the cross section

The analytical model described in this section is based on the following assumptions:

- The timber part of the composite member is not subjected to initial stresses due to placement of the concrete.
- The structure is subjected to a uniformly distributed vertical load.
- The assumptions for application of the γ-method in elastic conditions, illustrated in Section 2.3.2, are valid.
- The timber-concrete connections carry horizontal forces exclusively.
- The governing failure is a ductile connection failure because the composite member is designed so that all other failures do not occur.
- The connection behaviour is elastic-ideal plastic and can be simplified as shown in Fig. 3.4(a).
- The connections are designed proportional to the shear forces generated by a uniformly distributed vertical load. Thus, they yield simultaneously.

- The ultimate deformation capacities of the connections are sufficiently elevated and do not govern the structural behaviour.
- Yielding of the connections does not introduce secondary effects which compromise the structural behaviour of the composite member.
- Concrete subjected to compression exhibits ductile behaviour (Fig. 3.4(b)).
- No gap opening occurs. Thus, the timber and concrete bend with the same deflection and the same curvature.
- The distribution of the axial strains is linear in each part of the cross-section, and any plane sections remain plane.
- The shear deformations in the cross-section are neglected.

3.2.2 State I: connection elastic, concrete uncracked and elastic

In this state, the concrete part of the composite member is not yet cracked and so is able to carry tensile stresses. Fig. 3.5 illustrates the geometry and the axial stresses and strains of the composite member during state I. If the connections are not completely rigid, the diagram of the strains shows a gap at the interface due to the shear deformations of the connections. Since the model assumes that the concrete and timber do not separate vertically, the two parts of the cross-section exhibit the same curvature. To calculate the cross-sectional values, the stresses and the deformations, the γ-method is used according to Section 2.3.2. The limit of this phase is determined by cracking of the concrete.

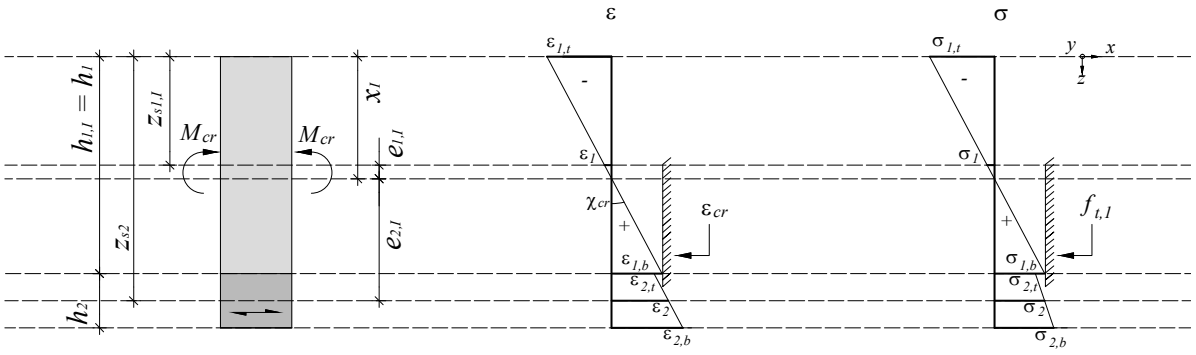

Figure 3.5: End of state I (concrete cracking): geometry, axial strains ε and axial stresses σ

Since the reference modulus of elasticity is that of timber, the different moduli of elasticity of timber E_2 and concrete E_1 are taken into account with the following factors:

$$n_1 = \frac{E_1}{E_2} \tag{3.1}$$

$$n_2 = \frac{E_2}{E_2} = 1 \tag{3.2}$$

Because of the dimensions of the slab elements assumed in this research project, the model is presented for the case where the zero-strain layer is located in the concrete. Thus, the γ-factors of the concrete and timber can be calculated with the following formulas:

$$\gamma_1 = 1 \tag{3.3}$$

$$\gamma_2 = \frac{1}{1 + \frac{\pi^2 E_2 A_2 s}{l^2 K}} \tag{3.4}$$

Since, during state I, the concrete section is not cracked, the entire concrete depth h_1 is taken into account. The areas and the moments of inertia correspond to:

$$A_{1,I} = b_1 h_{1,I} = b_1 h_1 \tag{3.5}$$

$$A_2 = b_2 h_2 \tag{3.6}$$

$$I_{1,I} = \frac{b_1 h_{1,I}^3}{12} \tag{3.7}$$

$$I_2 = \frac{b_2 h_2^3}{12} \tag{3.8}$$

The distances between the top of the composite cross-section ($z = 0$) and the centroids of the two parts of the composite member can be determined as follows:

$$z_{s,1,I} = \frac{h_{1,I}}{2} \tag{3.9}$$

$$z_{s,2} = h_1 + \frac{h_2}{2} \tag{3.10}$$

The centroid of the composite cross section (zero-strain layer) can be calculated as follows:

$$x_I = \frac{\sum_{i=1}^{2} \gamma_i n_i A_{i,I} z_{s,i,I}}{\sum_{i=1}^{2} \gamma_i n_i A_{i,I}} \tag{3.11}$$

The distances between the centroid of the composite cross-section x_I and the centroids of the timber and the concrete part $z_{s,1,I}$ and $z_{s,2,I}$ correspond to:

$$e_{1,I} = z_{s,1,I} - x_I \tag{3.12}$$

$$e_{2,I} = z_{s,2} - x_I \tag{3.13}$$

The moment of inertia of the composite cross section can be calculated as follows:

$$I_I = \sum_{i=1}^{2} n_i I_i + \sum_{i=1}^{2} \gamma_i n_i A_i e_{i,I}^2 \tag{3.14}$$

The effective static moment for the calculation of the theoretic elastic shear stress acting in the interface between the timber and concrete is:

$$S_{12,I} = n_1 \gamma_1 A_{1,I} e_{1,I} = n_2 \gamma_2 A_2 e_{2,I} \tag{3.15}$$

The effective bending stiffness of the composite cross section is:

$$EI_I = E_2 I_I \tag{3.16}$$

The section modulus of the concrete border close to the interface ($z = h_1$) can be determined as follows:

$$W_{1,b,I} = \frac{I_I}{\gamma_1 e_{1,I} + \frac{h_1}{2}} \tag{3.17}$$

Since the maximum tensile stress in the concrete occurs at the border close to the interface ($z = h_1$), the bending moment which generates cracking of the concrete and the associated curvature of the cross section can be calculated as follows:

$$M_{cr} = \frac{f_{t,1} W_{1,b,I}}{n_1} \tag{3.18}$$

$$\chi_{cr} = \frac{M_{cr}}{EI_I} \tag{3.19}$$

The axial strains which occur when the concrete part of the composite member cracks can be calculated according to Eq. 2.17 as follows:

$$\varepsilon_{1,t} = \chi_{cr}\left(\gamma_1 e_{1,I} - \frac{h_{1,I}}{2}\right) \tag{3.20}$$

$$\varepsilon_{1,b} = \chi_{cr}\left(\gamma_1 e_{1,I} + \frac{h_{1,I}}{2}\right) \tag{3.21}$$

$$\varepsilon_{2,t} = \chi_{cr}\left(\gamma_2 e_{2,I} - \frac{h_2}{2}\right) \tag{3.22}$$

$$\varepsilon_2 = \chi_{cr} \gamma_2 e_{2,I} \tag{3.23}$$

$$\varepsilon_{2,b} = \chi_{cr}\left(\gamma_2 e_{2,I} + \frac{h_2}{2}\right) \tag{3.24}$$

The axial stresses are obtained with Hooke's law as follows:

$$\sigma_1 = \varepsilon_1 E_1 \tag{3.25}$$

$$\sigma_2 = \varepsilon_2 E_2 \tag{3.26}$$

In the case of a single-span beam with a uniformly distributed vertical load, the cracking load q_{cr} can be calculated from M_{cr}, and the deflection at mid-span at cracking level w_{cr} can be estimated as follows:

$$w_{cr}(l/2) \approx \frac{5}{384} \cdot \chi_{cr} \cdot l^2 \cdot 8 \tag{3.27}$$

3.2.3 State II: connection elastic, concrete cracked and elastic

During the second state, the concrete is cracked and the behaviour of the composite member is elastic. Fig. 3.6 illustrates the geometry, the axial stresses and strains of the composite cross section during state II. The limit of this state corresponds to yielding of the connections.

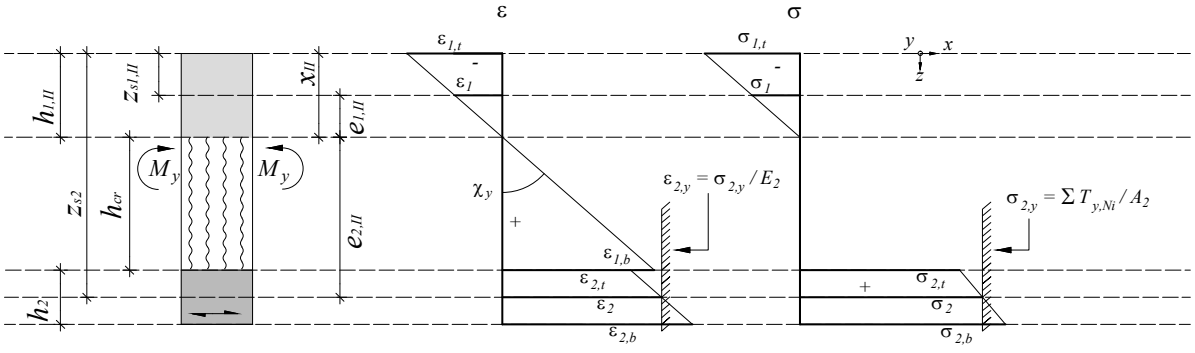

Figure 3.6: End of state II (connection yielding): geometry, axial strains ε and axial stresses σ

During this phase, the concrete part of the composite member is cracked and it is assumed that it does not carry tensile stresses. Therefore, the effective concrete surface has to be reduced depending on the crack depth h_{cr} as follows:

$$h_{1,II} = h_1 - h_{cr} \tag{3.28}$$

$$A_{1,II} = b_1 h_{1,II} \tag{3.29}$$

$$z_{s,1,II} = \frac{h_{1,II}}{2} \tag{3.30}$$

$$I_{1,II} = \frac{b_1 h_{1,II}^3}{12} \tag{3.31}$$

Since the concrete part does not carry tensile stresses, it is assumed that the depth of the effective concrete cross-section $h_{1,II}$ corresponds to the zero-strain layer x_{II} (centroid of the composite member). The effective concrete depth $h_{1,II}$ can be calculated using the following condition:

$$x_{II} = h_{1,II} \tag{3.32}$$

where x_{II} is the centroid of composite member during state II:

$$x_{II} = \frac{\sum_{i=1}^{2} \gamma_i n_i A_{i,II} z_{s,i,II}}{\sum_{i=1}^{2} \gamma_i n_i A_{i,II}} \tag{3.33}$$

Using the effective concrete dimensions of state II, the cross-sectional values $e_{1,II}$, $e_{2,II}$, I_{II} and EI_{II} can be calculated with the same procedure used for state I (Section 3.2.2).

State II ends due to yielding of the connections, and this point determines the end of the elastic behaviour. As illustrated in Fig. 3.7, the sum of the shear forces T_{Ni} transferred by the connections between the support and the point of maximal bending moment is equal to the resulting axial force N in the point of maximal bending moment. When the connections yield, this condition can be written as follows:

$$\sigma_{2,y} = \frac{\sum T_{y,Ni}}{A_2} \tag{3.34}$$

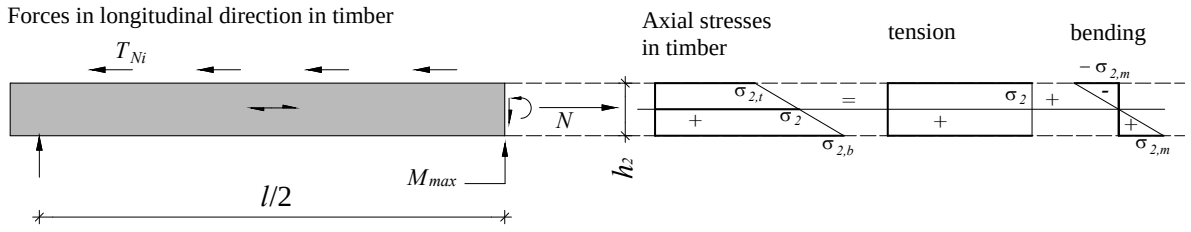

Figure 3.7: State II, equilibrium in the timber part of the composite member

The bending moment and the cross-section curvature corresponding to yielding of the connections can be calculated as follows:

$$M_y = M_{R,2C} = \sigma_{2,y} \cdot \frac{W_{2,II}}{n_2} = \frac{\sum T_{y,Ni}}{A_2} \cdot \frac{W_{2,II}}{n_2} \tag{3.35}$$

$$\chi_y = \frac{M_y}{EI_{II}} \tag{3.36}$$

Where $W_{2,II}$ is the section modulus corresponding to the centroid of the timber cross section:

$$W_{2,II} = \frac{I_{II}}{\gamma_2 e_{2,II}} \tag{3.37}$$

The strains which occur when the connections yield can be calculated according to Eq. 2.17 as follows:

$$\varepsilon_{1,t} = \chi_y\big(\gamma_1 e_{1,II} - \frac{h_{1,II}}{2}\big) \tag{3.38}$$

$$\varepsilon_{1,b} = \chi_y\big(\gamma_1 e_{1,II} + \frac{h_{1,II}}{2}\big) \tag{3.39}$$

$$\varepsilon_{2,t} = \chi_y\big(\gamma_2 e_{2,II} - \frac{h_2}{2}\big) \tag{3.40}$$

$$\varepsilon_2 = \chi_y \gamma_2 e_{2,II} \tag{3.41}$$

$$\varepsilon_{2,b} = \chi_y\big(\gamma_2 e_{2,II} + \frac{h_2}{2}\big) \tag{3.42}$$

The stresses are obtained with Hooke's law as follows:

$$\sigma_{1,t} = \varepsilon_{1,t} E_1 \tag{3.43}$$

$$\sigma_{1,b} = 0 \tag{3.44}$$

$$\sigma_{2,t} = \varepsilon_{2,t} E_2 \tag{3.45}$$

$$\sigma_2 = \varepsilon_2 E_2 = \sigma_{2,y} \tag{3.46}$$

$$\sigma_{2,b} = \varepsilon_{2,b} E_2 \tag{3.47}$$

In the case of a single-span beam with a uniformly distributed vertical load, the yielding load q_y can be calculated from M_y. Under the assumption that the composite cross section is cracked over the entire span, the deflection at mid-span at yielding level w_y can be estimated as follows:

$$w_y(l/2) \approx \frac{5}{384} \cdot \chi_y \cdot l^2 \cdot 8 \tag{3.48}$$

Failures in state II

Since the purpose of the design is to achieve a ductile connection failure, the connections should be able to yield, and all other failures of the composite member which can occur during state II should be prevented. In other words, the bending moment corresponding to connection yielding M_y must be smaller than the bending moments which cause the other possible failures, such as:

- combined tensile-bending failure of the timber part (2BT)
- shear/ rolling shear failure of the timber part (2V/ 2R)
- compressive failure of the concrete on the cross section top (1C,c)
- shear failures in the concrete
- brittle connection failures (which depend on the connection system)

A combined tensile-bending failure of the composite cross section (2BT) does not depend from the connection type and can be predicted using the interaction formula contained in the Swiss Standard SIA 265 [29] according to Section 2.4.5:

$$\frac{\sigma_2}{f_{t,0,2}} + \frac{\sigma_{2,m}}{f_{m,2}} \leq 1 \tag{3.49}$$

The tensile stress in the centroid of the timber is calculated using Eq. 3.37 as follows:

$$\sigma_2 = \frac{M}{W_{2,II}} \cdot n_2 \tag{3.50}$$

According to Fig. 3.7, the bending stress in the timber is:

$$\sigma_{2,m} = \sigma_{2,b} - \sigma_2 = \frac{M}{W_{2,b,II}} \cdot n_2 - \frac{M}{W_{2,II}} \cdot n_2 \tag{3.51}$$

where $W_{2,b,II}$ is the section modulus corresponding to the bottom edge of the timber cross-section:

$$W_{2,b,II} = \frac{I_{II}}{\gamma_2 e_{2,II} + \frac{h_2}{2}} \tag{3.52}$$

The bending moment which causes the combined tensile-bending failure of the timber part can be derived from Equations 3.50 to 3.49:

$$M_{R,2BT} = \frac{1}{\frac{1}{W_{2,II}} \cdot \frac{n_2}{f_{t,0,2}} + \left(\frac{1}{W_{2,b,II}} - \frac{1}{W_{2,II}}\right) \cdot \frac{n_2}{f_{m,0,2}}} \tag{3.53}$$

Reaching the compressive strength of the concrete $f_{c,1}$ at the top of the cross section does not imply a brittle failure. This condition should preferably occur after the connections begin to yield. The section modulus corresponding to the top edge of the concrete part of the composite member can be written as follows:

$$W_{1,t,II} = \frac{I_{II}}{\gamma_1 \cdot e_{1,II} - h_{1,II}} \tag{3.54}$$

The bending moment which causes the stress level of $f_{c,1}$ at the top of the cross section during state II is:

$$M_{R,1C,c} = \frac{f_{1,c} \cdot W_{1,t,II}}{n_1} \tag{3.55}$$

A shear failure in the timber cross-section is also independent from the connection type and can be predicted by calculating the elastic shear stress in the critical point. The failure occurs, when the elastic shear stress reaches the shear strength:

$$\tau = f_{v,2} \tag{3.56}$$

For instance, the elastic shear stress in the centroid of the timber part of the composite member can be determined as follows:

$$\tau = \frac{VS_{2,II}}{b_2 I_{II}} = \frac{V \cdot \gamma_2 \cdot n_2 \cdot \frac{h_2}{2} \cdot b_2 \cdot \left(e_{2,II} + \frac{h_2}{4}\right)}{b_2 I_{II}} \tag{3.57}$$

In the case of an LVL plate, the cross layers usually represent the weak point in shear transfer. Therefore, the shear stress should be calculated in the position of the cross layers and compared to the rolling shear strength of the material $f_{R,v,2}$.

Several other failure modes, like for instance shear failures in the concrete, depend on the connection system, and will be treated in Section 3.3.

3.2.4 State III: connection plastic, concrete cracked and elastic

The transition from state II to state III is due to the fact that the connections begin to develop plastic deformations parallel to the interface. Since the connections yield and are modelled without hardening (Fig. 3.4), the load which is transferred between the timber and the concrete during states III and IV is constant and corresponds to the sum of the yielding forces $T_{y,Ni}$ of the connections between the support and the point of maximum bending moment according to Frangi and Fontana [2]. Thus, according to Fig. 3.7, the tensile stress in the centroid of the timber cross-section during states III and IV is constant and can be calculated as follows:

$$\sigma_2 = \sigma_{2,y} = \frac{\sum T_{y,Ni}}{A_2} \tag{3.58}$$

Connection yielding can be modelled as an increase of the horizontal relative displacement at the interface. This implies an increase of the curvatures of the two parts of the composite member by constant tensile strain in the centroid of the timber. State III is characterised by ideal plastic connection behaviour and elastic behaviour of the timber and concrete. Since the timber and concrete are elastic, the stress distributions are linear. The composite member should be designed so that the state III ends due to exceedance of the compressive strength of concrete at the top of the composite cross-section (Fig. 3.8). This allows to develop ductility because the concrete is able to increase its compressive strain under stresses equal to the compressive strength $f_{c,1}$.

The depth of the compression zone at the end of state III can be calculated from the equilibrium condition in longitudinal direction:

$$x_{III} = \frac{2 \cdot \sigma_{2,y} \cdot A_2}{f_{c,1} \cdot b} = \frac{2 \cdot \sum T_{y,Ni}}{f_{c,1} \cdot b} \tag{3.59}$$

The curvature of the cross-section which occurs when the compressive strength of the concrete is reached can be calculated as follows:

$$\chi_{1C,c} = \frac{\varepsilon_{1,t}}{x_{III}} = \frac{f_{c,1}}{E_1 \cdot x_{III}} \tag{3.60}$$

Until the end of state III, no brittle failure of the timber should occur. Therefore, it must be checked that the curvature which causes a combined tensile-bending failure of the timber cross-section is not exceeded. Otherwise, the system will collapse abruptly after small plastic

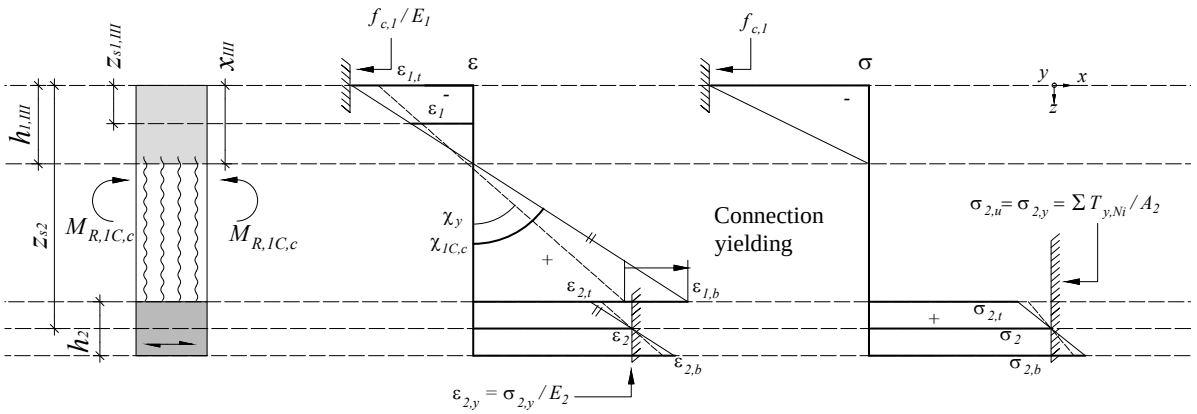

Figure 3.8: End of state III ($f_{c,1}$ at the cross section top is reached): geometry, axial strains ε and axial stresses σ

deformations. The allowed curvature can be calculated according to Frangi and Fontana [2] from Eq. 3.49 as follows:

$$\frac{\sigma_2}{f_{t,0,2}} + \frac{\sigma_{2,m}}{f_{m,2}} \leq 1 \tag{3.61}$$

$$\frac{\sigma_{2,y}}{f_{t,0,2}} + \frac{\chi_{1C,c} \cdot (h_2/2) \cdot E_2}{f_{m,2}} \leq 1 \tag{3.62}$$

$$\chi_{1C,c} \leq \frac{2 \cdot f_{m,2}}{h_2 \cdot E_2} \cdot \left(1 - \frac{\sigma_{2,y}}{f_{t,0,2}}\right) \tag{3.63}$$

The bending moment $M_{R,1C,c}$ corresponding to $\chi_{1C,c}$ can be calculated as follows:

$$M_{R,1C,c} = \sum T_{Ni} \cdot \left(h_1 - \frac{x_{III}}{3} + \frac{h_2}{2}\right) + \frac{b_2 h_2^2}{6} \cdot \chi_{1C,c} \cdot \frac{h_2}{2} \cdot E_2 \tag{3.64}$$

From the curvature $\chi_{1C,c}$, the zero strain layer x_{III} and the compressive strength of the concrete $f_{c,1}$, the axial strains of the composite member at the end of state III can be calculated as follows:

$$\varepsilon_{1,t} = -\chi_{1C,c} \cdot x_{III} \tag{3.65}$$

$$\varepsilon_{1,b} = \chi_{1C,c}\big(h_1 - x_{III}\big) \tag{3.66}$$

$$\varepsilon_{2,t} = \varepsilon_{2,y} - \chi_{1C,c} \cdot \frac{h_2}{2} = \chi_y \gamma_2 e_{2,II} - \chi_{1C,c} \cdot \frac{h_2}{2} \tag{3.67}$$

$$\varepsilon_2 = \varepsilon_{2,y} = \chi_y \gamma_2 e_{2,II} \tag{3.68}$$

$$\varepsilon_{2,b} = \varepsilon_{2,y} + \chi_{1C,c} \cdot \frac{h_2}{2} = \chi_y \gamma_2 e_{2,II} + \chi_{1C,c} \cdot \frac{h_2}{2} \tag{3.69}$$

The concrete part of the composite member is still elastic. Therefore, the stresses are obtained with Hooke's law as follows:

$$\sigma_{1,t} = -f_{1,c} \tag{3.70}$$

$$\sigma_{1,b} = 0 \tag{3.71}$$

$$\sigma_{2,t} = \varepsilon_{2,t} E_2 \tag{3.72}$$

$$\sigma_2 = \varepsilon_2 E_2 = \sigma_{2,y} \tag{3.73}$$

$$\sigma_{2,b} = \varepsilon_{2,b} E_2 \tag{3.74}$$

3.2.5 State IV: connection plastic, concrete cracked and plastic

During state IV, the connections yield (Eq. 3.58 is valid), and the compression zone of the concrete develops plastic deformations and redistributes the stresses. Thus, the curvature of the cross-section continues to increase until the ultimate failure. The ultimate failure can be due to exceedance of the ultimate compressive strain of the concrete $\varepsilon_{u,1}$ or to a combined tensile-bending failure of the timber part. The mechanism can be clarified with an analogy to the ductile failure of reinforced concrete cross sections subjected to bending according to Marti [4], Marti et al. [84], Bachmann [85], Kenel [65], Kaufmann [67] and SIA 262 [66] (Fig. 3.9).

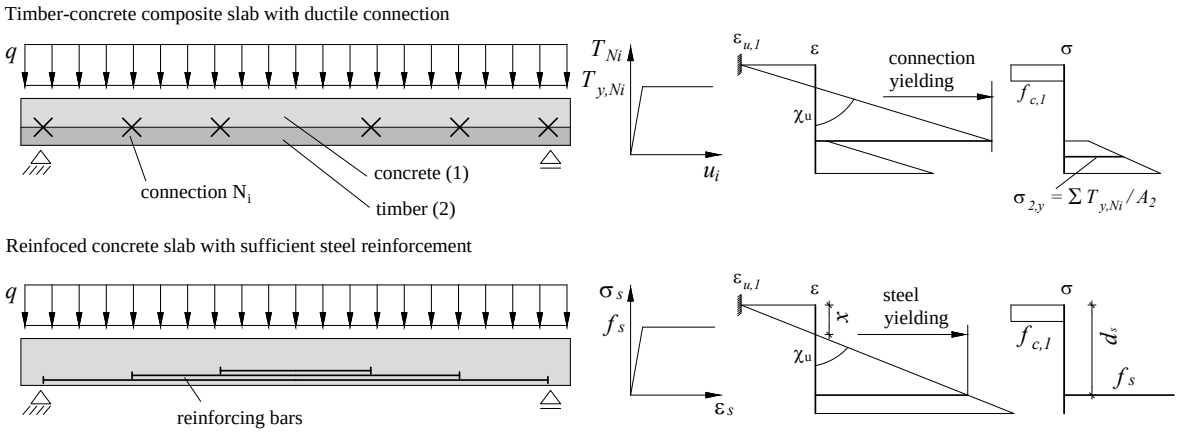

Figure 3.9: State IV, analogy with reinforced concrete cross-section

In a reinforced concrete member subjected to bending, if a sufficient amount of steel is provided, the failure is usually governed by yielding of the steel reinforcing bars [84], [85]. If the concrete member is cracked and the steel reinforcement is yielding, the structural behaviour can be modelled under the assumption of ductile behaviour of the reinforcement and the compressed

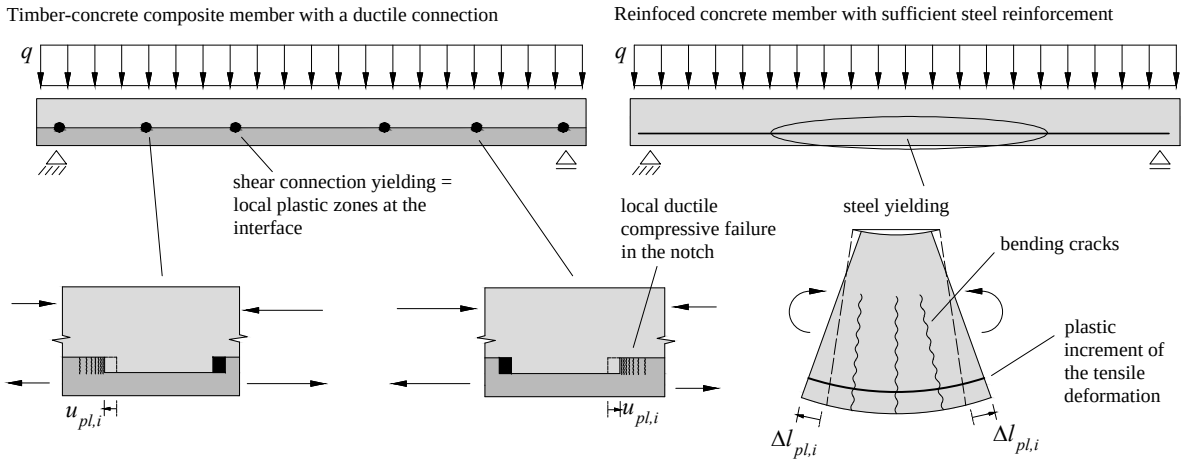

Figure 3.10: Difference between yielding of a steel reinforcing bar in a reinforced concrete member and plastic deformations of a shear connection of a timber-concrete composite member (e.g. notches)

concrete. This causes an increase of the curvature of the cross section. As stated in Section 2.5.1, due to the ductile failure of compressed concrete, the compressive stresses tend to redistribute across the compression depth x [65]. In the calculations, the compressive stresses in the concrete at the ultimate limit state are often assumed to be uniformly distributed over a depth of $0.85x$ [66]. The ultimate failure of the reinforced concrete member should be determined by exceedance of the ultimate compressive strain $\varepsilon_{u,1}$ of the concrete at the top of the cross section while steel is yielding [65], [67], [84]. The associated strain is usually assumed to be $\varepsilon_{u,1} \approx 0.003$ [66]. This failure is ductile and is marked by crack formation [67].

The plastic deformations of timber-concrete connections by constant tensile stress in the timber $\sigma_{2,y}$ activate mechanisms, which are similar to yielding of steel reinforcing bars due to constant tensile stress f_s (Fig. 3.9). Nevertheless, yielding of a steel reinforcing bar in the concrete and yielding of a timber-concrete shear connection are physically different (Fig. 3.10). Firstly, the plastic deformation of a steel reinforcing bar is due to an increment of its length [84], whereas yielding of timber-concrete shear connections is localised in plastic zones corresponding to the connections. In other words, in a timber-concrete composite member, the tensile part remains elastic, and the interface yields. In contrast, in a reinforced concrete member, the tensile reinforcement loses elasticity and yields. Depending on the connection type, the fact that the plastic zones are local may cause problems with crack propagation in the concrete. Secondly, in a timber-concrete composite member, the combination of tension and bending in the timber usually represents an important issue when the cross section curvature increases. A steel bar of a reinforced concrete structure is not subjected to this problem.

Fig. 3.11 illustrates the geometry of the effective timber-concrete composite cross-section and the qualitative distribution of the axial stresses and strains during state IV. The position of the zero strain layer x_{IV} can be estimated under the assumption that the compressive stress in the concrete is equal to the compressive strength [65], and is uniformly distributed over a depth of $0.85 \cdot x_{IV}$:

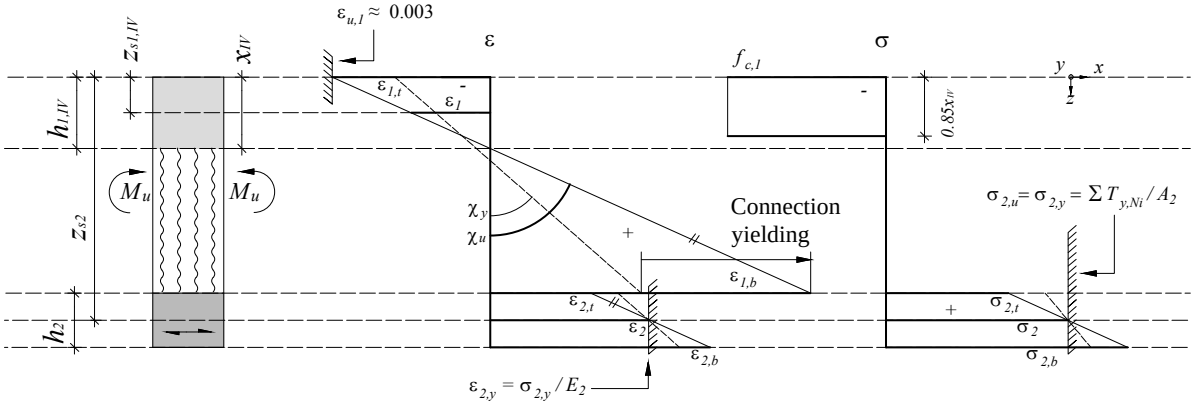

Figure 3.11: State IV: ultimate limit state

$$\sum F_x = 0 \tag{3.75}$$

$$x_{IV} = \frac{\sigma_2 A_2}{0.85 f_{c,1} b_1} = \frac{\sum T_{y,Ni}}{0.85 f_{c,1} b_1} \tag{3.76}$$

If the ultimate shear deformation capacity of the connections does not govern the structural behaviour and the connection yielding does not cause secondary effects, the ultimate failure of the composite cross-section can be caused by a combined tensile-bending failure of the timber (2BT) or a compressive failure of the concrete (1C,u).

The curvature of the cross-section which causes a combined tensile-bending failure in the timber part of the composite member can be calculated according to Frangi and Fontana [2] as shown in Section 3.2.4:

$$\chi_{u,2} = \frac{2\varepsilon_{2,m,u}}{h_2} = \frac{2}{h_2} \cdot \frac{f_{m,0,2}\left(1 - \frac{\sigma_{2,y}}{f_{t,0,2}}\right)}{E_2} \tag{3.77}$$

The increase of the curvature of the cross-section during state IV can also cause a compressive failure of the concrete at top of the composite cross-section. This occurs if the maximum compressive strain $\varepsilon_{u,1}$ is achieved [65], and the failure criterion can be written as follows:

$$\chi_{u,1} = \frac{\varepsilon_{u,1}}{x_{IV}} \tag{3.78}$$

The ultimate curvature can be determined as follows:

$$\chi_u = \min\left\{\chi_{u,1}; \chi_{u,2}\right\} \tag{3.79}$$

For the design of the composite member, it must be taken into account that a brittle failure of the timber part should occur as late as possible. If the end of state IV is determined by a combined tensile-bending failure of the timber, the composite member will fail abruptly. In contrast, if exceedance of the maximum compressive strain of the concrete $\varepsilon_{u,1}$ is governing, the

ultimate failure process is similar to that of reinforced concrete structures, which is ductile and announced by cracking [67]. Nevertheless, a further increase of the curvature of the cross section after exceedance of $\varepsilon_{u,1}$ can cause a combined tensile-bending failure of the timber part.

On the basis of the ultimate curvature χ_u, the zero strain layer x_{IV} and the tensile strain of timber $\varepsilon_2 = \varepsilon_{2,y}$, the axial strains of the composite member at the ultimate limit state can be calculated as follows:

$$\varepsilon_{1,t} = -\chi_u x_{IV} \tag{3.80}$$

$$\varepsilon_{1,b} = \chi_u \big(h_1 - x_{IV}\big) \tag{3.81}$$

$$\varepsilon_{2,t} = \varepsilon_{2,y} - \chi_u \cdot \frac{h_2}{2} = \chi_y \gamma_2 e_{2,II} - \chi_u \cdot \frac{h_2}{2} \tag{3.82}$$

$$\varepsilon_2 = \varepsilon_{2,y} = \chi_y \gamma_2 e_{2,II} \tag{3.83}$$

$$\varepsilon_{2,t} = \varepsilon_{2,y} + \chi_u \cdot \frac{h_2}{2} = \chi_y \gamma_2 e_{2,II} + \chi_u \cdot \frac{h_2}{2} \tag{3.84}$$

The axial stresses between the top of the composite cross section and the depth $z = 0.85 x_{IV}$ are assumed to be equal to the compressive strength of the concrete, and the remaining concrete cross-section is assumed to be free of tension:

$$\sigma_{1,t} = -f_{c,1} \tag{3.85}$$

$$\sigma_{1,b} = 0 \tag{3.86}$$

Except for the plastic zones in the notches, the timber part of the composite member is elastic, and the axial stresses of the timber cross section can be obtained with the Hooke's law as follows:

$$\sigma_{2,t} = \varepsilon_{2,t} E_2 \tag{3.87}$$

$$\sigma_2 = \sigma_{2,y} \tag{3.88}$$

$$\sigma_{2,b} = \varepsilon_{2,b} E_2 \tag{3.89}$$

Since the timber is elastic, the increase of the curvature causes an increase of the stresses and strains in the timber, which implies an increase of the bending moment acting on the slab. The bending stress acting on the timber is:

$$\sigma_{2,m,u} = \chi_u \cdot \frac{h_2}{2} \cdot E_2 \tag{3.90}$$

Also the change of the depth of the compression zone in concrete causes a variation of the bending moment due to the composite action. The resisting moment of the composite member at the ultimate state can be estimated as follows:

$$M_u = \sigma_2 A_2 \big(h_1 - \frac{0.85 x_{IV}}{2} + \frac{h_2}{2}\big) + \sigma_{2,m,u} \cdot \frac{h_2^2 b_2}{6} \tag{3.91}$$

3.2.6 Estimation of the deflections during states III and IV

The deflections during state III and state IV are more difficult to estimate than in the other states because the length of the zone where plastic deformations of the cross-section occur is unknown. An upper boundary of the deflection at mid-span can be obtained by considering the composite member as a continuum and inserting χ_u in Eq. 3.57.

However, in several research studies on ductility of reinforced concrete beams subjected to bending, it was observed that the ductile behaviour of the steel and concrete induces the formation of plastic hinges, which have a limited extension [65]. The deflection due to rotation of the hinge can be estimated under the assumption that the hinge provokes a rigid body rotation of the remaining parts of the structure [65]. According to Bachmann [85], the length of the plastic zone is an uncertain parameter, and can exceed two times the height of the beam.

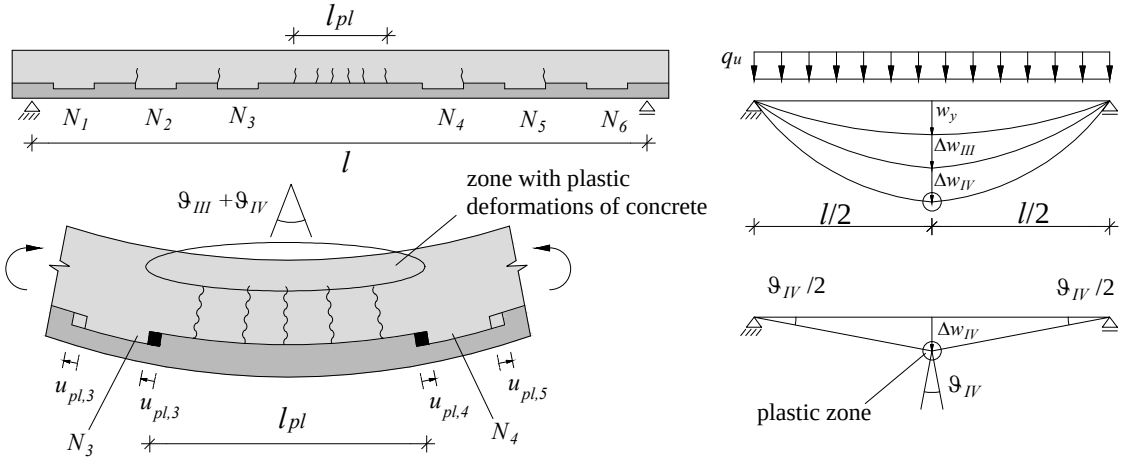

Figure 3.12: Estimation of the deflection of a timber-concrete composite member with notches designed proportional to the shear during state IV

The deflection of a timber-concrete composite member with a ductile connection during states III and IV can be estimated taking the models of reinforced concrete as an example. The following simplified model refers to a timber-concrete composite member with notched connections designed proportional to the distribution of shear stresses, so that all notches yield simultaneously (Fig. 3.12). Whereas ductility of a reinforced concrete beam is generated by plastic extensions of the longitudinal steel bars of concrete, in the timber-concrete composite member, ductility develops thanks to plastic longitudinal deformations of the notches (states III and IV). It can be interpreted that the moving away of the contact points is nearly equivalent to the plastic extension of a longitudinal steel reinforcing bar.

Since the width of the notches is designed proportional to the shear force distribution due to a vertical distributed load, the contact areas of all notches are subjected to the same stress:

$$\sigma_1 \approx \sigma_2 \approx \sigma_3 \approx \sigma_4 \approx \sigma_5 \approx \sigma_6 \tag{3.92}$$

This means that, in theory, all notches yield simultaneously and develop the same plastic deformation:

$$u_{pl,1} \approx u_{pl,2} \approx u_{pl,3} \approx u_{pl,4} \approx u_{pl,5} \approx u_{pl,6} \tag{3.93}$$

To simplify, the external concrete parts displace like rigid bodies in respect to the timber part of the composite member (Fig. 3.12). This means that, in theory, the zone where the curvatures of the parts of the cross-section increase due to the interface slip during states III and IV is located between the two central notches. However, this theory is a strong simplification of the real behaviour, and the effective length of the plastic zone l_{pl} is difficult to estimate.

When an assumption for l_{pl} is made, it is possible to estimate deformations. According to Bachmann [64], the rotation performed by the composite cross section in the plastic zone during states III and IV can be estimated as follows:

$$\theta_{III} \approx \frac{\frac{f_{c,1}}{E_1} - \varepsilon_{1,t,y}}{x_{III}} \cdot l_{pl} \tag{3.94}$$

$$\theta_{IV} \approx \frac{\chi_u \cdot x_{IV} - \frac{f_{c,1}}{E_1}}{x_{IV}} \cdot l_{pl} \tag{3.95}$$

According to Fig. 3.12, the deflection increments during states III and IV can be estimated as follows:

$$\Delta w_{III} \approx \frac{l}{2} \cdot \tan\left(\frac{\theta_{III}}{2}\right) \tag{3.96}$$

$$\Delta w_{IV} \approx \frac{l}{2} \cdot \tan\left(\frac{\theta_{IV}}{2}\right) \tag{3.97}$$

The deflection of the composite member when the concrete reaches the compressive strength $f_{c,1}$ (end of state III) can be calculated as follows:

$$w_{1C,c} \approx w_y + \Delta w_{III} \tag{3.98}$$

The deflection of the composite member at ultimate limit state (end of state IV) can be calculated as follows:

$$w_{1C,u} \approx w_y + \Delta w_{III} + \Delta w_{IV} \tag{3.99}$$

3.3 Structural behaviour of the notched connection

3.3.1 Introduction

This section illustrates several analytical models to estimate the structural behaviour of a notched timber-concrete connection. A series of parametric studies focused on a timber-concrete composite slab made of a beech LVL plate allow understanding the influence of the geometric and material parameters on the structural performance of the notch. These theoretical studies help to choose a notch layout for an optimal structural behaviour of the composite slab, with regard to the fact that brittle failures should be prevented.

3.3.2 Load-carrying behaviour

This section presents a simplified model based on equilibrium to visualise and understand the load-carrying mechanism of a timber-concrete composite member with a notched connection. If the geometry and the material properties are known, the elastic stresses acting on the composite cross-section σ_x and τ_{xz} due to a bending moment M and a shear force V can be quantified using the simplified analytical methods described in Section 2.3.2. To visualise the entire load-carrying mechanism of the composite member, truss models can be used. However, the use of truss models is correct only if tensile reinforcements are provided in the location of the tension ties. Also the load-carrying mechanism in the timber part of the composite member can be understood by means of a truss model; however, in this case, a truss model is correct provided that load-carrying capacity of the timber is not achieved.

Four-point bending

Fig. 3.13 represents the load-carrying mechanism of a timber-concrete composite member subjected to four-point bending with vertical forces F. The parameter h is the total thickness of the composite member, h_1 is the thickness of the concrete and h_2 the thickness of the timber. The following calculations are valid if the connections and the cross-sections are elastic (state II), and the centroid of the composite member x_{II} is located in the concrete ($x_{II} < h_1$). It is assumed that the concrete part of the composite member is cracked below the centroid x_{II}. As illustrated in Fig. 3.13(a), the vertical forces F generate elastic axial stresses σ_x in both parts of the composite member.

The resulting compression axial force in the concrete and tension force in the timber at a distance a from the support are named N, correspond to the integral of the axial stresses σ_x over the effective cross sections, and act in the centroids of the axial stress distributions:

$$N = -b \cdot \int_0^{x_{II}} \sigma_1(z)dx = b \cdot \int_{h_1}^{h} \sigma_2(z)dz \tag{3.100}$$

The axial stress at the top of the concrete cross-section at a distance a from the support is:

$$\sigma_{1,t} = \varepsilon_{1,t} \cdot E_1 = \frac{F \cdot a}{EI_{II}} \cdot \left(\gamma_1 e_{1,II} - \frac{x_{II}}{2}\right) \cdot E_1 \tag{3.101}$$

where:

$$e_{1,II} = -\frac{x_{II}}{2} \tag{3.102}$$

The equation of the axial stress which occurs in the effective area of the concrete cross section can be written as follows:

$$\sigma_1(z) = \sigma_{1,t} \cdot \left(1 - \frac{z}{x_{II}}\right) \tag{3.103}$$

The axial stress in the concrete integrated over the effective concrete depth corresponds to the resulting axial force N:

$$-N = b \cdot \int_0^{x_{II}} \sigma_1(z)dz = -F \cdot \frac{a \cdot n_1\gamma_1 b}{2I_{II}} \cdot x_{II}^2 \tag{3.104}$$

It can be assumed that the notches between the support and the point $x = a$ carry the integral of the theoretic elastic shear stress $\tau_{12,xz}$ which occurs on bottom edge of the effective concrete cross-section and on top edge of the timber cross-section:

$$\sum T_{Ni} = b \cdot \int_0^a \tau_{12,xz}(x)dx \tag{3.105}$$

The theoretic elastic shear stress $\tau_{12,xz}$ can be calculated referring to the concrete part of the composite member as follows:

$$\tau_{12,xz}(x) = \frac{V(x)S_{12,II}}{bI_{II}} = V(x) \cdot \frac{\gamma_1 n_1 e_{1,II} A_{1,II}}{bI_{II}} = V(x) \cdot \frac{\gamma_1 n_1 x_{II}^2}{2I_{II}} \tag{3.106}$$

Alternatively, the theoretic elastic shear stress at the interface can be calculated with the timber cross-section. The result will be the same, because the static moments are equal:

$$\tau_{12,xz}(x) = \frac{V(x)S_{12,II}}{bI_{II}} = V(x) \cdot \frac{\gamma_2 n_2 e_{2,II} A_{2,II}}{bI_{II}} \tag{3.107}$$

where:

$$e_{2,II} = h_1 + \frac{h_2}{2} - x_{II} \tag{3.108}$$

The integral of $\tau_{12,xz}(x)$ over the length a is:

$$\sum T_{Ni} = b \cdot \int_0^a \tau_{12,xz}(x)dx = F \cdot \frac{a \cdot n_1\gamma_1 b}{2I_{II}} \cdot x_{II}^2 \tag{3.109}$$

Eq. 3.104 and Eq. 3.109 show that the integral of the shear stress due to F acting on top edge of the timber cross-section and on bottom edge of the effective concrete cross-section between $x = 0$ and $x = a$ corresponds to the integral of the axial stresses of the concrete crosss-section due to F in the point $x = a$. Under the assumption that the notches carry the integral of $\tau_{12,xz}(x)$, it can be interpreted that the sum of the notch forces between $x = 0$ and $x = a$ is equal to the axial forces at $x = a$:

$$N = \sum T_{Ni} \tag{3.110}$$

The external load F causes vertical shear forces in both parts of the composite member. Since the axial force N has to be transferred from the centroid of the axial stress distributions to the notches, vertical internal forces must ensure the equilibrium of the two components. As described in Fig. 3.13(b), if the system is visualised as a truss model, diagonal and vertical struts occur.

Taking the concrete part as an example, since the axial compressive stress is triangularly distributed, the resulting axial compression force in the concrete N acts at a depth of $z = x_{II}/3$, where x_{II} is the position of the centroid of the composite member in the elastic-cracked state. The distance in z-direction between the notch force T_{Ni} and the resulting axial compression force in the concrete N can be calculated as follows:

$$h_1^* = \frac{t_N}{2} + h_1 - \frac{x_{II}}{3} \tag{3.111}$$

Concerning the concrete part of the composite member of Fig. 3.13(b), by considering the equilibrium requirements in the contact point between the timber and concrete in the notch Ni, the following equations can be written:

$$\sum F_x = 0 \Rightarrow D_i \cdot \frac{s}{\sqrt{s^2 + (h_1^*)^2}} = T_{Ni} \tag{3.112}$$

$$\sum F_y = 0 \Rightarrow D_i \cdot \frac{h_1^*}{\sqrt{s^2 + (h_1^*)^2}} = T_i \tag{3.113}$$

In the concrete, the vertical component of the diagonal strut D_i, which is equal to the vertical force T_i, corresponds to the shear force V_1. The vertical struts T_i are subjected to tension. As illustrated in Fig. 3.13(b), the load-carrying mechanism of the timber part can be simplified with a similar model.

Distributed load

The load-carrying mechanism in the case of a distributed load is governed by the same principle that governs the four-point bending. Fig 3.14 illustrates the load-carrying mechanism of a timber-concrete composite slab subjected to a distributed load. In contrast to the four-point bending configuration, the vertical load q is distributed over the entire span. The vertical shear force is divided in two parts and is carried by both parts of the composite member. Basically, the equilibrium in the contact points between the timber and concrete is analogue to the case of four-point bending. However, the diagonal and the vertical components are in equilibrium with the vertical loads resulting from q. Fig. 3.14(a) illustrates the forces acting on the composite member between the left support and the mid-span (which is the point where no shear force occurs). Fig. 3.14(b) shows a sector of the composite member between the left support and $x = a$, where a bending moment $M(a)$ and a shear force $V(a)$ are acting.

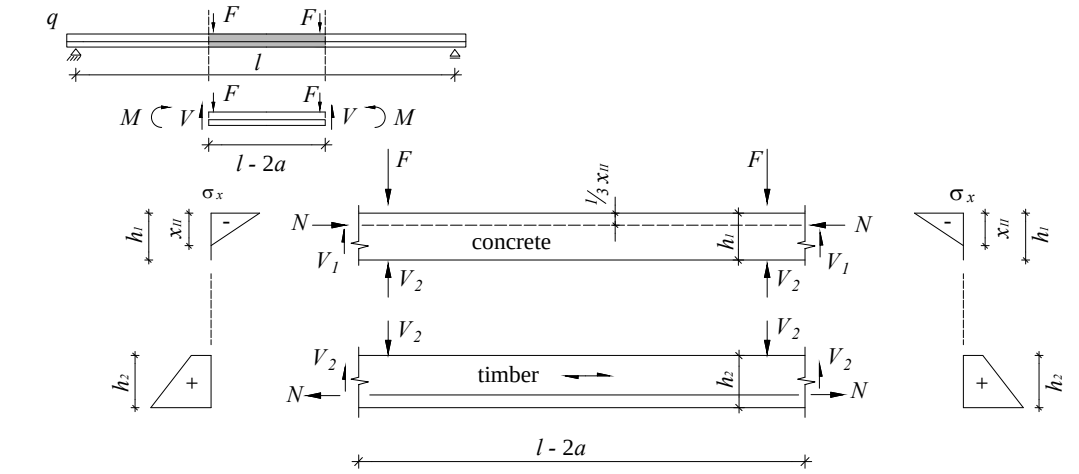

(a)

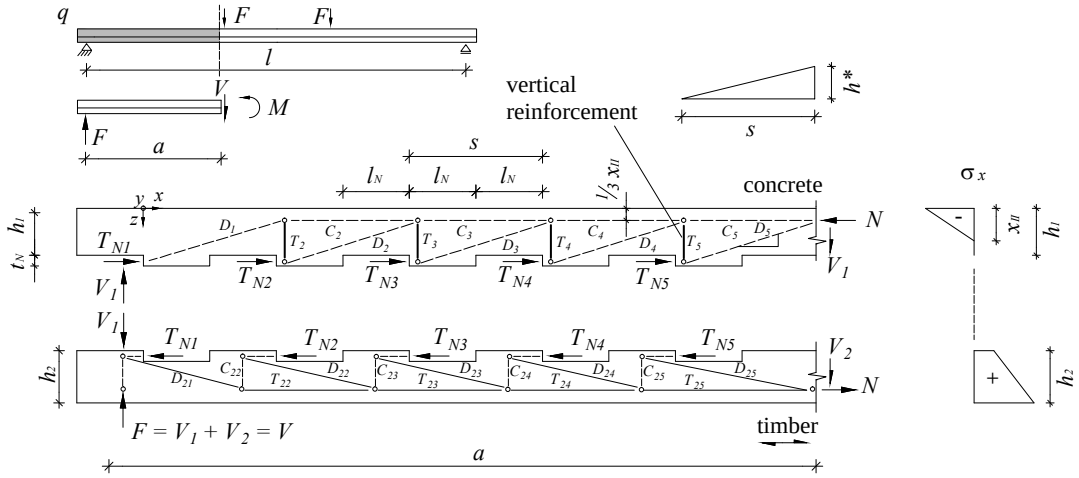

(b)

Figure 3.13: Simplified load-carrying mechanism of a timber-concrete composite member with a notched connection subjected to four-point bending: (a) forces acting on the middle sector; (b) forces acting on the left sector

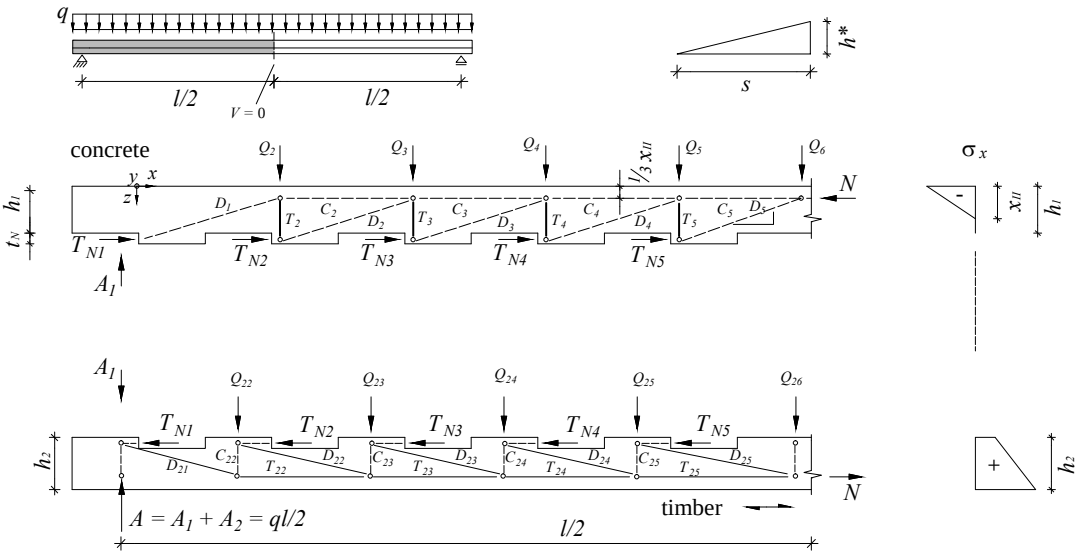

(a)

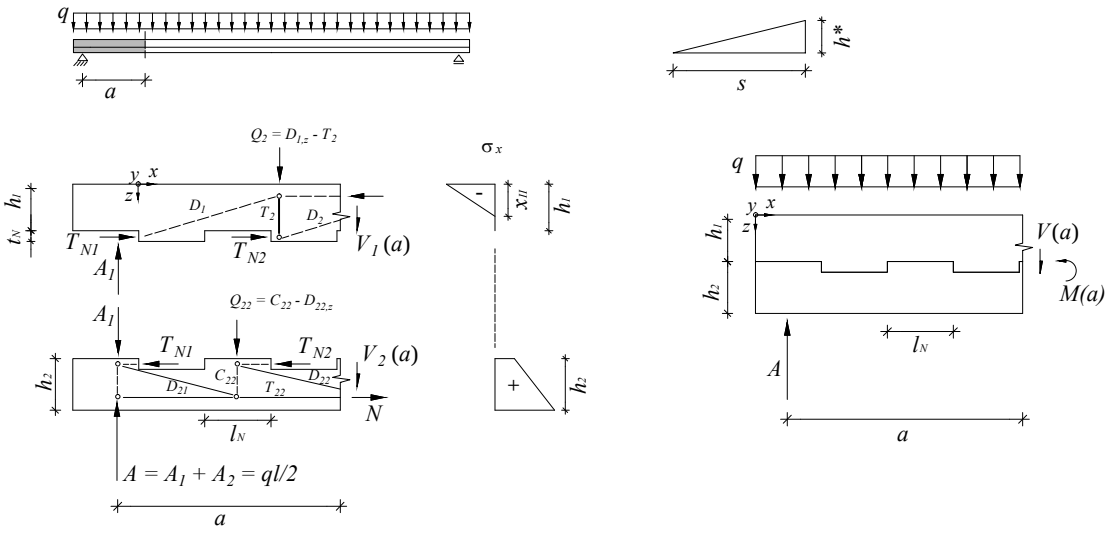

(b)

Figure 3.14: Simplified load-carrying mechanism of a timber-concrete composite member with a notched connection subjected to a distributed load: (a) forces acting between the left support and the mid-span; (b) forces acting between the left support and the point $x = a$

3.3.3 Calculation of the notch force

To investigate the structural behaviour of the notches, the forces acting on the notches must be calculated. This section presents a simplified model based on Eq. 3.105 to estimate the horizontal forces T_{Ni} to be carried by the notches. This method is based on the calculation of the theoretic elastic shear stress at the interface of the composite member, takes into account the flexibility of the connections, and is valid for every geometry of the parts (Fig. 3.15).

In this calculation, the theoretic shear stress $\tau_{12}(x)$ is assumed to be distributed over the interface. Since, in the case of a notched connection, the horizontal shear stresses are locally transferred through the notch edges, the notch force T_{Ni} can be estimated by integrating the theoretic shear stress τ_{12} over the length s. For most of the notches shown in Fig. 3.15, this length s can be assumed to be equal to the distance between two load transfer points:

$$s = 2 \cdot l_N \tag{3.114}$$

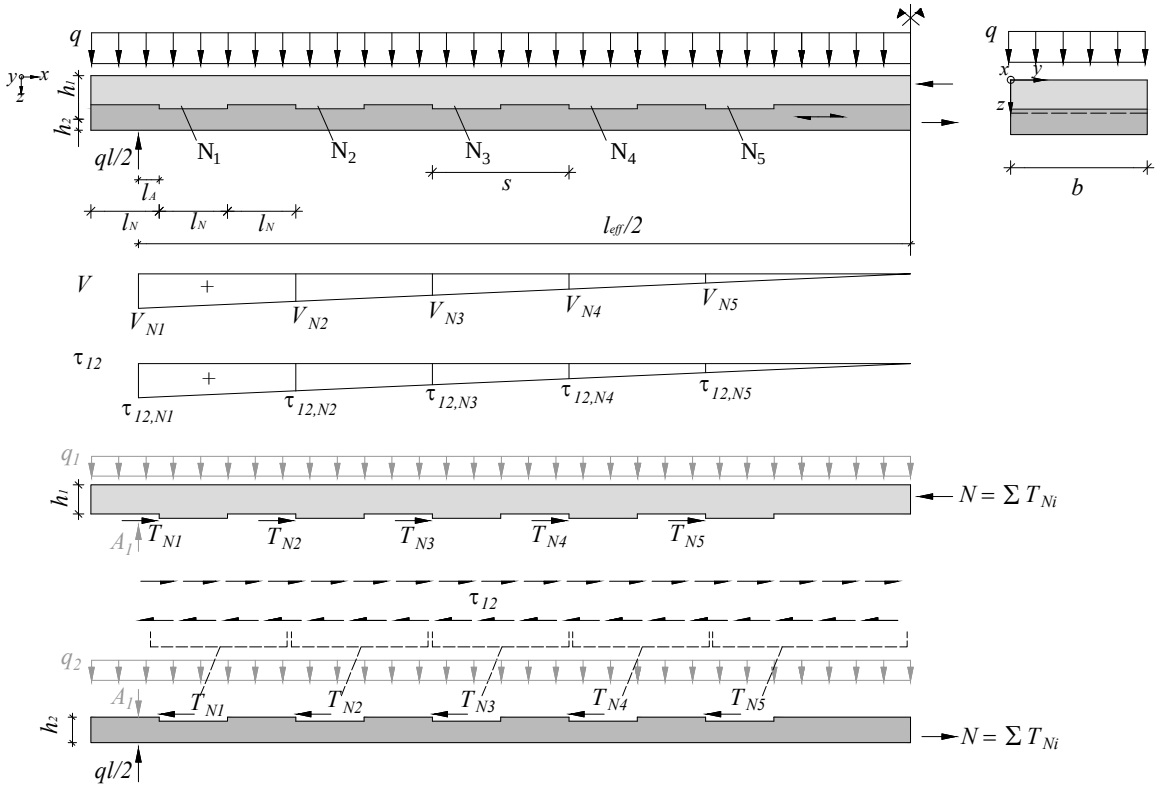

Figure 3.15: Calculation of the forces acting on the notches T_{Ni} by integrating the theoretical elastic shear stress at the interface between the timber and concrete

The theoretical elastic shear stress at the interface close to the notch Ni can be calculated on the basis of the shear force V_{Ni} and the elastic cross-sectional values by means of Eq. 3.106. If concrete is cracked, the elastic shear stress close to the notch Ni is:

$$\tau_{12,Ni} = \frac{V_{Ni} S_{12,II}}{b I_{II}} \tag{3.115}$$

where I_{II} is the moment of inertia of the composite cross-section obtained according to Section 3.2.3, and $S_{12,II}$ is the effective static moment calculated at the depth of the interface:

$$S_{12,II} = \gamma_i n_i e_{i,II} A_{i,II} \tag{3.116}$$

Based on the theoretical elastic shear stress distribution, the notch forces can be estimated as follows:

$$T_{Ni} = b \cdot s \cdot \frac{\tau_{Ni} + \tau_{N(i+1)}}{2} \tag{3.117}$$

For instance, the force T_{N1} acting on notch N1 of Fig. 3.15 due to a distributed force q per surface unit is:

$$T_{N1} = b \cdot (2l_N + l_A) \cdot \frac{\tau_{N1} + \tau_{N2}}{2} = q \cdot b \cdot \frac{2l_N + l_A}{2} \cdot (l_{eff} - l_A - 2l_N) \cdot \frac{\gamma_2 n_2 e_{2,II} A_{2,II}}{I_{II}} \tag{3.118}$$

The force T_{N2} acting on notch N2 of Fig. 3.15 is:

$$T_{N2} = b \cdot 2l_N \cdot \frac{\tau_{N2} + \tau_{N3}}{2} = q \cdot b \cdot l_N \cdot (l_{eff} - 2l_A - 6l_N) \cdot \frac{\gamma_2 n_2 e_{2,II} A_{2,II}}{I_{II}} \tag{3.119}$$

The force T_{N3} acting on notch N3 of Fig. 3.15 is:

$$T_{N3} = b \cdot 2l_N \cdot \frac{\tau_{N3} + \tau_{N4}}{2} = q \cdot b \cdot l_N \cdot (l_{eff} - 2l_A - 10l_N) \cdot \frac{\gamma_2 n_2 e_{2,II} A_{2,II}}{I_{II}} \tag{3.120}$$

The force T_{N4} acting on notch N4 of Fig. 3.15 is:

$$T_{N4} = b \cdot 2l_N \cdot \frac{\tau_{N4} + \tau_{N5}}{2} = q \cdot b \cdot l_N \cdot (l_{eff} - 2l_A - 14l_N) \cdot \frac{\gamma_2 n_2 e_{2,II} A_{2,II}}{I_{II}} \tag{3.121}$$

The force T_{N5} acting on notch N5 of Fig. 3.15 is:

$$T_{N5} = q \cdot b \cdot \frac{1}{2} \cdot \left(\frac{l_{eff}}{2} - l_A - 8l_N \right)^2 \cdot \frac{\gamma_2 n_2 e_{2,II} A_{2,II}}{I_{II}} \tag{3.122}$$

3.3.4 Concepts for designing the notch width

According to Section 3.1, to achieve a ductile behaviour of the slab, the notches should be designed so that a compressive failure of the timber parallel to the grain is governing. In this section, two possible approaches to choose the width of the notches are discussed relating to the case of a uniformly distributed load, which generally corresponds to the common design situation assumed in practice:

- constant notch width
- notch width proportional to the shear stresses generated by a uniformly distributed load

The notch force T_{Ni} generates a contact pressure between the timber and the concrete part, which can be calculated as a function of the width b_{Ni} and the depth t_{Ni} of the notch Ni:

$$\sigma_{2x,Ni} = \frac{T_{Ni}}{b_{Ni} \cdot t_{Ni}} \tag{3.123}$$

As shown in Fig. 3.16, if the slab is subjected to a uniformly distributed vertical load q and the notch width b_i is linearly proportional to the shear force V, all notches get the same contact pressure $\sigma_{2x,Ni}$ because the notch forces T_{Ni} are linearly proportional to V too:

$$\sigma_{2x,N1} \approx \sigma_{2x,N2} \approx \sigma_{2x,N3} \approx \sigma_{2x,N4} \approx \sigma_{2x,N5} \tag{3.124}$$

Consequently, all notches will exceed the compressive strength of the timber at the same level of q. In this case, the model of Section 3.2 can be directly applied to predict the structural behaviour of the composite slab.

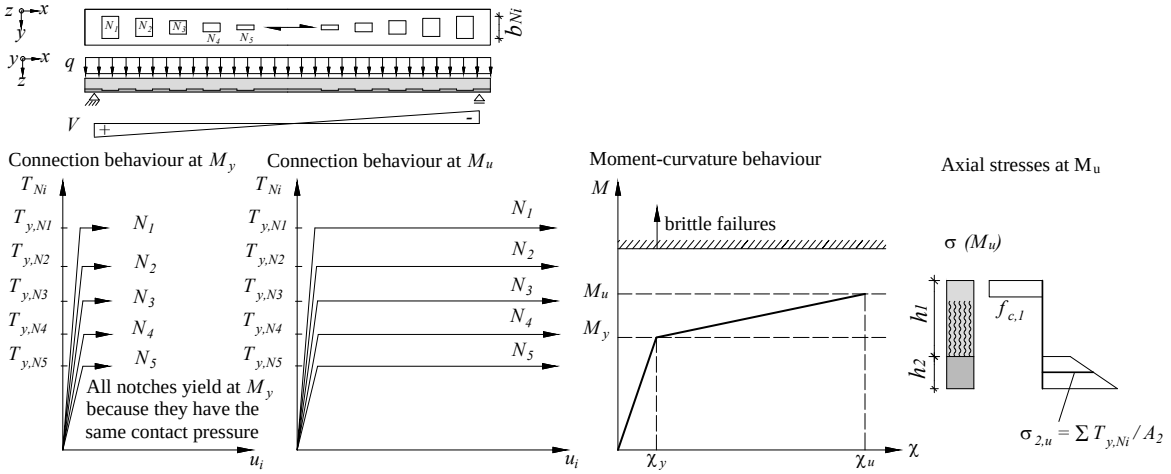

Figure 3.16: Qualitative structural behaviour of a composite slab with notch width proportional to the shear stresses generated by a uniformly distributed vertical load

As illustrated in Fig. 3.17, if the notch width is constant and the vertical load is uniformly distributed, when the compressive failure of the notch close to the support occurs, the other notches are still elastic because their contact areas are subjected to smaller compressive stresses parallel to the grain:

$$\sigma_{2x,N1} > \sigma_{2x,N2} > \sigma_{2x,N3} > \sigma_{2x,N4} > \sigma_{2x,N5} \tag{3.125}$$

In theory, this probably implies a hardening in the $M - \chi$ behaviour of the structure. In this case, when all notches reach the ductile failure, the timber part is subjected to a higher tensile stress than in the case of the notch width proportional to the shear force. In general, a hardening of the $M - \chi$ behaviour implies a higher risk that a premature brittle failure occurs (for instance a tensile-bending failure of the timber). Furthermore, the layout with the notch width proportional to the shear force, in contrast to the layout with constant notch width, allows saving timber material in the central area of the slab where the bending moment is elevated and

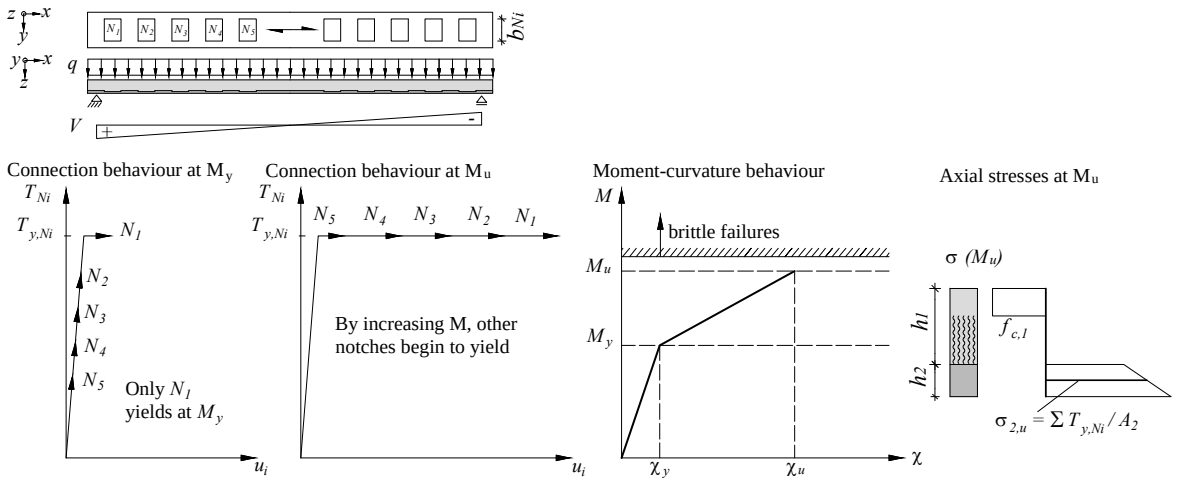

Figure 3.17: Qualitative structural behaviour of a composite slab with constant notch width subjected to a uniformly distributed vertical load

a sufficient active timber area is needed to prevent brittle failures of the timber and to ensure sufficient bending stiffness.

Another possibility to achieve the ductile notch failures at the same load level is to increase the notch distance inversely proportional to the shear force. The disadvantage of this solution is that each notch is cut over the same width. This causes a relevant reduction of the effective timber thickness in the areas with elevated bending moments and, thus, an increase of the risk of a brittle tensile-bending failure of the timber and a reduction of the bending stiffness, in particular for thin timber plates.

The following investigations are based on slab elements with a notch width proportional to shear force distribution.

3.3.5 Compressive failure of the timber

As illustrated in Section 2.4.3, the compressive failure of the timber parallel to the grain is a complex mechanism consisting of different states. For the following analyses, the behaviour of the timber subjected to compression parallel to the grain is assumed to be elastic-ideal plastic. Fig. 3.18 shows a simplified model to estimate the stresses acting on the notches. The critical element is located close to the edge of the notch and is subjected to a horizontal compressive stress parallel to the grain $\sigma_{2x,Ni}$ and to a vertical tensile stress perpendicular to the grain $\sigma_{2z,Ni}$. To simplify the failure prediction, it is assumed that the element considered is not subjected to shear. Although, in reality, stress peaks and non-linearities can occur, to simplify the calculation, the stress distributions represented in Fig. 3.18 are assumed to be linear.

The compressive stress parallel to the grain corresponds to the notch force distributed over the contact area between the timber and concrete. It is assumed to be constant and can be estimated as follows:

$$\sigma_{2x,Ni} = \frac{-T_{Ni}}{b_{Ni} \cdot t_{Ni}} \tag{3.126}$$

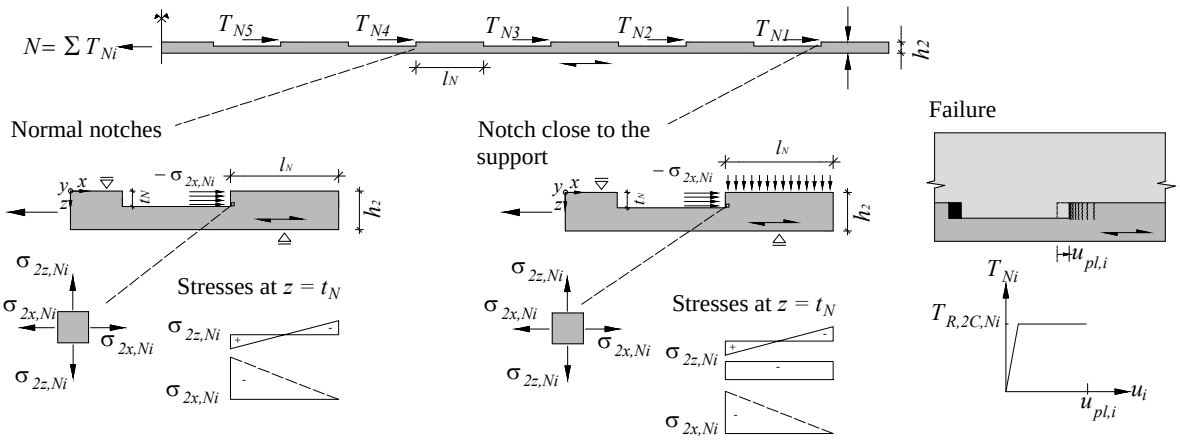

Figure 3.18: Simplified model for the compressive failure in the timber parallel to the grain

In addition to the compressive stress parallel to the grain, as stated by Steurer [63] in Section 2.4.4, in all notches, a vertical stress $\sigma_{2z,Ni}$ occurs because of the distance between the point of action of the notch force T_{Ni} and the position of the critical element. The tensile stress in this point can be estimated as follows:

$$\sigma_{2z,Ni} = \frac{3t_{Ni} \cdot T_{Ni}}{b_{Ni} \cdot l_{Ni}^2} \tag{3.127}$$

Close to the support, this stress has to be added to the vertical compressive stresses coming from the concrete compression diagonal strut. The mechanism is described in Fig. 2.12(b). It has to be noticed that, in practice, this effect is difficult to evaluate because it depends on the support dimensions. Under the assumption that the vertical compressive stresses are distributed over the entire width of the slab element, the following stress perpendicular to the grain results:

$$\sigma_{2z,Ni} = \frac{3t_{Ni} \cdot T_{Ni}}{b_{Ni} \cdot l_{Ni}^2} - \frac{T_{Ni} \cdot h_1^*}{2b \cdot l_{Ni}} \tag{3.128}$$

If the compressive stress in x-direction $\sigma_{2x,Ni}$ predominates over the vertical stress $\sigma_{2z,Ni}$, the bi-axial stress state can be neglected, and the load which causes a compressive failure of the timber parallel to the grain can be estimated as follows:

$$T_{R,2C,Ni}^* = f_{c,0,2} \cdot b_{Ni} \cdot t_{Ni} \tag{3.129}$$

However, if the vertical stress is relevant, since the critical element is subjected to a bi-axial stress state, a multi-axial strength criterion according to Section 2.4.1 should be used. In this case, the Tensor Polynomial theory [51] is used to predict the compressive failure of the timber parallel to the grain by taking into consideration the stress $\sigma_{2z,Ni}$ perpendicular to the grain. As explained in Eq. 2.29, for the notch Ni, the general formula of the failure function $F_{F,2C,Ni}$ for a bi-axial stress state without shear stress is:

$$F_{F,2C,Ni} = F_1\sigma_x + F_2\sigma_z + F_{11}\sigma_x^2 + 2F_{12}\sigma_x\sigma_z + F_{22}\sigma_z^2 = 1 \tag{3.130}$$

where $\sigma_x = \sigma_{2x,Ni}$ and $\sigma_z = \sigma_{2z,Ni}$ according to Fig. 3.18.
The force $T_{R,2C,Ni}$ with which the compressive failure of timber occurs can be estimated with the following inequality condition:

$$F_{F,2C,Ni} \geq 1 \tag{3.131}$$

For a beech LVL plate with mechanical properties according to Fig. 3.19(a), the coefficients can be calculated as follows:

$$F_1 = \frac{1}{f_{t,0,2}} - \frac{1}{f_{c,0,2}} = -4.79 \frac{\text{mm}^2}{\text{kN}} \tag{3.132}$$

$$F_2 = \frac{1}{f_{t,90,2}} - \frac{1}{f_{c,90,2}} = 434.1 \frac{\text{mm}^2}{\text{kN}} \tag{3.133}$$

$$F_{11} = \frac{1}{f_{c,0,2} \cdot f_{t,0,2}} = 370 \frac{\text{mm}^4}{\text{kN}^2} \tag{3.134}$$

$$F_{22} = \frac{1}{f_{c,90,2} \cdot f_{t,90,2}} = 37320 \frac{\text{mm}^4}{\text{kN}^2} \tag{3.135}$$

As explained in Section 2.4.1, there is no agreement about the determination of the interaction term F_{12}. However, as assessed by Narayanaswami and Adelman [52], it is possible to determine the two boundaries, in which F_{12} must lie:

$$F_{12} = \pm\sqrt{F_{11} \cdot F_{22}} = \pm 3716 \frac{\text{mm}^4}{\text{kN}^2} \tag{3.136}$$

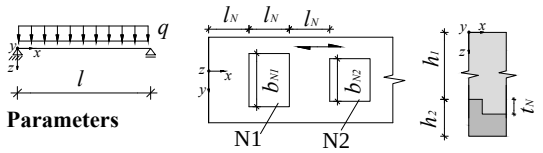

Parameters

$f_{c,0,2}$ = 45.7 N/mm^2
$f_{t,0,2}$ = 58.5 N/mm^2
$f_{c,90,2}$ = 13.6 N/mm^2
$f_{t,90,2}$ = 1.97 N/mm^2

l = 5.66 m
b = 530 mm
h_1 = 160 mm
h_2 = 40 mm

b_{N1} = 330 mm

t_N = 15 mm / 20 mm

l_N = 150 mm
b_{N2} (l_N = 150) = 293.3 mm

l_N = 200 mm
b_{N2} (l_N = 150) = 282.9 mm

l_N = 250 mm
b_{N2} (l_N = 150) = 260.0 mm

(a)

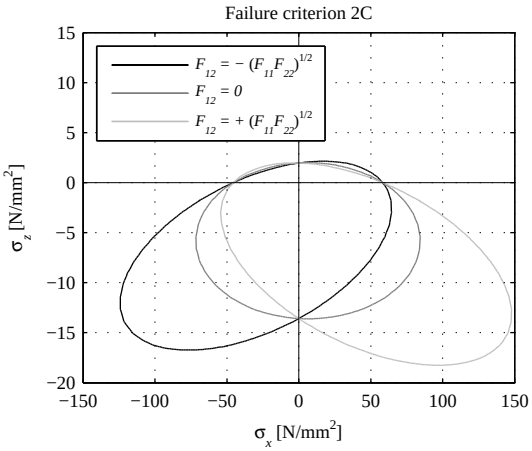

(b)

Figure 3.19: Parametric study on the compressive failure of beech LVL parallel to the grain: (a) geometry and material properties; (b) failure criterion according to the Tensor Polynomial model and influence of the interaction term F_{12} (as already shown in Fig. 2.8(b))

Figs. 3.19, 3.20 and 3.21 illustrate a parametric study concerning a timber-concrete composite member made of a beech LVL plate with a notched connection, in which the width of the

notches is proportional to the shear force generated by a uniformly distributed vertical load. The purpose of this study is to investigate the influence of a variation in length l_N and in depth t_N of the notch on the force $T_{R,2C,Ni}$ which causes a compressive failure of the LVL parallel to the grain, and to evaluate the difference between a failure prediction by considering the multi-axial stress state (Eq. 3.130) or by neglecting it (Eq. 3.129). The geometry and the relevant material properties used in the calculations are illustrated in Fig. 3.19(a).

Fig. 3.19(b) shows the theoretical interaction between the stresses parallel and perpendicular to the grain according to Eq. 3.130. The analysis is performed according to Section 2.4.1. It can be seen that the influence of F_{12} depends on the stress situation, and in some cases can be critical. The combinations of $\sigma_{2x,Ni}$ and $\sigma_{2z,Ni}$ which cause the compressive failure of the LVL parallel to the grain (in x-direction) are outside of the envelopes. In general, until a determinate level, a vertical pressure perpendicular to the grain ($\sigma_z < 0$) increases σ_x. In contrast, a tension perpendicular to the grain ($\sigma_z > 0$) causes a significant decrease of σ_x.

Fig. 3.20(a) illustrates the influence of the notch length l_N on the failure force $T_{R,2C,Ni}$ of the notch close to the support (N1) and the second notch (N2) calculated according to Eq. 3.130 for a notch depth of $t_N = 15$ mm, and compares the results with the failure load $T^*_{R,2C,Ni}$ calculated neglecting the vertical stress (Eq. 3.129). All other notches (except notch N1) are subjected to similar conditions as notch N2. As shown in Fig. 3.20(a), in notch N2, an increase of l_N causes a decrease of $\sigma_{2z,N2}$ according to Eq. 3.127; thus, $T_{R,2C,N2}$ increases in an asymptotic way and tends to become equal to $T^*_{R,2C,N2}$. In the notch close to the support (N1), under the assumptions made in this model, the compression perpendicular to the grain stresses compensate the tension perpendicular to the grain stresses according to Eq. 3.128 and the curve shows just a small influence of the resulting compression stresses for notches shorter than 200 mm. Furthemore, with increasing notch length, the ratio between $T_{R,2C,N1}$ and $T_{R,2C,N2}$ decreases. It can be seen that, for this stress situation, the interaction term F_{12} slightly shifts the curves, and the curve calculated with $F_{12} = 0$ lies between the two boundaries.

Fig. 3.20(b) shows the influence of the notch depth t_N on the notch failure force $T_{R,2C,Ni}$ calculated according to Eq. 3.130 in the case of a notch length of 250 mm. The results of $T_{R,2C,Ni}$ are compared to the load $T^*_{R,2C,Ni}$ calculated without the influence of the vertical stresses according to Eq. 3.129, which are directly proportional to the notch depth. The notch depth influences $T_{R,2C,Ni}$ as follows:

- An increase of t_N implies a decrease of the compressive stress $\sigma_{2x,Ni}$ according to Eq. 3.126, which causes an increase of the failure load $T_{R,2C,Ni}$.
- An increase of t_N causes an increase of the tension perpendicular to the grain stresses $\sigma_{2z,Ni}$ according to Eq. 3.127 due to the increasing eccentricity. This implies a non-linearity in the curve of $T_{R,2C,N2}$. However, in the practical range of t_N, $T_{R,2C,Ni}$ increases with increasing depth.
- An increase of t_N implies an increase of the ratio between $T_{R,2C,N1}$ and $T_{R,2C,N2}$

As shown in Fig. 3.20(b), in the notch close to the support N1, the influence of the vertical compression stresses predominates. This slightly increases the failure load $T_{R,2C,N1}$ in

comparison to $T^*_{R,2C,N1}$. In the notch N2, the sum of all effects tends to decrease $T_{R,2C,N2}$ in comparison to $T^*_{R,2C,N2}$.

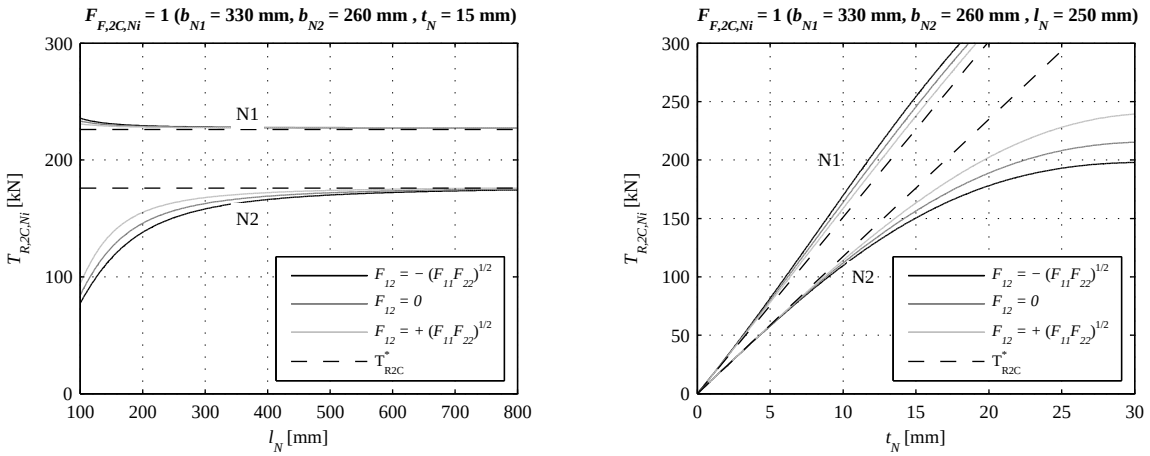

Figure 3.20: Parametric study of the compressive failure of beech LVL parallel to the grain: (a) influence of the notch length on the failure load; (b) influence of the notch depth on the failure load

Fig. 3.21 illustrates the relationship between the vertical load q acting on the slab element and the failure function $F_{F,2C,Ni}$ obtained from Eq. 3.130 with $F_{12} = 0$. The load q is calculated from the notch forces T_{Ni} according to Section 3.3.3. According to the Tensor Polynomial theory, the load $q_{R,2C,Ni}$, which causes the compressive failure of the LVL parallel to the grain, corresponds to the intersection between the failure function $F_{F,2C,Ni}$ and the horizontal line $F_{F,2C,Ni} = 1$. The load $q^*_{R,2C}$ does not take the influence of vertical stresses into account and is derived from $T^*_{R,2C,Ni}$ (Eq. 3.129). Also these diagrams show that, if the notches are shorter and deeper, the effects of the stresses perpendicular to the grain increase. This can be assessed by observing the difference between $q_{R,2C,N2}$ and $q^*_{R,2C}$. Furthermore, if the stresses perpendicular to the grain are not taken into account, the vertical load $q^*_{R,2C}$, which causes a compressive failure of the LVL parallel to the grain, increases with decreasing notch length. This dependency is explained in Section 3.3.3.

In summary, for the development of timber-concrete composite slabs made of beech LVL with a notched connection, the following conclusions concerning the modelling of the compressive failure of the LVL can be drawn :

- The model and the strength criterion illustrated are strongly simplified. They help understanding the influence of several parameters on the failure force. Nevertheless, a compressive failure of the LVL is complicated by a multitude of complex mechanisms, which are difficult to quantify.

- If the notches are too short, the problem could be that the notch over the support is not able to yield when the other notches are yielding.

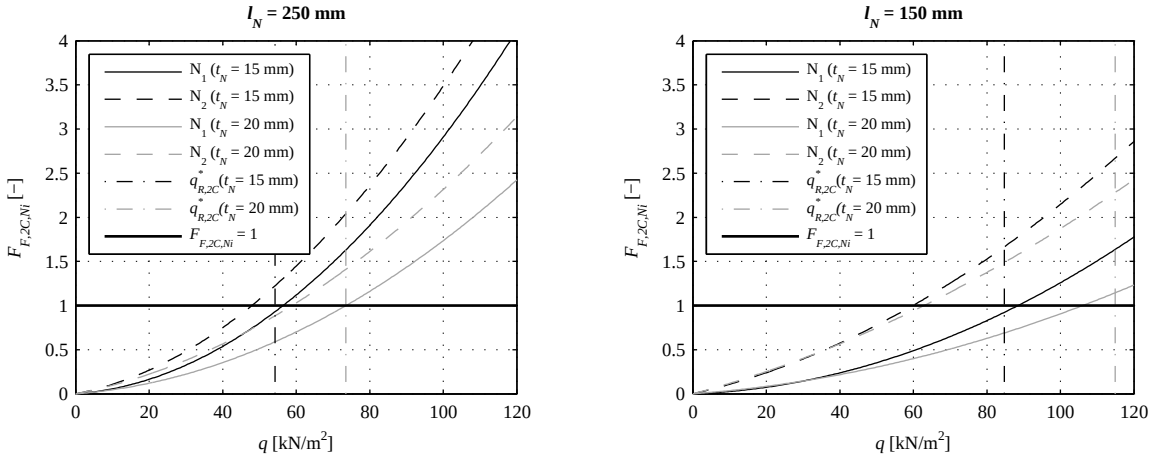

Figure 3.21: Parametric study of the compressive failure of beech LVL parallel to the grain: (a) relationship between vertical load q and failure function $F_{F,2C,Ni}$ for a notch length $l_N = 250$ mm; (b) relationship between vertical load q and failure function $F_{F,2C,Ni}$ for a notch length $l_N = 150$ mm

- If the notches are too deep, it becomes more difficult to reach the ductile compressive failure in the LVL because $T_{R,2C,Ni}$ increases and maybe other failure modes become governing.
- In the cases studied, neglecting of the interaction term F_{12} does not introduce substantial changes in the failure prediction.
- From the parametric study results that, if the notches are 250 mm long and 15 mm deep, the difference between $q_{R,2C,Ni}$ and $q^*_{R,2C}$, as well as the difference between the behaviour of the notches N1 and N2, is limited.
- Since compressive failure of LVL parallel to the grain is ductile, a small underestimation of the failure load does not imply dramatic consequences like in the case of a brittle failure.
- It has to been taken into account that the estimation of the vertical load q from the notch forces T_{Ni} contains several uncertainties, which sum up to the model simplifications in failure prediction.

3.3.6 Shearing-off failure of the timber

In practice, a shearing-off failure of the timber close to a notch can be characterised as a brittle failure, and, in the design of timber-concrete composite members, should be prevented. As explained in Section 2.4.4, the estimation of the shear stress distribution in the shear plane of the timber is very difficult.

In this work, the following approach was adopted:

- During the elastic state, the elastic shear stress distribution can be studied using the theory of the composite problems formulated for instance by Marti [5].

- At failure, based on theoretical studies, it is assumed that stress peaks are reduced (Fig. 3.27).

Analytical model for the elastic shear stress distribution

The elastic distribution of the horizontal relative displacement δ and the shear stress τ in the shear plane of the timber close to the notch are estimated using a similar approach to the composite problems solved by Marti [5] and Kaiser [58]. Similar to the approach presented by Kaiser [58] for pulling-out of carbon fibres glued to timber, the timber close to the notch is divided into three areas (Fig. 3.22(a)):

- An upper part with a depth of h_{sup} and a cross-section area of $A_{sup} = b \cdot h_{sup}$, which is subjected to compression and becomes shorter due to T_{Ni}.
- A lower part with a depth of h_{inf} and a cross-section area of $A_{inf} = b \cdot h_{inf}$, which is subjected to tension and becomes longer due to T_{Ni}.
- A middle part with a depth of h_s which connects the upper and the lower part, and is subjected to shearing.

It has to be noticed that the assumption that the shear deformations are concentrated in the middle part with a depth of h_s is a strong simplification of reality.

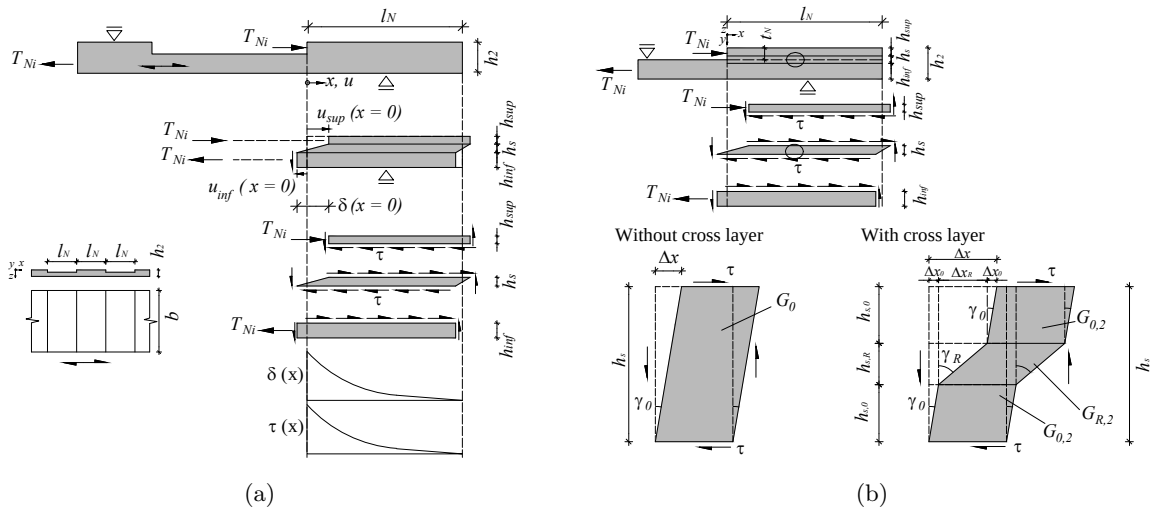

Figure 3.22: Estimation of the elastic shear stress distribution: (a) model for the calculation of the relative displacement and the shear stress; (b) model to calculate the shear stiffness of the shear zone

The problem illustrated in Fig. 3.22(a) is solved in analogy to the situation of two beams connected as treated by Marti [5]. As a consequence of the condition of equilibrium in x-direction, $N_{sup} = -N_{inf}$. The horizontal relative displacement between the upper and the lower part is defined as follows:

$$\delta(x) = u_{sup}(x) - u_{inf}(x) \tag{3.137}$$

The shear force per length unit $dN_{sup}/dx = -dN_{inf}/dx$ is assumed to be proportional to the horizontal relative displacement $\delta(x)$:

$$p(x) = k \cdot \delta(x) = \frac{dN_{sup}}{dx} = -\frac{dN_{inf}}{dx} \tag{3.138}$$

The shear stress is:

$$\tau = \frac{p(x)}{b} \tag{3.139}$$

The axial deformations of the upper and the lower part are governed by the following equations [5]:

$$N_{sup} = E_{sup}A_{sup} \cdot \frac{du_{sup}}{dx} \tag{3.140}$$

$$N_{inf} = E_{inf}A_{inf} \cdot \frac{du_{inf}}{dx} \tag{3.141}$$

Eq. 3.137 inserted in Eq. 3.138:

$$k(u_{sup} - u_{inf}) = \frac{dN_{sup}}{dx} \tag{3.142}$$

$$k(u_{sup} - u_{inf}) = -\frac{dN_{inf}}{dx} \tag{3.143}$$

By differentiating Eq. 3.140 and Eq. 3.141, and inserting in Eq. 3.142 and Eq. 3.143, the following system of homogeneous differential equations of II. Order is obtained:

$$\frac{dN_{sup}}{dx} = E_{sup}A_{sup}\frac{d^2u_{sup}}{dx^2} = k(u_{sup} - u_{inf}) = k\delta \tag{3.144}$$

$$\frac{dN_{inf}}{dx} = E_{inf}A_{inf}\frac{d^2u_{inf}}{dx^2} = -k(u_{sup} - u_{inf}) = -k\delta \tag{3.145}$$

The horizontal relative displacement is governed by the following differential equation. Eq. 3.137 combined with Eq. 3.140 and Eq. 3.141 can be written as follows:

$$\frac{d\delta(x)}{dx} = \frac{du_{sup}}{dx} - \frac{du_{inf}}{dx} = \frac{N_{sup}}{E_{sup}A_{sup}} - \frac{N_{inf}}{E_{inf}A_{inf}} \tag{3.146}$$

As shown by Marti [5], Eq. 3.146 differentiated and combined with Eq. 3.138 becomes:

$$\frac{d^2\delta(x)}{dx^2} - \delta(x)k\Big(\frac{1}{E_{sup}A_{sup}} + \frac{1}{E_{inf}A_{inf}}\Big) = 0 \tag{3.147}$$

The solution can be written as follows:

$$\delta(x) = C_1e^{\lambda x} + C_2e^{-\lambda x} \tag{3.148}$$

Where:

$$\lambda = \sqrt{\frac{k}{EA}} \tag{3.149}$$

$$\frac{1}{EA} = \frac{1}{E_{sup}A_{sup}} + \frac{1}{E_{inf}A_{inf}} \tag{3.150}$$

To determine the coefficients of the differential equation, the following boundary conditions are used according to Fig. 3.22(a):

$$N_{sup}(x = 0) = -T_{Ni} \tag{3.151}$$

$$N_{inf}(x = 0) = T_{Ni} \tag{3.152}$$

$$N_{sup}(x = l_N) = 0 \tag{3.153}$$

$$N_{inf}(x = l_N) = 0 \tag{3.154}$$

The coefficients are:

$$C_1 = \frac{T_{Ni} \cdot \frac{1}{EA}}{\lambda e^{\lambda \cdot 2l_N} - \lambda} \tag{3.155}$$

$$C_2 = \frac{T_{Ni} \cdot \frac{1}{EA}}{\lambda - \lambda e^{-\lambda \cdot 2l_N}} \tag{3.156}$$

The shear stiffness k of the middle zone can be estimated according to Fig. 3.22(b). If it can be assumed that the timber is homogeneous and does not contain cross layers, the transverse displacement of the middle zone Δx can be written as follows:

$$\Delta x = \frac{\tau}{G_0} \cdot h_s = \frac{p}{b \cdot G_0} h_s \tag{3.157}$$

The shear stiffness k can be calculated by inserting Eq. 3.157 in Eq. 3.138:

$$k = \frac{p}{\Delta x} = \frac{b \cdot G_0}{h_s} \tag{3.158}$$

If the timber member contains a cross layer with a thickness of $h_{s,R}$ in the middle of the shear zone, under the assumption that $G_R = 0.1G_0$, the transverse displacement of the middle zone Δx can be written as follows::

$$\Delta x = 2\Delta x_0 + \Delta x_R = 2 \cdot \frac{p \cdot h_{s,0}}{b \cdot G_0} + \frac{p \cdot h_{s,R}}{b \cdot G_R} \tag{3.159}$$

The shear stiffness k can be calculated by inserting Eq. 3.159 in Eq. 3.138:

$$k = \frac{p}{\Delta x} = \frac{b \cdot G_0}{2h_{s,0} + 10h_{s,R}} \tag{3.160}$$

Figs. 3.23 - 3.26 illustrate a parametric study concerning a 15 mm deep notch of a timber-concrete composite slab made of a 40 mm thick beech LVL plate. The middle shear zone is assumed to be 10 mm deep. The geometric and material parameters assumed for the calculations are summarised in Fig. 3.23. Basically, two different veneer configurations were treated (Fig.

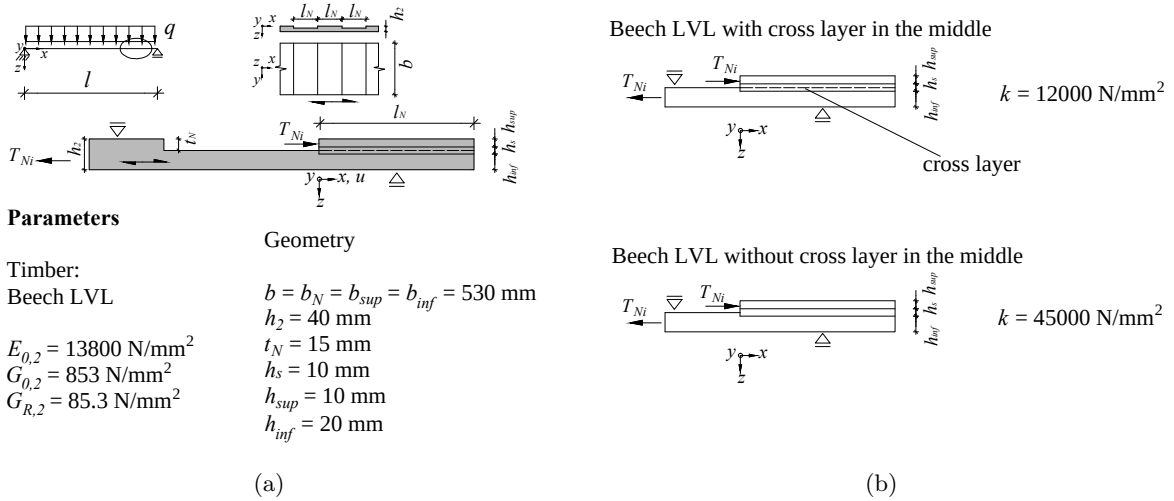

Figure 3.23: Parametric study on the elastic shear stress distribution in beech LVL: (a) geometry and material parameters; (b) veneer configurations

3.23(b)): a beech LVL plate with or without a cross layer in the middle of the shear zone h_s. This influences the parameter k according to Eq. 3.158 and Eq. 3.160 .

Fig. 3.24 illustrates the distribution of the horizontal relative displacement δ calculated according to Eq. 3.148 for four notch lengths used in practice between 150 and 300 mm. The curves denote a non-linear distribution of δ with a peak close to the notch edge where the load T_{Ni} is introduced ($x = 0$). A decrease in the parameter k causes an increase in relative displacement due to lower stiffness of the system. For both parameters k, in the cases studied, the value of the peak is not significantly influenced by a variation of the notch length.

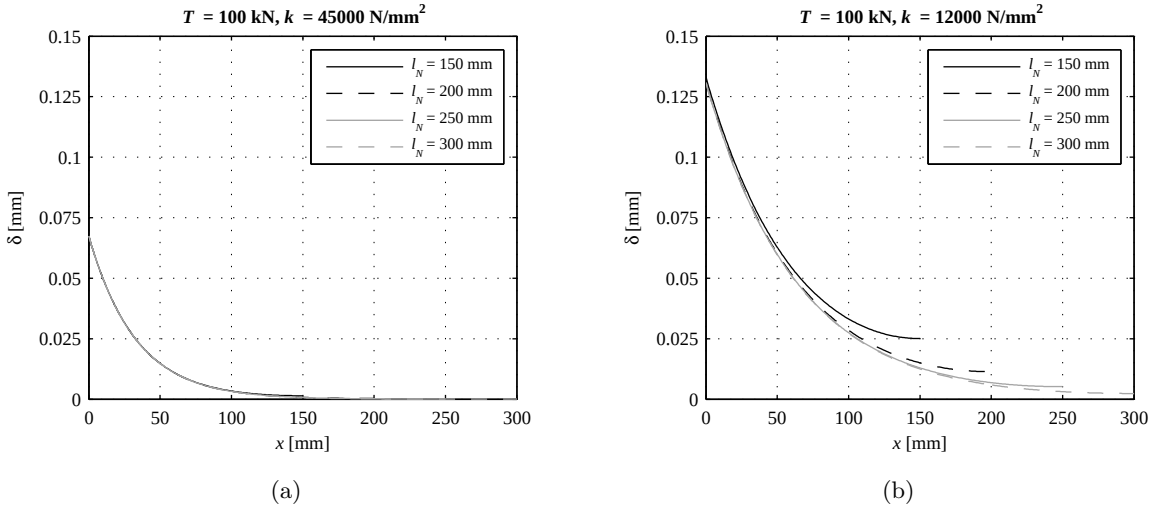

Figure 3.24: Parametric study of the elastic distribution of the horizontal relative displacement in beech LVL: (a) without cross layer; (b) with cross layer

Fig. 3.25 illustrates the elastic shear stress distribution calculated according to Eq. 3.148, Eq. 3.138 and Eq. 3.139 for four notch lengths used in practice between 150 and 300 mm. In a similar way to the relative displacement δ, the curves of the elastic shear stress τ denote a non-linear distribution with a peak close to the notch edge where the load T_{Ni} is introduced. However, in this case, a decrease in the parameter k causes a decrease in the shear stress peak due to lower stiffness. If k decreases, the peak decreases, and the shear stress is distributed over a longer effective length (3.25(b)). Also in the case of τ, for both parameters k, the value of the peak is not significantly influenced by a variation of the notch length.

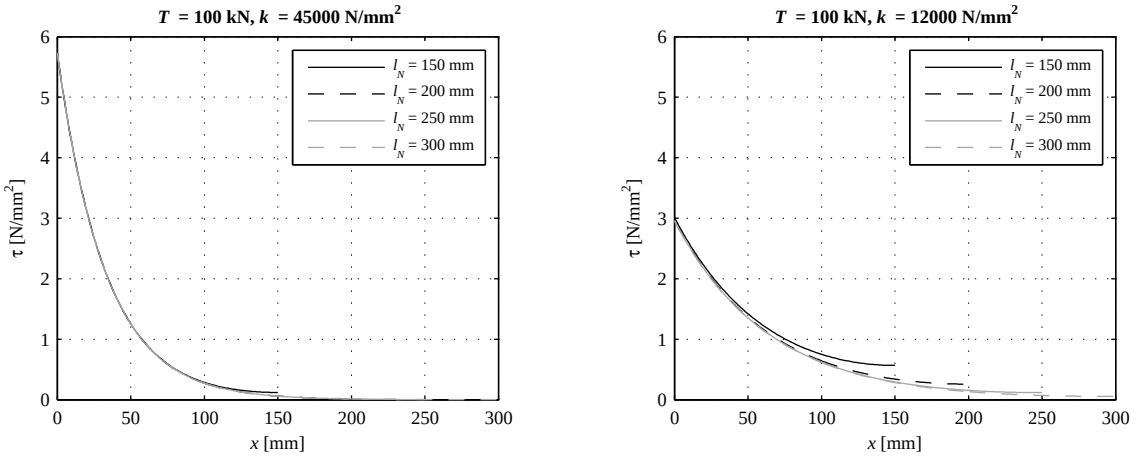

(a) (b)

Figure 3.25: Parametric study of the elastic shear stress distribution in beech LVL: (a) without cross layer; (b) with cross layer

Fig. 3.26 shows the peak values of the shear stress τ and the horizontal relative displacement δ in the case of a notch subjected to a force of $T = 100$ kN as a function of the notch length l_N. The peaks of τ and δ decrease in a non-linear way and follow an asymptotic behaviour. From a determinate value of the notch length l_N, the peaks of δ and τ remain constant. This limit length increases with decreasing stiffness parameter k. The higher the parameter k, the smaller $\delta(x = 0)$, the higher $\tau(x = 0)$, and the faster the decrease in $\delta(x = 0)$ and $\tau(x = 0)$.

It must be reminded that this model, which divides the timber in three sectors, is strongly simplified. The stiffness parameter k has a relevant influence on τ and δ, but is very difficult to quantify because the thickness of the middle part subjected to shear h_s in unknown and must be assumed. In general, a thicker shear zone h_s and a weaker timber cause a smaller value of k.

Concerning the development of timber-concrete composite slabs made of beech LVL plates, the following conclusions can be made:

- This study is valid for the estimation of a completely elastic behaviour, in other words, for low load levels.
- Although the model is a rough simplification of the reality, it allows to understand the mechanism of elastic shear-carrying in a timber notch.

- Regarding the notches of timber-concrete composite members made of beech LVL plates with dimensions similar to the cases studied, a variation of the notch length l_N between the values considered (150-300 mm) does not influence the peak of the elastic horizontal relative displacement in a significant way because the notch lengths considered are located in the asymptotic part of Fig. 3.26(a). Therefore, according to this model, the part of the notch shear stiffness at service level due to the LVL deformations is not significantly influenced by the notch length.

- For the notches made of beech LVL analysed, the part of the LVL which carries most of the elastic shear stress corresponds only to the first part of the notch length l_N (Fig. 3.25). This result agrees with previous investigations cited in Section 2.4.4. The fact that the peak of τ decreases asymptotically agrees with the numerical simulations conducted by Michelfelder [33]. However, since the value of h_s is very difficult to quantify, an exact comparison of the results is challenging.

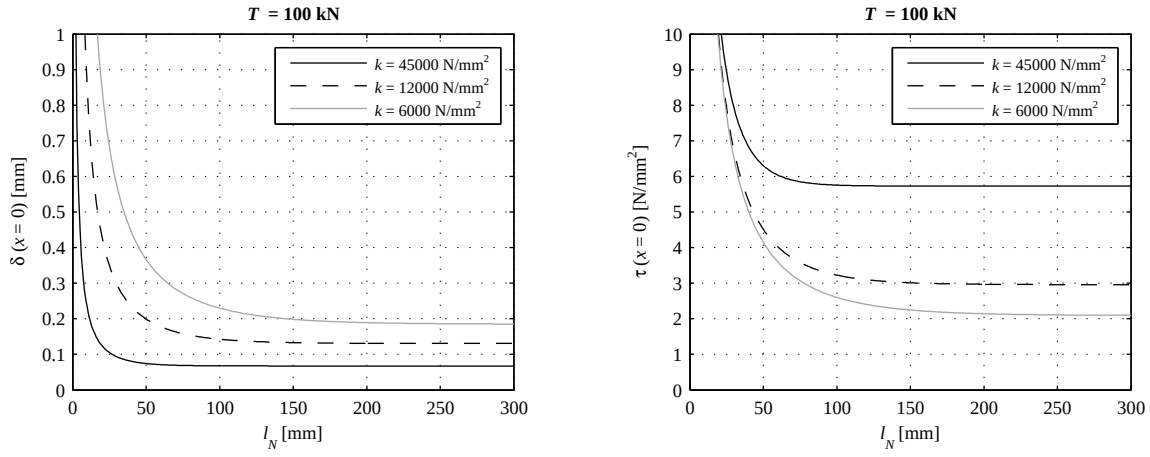

(a) (b)

Figure 3.26: Influence of the notch length on the peak values of the relative displacement and the shear stress: (a) relationship between the notch length l_N and the peak of the horizontal relative displacement $\delta(x = 0)$; (b) relationship between the notch length l_N and the shear stress peak $\tau(x = 0)$

Model for the failure prediction

The mechanism of a shearing-off failure in timber is very difficult to model because timber can be classified as a semi-brittle material and a series of micro structural mechanisms are capable of dissipating strain energy [45]. Because of the complexity of the micro-structure of wood, these mechanisms are difficult to quantify.

In Fig. 2.10(b), Smith at al. [45] idealised the behaviour of timber subjected to tension perpendicular to the grain by means of an elastic phase, a pre-peak non-linearity, and a strain softening. This implies that probably also a shearing-off failure in the timber close to the notch is governed by similar principles (Fig 3.27). When the elastic shear stress peak at $x = 0$ reaches

a value which is enough to initiate a fracture of the material, the timber part of the composite member does not fail in a brittle way, but probably begins a softening process close to $x = 0$ and the shear stress in the other zones increases. This means that, at failure level, the shear stress distribution probably differs from the elastic distribution.

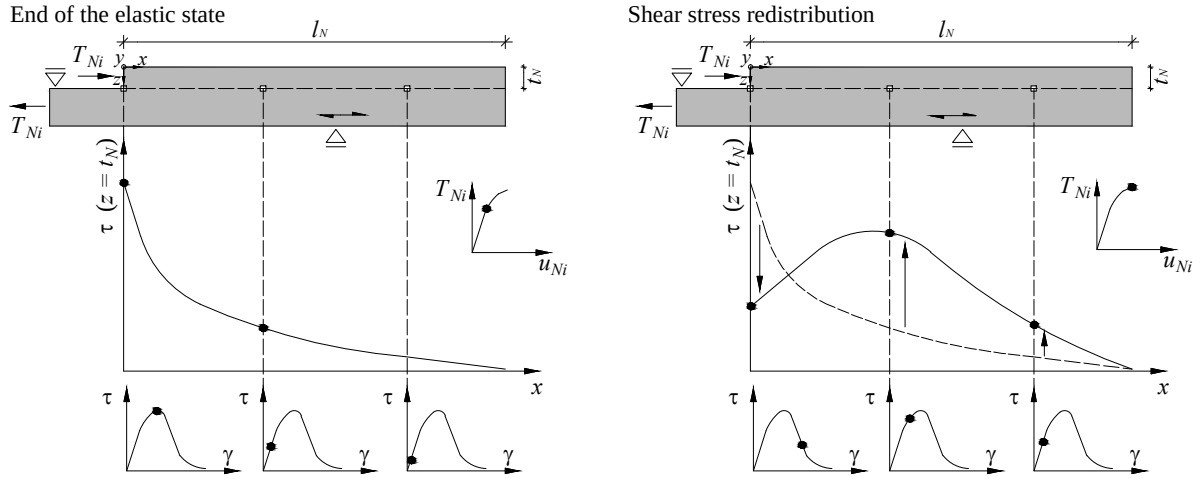

Figure 3.27: Qualitative stress redistribution during the shearing-off failure of the timber

Since the mechanisms, which are capable of dissipating strain energy, depend on the microscopic structure and imperfections of wood, the shear stress redistributions at failure level is very difficult to quantify. Therefore, for the following calculations, it is assumed that, at failure, the shear stress redistributes rectangularly over the length $8 \cdot t_N$ [59]. This rule is widely used in practice and was described in Section 2.4.4. Furthermore, Colling [59] suggested that the notch length must be at least equal to $8 \cdot t_N$. Nevertheless, it has to be taken into account that this stress distribution, although it is suitable for engineering applications, is a rough simplification of reality.

Fig. 3.28 illustrates the model adopted to study the shearing-off failure of the timber close to the notch caused by the introduction of the force T_{Ni}. It is assumed that the shear stress is transferred over a shear area located at a depth of $z = t_N$. Furthermore, it is assumed that, along the shear area, no axial stresses in x-direction occur. The critical element is located in the shear area at a depth of t_N, close to the notch edge. This element is subjected to a shear stress $\tau_{2,Ni}$ and to a vertical stress perpendicular to the grain $\sigma_{2z,Ni}$.
According to the approach by Colling [59], the shear stress is assumed to be constant over the length $8t_N$ and is estimated as follows:

$$\tau_{2,Ni} = \frac{T_{Ni}}{b_{Ni} \cdot 8t_{Ni}} \tag{3.161}$$

The vertical stress $\sigma_{2z,Ni}$ is due to the distance in z-direction between the point of action of the notch force T_{Ni} and the shear plane and can be calculated according to Eq. 3.127. The influence of the vertical stresses close to the support can be quantified with Eq. 3.128.

If the vertical stress perpendicular to the shear surface $\sigma_{2z,Ni}$ is neglected, the notch force, which causes a shear failure of the timber, can be calculated as follows:

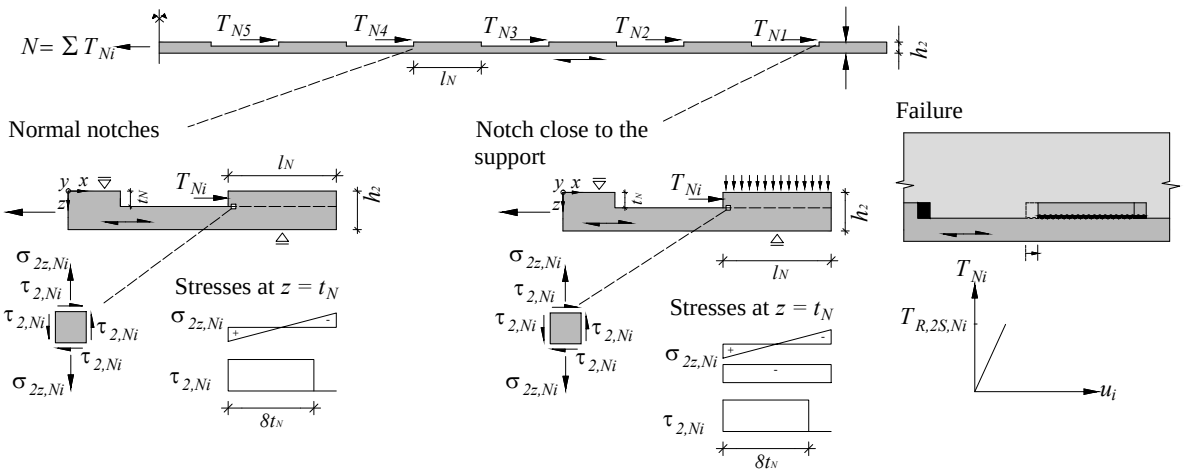

Figure 3.28: Model for the prediction of the shearing-off failure of the timber close to the notch

$$T^*_{R,2S,Ni} = f_{v,2} \cdot b_{Ni} \cdot 8 \cdot t_N \tag{3.162}$$

If the stress perpendicular to the shear area must be taken into account, the problem can be investigated using the Tensor Polynomial theory (Eq. 2.29) [51] explained in Section 2.4.1. Since it is assumed that no axial stress in x-direction occurs close to the shear area, the interaction term F_{12} is not needed, and the failure function can be written as follows:

$$F_{F,2S,Ni} = \left(\frac{1}{f_{t,90,2}} - \frac{1}{f_{c,90,2}}\right) \cdot \sigma_{2z,Ni} + \frac{1}{f_{t,90,2} f_{c,90,2}} \cdot \sigma^2_{2z,Ni} + \frac{1}{f^2_{v,2}} \cdot \tau^2_{2,Ni} = 1 \tag{3.163}$$

The force $T_{R,2S,Ni}$, when a shearing-off failure of the timber occurs close to the notch Ni, can be estimated using the following inequality condition:

$$F_{F,2C,Ni} \geq 1 \tag{3.164}$$

Figs. 3.29 - 3.31 summarise a parametric study on the application of the Tensor Polynomial model (Eq. 3.163) to predict a shearing-off failure of the timber close to the notch. The calculations refer to a timber-concrete composite slab made of a beech LVL plate, in which the width of the notches is proportional to the shear force generated by a uniformly distributed vertical load. This parametric study concentrates on the influence of the notch length l_N and depth t_N on the failure load of the notch. The material and geometric parameters are shown in Fig. 3.29(a).

Fig. 3.29(b) illustrates the theoretical interaction between the shear stress τ_2 and the vertical stress perpendicular to the grain σ_{2z} according to the Tensor Polynomial theory expressed in Eq. 3.163. The stress combinations, which cause a failure, are located above the envelope of the failure criterion. A compressive stress perpendicular to the shear plane ($\sigma_z < 0$) increases the shear strength until a determinate level, whereas a tensile stress perpendicular to the shear plane ($\sigma_z > 0$) facilitates the shear failure.

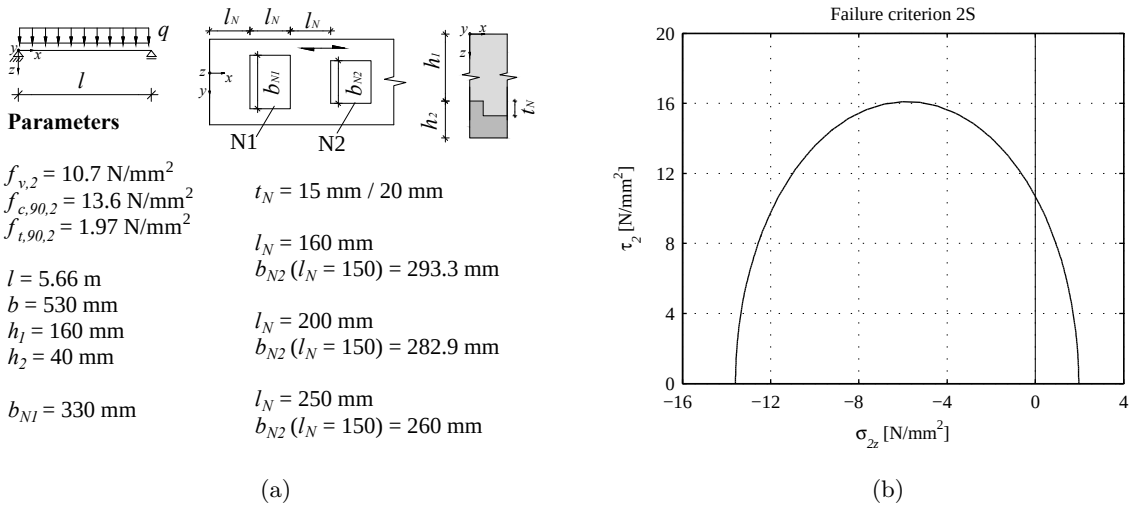

Figure 3.29: Parametric study on the prediction of the shearing-off failure of the beech LVL plate close to the notch: (a) geometry and material properties; (b) envelope of the Tensor Polynomial theory according to Eq. 3.163

Fig. 3.30 refers to the prediction of the shearing-off failure of the second notch from the support (N2) by means of the Tensor Polynomial model (Eq. 3.163) and the simplified formula of Eq. 3.162. The notch N2 is subjected to shear and tension perpendicular to the shear area according to Fig. 3.28, and the same principles govern the behaviour of all other notches except for the notch close to the support (N1), which has the positive influence of the compression stresses coming from the load introduction in the support.

As shown in Fig. 3.30(a), an increase of the notch length l_N causes a non-linear increase of the failure load $T_{R,2S,Ni}$ with asymptotic behaviour. The reason is that an increasing length provokes a decrease of the vertical tensile stress according to Eq. 3.127, whereas, according to the model of Fig. 3.28, the area of distribution of the shear stress depends only on the notch depth t_N. Therefore, from a determinate notch length forward, the vertical tensile stress does not play a significant role, and the outcome of Eq. 3.163 gets closer to Eq. 3.162.

As illustrated in Fig. 3.30(b), an increase in depth t_N has two opposing consequences on the failure load calculated according to the Tensor Polynomial theory:

- According to Eq. 3.161, the area of the shear plane where the notch force is distributed increases, and the shear stress decreases. Thus, the failure load $T_{R,2S,N2}$ tends to increase.
- From a determinate value of t_N, the tensile stresses generated by the eccentricity between the shear plane and the action point of the notch force become relevant and cause a decrease in failure load $T_{R,2S,N2}$ according to Eq. 3.127.

As a result, with increasing notch depth t_N, the curve of the failure load $T_{R,2S,Ni}$ calculated according to the Tensor Polynomial theory (Eq. 3.163) tends to shift from the failure load $T^*_{R,2S,Ni}$ obtained by neglecting the vertical stress (Fig. 3.30(b)).

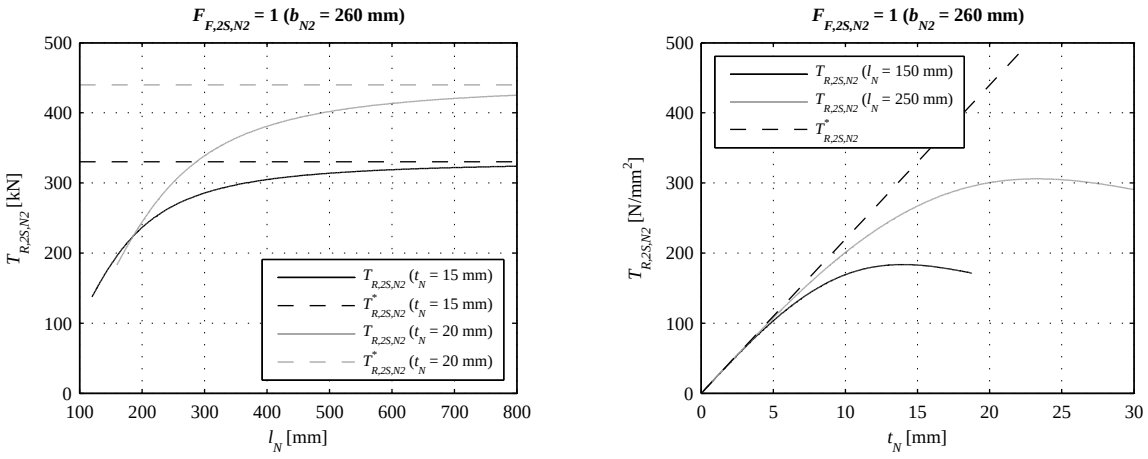

(a) (b)

Figure 3.30: Parametric study on the prediction of the shearing-off failure in beech LVL: (a) influence of the notch length l_N on the failure force of the second notch $T_{R,2S,N2}$ calculated according to Eq. 3.163, and comparison with $T^*_{R,2S,N2}$ calculated without the influence of $\sigma_{2z,N2}$ according to Eq. 3.162; (b) influence of the notch depth t_N on the failure force of the second notch $T_{R,2S,N2}$ calculated according to Eq. 3.163, and comparison with $T^*_{R,2S,N2}$ calculated without the influence of $\sigma_{2z,N2}$ according to Eq. 3.162

Fig. 3.31 shows the relationship between the vertical load q acting on the slab and the value of the failure function $F_{F,2S,Ni}$ according to Eq. 3.163. The vertical load q is calculated according to Section 3.3.3 from T_{Ni}. The load $q_{R,2S,Ni}$, which causes the shear failure of the LVL, corresponds to the intersection between the failure function $F_{F,2S,Ni}$ and the horizontal line $F_{F,2C,Ni} = 1$. These diagrams also show the shear failure load $q^*_{R,2S}$ calculated without the influence of the vertical stress according to Eq. 3.162. Fig. 3.31(a) refers to a notch length of 250 mm and Fig. 3.31(b) to a notch length of 160 mm. In both cases, the failure function is calculated for a notch depth of 15 and 20 mm.

For notch N2 (and basically for all notches except for the notch close to the support), an increase of l_N implies two opposing consequences:

- According to Section 3.3.3, the notch gets a higher force T_{Ni}. Therefore, the load q which causes the failure tends to decrease.
- On the other hand, as shown in Fig. 3.30(a), an increase of l_N has a positive influence on the shearing-off failure and contributes to increase T_{Ni} and q.

As shown in Fig. 3.31, according to the model of Fig. 3.28, in the notch close to the support (N1), the vertical pressure compensates the tensile stresses due to the eccentricity, and the prediction made with the Tensor Polynomial theory corresponds approximately to the load $q^*_{R,2S}$ calculated without the vertical stress according to Eq. 3.162. However, for the other notches of the composite member, the failure load $q_{R,2S,Ni}$ is considerably smaller than $q^*_{R,2S}$, and this tendency increases with decreasing notch length.

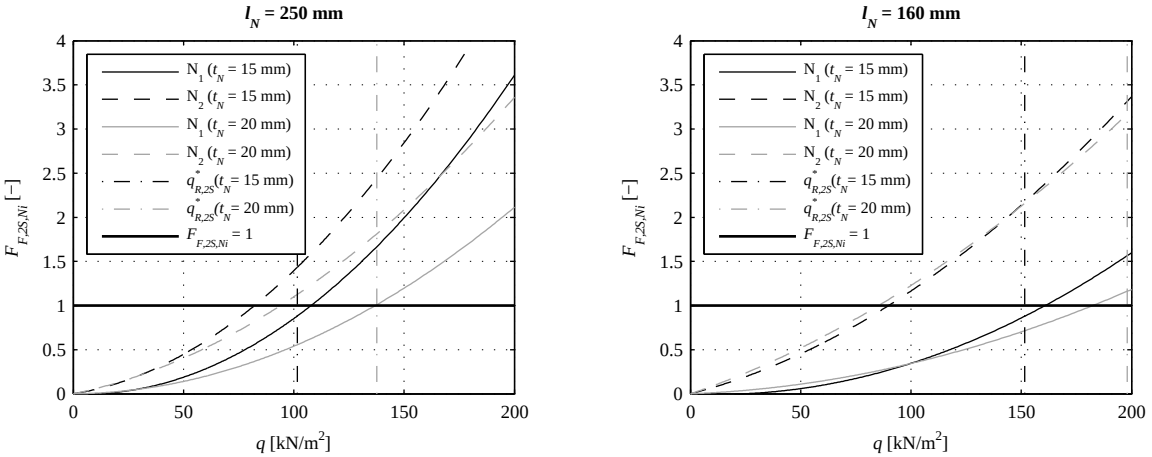

Figure 3.31: Relationship between the vertical load acting on the slab and the failure function of Eq. 3.163, and comparison with the failure loads obtained without considering the vertical stress: (a) notch length $l_N = 250$ mm; (b) notch length $l_N = 160$ mm

For the development of a timber-concrete composite slab made of a beech LVL plate with a notched connection, the following conclusions regarding the shearing-off failure can be drawn:

- The model and the strength criterion presented help to understand the influence of several parameters, but contain rough idealisations of reality. The uniform shear stress distribution over a length of $8t_N$ is a rough idealisation. Furthermore, the assumption of linear distribution of the stress perpendicular to the shear area over the entire length l_N is a simplification. Non-linearities and stress peaks may occur.
- The influence of tensile stresses perpendicular to the shear plane should be taken into account as it is accounted for in Eq. 3.163.
- The shorter and deeper the notches, the higher the influence of the tensile stress perpendicular to the shear plane generated by the eccentricity.
- For design purposes, since the shearing-off failure of LVL should be prevented, the positive influence of the vertical pressure on the behaviour of the notch close to the support (N1) should be neglected.

3.3.7 Failures of the timber cross-section

In a timber-concrete composite member, the timber cross section is subjected to axial tension, bending and shear (Section 3.2.3). For engineering applications, the following two failure modes are considered:

- combined tensile-bending failure of the cross-section
- shear failure of the cross-section

The equations to predict these failures are presented in Section 3.2.3. To design a LVL-concrete composite member with ductile notched connection, these failure modes should be prevented. In contrast to other connection systems, notches imply a local weakening of the timber cross-section, because they are cut out from the timber part. Thus, the cross section of the timber is locally reduced. A load-carrying capacity analysis of the timber cross-section should take into account this effect.

For design purposes, a simple and conservative approach to take into account this problem is to neglect the height of the timber corresponding to the notch depth (Fig. 3.32). In this way, the stress calculation is performed using a reduced cross-section of the timber part.

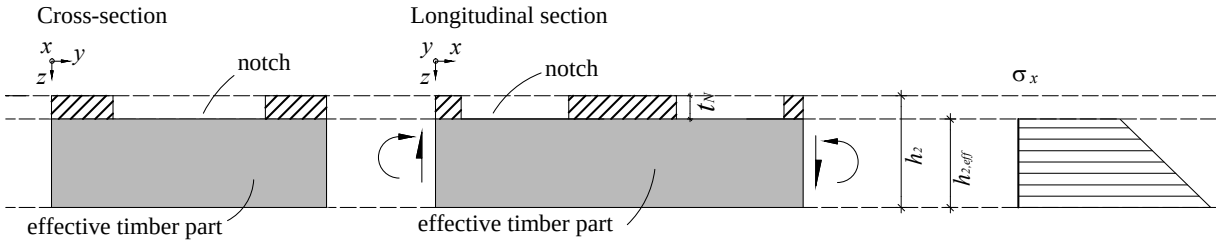

Figure 3.32: Simplified model to take into account the influence of notches in the load-carrying capacity analysis of the timber cross-section

3.3.8 Concrete failures close to the notch

Combination of shear and tension

In timber-concrete composite slabs with notched connections, the transfer of the shear forces in the concrete represents a critical point, in particular, if the notches are located in a zone where the concrete part is cracked. To develop a ductile timber-concrete composite slab, shear and flexural-shear failures of the concrete should be prevented because they are brittle. One of the main discussion points is if it is possible to design timber-concrete composite members with notched connections without vertical reinforcement in the concrete. To answer this question, a model to study the shear transfer in the concrete without vertical reinforcement is necessary.

As explained in Section 2.5.3, the development of a reliable model for the transfer of shear and tensile stresses in a concrete member without vertical reinforcement is considerably more difficult than in the case of a member with vertical reinforcement. The difference can be summarised as follows:

- If the concrete member is provided with a vertical shear reinforcement, the load-carrying mechanism can be modelled by means of a truss model: the reinforcement is subjected to tension, and the concrete to compression.

- If the structure lacks of vertical reinforcement, the shear and the tensile stresses are carried by the concrete, and the failure is governed by the crack layout, the tensile strength and the aggregate interlock of concrete. The tensile strength of concrete and the aggregate

interlock of cracks are subject to a high variability and the crack layout is difficult to predict. Thus, failure is challenging to predict.

The purpose of this section is to develop a simplified model to study the shear and flexural-shear failures in the concrete part of a timber-concrete composite slab with a notched connection lacking of vertical reinforcement, to understand its limits, and to judge its suitability for design. This model is based on the cantilever models (e.g. [73]) and does not take into account crack friction (i.e. diverges from the current state-of-art in reinforced concrete where accounting for shear on crack face has become common in members without shear reinforcement). Fig. 3.33 shows a sector of the concrete part separated from the timber part. The forces transferred in the notches are represented with T_{Ni} and the model assumes that the flexural-shear cracks are located close to the force transfer points of the notches. This crack configuration is based on experimental observations and, in the model, the cracks are assumed to grow with an angle of about 45° (Sections 4.2 and 4.4). The crack depth h_{cr} is calculated according to Eq. 3.28. The concrete layer is modelled with a series of cantilevers delimited by the flexural-shear cracks, fixed in the compression zone, and subjected to the notch forces T_{Ni}.

As shown in Fig. 3.33, each cantilever can be separated and the forces necessary for the equilibrium can be calculated. Then, the critical planes can be determined. In this case, they are indicated with the abbreviations 1V, 1S and 1F. The planes 1S and 1F are subjected to shear stresses τ_{1x} parallel to the plane and axial stresses σ_{1z} perpendicular to the plane generated by the eccentricity of the notch force T_{Ni}. In contrast, on the plane 1V, vertical shear stresses τ_{1z} and compressive axial stresses σ_x act. The shear stresses are assumed to be constant over the entire shear plane and the axial stresses due to the eccentricity of T_{Ni} are assumed to be linearly distributed over the plane.

In each plane, there exists a point, where the combination of axial and shear stress is critical. The identification of the critical points is shown is Figs. 3.34 and 3.35. In these critical points, the stress interaction is analysed using the modified Mohr-Coulomb failure criterion according to Marti [5] described in Section 2.5.2.
The equation of the line which describes the interaction between shear and compression is:

$$\tau = -\frac{3}{4}\sigma + \frac{f_{c,1}}{4} \tag{3.165}$$

The equation of the circle which refers to the interaction between shear and tension can be written as follows:

$$\left(\sigma + \frac{f_{c,1}}{2} - \frac{sin(\varphi) f_{t,1}}{1 - sin(\varphi)} - f_{t,1}\right)^2 + \tau^2 = \left(\frac{f_{c,1}}{2} - \frac{sin(\varphi) f_{t,1}}{1 - sin(\varphi)}\right)^2 \tag{3.166}$$

Where φ is the angle of the internal friction, $f_{c,1}$ is the compressive strength of concrete, and $f_{t,1}$ the tensile strength of concrete.

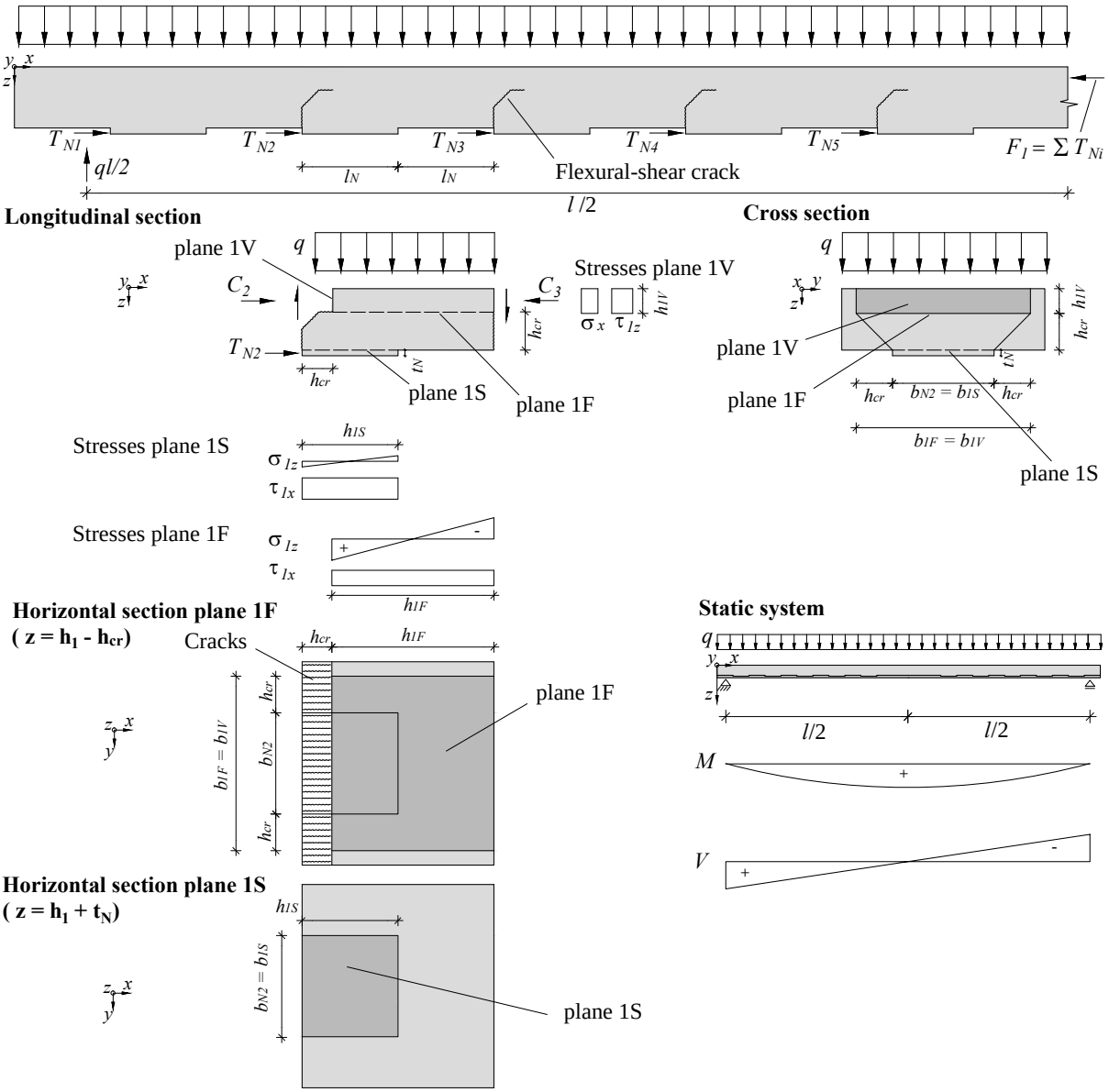

Figure 3.33: Cantilever model to describe the structural behaviour of the concrete part of a timber-concrete composite slab with a notched connection lacking of vertical reinforcement

As shown in Fig. 3.34, the failure in plane 1S can be simplified to a combination of shear and tensile stresses. The critical point for this stress combination is the notch edge close to the introduction of T_{Ni} because the tensile stress in this point is maximal. The failure load is estimated using Eq. 3.166. This failure does not depend on the layout of the flexural-shear cracks. Nevertheless, the distribution of the stresses over the entire notch length is a rough assumption.

The shear stress in the plane 1S can be estimated as follows:

$$\tau = \tau_{1x} = \frac{T_{Ni}}{b_{Ni} h_{1S}} \tag{3.167}$$

The tensile stress in the critical point of the plane 1S is due to the eccentricity of T_{Ni} in respect of the plane 1S and can be estimated as follows:

$$\sigma = \sigma_{1z} = \frac{3T_{Ni}t_N}{b_{Ni}h_{1S}^2} \tag{3.168}$$

By inserting Eq. 3.167 and Eq. 3.168 in Eq. 3.166, it is possible to estimate the notch force $T_{R,1S,Ni}$ which causes failure along plane 1S.

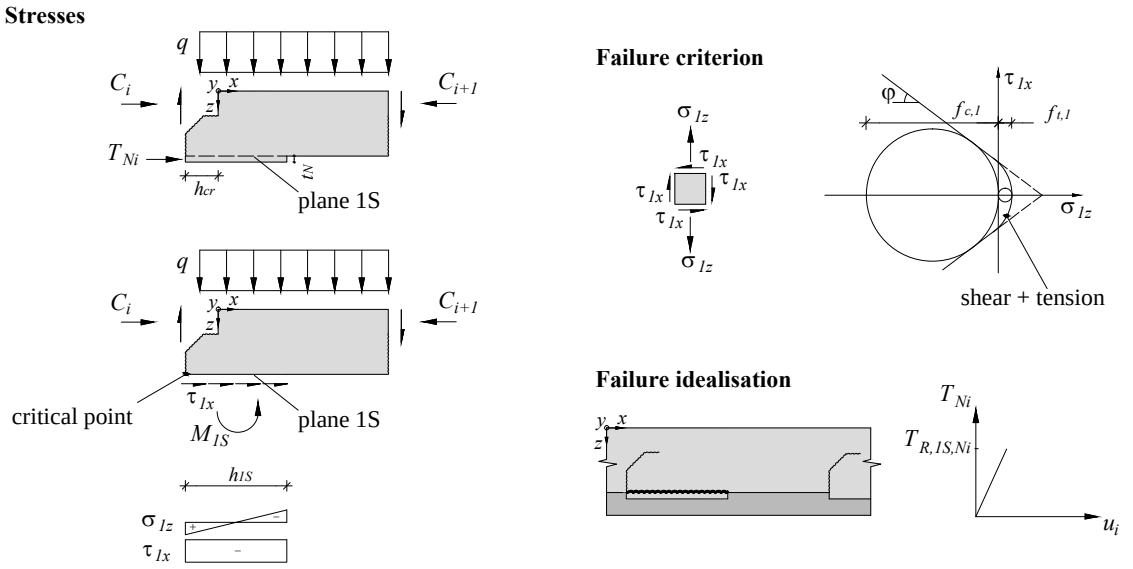

Figure 3.34: Concrete failure 1S

The failure along the plane 1F can be idealised as a sudden propagation of an existing flexural-shear crack due to a combination between shear and tensile stress according to Fig. 3.35. As summarised in Section 2.5.3, this mechanism was observed in reinforced concrete slabs without vertical reinforcement [68]. This failure is difficult to predict because it depends on the position and the length of the cracks.
The width of the effective area of the plane 1F can be estimated by means of two limits. If there is no load expansion in y-direction, the effective width of the plane 1F is:

$$b_{1F,inf} = b_{Ni} \tag{3.169}$$

Under the assumption of a load expansion of 45°, the effective width of the plane 1F is:

$$b_{1F,sup} = b_{Ni} + 2h_{cr} \tag{3.170}$$

Since it was observed that the cracks grow approximately in a diagonal way (Sections 4.2 and 4.4), the flexural-shear cracks are assumed to be inclined by 45°. The effective height of the plane 1F is simplified as follows:

$$h_{1F} = 2l_N - h_{cr} \tag{3.171}$$

The shear stress acting on the plane 1F can be estimated as follows:

$$\tau = \tau_{1x} = \frac{T_{Ni}}{b_{1F} h_{1F}} \tag{3.172}$$

The tensile stress in the critical point of the plane 1F can be estimated as follows:

$$\sigma = \sigma_{1z} = \frac{6 T_{Ni} \left(h_{cr} + \frac{t_N}{2} \right)}{b_{1F} h_{1F}^2} \tag{3.173}$$

The critical point of the plane 1F is subjected to a combination of shear and tension. Thus, by inserting Eq. 3.172 and Eq. 3.173 in Eq. 3.166, it is possible to estimate the notch force $T_{R,1F,Ni}$ which causes failure along the plane 1F.

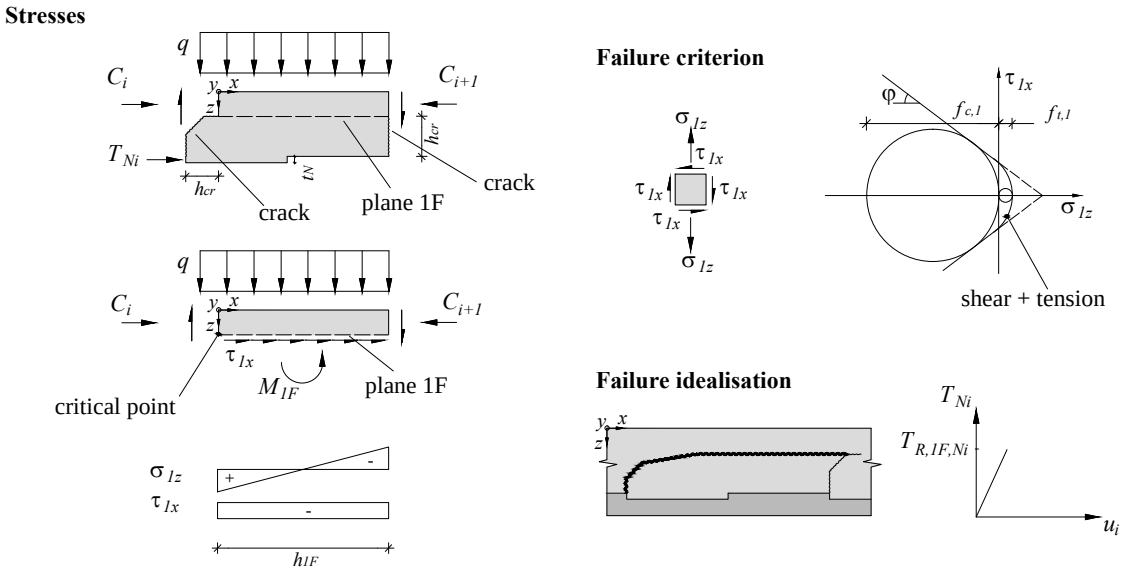

Figure 3.35: Concrete failure 1F

The model for vertical shear failure along the plane 1V is described in Fig. 3.36. In this zone, there is a combination of shear and compression stresses. Since, according to the Mohr-Coulomb failure criterion, the axial compression stresses have a positive influence on the shear failures, the worst case is represented by the areas close to the supports, where the compression stresses in the concrete are minimal. Therefore, in the following calculations, the axial compression stresses in the concrete are neglected.
According to Fig. 3.36, if the notch is subjected to a horizontal force T_{Ni}, the vertical shear force in the concrete $V_{1z,Ni}$, which ensures equilibrium, can be written as follows:

$$V_{1z,Ni} = T_{Ni} \cdot \frac{h_1^*}{2 l_N} \tag{3.174}$$

where h_1^* is the distance between the action points of the notch force T_{Ni} and the horizontal concrete compression forces C_i and C_{i+1}. For state II, this parameter can be calculated as follows:

$$h_1^* = h_1 - \frac{1}{3}x_{II} + \frac{t_N}{2} \tag{3.175}$$

The effective width of the plane 1V can be estimated by means of two limits:

$$b_{1V,inf} = b_{1F,inf} = b_{Ni} \tag{3.176}$$

$$b_{1V,sup} = b_{1F,sup} = b_{Ni} + 2h_{cr} \tag{3.177}$$

The shear stress acting in the plane 1V is:

$$\tau_{1z} = \frac{V_{1z}}{h_{1V} b_{1V}} \tag{3.178}$$

Since the concrete compression is neglected, the failure load can be estimated using the following equation:

$$\tau_{1z} = \frac{f_c}{4} \tag{3.179}$$

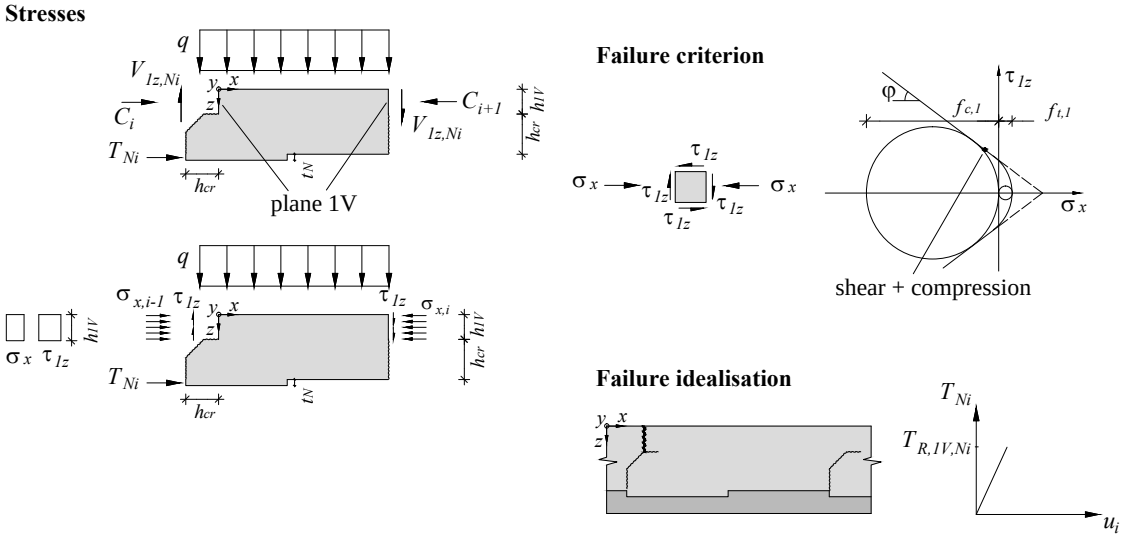

Figure 3.36: Concrete failure 1V

Figures 3.37 and 3.38 illustrate the influence of a variation of the geometric parameters of the composite member on the failure modes 1S, 1F and 1V predicted according to the model. The calculations are performed for the second notch (N2) of a timber-concrete composite slab made of a beech LVL plate and a concrete C50/60 according to the Swiss Standard SIA 262 [66] (Fig. 3.37(a)). The reason for the choice of such a high quality concrete is that the behaviour of the LVL-concrete composite members developed in this thesis should be governed by compressive failure of the LVL in the notch. Since the LVL and concrete are subjected to the same compressive stress in the notch edge, the compressive strength of the concrete must be

higher than the compressive strength of the beech LVL (Tab. 2.1). The thickness of the timber and concrete are varied, but the total thickness of the slab is constant and amounts to 200 mm.

Fig. 3.37(b) illustrates the influence of the notch depth t_N on the failure loads T_{Ni} of a composite member made of beech LVL with a timber thickness of 40 mm and a concrete thickness of 160 mm.

- The most sensible failure is the combined shear-tensile failure along the plane 1S because $t_N/2$ is the lever which generates tension due to the eccentricity of T_{Ni}.
- The concrete failures 1F and 1V are just slightly influenced because t_N, in the cases studied, represents only a small part of the lever.

Fig. 3.38 describes the influence of the notch length l_N on the concrete failure loads T_{Ni} of a composite slab made of beech LVL predicted with the model. Two cases are investigated: a timber thickness of 40 mm (Fig. 3.38(a)) and a timber thickness of 80 mm (Fig. 3.38(b)). From this parametric study, it results that the notch length influences the failures 1S, 1F and 1V in a marked way:

- The failure load $T_{R,1S,Ni}$ increases with increasing notch length l_N because the distribution of the shear and tensile stresses depends on this dimension (Eq. 3.167 and Eq. 3.168). Furthermore, this failure load does not depend from the thickness of the timber and concrete.
- The upper and the lower limit of the failure load $T_{R,1F,Ni}$ increase in a non-linear way with increasing notch length l_N because this dimension influences the distribution of the shear and tensile stresses. Furthermore, if the timber thickness increases and the concrete thickness decreases, the failure load $T_{R,1F,Ni}$ increases. The reason is that the concrete thickness determines the lever which causes the tensile stress in the critical point of the plane 1F. It has to be noticed that, for most of the notch lengths studied, this failure happens with the smallest failure loads.
- The upper and the lower limit of the failure load $T_{R,1V,Ni}$ increase in a non-linear way with increasing notch length l_N because the vertical shear force $V_{1z,Ni}$ generated by T_{Ni} is inversely proportional to l_N. The member with a timber thickness of 80 mm shows higher shear failure loads in plane 1V because the parameter h_1^* decreases and hence, $V_{1z,Ni}$ decreases too. The failures in the plane 1V are calculated by neglecting the concrete compression stresses. Nevertheless, these failures show very high failure loads in comparison to the other failures of the concrete.

In conclusion, the models presented are appropriate to understand the causes of the failures of the concrete, and the influence of several geometric and material parameters. However, the design of the notches of a timber-concrete composite member without vertical reinforcement based on these models is critical because of three reasons.

The first reason is the nature of the models. Although the models presented allow understanding the stress state of the concrete layer, they contain several factors, which are very

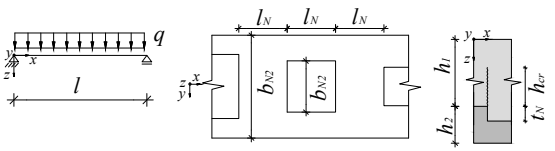

Parameters

Concrete	Geometry
C50/60	b = 530 mm
$f_{c,l}$ = 58 N/mm^2	$h_1 + h_2$ = 200 mm
$f_{t,l}$ = 4.1 N/mm^2	b_{N2} = 257 mm
	t_N = 15 mm
φ = 36.9°	

(a)

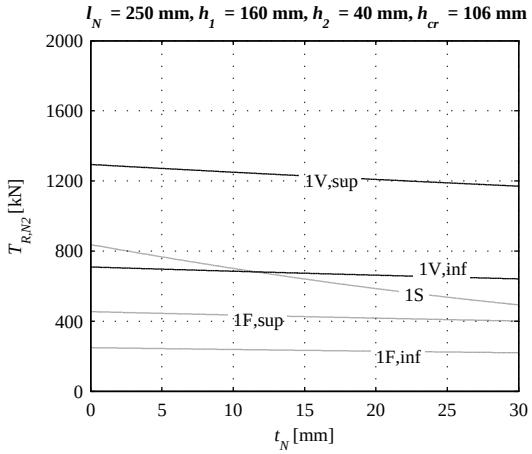

(b)

Figure 3.37: Parametric study on the prediction of shear and flexural-shear failures in the concrete: (a) parameters; (b) influence of the notch depth t_N

difficult to predict, in particular if the notched connection is located in a zone where the concrete is cracked. Although, during several experiments, the cracks were concentrated close to the notch edges (Sections 4.2 and 4.4), it is possible that, in reality, the cracks grow in a different way, or that internal stresses, which are very difficult to predict, cause modifications of the crack layout as well as the growth of new cracks. Therefore, since the cantilever model assumes a determinate crack layout, its application will imply significant uncertainties. Furthermore, there is probably a limited length for the distribution of σ_{1z} and τ_{1x} on the planes 1S and 1F, which is very difficult to quantify and is not taken into account by the model. In the model, h_{1S} and h_{1F} correspond to the maximum length available. Since these parameters govern section modules, their variation implies significant deviations in prediction. In addition, if the notch is very long (for instance $l_N = 400$ mm), probably, during the loading of the slab, also additional cracks between two notches might occur.

The second reason is that, in a timber-concrete composite member with a notched connection, the cracks are usually concentrated in the notch edges and, consequently, they tend to be wide. This implies the risk that there is no interlocking action which can contribute to the load-carrying mechanism. Thus, the shear resistance of the concrete part is based only on the tensile and shear strength of concrete, and a design without reinforcement becomes critical.

The third reason is that, if unexpected factors cause a shear or a flexural-shear failure, the slab fails in a brittle way and the consequences are dramatic. This may happen because of unexpected additional cracks or because of a load configuration which does not correspond to the model assumptions, like for instance an isolated concentrated force. This possibility makes a design without vertical reinforcement critical.

Therefore, although, according to the model, the notches of a timber-concrete composite member can be theoretically designed to prevent shear or flexural-shear failures in the concrete, it is recommended to provide vertical reinforcement. If the vertical reinforcement is designed to

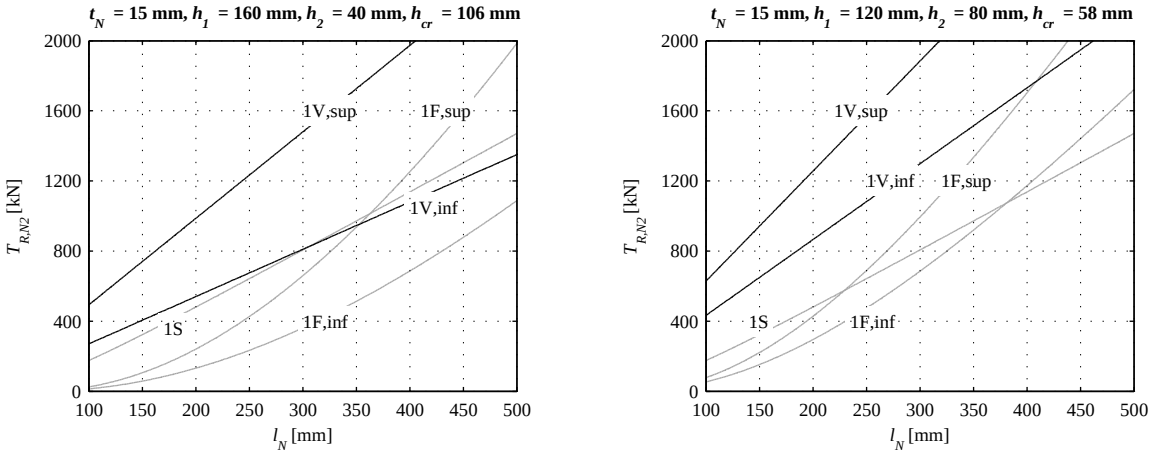

(a) (b)

Figure 3.38: Parametric study on the prediction of shear and flexural-shear failures in the concrete: (a) influence of the notch length l_N in the case of a timber thickness of 40 mm and a concrete thickness of 160 mm ; (b) influence of the notch length l_N in the case of a timber thickness of 80 mm and a concrete thickness of 120 mm

carry the vertical tension which occurs in the concrete, the system is able to activate a ductile load-carrying mechanism, and unexpected brittle failures are prevented.

Compressive failure

In a timber-concrete composite member with a notched connection, the transfer of the longitudinal forces necessary for composite action generates compressive stresses in the notch edges where the forces are transferred. Thus, both the timber and concrete are subjected to local compressive stresses close to the notch edges. If the compressive concrete stress exceeds the strength, failure of the concrete part of the composite member may occur.

The compressive stress state in the concrete depends on the geometric properties of the composite member and the vertical reinforcement installed. Fig. 3.39(a) shows the compressive stresses close to the notch edge acting on the concrete part of a composite member provided with vertical steel reinforcement as an example. If a composite member is provided with vertical steel reinforcement, the internal forces can be modelled by means of a truss model according to Section 3.3.2. The vertical reinforcement carries the vertical tension forces, and the concrete part is subjected to compression. The compressive force in the upper part of the concrete cross-section is transferred to the notch edge by means of a diagonal compressive strut C_i, which can be simplified as a concrete zone subjected to uniaxial stress. Fig. 3.39(a) represents a simplified stress field of a zone of the concrete layer close to the notch edge drawn according to Muttoni et al. [76]. As shown in Fig. 3.39(a), close to the notch edge, there is a concrete zone subjected to biaxial stress (node).

With regard to the compressive failure of the concrete, the critical zone is the smallest cross section area of the diagonal compressive strut, which usually corresponds to the interface

between the node and the diagonal strut. The situation of the node is more favourable because the restraint of transverse strain due to biaxial stress increases the compressive strength and the ductility of the concrete [76]. The failure criterion for the critical cross section area of the diagonal strut can be formulated as follows:

$$\sigma_i = \frac{C_i}{\frac{t_N}{\cos(\alpha)} \cdot b_N} = \frac{C_i \cdot \cos(\alpha)}{t_N \cdot b_N} = \frac{T_{Ni}}{t_N \cdot b_N} \leq f_c \tag{3.180}$$

The compressive failure of the diagonal strut is characterised by the formation of cracks parallel to the stress direction, which generates small plastic compressive strains followed by a softening process (Fig. 3.39(b)) [76]. The ductility of the compressive failure of such a diagonal compressive strut is much smaller than the plastic compressive deformations of LVL which occur in the notches (which can exceed 10 mm (Section 4.4)). Thus, since the LVL and concrete are subjected to the same contact pressure close to the notch edge, compressive failure of the concrete must be prevented by choosing a concrete with a compressive strength which is higher than the compressive strength of the LVL parallel to the grain.

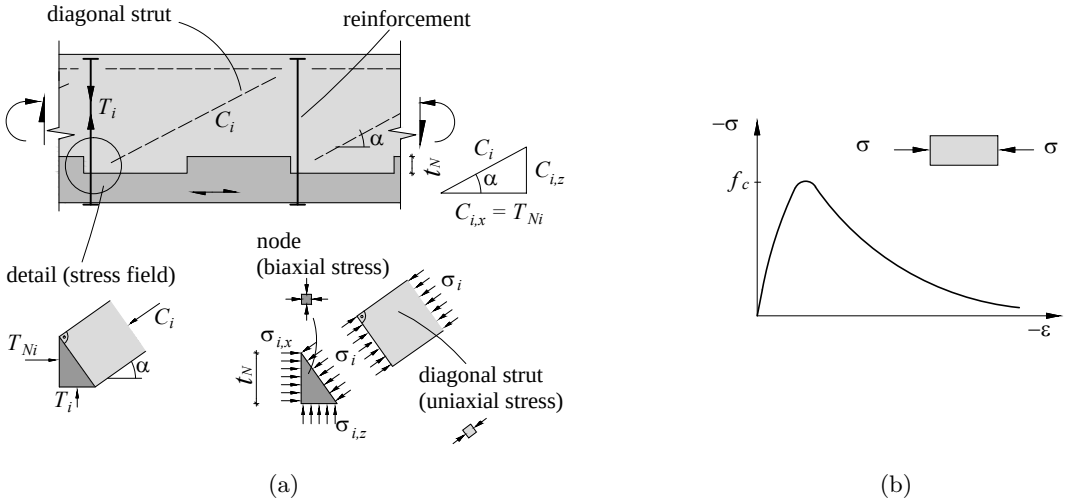

Figure 3.39: (a) Compressive stress acting in the concrete close to the notch edge of a composite member with vertical reinforcement; (b) stress-strain relationship of a concrete member subjected to uniaxial compression [76]

3.3.9 Secondary effects during notch yielding (states III and IV)

If a timber-concrete composite member with a notched connection is designed so that a compressive failure of the timber in the contact areas of the notches is governing, secondary effects due to local plastic deformations of the timber can compromise the structural behaviour and the ductility of the system during the plastic phase.

Firstly, since the concrete is more rigid than the timber and is brittle when subjected to tension, it is not able to follow the compressive plastic deformations of the timber part. If two notches close to each other develop slightly different plastic deformations, the existing concrete

cracks tend to open and to become longer. This crack propagation can cause problems with the shear transfer in the concrete and cause it to fail. This failure determined the end of several experiments (Section 4.4). Fig. 3.40 illustrates a timber-concrete composite member where notch N3 develops a larger plastic deformation than notch N4. The consequence is that the existing flexural-shear crack, close to the edge of notch N4, grows. The problem of the different plastic deformations of the notches is difficult to predict because it can be influenced by several factors. These include the position of the compression zone, the crack height, and the load position, which, in reality, can deviate from the distributed load assumed in the model.

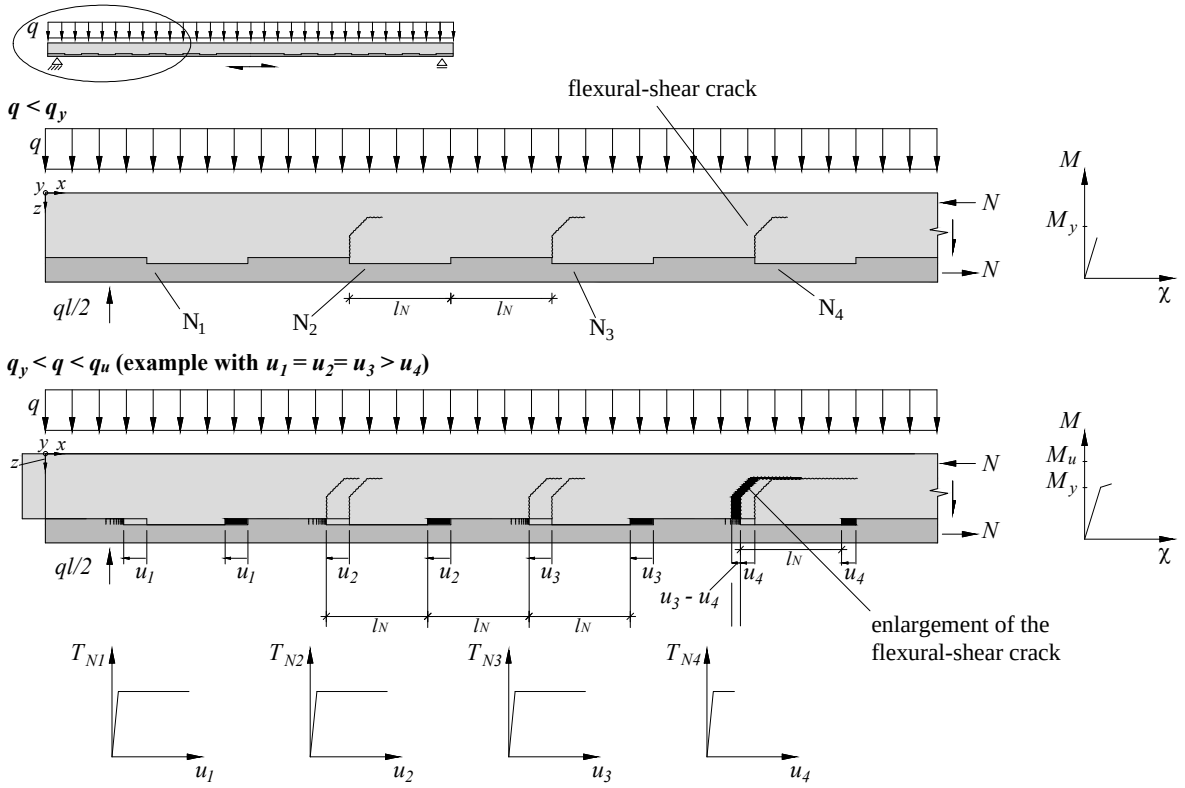

Figure 3.40: Enlargement of the existing cracks due to plastic compressive deformations of the timber

Secondly, during yielding of the notches, a vertical opening of the gap between the timber and concrete may occur and compromise composite action (Fig. 3.41). This was observed during the plastic phases of composite members with notched connections, tested in bending with uniformly distributed vertical loads (e.g. Section 4.4). This gap opening is difficult to quantify and to predict, but is likely caused by a combination of the following phenomena:

- The compressive failure of the timber in the notch in the longitudinal direction causes a volume expansion of the timber in vertical direction, which pushes the concrete part of the composite member out of the notch (Fig. 3.41(a)).

- The notch edge subjected to compression yields, and hence, the concrete may slide out of the notch (Fig. 3.41(b)). This phenomenon was observed by Frangi and Fontana [2]

during shear tests on notches. The plastic deformation capacity of the notches without mechanical fasteners was limited by the sliding out of the concrete.

- The crack opening, described previously, causes a sort of hinge in the concrete part of the composite member. Therefore, the concrete tends to bend in an angled way, whereas the timber part bends in a parabolic way (Fig. 3.41(c)).
- During state IV, a plastic zone develops, in which rotation of the cross-section occurs (Fig. 3.41(d)). Due to the yielding of the interface, the compressive strain of the concrete increases until a value of about $\varepsilon_{u,1} \approx 0.003$. According to Section 3.2.5, the behaviour can be simplified by assuming that the plastic zone behaves like a hinge, and the other zones of the slab tend to rotate like rigid bodies. Therefore, if the two parts of the composite member are not connected vertically, the gap tends to open. The reason is that the timber part is a continuum and tends to bend following a parabola.

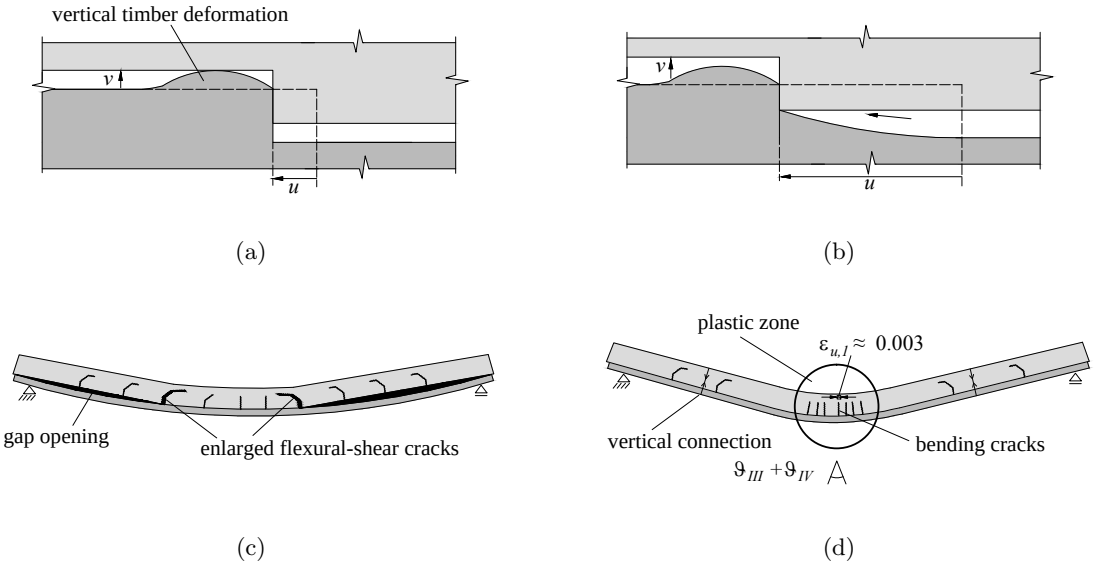

Figure 3.41: Causes of gap opening during plastic deformation of the notches (states III and IV); (a) vertical extension of the timber due to a longitudinal compressive failure; (b) sliding out of the concrete part due to deformations of the contact area; (d) enlargement of flexural-shear cracks; (c) local rotation of the plastic zone

These secondary effects, which occur during yielding of the notches, represent a problem because they may compromise the structural behaviour of the composite member. Since notch yielding is characterised by large deformations under large loads, these secondary phenomena are very unstable and difficult to predict. One solution is to provide end-to-end vertical reinforcement to:

- transfer the vertical tension in the concrete even if the cracks occur due to notch yielding and to keep these cracks closed
- prevent gap opening after compressive failure of the timber

Further details of this reinforcement are illustrated in Sections 3.3.10 and 3.3.11.

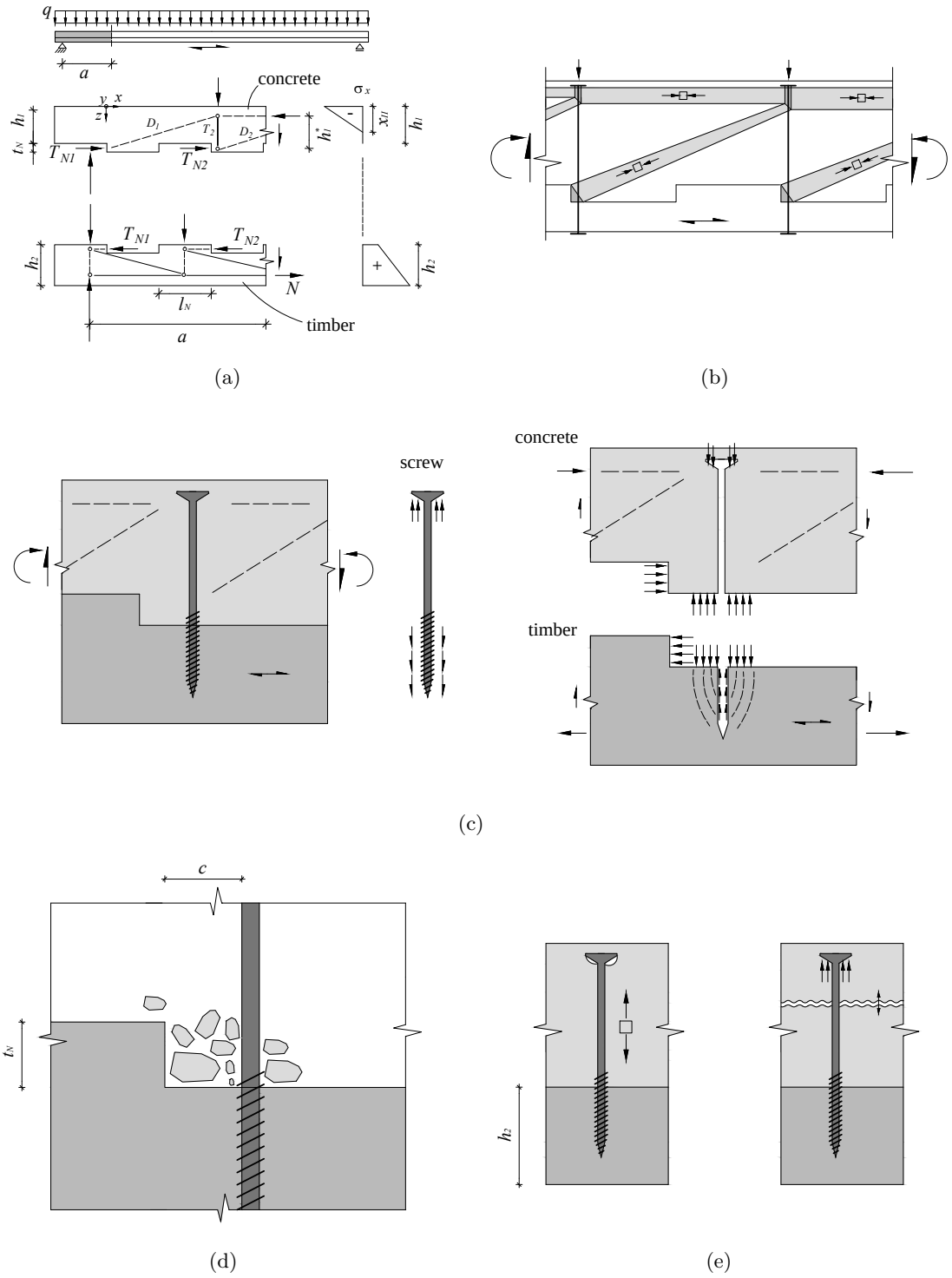

Figure 3.42: Vertical reinforcement to carry the vertical tension in the concrete: (a) truss model according to Section 3.3.2; (b) qualitative stress field in the concrete generated by the vertical reinforcement; (c) internal forces acting on a notch with a screw; (d) minimum distance between the notch edge and the vertical reinforcement; (e) activation of the screw after concrete cracking

3.3.10 Vertical reinforcement to carry the vertical tension in the concrete

The vertical reinforcement has to be designed to carry the vertical tension which occurs in the concrete part of the composite member. When the vertical reinforcement becomes active, the load-carrying mechanism in the concrete acts as a truss. This section presents a simple method to design such reinforcement.

The first issue is the position of the vertical reinforcement. Fig. 3.43(a) shows a composite member with notched connections cut free between the support and the mid-span. As illustrated in Section 3.3.2, the notches carry the longitudinal forces T_{Ni} to ensure composite action. As explained in Section 3.3.8, a notch subjected to a force T_{Ni} can be modelled as a cantilever fixed in the compression zone (Fig. 3.43(a)). Therefore, the impact of vertical steel reinforcement on the notch can be compared to the effect of longitudinal tensile reinforcement in a console.

Figs. 3.43(b), 3.43(c) and 3.43(d) show a qualitative representation of the influence of a vertical steel reinforcing bar on the structural behaviour of a concrete notch located between the left support and the mid-span of a composite member, subjected to a positive bending moment. The stresses represented are greatly simplified and are derived from theoretic considerations. Fig. 3.43(b) represents the elastic stresses and strains in z- direction due to the notch force T_{Ni} when the concrete is elastic and uncracked in x-direction. It can be seen that the maximal elastic tensile stress occurs close to the left edge of the notch. As in all reinforced concrete structures, the tensile reinforcement must be placed where the tensile stresses are maximal, so that the reinforcement is ready to carry the tensile stresses after the concrete begins to crack. Furthermore, the lever which generates the resisting moment is maximal here. Fig. 3.43(c) shows the elastic-cracked state, in which only the vertical steel reinforcement carries the tension, and the tensile stress in the steel is smaller than the yielding limit. The plastic state is shown in 3.43(d): the steel reinforcement yields and the stresses in the concrete redistribute. Thus, vertical reinforcement should be placed where the tensile stresses in the concrete are maximal. If the reinforcement is installed in a different position, the crack has to open more before the reinforcement carries tension.

To be able to carry tensile stresses, the reinforcement must be anchored in the compression zone (3.42(b)). Furthermore, between the reinforcement and the notch border, a minimum spacing, which depends on the maximum aggregate size, must be respected, according to Fig. 3.42(d).

When the position of the vertical reinforcement is determined, the composite member can be cut free, and truss models can be drawn according to Section 3.3.2, as shown in Fig. 3.42(a). As explained in Section 3.3.2, the vertical tensile force in the concrete T_i, carried by the vertical reinforcement close to notch Ni, corresponds to the vertical shear force in the concrete (V_1) close to this notch and to the vertical component of the compression diagonal D_i. The simplest way to calculate the tensile forces of the reinforcement is to determine the notch forces T_{Ni} according to Section 3.3.3 by integrating the elastic shear stresses at the interface. As shown in Section 3.3.2, since a horizontal force T_{Ni} is transferred in notch Ni, the tensile force in the concrete T_i can be calculated by considering the equilibrium of the node of the truss model close to notch Ni as follows:

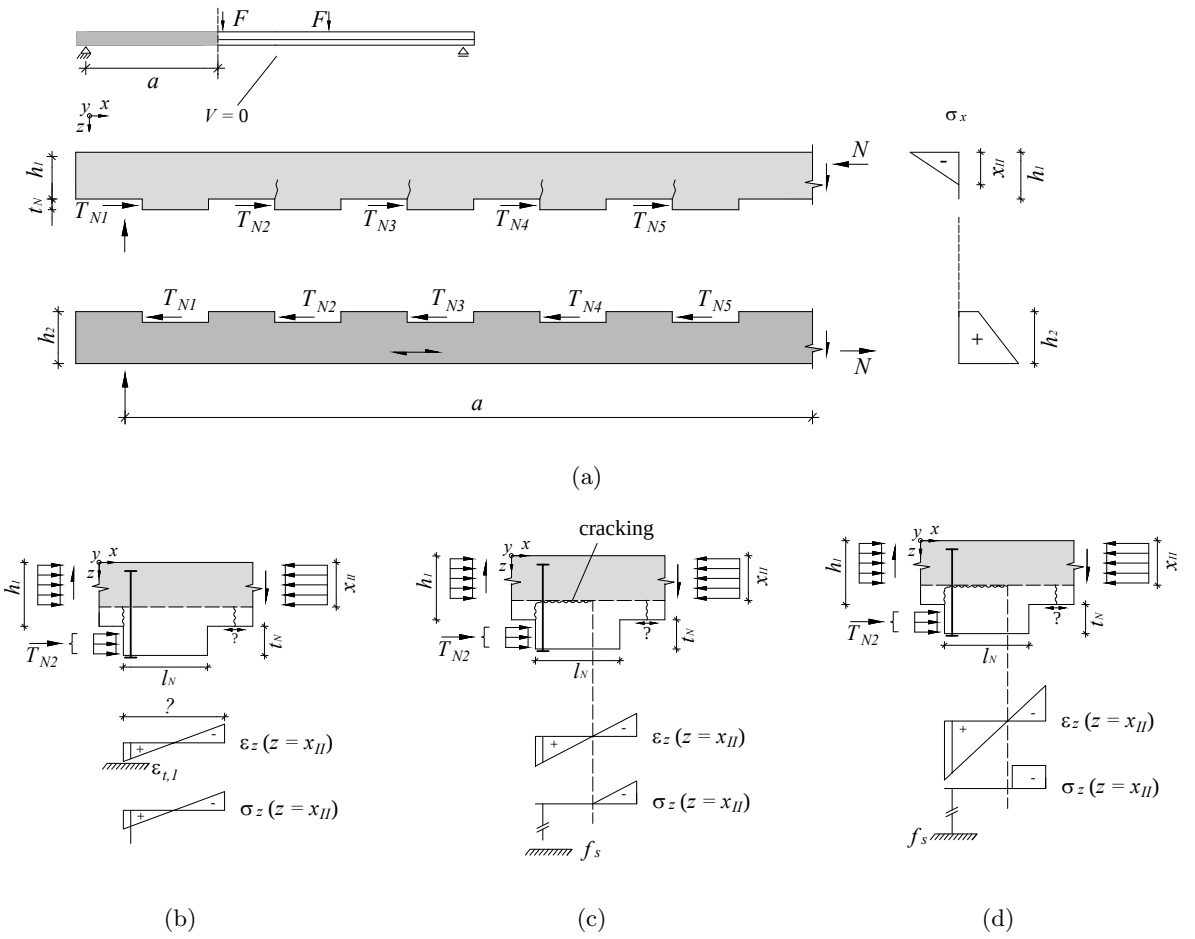

Figure 3.43: Stresses and strains in the concrete and in the vertical reiforcement due to the horizontal shear force T_{Ni}: (a) timber-concrete composite member with notched connections cut free between the left support and the mid-span; (b) elastic uncracked state; (c) elastic cracked state; (d) plastic state

$$\sum F_y = 0 \Rightarrow T_i = T_{Ni} \cdot \frac{h_1^*}{s} \tag{3.181}$$

where s is the distance between two points where the notch force T_{Ni} is introduced and h_1^* is the distance between T_{Ni} and the resulting compression in the concrete, calculated in Eq. 3.111.

The steel area, which is needed to carry the vertical tension T_i due to T_{Ni}, can be calculated as:

$$A_{s,T,Ni} = \frac{T_i}{f_s} = \frac{T_{Ni} \cdot h^*}{s \cdot f_s} \tag{3.182}$$

where f_s is the tensile strength of the reinforcement.

The critical cross-section of the diagonal compression strut is located close to the notch edge and can be estimated with the notch depth. Therefore, the problem can be reduced to the failure 1C,n, explained in Section 3.3.8.

In the case of a timber-concrete composite member with common notch dimensions at the ultimate limit state, the presence of a vertical reinforcing bar in z-direction generates a direct

bracing like in a short console (Fig. 3.42(b)). However, if the compressive diagonal strut were to be long and have a small angle to the tensile reinforcement, the load-carrying capacity would be compromised by concrete cracks. For practical dimensions, this is not the case. This means that, if a timber-concrete composite member with a notched connection is provided with a sufficient area of vertical steel $A_{s,T,Ni}$, shear failures (1S and 1V) and flexural-shear failures in the concrete (1F) are unlikely to occur.

Fig. 3.42(c) shows a detailed qualitative representation of the load transfer in a notch with a screw fixed in the timber under the assumption that the screw does not transfer shear (the dowel action is neglected). In this case, the timber can be idealised as the lower head of the screw. The horizontal component of the diagonal concrete strut corresponds to T_{Ni} and is transferred to the timber part through the notch edge. In contrast, the vertical component of the diagonal strut pushes the timber plate vertically. This vertical component is transferred to the screw through the screw thread. The screw transfers the vertical component to the concrete by means of the pressure of the head. Therefore, all timber stresses generated by the screw are locally in equilibrium. However, the screw and the thickness of the timber part should be designed to prevent a pull-out failure perpendicular to the grain. Furthermore, in reality, the screws represented in Fig. 3.42(c) carry a part of the horizontal shear stresses, which occur between the two layers.

If this reinforcement is provided by means of screws, the load is transferred from the concrete to each screw by means of compressive contact in the head. Since the fresh concrete is subjected to gravity, it is possible that a small gap exists below the head of each screw. Therefore, in this case, the screw becomes active only after the concrete makes a determinate deformation, and it can happen that the screw begins to carry the tensile force only after cracks occur (Fig. 3.42(e)).

Even though, in the ductile LVL-concrete composite members developed in this thesis, vertical steel reinforcement (e.g. screws) is recommended, it makes no sense to use this type of reinforcement as a shear connector. The shear flow between the two parts of the composite member should be carried by the notches, and the reinforcement should carry the vertical forces. The first reason is that screws as shear connectors are markedly less stiff than notches [18]. The consequence is an increase of the deformations of the composite member at the service level. The second reason is that the ultimate shear deformation capacity of nails and screws, installed as timber-concrete shear connections [86], is smaller than the maximum plastic deformation of the timber subjected to compression in the notches [2], [87]. Therefore, the plastic shear deformations of nails and screws will contribute to the ductility of the composite member in a less effective way than notches.

Reinforced concrete structures should be provided with a minimum amount of reinforcement. The most important reason is to prevent brittle failure as soon as the concrete cracks. When a crack occurs, the reinforcement must not yield. Otherwise, since the reinforcement would be in plastic conditions, it would not be able to carry the necessary tensile forces, and hence, a brittle failure would occur. For conventional reinforced concrete structures subjected to bending, analytical models to assess the minimum longitudinal reinforcement are well-established [88].

For vertical shear reinforcement, due to the higher complexity of the shear-carrying mechanism, semi-empirical equations are used (e.g. [74]).

For timber-concrete notched connections with vertical steel reinforcement, the same principle should be valid. In this section, a simplified analytical model to understand the most important factors, which influence the minimum vertical reinforcement, is presented. The horizontal cracks are assumed to open when the tensile stress exceeds the tensile strength of the concrete, according to the cantilever model shown in Fig 3.35.

Since, until the end of the elastic uncracked state, the tensile force carried by the steel is not relevant in comparison to the tensile force carried by the concrete, the influence of the reinforcement is neglected. Hence, the notch force $T_{N,cr}$, which causes concrete cracking, can be estimated according to Fig 3.35 as follows:

$$T_{N,cr} \approx \frac{b_{1F} \cdot h_{1F}^2 \cdot f_{t,1}}{6 \cdot (h_{cr} + t_N/2)} \tag{3.183}$$

The horizontal notch force $T_{N,y}$, which occurs when the concrete is cracked and the vertical reinforcement yields, can be estimated according to Eq. 3.182 as follows:

$$T_{N,y} \approx A_s f_y \cdot \frac{s}{h^*} \tag{3.184}$$

To prevent brittle failure, the following condition should be valid:

$$T_{N,y} \geq T_{N,cr} \tag{3.185}$$

By inserting Eq. 3.183 and Eq. 3.184 in Eq. 3.185, the minimal amount of vertical reinforcement close to notch i can be calculated as follows:

$$A_{s,min} \approx \frac{h^* \cdot b_{1F} \cdot h_{1F}^2}{6 \cdot s \cdot (h_{cr} + t_N/2)} \cdot \frac{f_{t,1}}{f_s} \tag{3.186}$$

This approach could be the starting point to develop a reliable criterion. However, some significant simplifications are made. First of all, the crack position and the effective part of the concrete which carries the stresses are unknown and must be assumed. Secondly, the interaction between the tensile and the shear stresses in the concrete is neglected. In reality, as previously described by means of the Mohr-Coulomb failure criterion, shear stresses acting in the critical zone facilitate crack opening. However, a calculation neglecting the shear leads to a safe design of the minimum reinforcement.

In conclusion, this section provides a simple method to decide the position and the amount of reinforcement. The approach presented is based on theoretic considerations and analogies to the current models available to design reinforced concrete members [76]. However, to validate the models presented, further theoretic and experimental analyses are needed.

3.3.11 Vertical reinforcement to prevent gap opening

The amount of vertical reinforcement necessary to prevent gap opening can be estimated based on the maximum deflection w_u, which the composite slab should theoretically reach. It is

assumed that, at mid-span, there is an enlarged crack, and, consequently, the concrete layer deforms in an angled way, whereas the timber plate bends as a parabola (Fig. 3.44). The reason for this conservative assumption is that it is very difficult to estimate the length of the sector in which the gap opens.

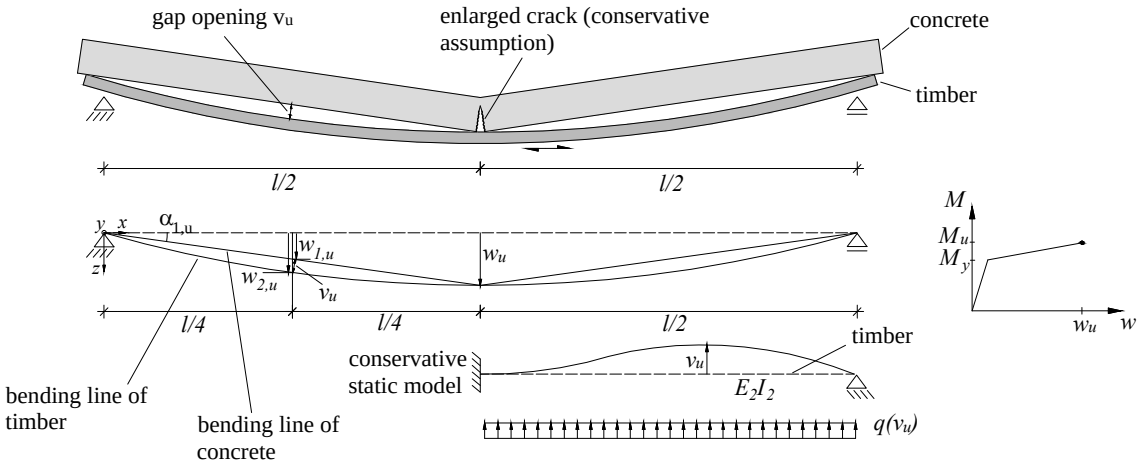

Figure 3.44: Model to deign vertical reinforcement to prevent gap opening

The angle of the concrete deformation is:

$$\alpha_{1,u} = \arctan(\frac{w_u}{l/2}) \tag{3.187}$$

Since it is assumed that the timber part of the composite member bends as a parabola, the angled deformation of the concrete part causes a gap opening which can be idealised as the projection v_u of the difference between the deflection of the timber $w_{2,u}$ and the concrete $w_{1,u}$ at $x = l/4$:

$$v_u = (w_{2,u} - w_{1,u}) \cdot \cos(\alpha_{1,u}) = \left(\frac{3}{4} \cdot w_u - \frac{1}{2} w_u\right) \cdot \cos(\alpha_{1,u}) \tag{3.188}$$

Since the bending stiffness of the concrete part is usually greater than that of the timber part, an upper bound for the required force can be determined by applying a vertically distributed force $q(v_u)$ on the timber part, which deforms it by v_u. If it is assumed that the timber plate has a hinge at the support and is rigidly fixed at mid span (Fig. 3.44), $q(v_u)$ can be estimated as follows:

$$q(v_u) = v_u \cdot \frac{369}{2} \cdot \frac{E_2 I_2}{(l/2)^4} \tag{3.189}$$

Finally, the steel reinforcement which is necessary to prevent the gap opening of the slab element can be estimated as follows:

$$A_{s,v} = \frac{q(v_u) \cdot l}{f_s} \tag{3.190}$$

3.3.12 Design strategies to achieve ductility

As a conclusion of the analytical models presented in this chapter, this section illustrates a design procedure to achieve ductility in a timber-concrete composite member with a notched connection.

A timber-concrete composite member with a notched connection shows a ductile behaviour if a compressive failure of the timber inside the notch is governing. This means that the ultimate load in plastic conditions q_u, calculated according to the model presented in Section 3.2.5, must be smaller than the loads corresponding to all the unwanted failure modes of the composite member. To achieve this, it makes sense to use LVL materials instead of solid wood or glued laminated timber, so that the failures of the timber part can be predicted with sufficient accuracy. According to Fig. 3.45(a), the failures of a timber-concrete composite member with a notched connection made of LVL should be designed to occur in the following order:

- Initially, the entire structure is elastic, and the concrete does not exhibit cracks. Then, when the critical tensile stress of the concrete is reached, which mainly depends on the geometrical properties of the cross-section, cracks occur. The corresponding bending moment is named M_{cr}. This occurrence mainly depends .

- Afterwards, yielding of the notches should occur. This means that the bending moment $M_{R,2C}$, which causes a compressive failure of the LVL, should be the smallest of all failure moments of the composite member ($M_y = M_{R,2C} = min\{M_{R,i}\}$). After that, the curvature of the cross-section begins to increase.

- Then, the compressive strength of the concrete $f_{c,1}$ should be reached at the top of the cross-section, making the end of the elastic behaviour of concrete ($M_{1C,c}$). After that, both the notches and the compression zone of concrete behave in a ductile way.

- The ultimate failure of the composite cross-section should be governed by the ultimate compressive strain of concrete ($\varepsilon_{u,1} \approx 0.003$) on the top edge of the concrete cross-section ($M_u = M_{1C,u}$). This should cause a delamination of the concrete followed by a load decrease and a further increase of the curvature.

- Eventually, the increase of the curvature after the concrete failure causes a combined bending-tensile failure of the LVL cross-section (2BT). The ductility of this composite system is limited by the rotation capacity of the LVL.

As illustrated in Section 3.3.9, a sufficient amount of vertical end-to-end reinforcement must be provided to ensure ductility. The slab should contain $A_{s,v}$ to prevent gap opening plus $A_{s,T,Ni}$ to carry the vertical tension in the concrete. It is important to note that the model calculates q_y and q_u without taking into account a hardening of the notch during the compressive failure of the LVL (2C). In reality, during compressive tests, a hardening of the LVL can be observed. Thus, the load-carrying capacity of the vertical reinforcement must have a reserve in comparison to the load q_u calculated by the model. It is suggested to calculate the forces T_i from the notch

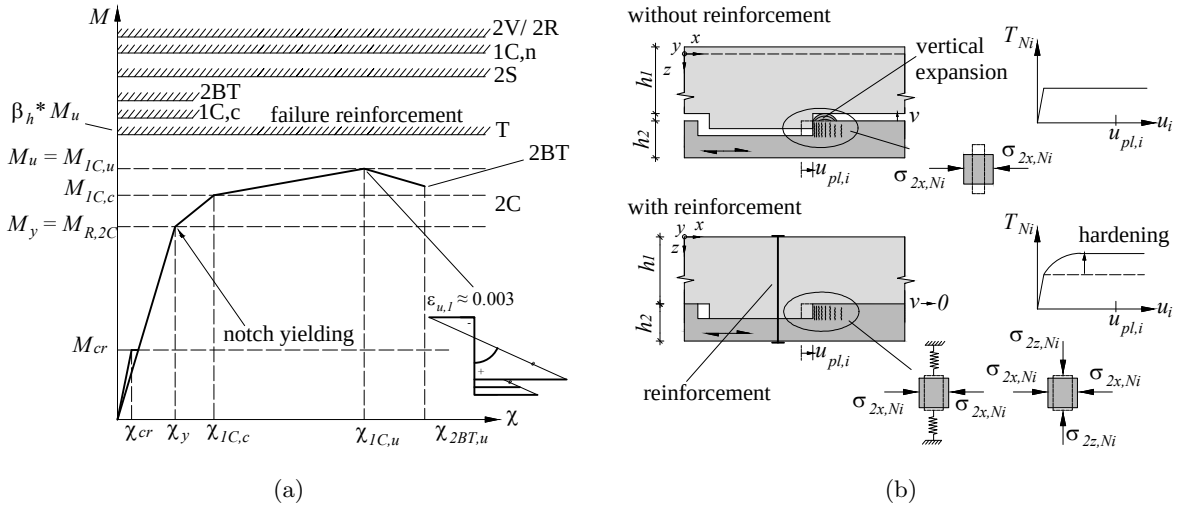

Figure 3.45: (a) Design strategies to achieve ductility; (b) restraint due to vertical reinforcement

forces $T_{Ni} = f(\beta_h \cdot q_u)$ where β_h is a factor, which takes into account the hardening phenomena during the compressive failure (Fig. 3.45(a)).

Thirdly, it must be ensured that the vertical reinforcement allows the plastic deformations of the LVL:

- This means that the horizontal shear forces T_{Ni} must be carried mostly by the notches, and the vertical reinforcement should carry the vertical forces almost exclusively. Thus, the vertical reinforcement must be as soft as possible if subjected to shear parallel to the interface. This aspect can be quantified with the theory of Johansen [80], as shown by Frangi [25]. For instance, screws should be as slender as possible.

- Since a compressive failure of the LVL part of the composite member implies significant horizontal relative displacements at the interface, the end-to-end vertical reinforcement must be able to follow these deformations without failing due to shear. A high slenderness of the screws would contribute to fulfil this requirement. However, as shown by Timmermann and Meierhofer [86], the ultimate deformation capacity of screws and nails ($0.3 - 1.4$ mm) is markedly smaller than the expected compressive plastic deformations of the LVL in the notches, which reach more than 10 mm (Fig. 4.31). This means that the vertical reinforcement should be provided with additional elements, which allow the development of high relative displacements between the two parts of the composite member.

- The compressive failure of the LVL parallel to the grain implies a volume expansion in the vertical direction. As illustrated in Fig 3.45(b), if a vertical reinforcement prevents gap opening during yielding of the LVL, a restraint $\sigma_{2z,Ni}$ can develop. This causes a hardening in the notch behaviour which has to be added to the hardening which usually occurs during a compressive failure of the LVL. Thus, if the vertical reinforcement is too stiff under tension or is pre-stressed, ductility can be compromised.

3.3.13 Gap opening during state II

In many cases, in particular during four-point bending tests, a gap opening was already observed during the elastic states (I and II) (e.g. [33], [89]). Gap opening may directly cause collapse of the composite member, or facilitate other failure modes. For instance, in the timber part of a timber-concrete composite member with a notched connection, if the gap opens, the eccentricity between the notch force and the notch bottom increases, and thus, the tensile stresses in the timber perpendicular to the grain increase. As a consequence, a shearing-off failure is facilitated. However, this phenomenon is difficult to treat and there is no agreement about its causes.

As illustrated in Section 2.3.5, the existing studies assess several reasons for gap opening in a composite system, such as differential bending deflections of the parts [19], different deflections due to shear [43], and eccentricity between the interface and the centroids of the parts [43]. However, these phenomena are difficult to predict because they depend on the connection type, the geometry and the material properties. In reality, a combination of these effects probably occurs.

This section focuses on the uplift due to the eccentricity between the centroids of the members and the interface, which was qualitatively explained by Chapman [43]. This phenomenon is difficult to quantify, because it strongly depends on the boundary conditions, but can be understood with the simplified model presented in this section. Fig 3.46 shows a timber-concrete composite member with a notched connection subjected to four-point bending as an example. In this composite member, there are no connections which are able to carry vertical tensile stresses in the interface. The shear forces T are transferred through the notches and are in equilibrium with the axial forces N. The eccentricity in z-direction h_i^* between the interface and the action points of the axial forces causes bending of the parts of the composite member. The simplified model illustrated in Fig 3.46 only considers the forces in x-direction acting in the zones subjected to shear. To simplify the calculations, it is roughly assumed that the considered part of the slab is simply supported.

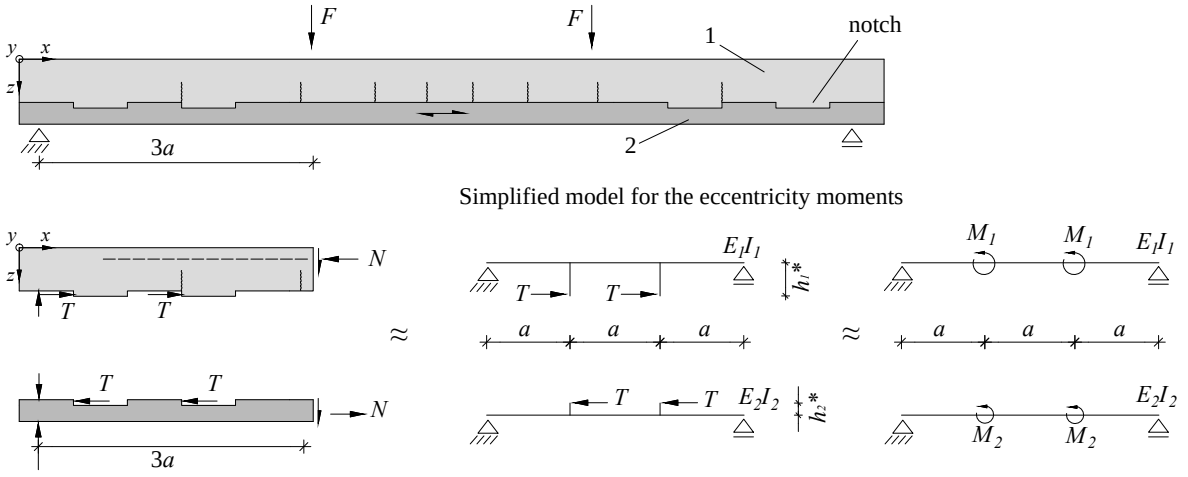

Figure 3.46: Simplified model to understand the gap opening during state II

The distances in z-direction between T and N cause bending moments in the parts of the composite member. Since the eccentricities h_i^* are different, the moments M_i are different:

$$M_i = T \cdot h_i^* \tag{3.191}$$

These moments M_i due to the eccentricity cause bending moments and curvatures in the parts of the composite member. For the simplified situation of Fig. 3.46, the bending deformations of the members can be calculated with the equation of kinematics according to Fig. 3.47.

As shown in Fig. 3.47, the maximum vertical displacement δ_i due to M_i, which takes place at a distance of $3/4 \cdot a$ from the supports, is calculated as:

$$\delta_i = \int \overline{M} \cdot \frac{M_i}{E_i I_i} dx = \frac{115 \cdot M_i a^3}{1152 \cdot E_i I_i} \tag{3.192}$$

Since the two parts of the composite member are subjected to different bending moments and have different geometrical and mechanical properties, they tend to exhibit different deformations δ_i, which can cause a gap opening. These phenomena take place mainly in the zones of the slab where connection forces are transferred. For instance, in the case of a composite member subjected to four-point bending, the gap opening due to these deformations will occur between the supports and the load.

The form of the bending line and the values of the displacements of the parts of the composite member due to the eccentricity significantly depend on the boundary conditions, the number of connections and the distance between the connections. Therefore, it can be concluded that this phenomenon exists, but it is very difficult to quantify. A pragmatic solution is to install vertical reinforcement which connects the two layers of the composite member.

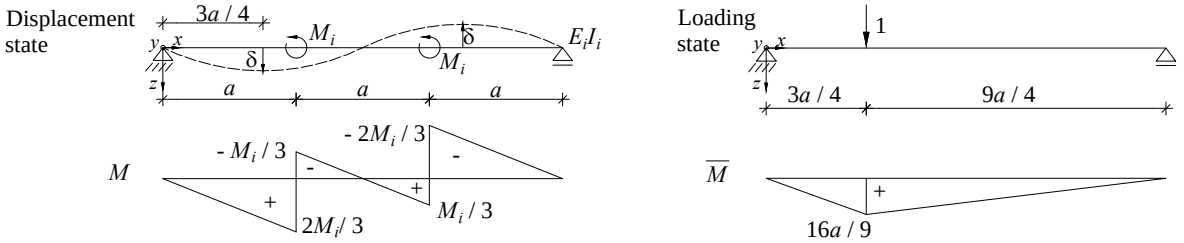

Figure 3.47: Static system for the equation of kinetics to find the deformations δ_i due to the eccentricity between the action point of the axial force and the interface

3.4 Parametric study

In this section, the structural behaviour of several timber-concrete composite slabs with notched connections is predicted applying the analytical models of Sections 3.2 and 3.3. The influence of several parameters like the thickness of the parts of the composite member, the LVL properties, the concrete properties and the span is studied.

3.4.1 Materials and geometry

The timber-concrete composite members studied in this section are made of beech LVL and spruce LVL, have a width of 530 mm, and a total thickness of 200 mm. The length of the slab elements is 6 or 8 m, the notch width is proportional to the shear force generated by a uniformly distributed vertical load, and the thickness of the LVL part is varied between 40 and 100 mm. Four LVL plates are considered: 40 mm, 60 mm, 80 mm, and 100 mm thickness. Tables 3.3 and 3.4 summarise the mechanical properties assumed for LVL, concrete and vertical reinforcement.

It is assumed that the properties of the beech LVL plates considered in the parametric study (Fig. 3.48(b)) correspond to the mean values of the material with cross layers developed by the company Pollmeier (Fig. 3.48(a)) tested by van de Kuilen and Knorz [14], [15] described in Section 2.2 (Tab. 2.1). In reality, there are slight differences in amount and position of cross layers. All LVL plates of the parametric study (Fig. 3.48(b)) contain two cross layers in the third position from outside to ensure form stability. Furthermore, in contrast to the approved configuration (Fig. 3.48(a)), the LVL plates of the parametric study never contain cross layers in the zones with high shear stresses just below the notch bottom. In this way, a shearing-off failure of the LVL close to the notch can be predicted using the shear strength parallel to the grain, which is significantly higher than the rolling shear strength of the cross layer (Section 3.3.6). Because of the higher thickness, the 80 mm and the 100 mm thick LVL plates contain a third cross layer. This cross layer is placed as far as possible from the notch bottom, i.e. at mid height. This cross layer is taken into account in the prediction of shear failure of the LVL cross-section.

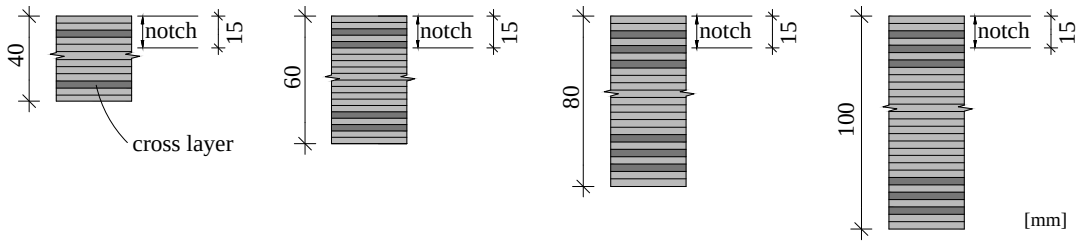

(a)

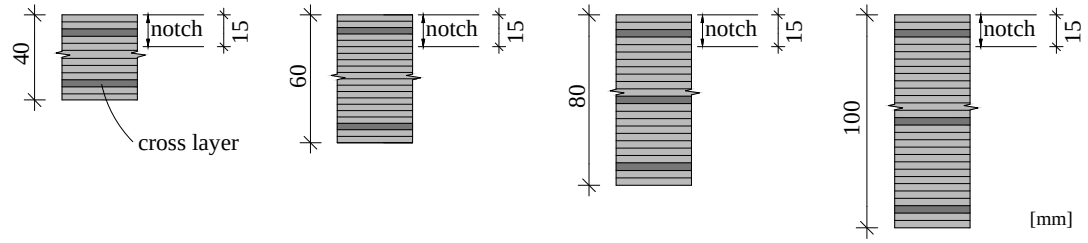

(b)

Figure 3.48: (a) Veneer configurations related to the mechanical properties determined by Van de Kuilen and Knorz [14], [15] in preparation of the European Technical Approval [3]; (b) veneer configuration of the LVL plates considered in the parametric study

The mean values of spruce LVL are obtained with a rough estimation. The characteristic values of LVL made of spruce Kerto Q [83] are multiplied by the ratios between the mean values and the characteristic values of the beech LVL tested by Van de Kuilen and Knorz [14], [15].

The concrete of Tab. 3.4 has elevated mechanical properties because a compressive failure of the LVL in the contact area should occur before the compressive failure of the concrete ($f_{c,0,2} < f_{c,1}$).

From own tests (Section 4.3), it is assumed that the behaviour of the LVL subjected to compression parallel to the grain is linear-elastic until $f_{c,0,2}$ and then ideal plastic without hardening. Based on the shear tests presented in Section 4.3, it is assumed that the shear stiffness of the notched connections is about 200 kN/mm.

In this parametric study, the variation of the mechanical properties is not studied. However, although the considered beech LVL is more homogeneous than solid timber or glued laminated timber, the mechanical properties are subjected to variations (according to Tab. 2.1). In design of the composite members, the influence of such variations should be taken into account. In this way, it can be ensured that the structural behaviour of the LVL plate is governed by compressive failure of the LVL.

Table 3.3: Parametric study on the structural behaviour of timber-concrete composite slabs with notched connection: mean values of the mechanical properties of LVL with cross layers in [N/mm^2]

		Beech LVL	Spruce LVL
Modulus of elasticity	$E_{0,2}$	13800	10500
Compressive strength parallel to the grain	$f_{c,0,2}$	45.7	32.9
Tensile strength parallel to the grain	$f_{t,0,2}$	58.5	36.5
Compressive strength perpendicular to the grain	$f_{c,90,2}$	13.6	2.72
Tensile strength perpendicular to the grain	$f_{t,90,2}$	1.97	0.98
Bending strength parallel to the grain	$f_{m,0,2}$	77.9	42.12
Shear strength parallel to the grain	$f_{v,2}$	10.7	5.7
Rolling shear strength	$f_{Rv,2}$	3.6	1.67

Table 3.4: Parametric study on the structural behaviour of timber-concrete composite slabs with notched connection: mechanical properties of concrete (mean values of C50/60 according to the Swiss Standard SIA 262 [66]), and assumed yield strength of the vertical reinforcement

Modulus of elasticity of uncracked concrete	E_1	38800 N/mm^2
Compressive strength of concrete	$f_{c,1}$	58 N/mm^2
Tensile strength of concrete	$f_{t,1}$	4.1 N/mm^2
Maximum compressive strain of concrete	$\varepsilon_{u,1}$	0.003
Angle of friction of concrete	φ	36.9 °
Yield strength of vertical reinforcement (class 10.9)	f_s	1000 N/mm^2

3.4.2 Structural behaviour of the notch

As shown in Section 3.3, the notch failures depend on the notch geometry, the thickness of the LVL and concrete and the material properties. Fig. 3.49 illustrates a parametric study on the structural behaviour of the second notch N2 of a composite slab made of a beech LVL plate without vertical reinforcement. Two 200 mm thick composite slabs are studied: in the first case, the beech LVL plate is 40 mm thick, and in the second case its thickness is 80 mm. The two most significant parameters are varied: the notch length l_N and the notch depth t_N (Fig. 3.49(a)). The failure modes considered are illustrated in Fig. 3.49(a), and the failure loads are calculated according to Section 3.3. It must be reminded that, if vertical reinforcement is provided, only failures of type 2C, 2S and 1C,n can occur.

The most important diagram is shown in Fig. 3.49(b), because a brittle shearing-off failure of the LVL (2S) must absolutely happen at a higher load level than a compressive failure of LVL parallel to the grain (2C). Fig. 3.49(b) shows that, for both notch depths studied (15 and 20 mm), this is the case. Furthermore, the difference between the failure loads increases with increasing notch length. If a shearing-off failure of the LVL was governing, the LVL part of the composite member would not be able to induce a ductile failure of the composite system.

Figs. 3.49(c) to (f) compare all theoretical failure loads of the second notch (N2) calculated according to the models presented in Section 3.3:

- The compressive failure of the LVL is governing for most of the cases studied.
- The safety margin between the compressive failure of the LVL parallel to the grain and the other notch failures theoretically increases with increasing notch length.
- A change of the notch depth from 15 mm to 20 mm increases the LVL failure loads, but does not introduce substantial changes.
- An increase of the LVL thickness and a decrease of the concrete thickness improve only the situation with regard to the concrete failures.
- The flexural-shear failures of the concrete are the most critical brittle failures, and are markedly sensible to the length of the notch. However, flexural-shear failures can be prevented using vertical reinforcement.

In conclusion, this part of the parametric study demonstrated that notches as connection system for timber-concrete composite members made of beech LVL can be designed so that their structural behaviour is governed by a ductile compressive failure of the LVL.

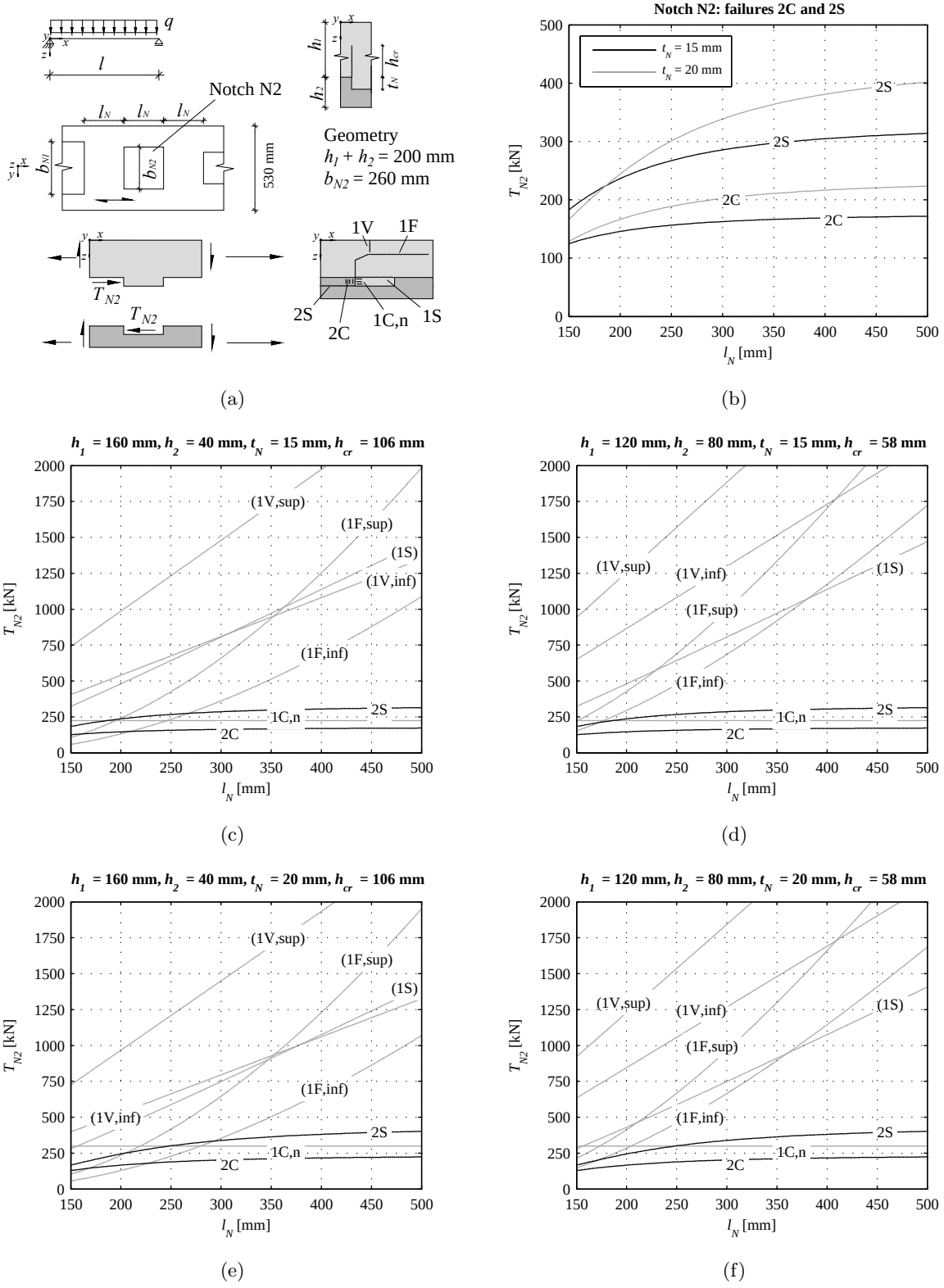

Figure 3.49: Parametric study on the notch failures ((...) = prevented by vertical reinforcement): (a) parameters and possible failure modes; (b) comparison between shearing-off failure in LVL (2S) and compressive failure in LVL parallel to the grain (2C); (c) $h_1 = 160$ mm, $h_2 = 40$ mm, $t_N = 15$ mm; (d) $h_1 = 120$ mm, $h_2 = 80$ mm, $t_N = 15$ mm; (e) $h_1 = 160$ mm, $h_2 = 40$ mm, $t_N = 20$ mm; (f) $h_1 = 120$ mm, $h_2 = 80$ mm, $t_N = 20$ mm

3.4.3 Structural behaviour of the composite member

This section deals with the influence of the concrete thickness h_1, the LVL thickness h_2, the notch length l_N, the span l and the LVL type on the structural behaviour of a timber-concrete composite slab, calculated applying the model presented in Sections 3.2 and 3.3. Fig. 3.50 summarises the failure modes of an LVL-concrete composite slab with a notched connection. It must be reminded that the failure modes 1S, 1F and 1V, as well as the secondary effects during states III and IV, are prevented if vertical reinforcement is provided.

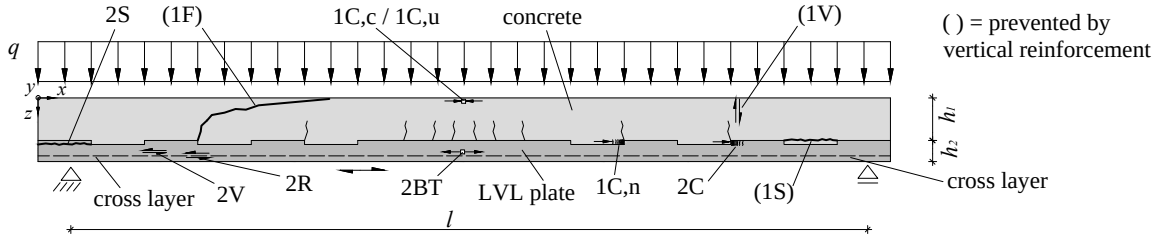

Figure 3.50: Failure modes of a LVL-concrete composite slab with a notched connection

Span of 6 m and notch length of 250 mm

In this section, the analytical models presented in Section 3.2 are applied to study the influence of several parameters on the behaviour of a 6 m long composite member with a notched connection. In all slab elements considered, the notches are 250 mm long and 15 mm deep, and their width is proportional to the shear force generated by a uniformly distributed vertical load. As shown in Tab. 3.5, four composite members made of beech LVL and two composite members made of spruce LVL are analysed. The thickness of the LVL is varied between 40 and 100 mm, whereas the total thickness of the composite slab has a constant value of 200 mm.

Table 3.5: Parametric study on the structural behaviour of 6 m long LVL-concrete composite slabs with notched connections (l = 5.66 m, b = 530 mm, $h_1 + h_2$ = 200 mm, l_N = 250 mm, t_N = 15 mm): geometry of the composite members

Timber	Concrete	h_1 [mm]	h_2 [mm]	Number of cross layers	l [m]
Beech LVL	C50/60	160	40	2	5.66
		140	60	2	5.66
		120	80	3	5.66
		100	100	3	5.66
Spruce LVL	C50/60	160	40	2	5.66
		120	80	3	5.66

Table 3.6: Parametric study on the structural behaviour of LVL-concrete composite slabs with notched connections ($l = 5.66$ m, $b = 530$ mm, $h_1 + h_2 = 200$ mm, $l_N = 250$ mm, $t_N = 15$ mm): results

Timber		Beech LVL				Spruce LVL	
Concrete		C50/60				C50/60	
h_1	[mm]	160.0	140.0	120.0	100.0	160.0	120.0
h_2	[mm]	40.0	60.0	80.0	100.0	40.0	80.0
n_1	[-]	2.81	2.81	2.81	2.81	3.70	3.70
n_2	[-]	1.00	1.00	1.00	1.00	1.00	1.00
γ_1	[-]	1.00	1.00	1.00	1.00	1.00	1.00
γ_2	[-]	0.82	0.75	0.70	0.65	0.86	0.75
Governing failure	[-]	2C	2C	2C	2C	2C	2C
Ultimate failure	[-]	1C	1C	2BT	2BT	2BT	2BT
x_I	[mm]	86.8	80.3	74.1	68.7	85.5	71.9
x_{II}	[mm]	54.2	59.6	62.2	63.2	49.3	57.6
x_{III}	[mm]	44.2	44.2	44.2	44.2	31.8	31.8
x_{IV}	[mm]	26.0	26.0	26.0	26	18.7	18.7
M_{cr}	[kNm]	13.4	13.8	15.6	20.8	12.6	13.5
M_y	[kNm]	110.8	104.3	99.8	97.6	80.5	72.2
$M_{R,1C,c}$	[kNm]	113.5	109.8	109.2	112.4	84.2	84.2
M_u	[kNm]	119.1	123.1	133.1	148.1	84.1	90.6
q_y	[kN/m^2]	52.2	49.2	47.0	46.0	37.9	34.0
q_u	[kN/m^2]	56.2	58.0	62.7	69.8	40.6	42.7
$\chi_{cr} \cdot 10^{-3}$	[1/m]	1.44	1.77	2.31	3.37	1.42	2.20
$\chi_y \cdot 10^{-2}$	[1/m]	2.25	1.86	1.71	1.65	1.96	1.43
$\chi_{1C,c} \cdot 10^{-2}$	[1/m]	3.39	3.39	3.39	3.39	4.70	
$\chi_u \cdot 10^{-2}$	[1/m]	11.55	11.55	10.30	8.82	7.39	6.86
w_y	[mm]	75.0	62.1	56.9	55.2	63.6	46.4
$EI_I \cdot 10^{12}$	[Nmm^2]	9.29	7.80	6.77	6.16	8.85	6.14
$EI_{II} \cdot 10^{12}$	[Nmm^2]	4.93	5.61	5.85	5.90	4.11	5.05
χ_u/χ_y	[-]	5.16	6.21	6.01	5.33	3.95	4.96
M_u/M_y	[-]	1.07	1.18	1.33	1.52	1.07	1.26

The most important outcomes of the analytical calculations are illustrated in Tab. 3.6. Fig. 3.51 summarises the results of a composite member made of beech LVL with a timber thickness of 40 mm and a concrete thickness of 160 mm as an example, including the moment-curvature behaviour (M-χ), the estimated load-deflection behaviour (q-w), and the distributions of the axial stresses and strains across the height. Fig. 3.52 shows the results in the case of a thickness of the beech plate of 80 mm instead of 40 mm. Fig. 3.53(a) compares the axial strains of the four composite cross-sections made of beech LVL, plotted in the instant, in which the notches begin to yield. Fig. 3.53(b) compares the axial strains of the four composite members made of

beech LVL at the ultimate limit state. Fig. 3.53(c) compares the moment-curvature behaviours of the four slab elements made of beech LVL. Fig. 3.53(d) shows the influence of the use of spruce instead of beech for a timber thickness of 40 mm and 80 mm.

In the M-χ-diagrams included in Figs. 3.51(b) and 3.52(b), the predicted failures are represented with horizontal lines. The failures, which are prevented by means of vertical reinforcement, are represented with dashed lines. As explained in Section 3.3.9, to ensure the development of ductility, vertical end-to-end reinforcement should be provided. Thus, the failures 1S, 1F and 1V do not occur and can be neglected.

Cracking of the concrete (cr), yielding of the notches (y), and exceedance of the compressive strength of the concrete (1C,c) occur in the same order in all six composite members studied (Fig. 3.51(b), Fig. 3.52(b), Fig. 3.53(c) and Fig. 3.53(d)). First, the concrete subjected to tension cracks; second, the notches begin to yield, and then the compressive strength of the concrete is reached at the top of the cross-section. This means that the compressive failure of the LVL parallel to the grain (2C) governs the structural behaviour and generates ductility. However, as described in Tab. 3.6, the theoretic ultimate limit of the composite member depends on the LVL thickness. In the case of an LVL thickness of 40 and 60 mm, the ultimate limit is determined by the exceedance of the maximum compressive strain of the concrete $\varepsilon_{u,1}$ at the top of the composite cross-section (1C,u), whereas the specimens with an LVL thickness of 80 mm and 100 mm fail due to a combined tensile-bending failure of the LVL (2BT) before $\varepsilon_{u,1}$ can be reached. Thus, according to this parametric study, a thinner LVL plate has a greater rotation capacity and postpones a brittle tensile-bending failure of the LVL.

The M-χ-behaviour is related to the axial deformations of a cross-section at mid-span, and can be analytically estimated with a certain degree of accuracy. In contrast, the deflections which occur after yielding, are more difficult to predict and imply uncertainty. The plastic amounts of the deflections shown in Fig. 3.51(c) and Fig. 3.52(c) are calculated according to the simplified model of Section 3.2.6, and depend on the assumed length l_{pl} of the plastic zone. The longer the plastic zone, the higher the deflection.

By observing Figures 3.51 to 3.53, it can be seen that the ratio between the thickness of the LVL and concrete influences the failure loads and the structural behaviour of the composite member in a marked way. In general, the thicker the LVL part in comparison to the concrete part of the composite member:

- the marked the hardening in the moment-curvature behaviour
- the smaller the theoretic maximum curvature
- the higher the tendency to reach a combined tensile-bending failure in the LVL before the maximum compressive strain of the concrete is reached
- the higher the theoretical shear- and flexural-shear failure loads of the concrete
- the higher the tendency to a small increase of the bending stiffness of the composite slab during state II.

The diagrams of the distributions of the axial strains ε and stresses σ of the composite member across the height included in Figs. 3.51 to 3.53 suggest the following remarks:

- Since the analytical model assumes that no gap opening occurs between the LVL and concrete, the two parts are assumed to exhibit the same curvature and the planes of the axial strains of the LVL and concrete are consequently parallel.

- The planes of the axial stresses of the LVL and concrete are not parallel because the two parts have different moduli of elasticity.

- The step between the LVL and concrete in the distribution of axial stresses and strains during the elastic states is due to connection flexibility, which is taken into account in the model by means of the γ-factor. If the connection was fully rigid, there would be theoretically no step.

- Between yielding of the connection (y) and the estimated ultimate failure of the system (u), the increase of the axial strain at the interface is due to the plastic compressive deformations of the LVL in the notches.

- For a determinate composite cross-section, it can be seen that, from the yield point (y) to the ultimate failure (u), the axial strain and stress of the centroid of the LVL is constant. The reason for is that, in the model, the behaviour of the connections is assumed to be elastic-ideal plastic.

- As illustrated in Fig. 3.53(a), the axial stress in the centroid of the LVL cross section at yielding $\sigma_{y,1}$ is different in each composite member, although the notches are always the same. This is due to the fact that the LVL area changes, influencing the axial stress.

Fig. 3.53(d) illustrates a comparison between composite members with notched connections made of beech LVL and spruce LVL. Basically, if beech LVL is substituted with spruce LVL, the mechanical properties of the timber part decrease. By observing Fig. 3.53(d), following remarks can be made:

- Since all strengths of the LVL decrease, the curves of the structural behaviour of the composite members made of spruce LVL are similar to those of beech LVL but show smaller failure loads and smaller ultimate deformations (Fig. 3.53(d)).
- With the assumed mechanical properties of spruce LVL and a concrete C50/60, the tendency to get a ultimate tensile-bending failure of the LVL part of the composite member increases. Indeed, the theoretical ultimate failure of the composite slab with LVL thickness 40 mm and concrete thickness 160 mm becomes a tensile-bending failure of the LVL instead of a compressive failure of the concrete on top edge of the slab.
- From the analytical calculations it results that, during the elastic states, the influence of the wood species on the deformations of the composite members is small. This is due to the fact that the difference between the stiffness of beech LVL and spruce LVL is less marked than the difference between the strengths. Nevertheless, it has to be noticed that, since no data are available, it is assumed that notches cut in a spruce LVL plate have the same connection stiffness as those in beech LVL. This assumption is not verified. Blass et al. [28] calculated the shear stiffness of notched connections in spruce LVL-concrete composite members. However, the composite specimens tested had round notches, steel reinforcement in the notches, and were made of a different concrete. Thus, these experimental results were not considered for the parametric study included in this section.
- Furthermore, since the mechanical properties of spruce LVL are inferior to those of beech LVL, a concrete with a smaller strength than C50/60 can be used. However, the compressive strength of the concrete should be bigger than the compressive strength of spruce LVL parallel to the grain. The reason for is that the structural behaviour of the composite member should be governed by a compressive failure of the LVL in the notches.

Span of 6 m and notch length of 150 mm

The parametric studies of the previous section were related to a notch length of 250 mm. A reduction of the notch length l_N from 250 mm to 150 mm, under the condition that the notch spacing equals twice the notch length, has two consequences:

- As explained in Section 3.3, the smaller l_N, the more relevant the influence of the stresses perpendicular to the interface on the failure loads of the notch.
- As shown in Section 3.3.3, the notch force T_{Ni} depends on the notch length l_N. A higher number of notches between the point of maximum bending moment and the support implies smaller notch forces. For instance, the load $q_{R,2C,N2}$, which is needed to cause a compressive failure in the LVL, is higher with a notch length of 150 mm than with a

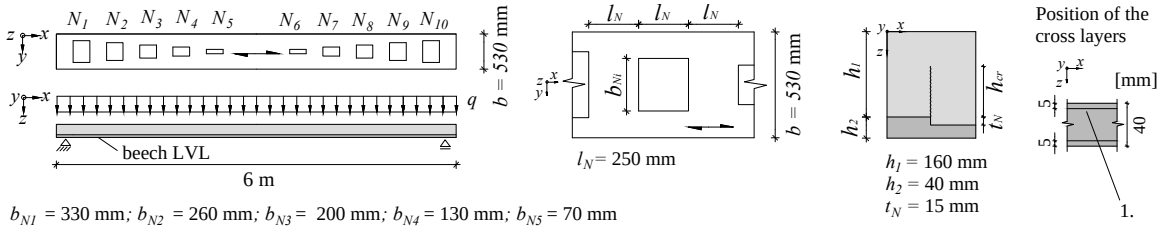

(a)

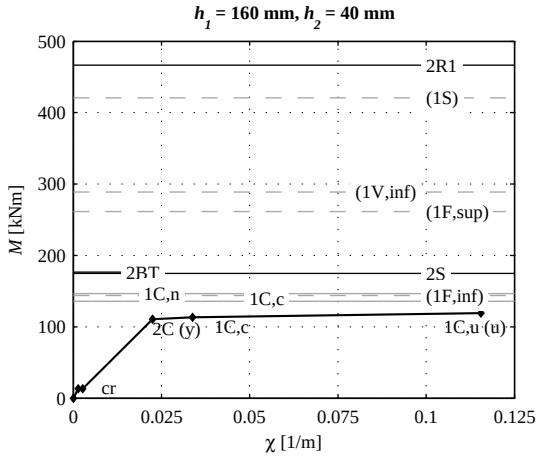

(b)

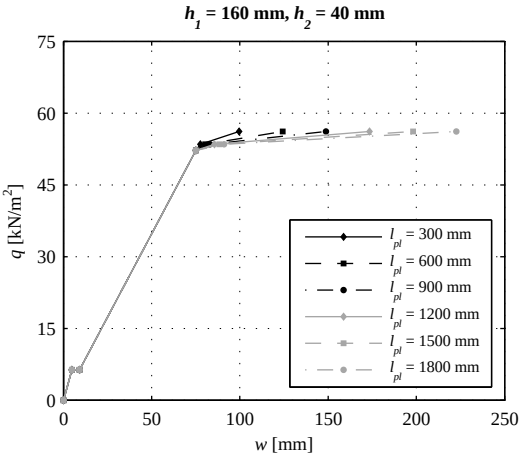

(c)

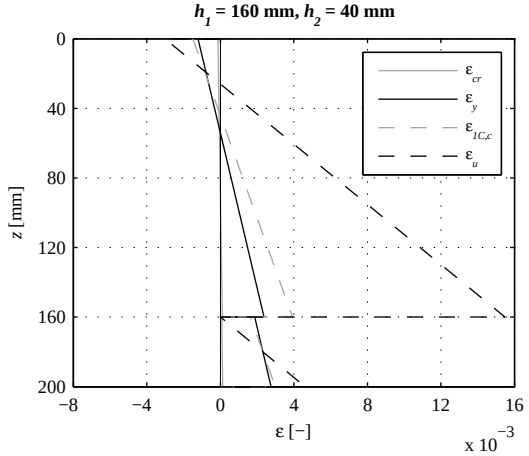

(d)

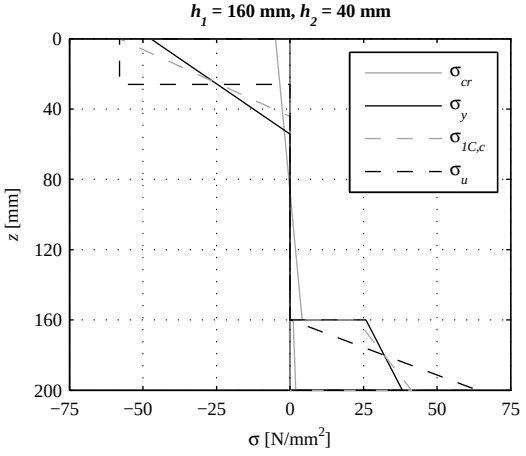

(e)

Figure 3.51: Parametric study about the structural behaviour of timber-concrete composite slabs made of beech LVL ($l = 5.66$ m, $b = 530$ mm, $h_1 = 160$ mm, $h_2 = 40$ mm, $l_N = 250$ mm, $t_N = 15$ mm): (a) geometry; (b) moment-curvature behaviour and failure modes; (c) load-deflection behaviour; (d) axial strains ; (e) axial stresses

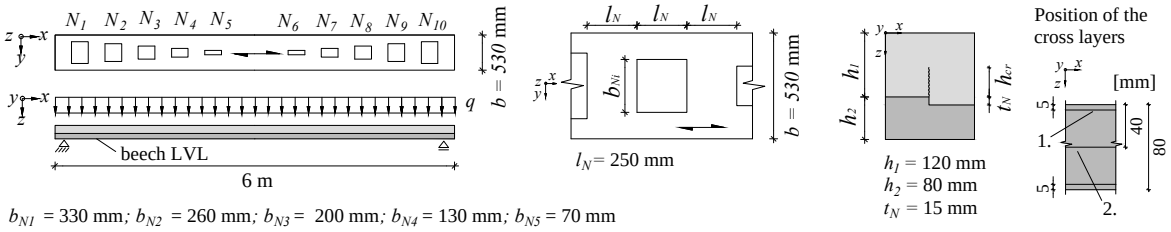

(a)

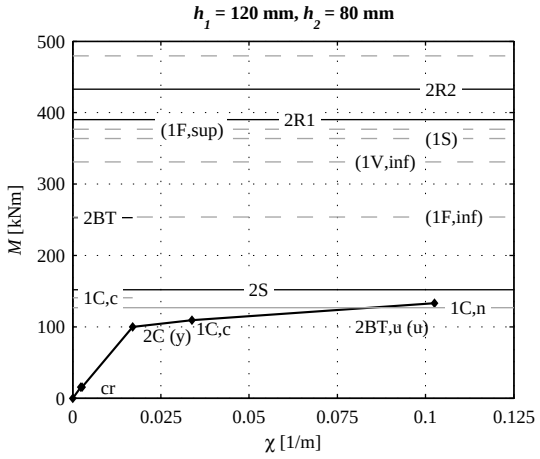

(b)

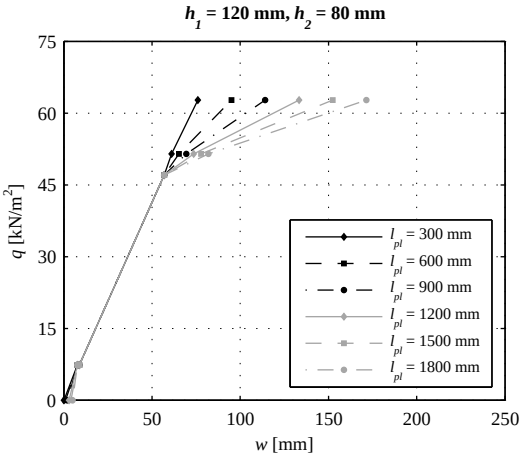

(c)

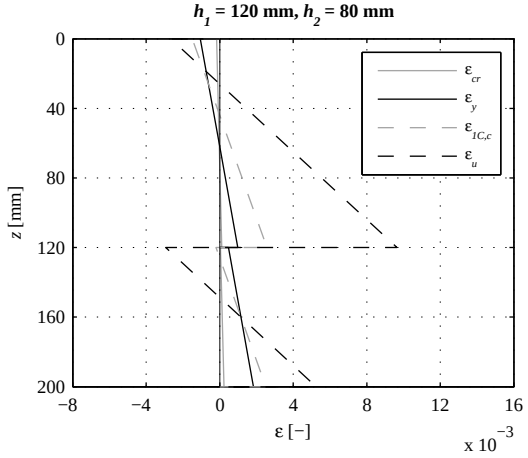

(d)

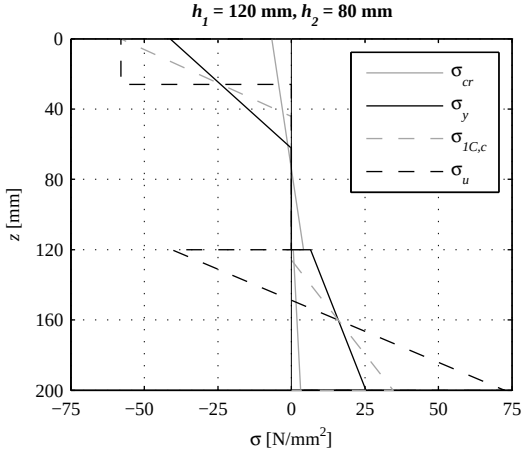

(e)

Figure 3.52: Parametric study about the structural behaviour of timber-concrete composite slabs made of beech LVL ($l = 5.66$ m, $b = 530$ mm, $h_1 = 120$ mm, $h_2 = 80$ mm, $l_N = 250$ mm, $t_N = 15$ mm): (a) geometry; (b) moment-curvature behaviour and failure modes; (c) load-deflection behaviour; (d) axial strains ; (e) axial stresses

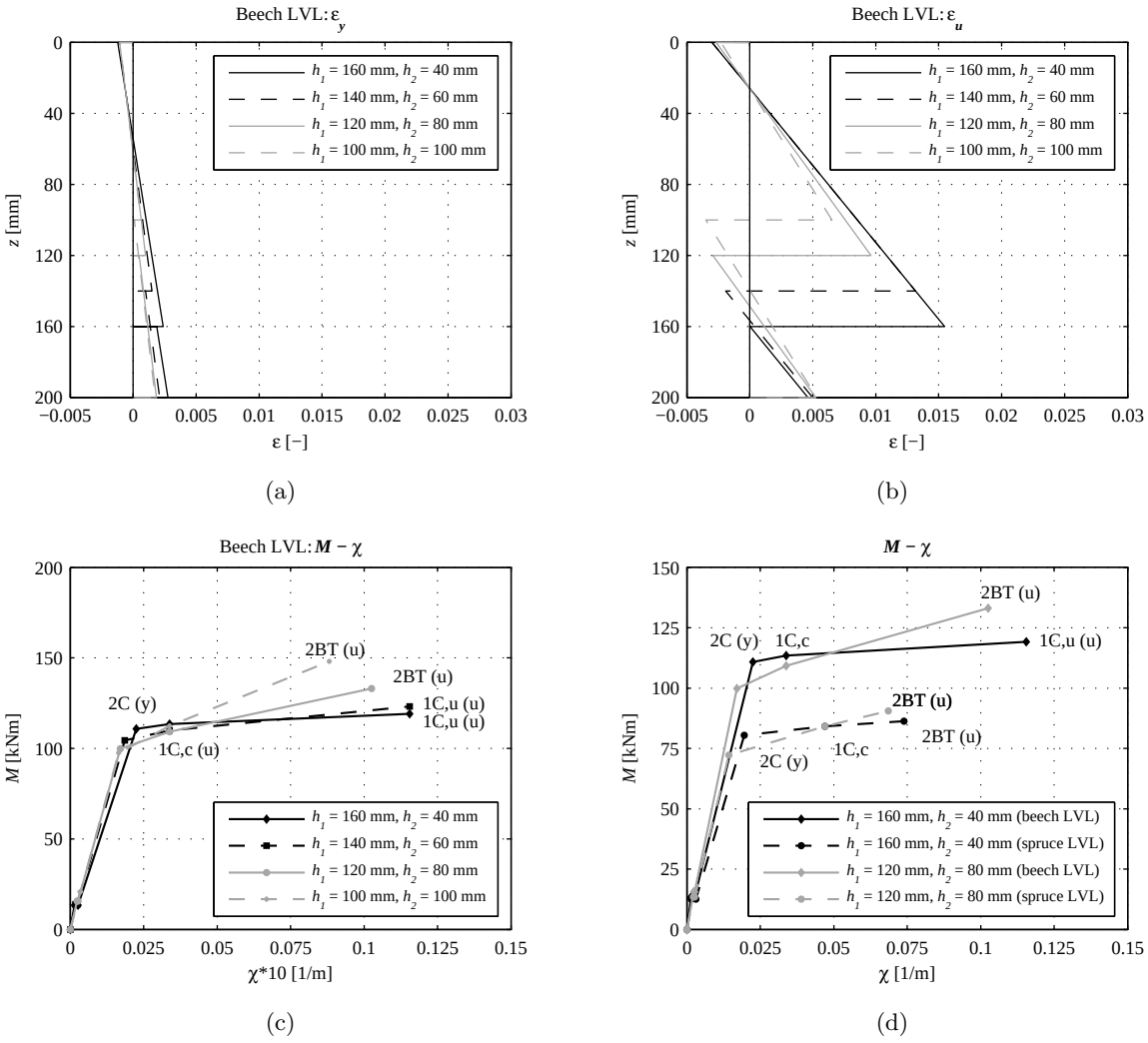

Figure 3.53: Parametric study about the structural behaviour of LVL-concrete composite slabs with a notched connection (l = 5.66 m, b = 530 mm, l_N = 250 mm, t_N = 15 mm): (a) comparison of the axial strains at yielding ε_y; (b) comparison of the axial strains at ultimate failure ε_u; (c) comparison of the moment-curvature behaviour; (d) comparison between composite members made of beech LVL and spruce LVL

notch length of 250 mm, if the notch depth is constant. Therefore, the shorter the notches, the higher the tendency that a brittle failure mode governs the structural behaviour of the composite member. This aspect represents the most important problem caused by a reduction of the notch length.

Fig. 3.54 shows the structural behaviour of a 6 m long timber-concrete composite slab made of beech LVL with 18 150 mm long notches. The structural behaviour of the composite member is not governed by a compressive failure of the LVL in the notch (2C). First, the compressive strength of the concrete $f_{c,1}$ is reached at the top of the cross-section at a bending moment of $M_{R,1C,c} = 136$ kNm. Starting from this point, the stresses in the compression zone should begin to redistribute. The following failure predicted is a combined tensile-bending failure of the LVL cross-section which should occur at a bending moment of $M_{R,2BT} = 177$ kNm. In contrast to the exceedance of $f_{c,1}$, the combined tensile-bending failure of the LVL implies a sudden collapse of the structure. A compressive failure of the LVL would theoretically occur at a bending moment of $M_{R,2C} = 187$ kNm. Therefore, this notch layout does not allow reaching a ductile failure of the composite member. This case study shows the importance of a sufficient notch length.

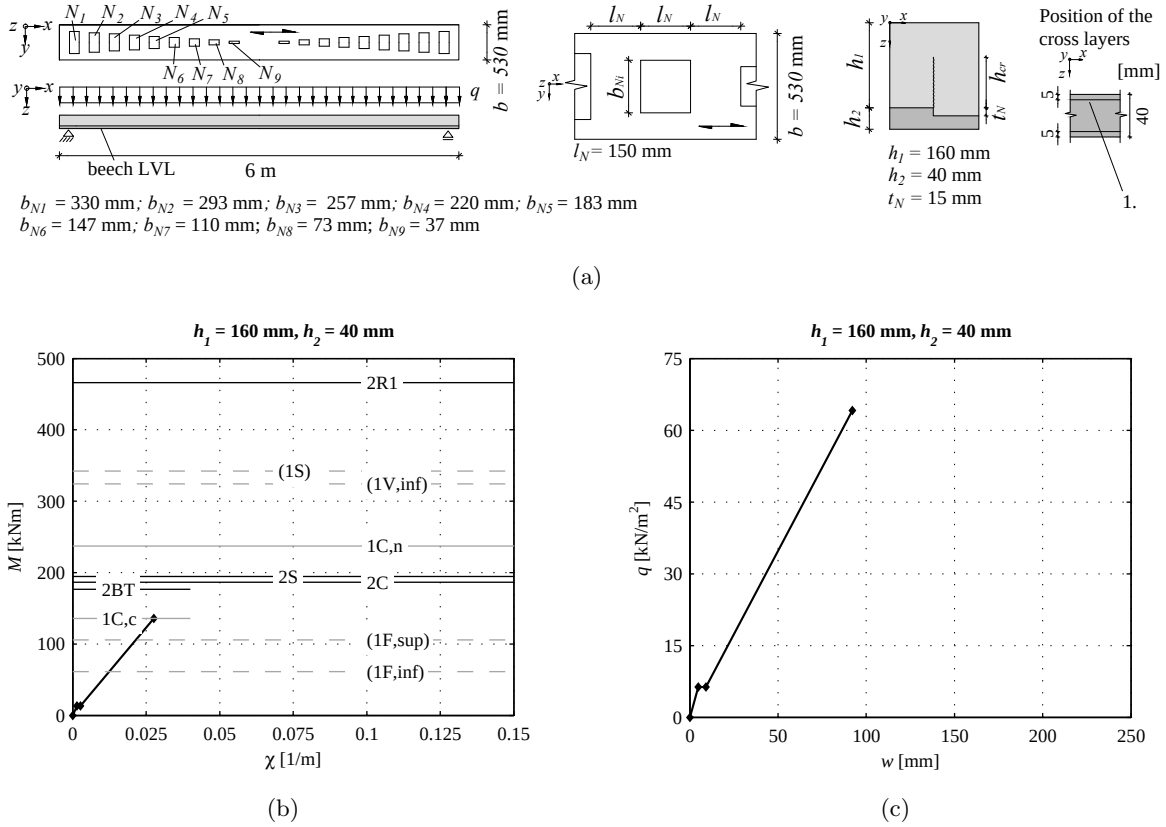

Figure 3.54: Parametric study about the structural behaviour of timber-concrete composite slabs made of beech LVL with notch length $l_N = 150$ mm and notch depth $t_N = 15$ mm ($l = 5.66$ m, $b = 530$ mm, $h_1 = 160$ mm, $h_2 = 40$ mm): (a) geometry; (b) moment-curvature behaviour and failure modes; (b) load-deflection behaviour

Span of 8 m and notch length of 250 mm

Fig. 3.55 illustrates the structural behaviour of a timber-concrete composite slab made of beech LVL with a length of 8 m instead of 6 m. As shown in Fig. 3.55(a), the concrete layer is 160 mm thick, the beech LVL plate 40 mm thick and the 250 mm long and 15 mm deep notches are designed proportional to the shear generated by a uniformly distributed vertical load.

As illustrated in Figs. 3.55(d) and 3.55(e), at the ultimate limit state, the 8 m long composite slab shows a higher strain and stress in the centroid of the LVL cross-section in comparison to the 6 m long slab. This is due to the fact that the 8 m long slab contains more notches. Under the assumption that the compressive failure of the LVL in the notch is ideal-plastic, the axial stress in the centroid of the LVL at yielding and at the ultimate state is calculated as follows:

$$\sigma_{2,u} = \sigma_{2,y} = \frac{\sum T_{y,Ni}}{A_2} \tag{3.193}$$

If the number of notches increases and the cross section area of the LVL A_2 is constant, the stress in the centroid of the LVL $\sigma_{2,y}$ increases. Therefore, when the notches yield, the LVL part of the 8 m long slab is subjected to a higher tensile stress than the 6 m long slab.

Fig. 3.55(b) shows the moment-curvature behaviour of the 8 m long slab compared to the 6 m long slab:

- In the 8 m long slab, in contrast to the 6 m long slab, exceedance of the compressive strength of the concrete occurs at approximately the same load level as the compressive failure of the LVL in the notches ($M_{R,2BT} \approx M_{R,1C,c} \approx 140$ kNm).
- To achieve yielding of the notches in the 8 m long slab, a higher bending moment M_y is needed. The reason is that in the 8 m long slab there are more notches, and hence, in the centroid of the LVL, higher axial stresses occur.
- Due to this higher axial tensile stress in the LVL at yielding level $\sigma_{2,y}$, a smaller bending deformation is necessary to reach a tensile-bending failure of the LVL. Thus, the 8 m long slab fails due to a tensile-bending failure of the LVL instead of a concrete failure, and its ultimate curvature χ_u is smaller than the ultimate curvature of a 6 m long slab.

Fig. 3.55(c) shows the moment-curvature behaviour of the 8 m long slab represented with all failure loads calculated by means of the analytical model. Since the moment-curvature curve of the 8 m long slab lies under the lines of the brittle failures, according to the model, an elastic-plastic behaviour should occur. Nevertheless, the yielding moment M_y and the moment corresponding to the tensile-bending failure of the LVL during state II ($M_{R,2BT}$) are closer than in the case of a length of 6 m (Fig. 3.51(c)). Since the model contains simplifications and the material shows a variability in properties, this can represent a problem in the case of a span longer than 6 m. A solution could be to reduce the width of the notches or to increase the LVL thickness.

The deflections of the composite member strongly depend on the span. Since the thickness of the LVL and concrete are the same in both composite slabs studied, a composite member with a span of 8 m exhibits higher deflections than one with a span of 6 m subjected to the same vertical load. Furthermore, because of the longer span, the yielding load q_y of the 8 m long slab is smaller then in the case of a 6 m long slab.

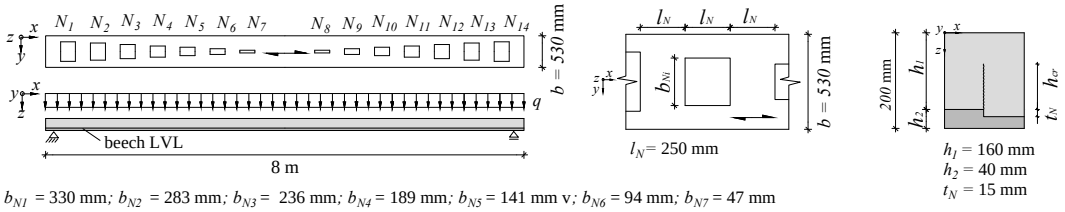

(a)

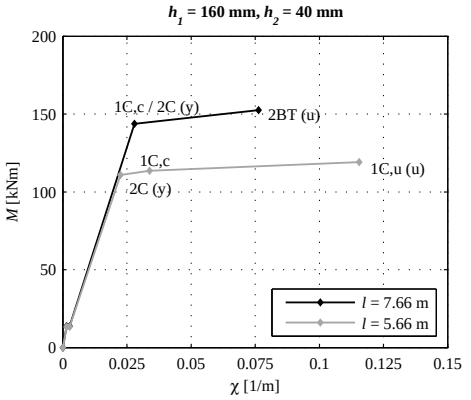

(b)

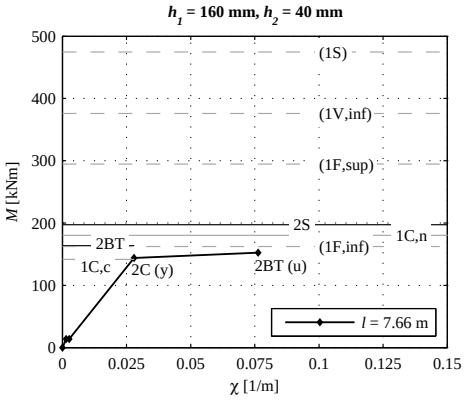

(c)

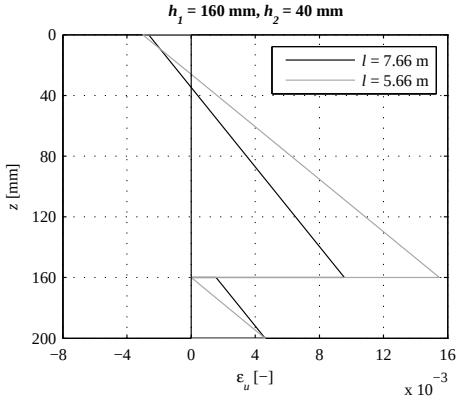

(d)

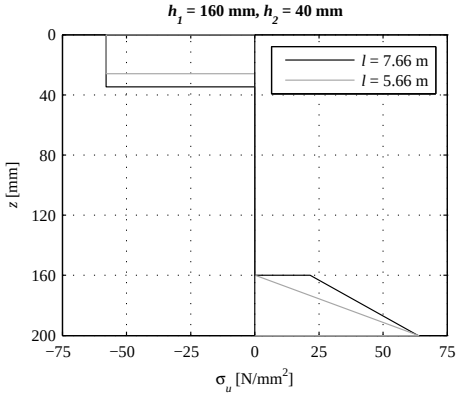

(e)

Figure 3.55: Parametric study about the structural behaviour of timber-concrete composite slabs made of beech LVL (l = 7.66 m, b = 530 mm, h_1 = 160 mm, h_2 = 40 mm, l_N = 250 mm, t_N = 15 mm): (a) geometry; (b) moment-curvature behaviour; (c) moment-curvature behaviour and failure modes; (d) axial strains at ultimate limit state ε_u; (e) axial stresses at ultimate limit state σ_u

This section presented a comparison between two spans with constant thickness of the layers. In practice, the 8 m long slab will be designed with a higher thickness of the LVL

and concrete layers to fulfil the deformation requirements suggested by the design codes. This influences the structural behaviour of the composite member.

3.4.4 Vertical reinforcement

This section deals with the estimation of the amount of vertical reinforcement with a yield strength of $f_s = 1000$ N/mm^2, which is necessary to ensure that the composite member is able to achieve the theoretical ultimate failure load q_u and the ultimate deflection w_u. The model assumes that this reinforcement carries exclusively vertical forces. The following calculations deal only with the necessary steel area and not with the flexibility requirements of the reinforcement presented in Section 3.3.12. Fig. 3.56 shows the location of the steel reinforcements, which is chosen as shown in Section 3.3.10. The vertical reinforcement should be end-to-end, and is divided in two groups:

- reinforcement to carry the vertical tension in the concrete ($A_{s,T,Ni}$), which is located close to the action point of the horizontal notch force T_{Ni} due, in this case, to q_u, and is estimated according to Section 3.3.10
- reinforcement to prevent the gap opening ($A_{s,v}$), which is distributed over the entire span, and is designed under the assumption that the composite member reaches a maximum deflection at mid-span of $w_u \approx 300$ mm according to Section 3.3.11

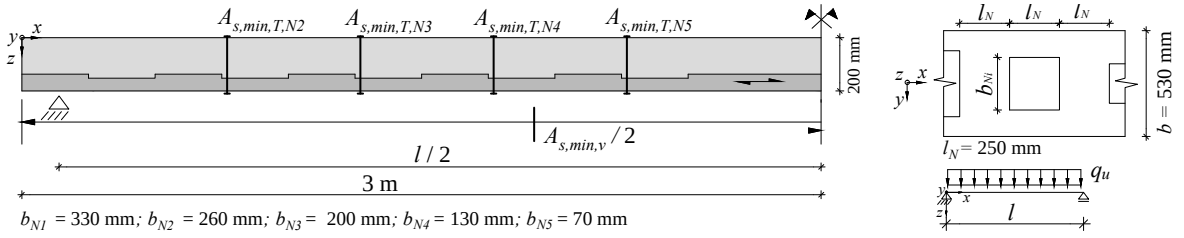

Figure 3.56: Vertical reinforcements

The total amount of vertical steel reinforcement in the composite member shown in Fig. 3.56 can be quantified as follows:

$$A_s = \sum A_{s,T,Ni} + A_{s,v} = 2\sum_{i=1}^{5} A_{s,T,Ni} + A_{s,v} \tag{3.194}$$

To estimate the magnitude of the vertical reinforcement necessary, an equivalent number of vertical bars with diameter $\oslash_{bars} = 6$ mm is calculated from A_s as follows:

$$n_{bars} = \frac{4 \cdot A_s}{\oslash_{bars}^2 \cdot \pi} \tag{3.195}$$

The results of the calculation are shown in Tab. 3.7, and Fig. 3.57 illustrates the influence of the LVL thickness by a constant total thickness of 200 mm on the necessary steel surface.

Concerning the estimated necessary amount of end-to-end vertical reinforcements in a timber-concrete member with notched connection, following conclusions can be drawn:

Table 3.7: Amount of vertical reinforcement to achieve q_u and $w_u \approx 300$ mm in a timber-concrete composite member with a notched connection made of LVL ($l = 6$ m, $b = 530$ mm, $l_N = 250$ mm, $t_N = 15$ mm)

		Beech C50/60				Spruce C50/60	
h_1	[mm]	160	140	120	100	160	120
h_2	[mm]	40	60	80	100	40	80
Vertical tension							
h_1^*	[mm]	149.4	127.6	106.8	86.4	151.1	108.3
q_u	[kN/m^2]	56.2	58	62.7	69.8	39.6	41.8
T_{N2}	[kN]	182.5	199.9	225.9	257.3	127.4	150.0
T_2	[kN]	54.5	51.0	48.2	44.5	38.5	32.5
$A_{s,T,N2}$	[mm^2]	54.5	51.0	48.2	44.5	38.5	32.5
T_{N3}	[kN]	136.9	149.9	169.4	192.9	95.5	112.5
T_3	[kN]	40.9	38.3	36.2	33.4	28.9	24.4
$A_{s,T,N3}$	[mm^2]	40.9	38.3	36.2	33.4	28.9	24.4
T_{N4}	[kN]	91.2	100.0	112.9	128.6	63.7	75.0
T_4	[kN]	27.3	25.5	24.1	22.2	19.2	16.2
$A_{s,T,N4}$	[mm^2]	27.3	25.5	24.1	22.2	19.2	16.2
T_{N5}	[kN]	45.8	50.2	56.8	64.6	32.0	37.7
T_5	[kN]	13.7	12.8	12.1	11.2	9.7	8.2
$A_{s,T,N5}$	[mm^2]	13.7	12.8	12.1	11.2	9.7	8.2
$\sum A_{s,T,Ni}$	[mm^2]	272.8	255.3	241.3	222.5	192.5	162.5
Gap opening							
w_u	[mm]	300	300	300	300	300	300
$w_{1,u}$	[mm]	150	150	150	150	150	150
$w_{2,u}$	[mm]	225	225	225	225	225	225
$\alpha_{1,u}$	[rad]	0.106	0.106	0.106	0.106	0.106	0.106
v_u	[mm]	74.58	74.58	74.58	74.58	74.58	74.58
$q(v_u)$	[kN/m]	8.37	28.24	66.95	130.76	8.37	66.95
$A_{s,v}$	[mm^2]	47.4	159.9	378.9	740.1	47.4	378.9
Total							
A_s		320.2	415.2	620.2	962.6	239.9	541.4
$n_{bars\varnothing 6}$	[-]	12	15	22	34	9	20

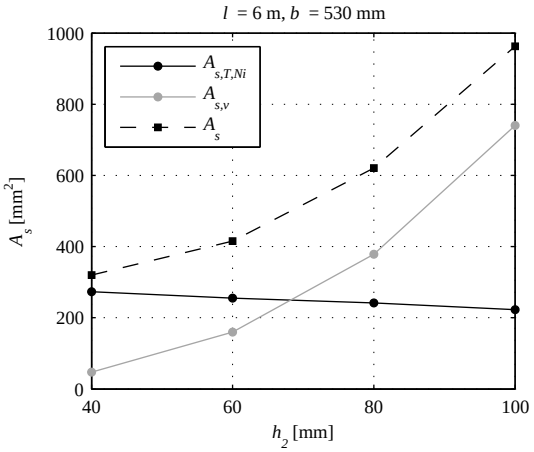

Figure 3.57: Amount of vertical reinforcements to achieve q_u and $w_u \approx 300$ mm in a timber-concrete composite member with notched connection made of beech LVL ($l = 6$ m, $b = 530$ mm, $l_N = 250$ mm, $t_N = 15$ mm)

- In general, the amount of vertical reinforcements to carry the vertical tension in the concrete and to prevent gap opening in a 6 m long and 0.53 m wide composite slab is contained. For the considered slabs made of beech LVL, the necessary number of vertical bars with a diameter of 6 mm and a tensile strength of $f_s = 1000$ N/mm^2 is between 12 and 34.

- Regarding the reinforcement to carry the vertical tension in the concrete $A_{s,min,T,Ni}$, the vertical components T_i decrease with decreasing concrete thickness. Therefore, the necessary steel amount decreases.

- Regarding the reinforcement to prevent gap opening $A_{s,v,min}$, a thicker timber plate implies higher stiffness and hence, a higher load to bend it. Thus, according to the simplified model presented in Section 3.3.11, the necessary number of vertical reinforcement bars increases.

- Since spruce implies lower failure load and is less stiff, the amount of necessary reinforcement bars is smaller.

3.4.5 Remarks for the design

This section investigates if composite slabs made of beech and spruce LVL with notched connections, designed according to the analytical model developed in Sections 3.2 and 3.3, are able to achieve the requirements of structural safety and serviceability at design level. Fig. 3.58 shows the prediction of the load-deflection behaviour of the composite member calculated using the mechanical properties of beech and spruce LVL at design level. The thickness of the LVL is 40 mm, the concrete thickness is 160 mm, and the slab length is either 6 or 8 m. The deflections are calculated under initial conditions ($t = 0$), and considering long-term effects ($t = \infty$). According to the Swiss Standard SIA 265 [29], the long-term effects can be estimated with a reduction of the modulus of elasticity depending on the creep factor φ:

$$E_\infty = \frac{E_0}{1+\varphi} \tag{3.196}$$

It is assumed that the creep factor of the LVL is $\varphi_2 = 0.8$. The long term effects on the elasticity of concrete are calculated using Eq. 3.196 as well and assuming a creep factor of $\varphi_1 = 2.1$.

In this analysis, it is assumed that the composite members are strengthened with vertical reinforcement bars. This ensures the development of ductility.

In Fig. 3.58 the design loads for ultimate limit state analysis ($q_{d,ULS}$) and for the control of appearance ($q_{d,app}$) according to the Swiss Standard SIA 260 [90] are shown as well. The limit deflection for the control of appearance corresponds to $l/300$ and is represented with a vertical line [90]. For a characteristic value of self-weight of $g_k = 4.3$ kN/m^2, and under the assumption of a permanent load of $q_{Ak} = 2.33$ kN/m^2 and a live load of $q_{Nk} = 3$ kN/m^2 at characteristic level, the design loads are calculated as follows:

$$q_{d,ULS} = \gamma_G \cdot (g_k + q_{Ak}) + \gamma_Q \cdot q_{Nk} = 13.5\text{kN/m}^2 \tag{3.197}$$

$$q_{d,app} = g_k + q_{Ak} + \psi_2 \cdot q_{Nk} = 7.5\text{kN/m}^2 \tag{3.198}$$

In the case of a length of 6 m (Fig. 3.58(a)), the following conclusions can be drawn:

- The structural safety of the composite member is fulfilled with both LVL materials.
- Both LVL materials allow a ductile design.
- The composite slab made of beech LVL has a higher reserve in load-carrying capacity.
- At service level, the deflection of the composite slab made of beech LVL calculated by taking into account long-term effects ($t = \infty$) coincides approximately with the limit deflection of $l/300$, and the deflection of the composite slab made of spruce LVL is slightly higher.

Concerning a slab length of 8 m (Fig. 3.58(b)), it can be concluded that:

- Only the composite slab made of beech LVL achieves the requirements for the structural safety. The composite slab made of spruce LVL shows insufficient load-carrying capacity at design level.
- The slab made of beech LVL shows ductility at failure, whereas the slab made of spruce LVL is governed by a brittle failure (combined bending-tensile failure of the LVL).
- Nevertheless, with a length of 8 m, the design of the composite member is governed by the deflections at service level. Therefore, to fulfil the serviceability requirements (e.g. aesthetics), the thickness must be increased, and hence, the load-carrying capacity of the composite member will be considerably improved.

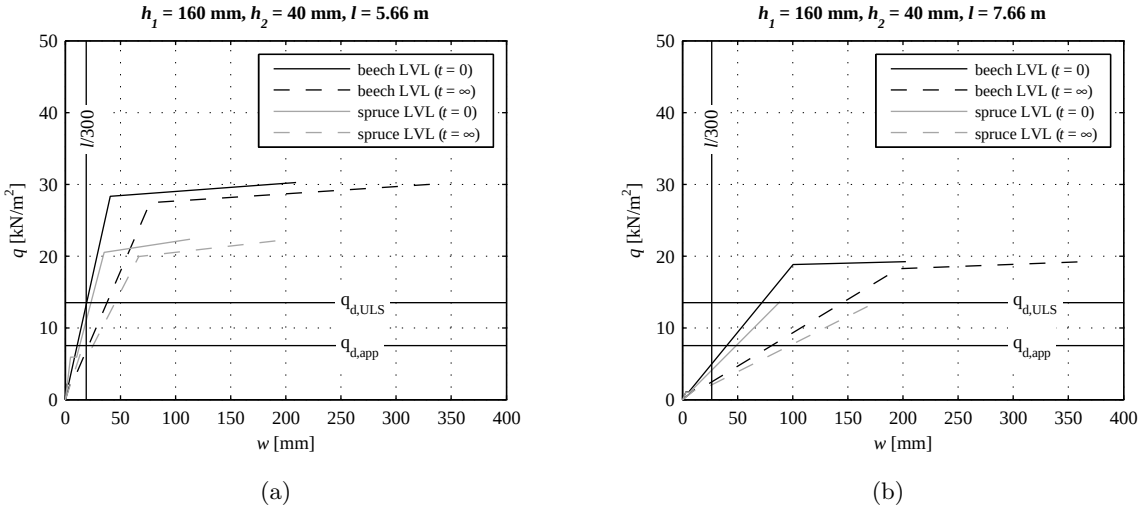

Figure 3.58: Design of timber-concrete composite slabs made of beech LVL and spruce LVL ($b = 530$ mm, $h_1 = 160$ mm, $h_2 = 40$ mm, $l_N = 250$ mm, $t_N = 15$ mm): (a) $l = 5.66$ m ; (b) $l = 7.66$ m

3.4.6 Conclusions from the parametric study

This parametric study dealt with the influence of several material and geometrical properties on the structural behaviour of LVL-concrete composite members with notched connections. In all composite memberss the notches were designed proportional to the shear force generated by a uniformly distributed vertical load. The calculations were performed according to the analytical models developed in Sections 3.2 and 3.3. The following conclusions can be drawn:

- The notch length and depth influence the failure modes and the failure load. They must be chosen so that a compressive failure of the LVL is governing and the load-carrying capacity is sufficient. In the cases studied, a length of 250 mm and a depth of 15 mm ensure a satisfying structural behaviour. A reduction of the notch length increases the tendency that brittle failures become governing.

- If a compressive failure of the LVL is governing, the composite cross section exhibits high theoretical ultimate curvatures.

- The nature of the ultimate failure of the composite member depends on several factors such as material properties and geometry. Some of the cases studied are governed by the exceedance of the maximum compressive strain of the concrete. Otherwise, a tensile-bending failure of the LVL occurs.

- The amount of vertical reinforcement bars to ensure the theoretical ultimate deformations results to be moderate and increases with increasing LVL thickness.

- The use of LVL materials is important to ensure consistency in mechanical properties of the timber component of the composite slab.

- The wood species influences the structural behaviour. If spruce instead of beech is used, all timber failure loads decrease. The advantage is that it is possible to reduce the concrete quality. On the other hand, the stiffness, the load-carrying capacity and the ultimate deformations are lower.

The choice of the thickness of the LVL in respect to the concrete is a compromise between many requirements. An increase of the LVL thickness in comparison to the concrete implies:

- slightly smaller deflections
- higher hardening after the compressive failure of the LVL, but smaller theoretical ductility
- more favourable loading of the concrete, and so a smaller tendency to flexural-shear failures
- higher need in vertical reinforcement to ensure ductility
- better suitability for anchoring of the screws
- less propping during construction
- reduction of the self-weight
- higher fire resistance
- more vulnerable for vibration

In conclusion, this parametric study demonstrates that the analytical model allows to determine the phases of the structural behaviour of a LVL-concrete composite member with a notched connection in a simple and clear way. Furthermore, this study shows that, depending on the geometry and the mechanical properties of the parts of the composite member, the theoretic requirements for ductile behaviour summarised in Section 3.3.12 can be fulfilled.

3.5 Conclusion

The presented analytical models are suitable to analyse the structural behaviour of timber-concrete composite members with notched connections. These models are efficient and clear, and allow studying the influence of the most significant geometrical and material parameters. Based on these theories, a design procedure to achieve ductility in timber-concrete composite members made of LVL with notched connections was developed. The structural aspects of the composite member which are most critical to model are the shear resistance of the plain concrete and the secondary effects, which may occur during connection yielding. These problems are influenced by several factors which are difficult to quantify, but can be solved by designing vertical reinforcement.

When a timber-concrete composite member made of LVL with a ductile notched connection is designed, the position of the cross layers should be taken into account. The cross layers decrease the resistance against shearing-off failure of the LVL in front of the notch and shear

failure of the LVL cross section. The parametric studies presented in this section were performed for LVL plates without cross layers in the critical zones. If it is possible, cross layers should not be placed in zones subjected to high shear stresses.

Chapter 4

Experimental investigations

4.1 Introduction

In this research study, three series of experiments were performed. In the beginning, a series of timber-concrete composite members made of beech LVL with different notched connections were tested in bending, to evaluate the potential of this innovative concept (Section 4.2). At that time, the analytical model described in Chapter 3 did not yet exist. Then, a series of shear tests allowed observing several failure modes of notched timber-concrete connections, among which the compressive failure of the timber (Section 4.3). Finally, the ductile design procedure summarised in Section 3.3.12 was validated with a series of bending tests presented in Section 4.4. A test report [6] includes additional details on the test procedures and a complete evaluation of the test results.

4.2 Preliminary bending tests

4.2.1 Introduction

At the beginning of this research project, to evaluate feasibility and the structural potential of timber-concrete composite slabs made of beech LVL with notched connections, a series of four-point bending tests was performed in the laboratory of the Institute of Structural Engineering (IBK) at ETH Zurich. These experiments represented the first study on the use of beech wood in timber-concrete composite slabs and gave significant initial information about the structural behaviour of this type of slabs [89], [91], [87].

4.2.2 Materials and methods

As illustrated in Fig. 4.2, four 15 mm deep notch types were tested to study the influence of the notch geometry on the load-displacement behaviour and the load-carrying capacity of the composite slabs. The specimens tested were 6 m long, 600 mm wide and 160 mm deep. Each beech LVL plate was 40 mm deep with a 120 mm thick concrete layer.

The beech LVL plates were produced by the company Pollmeier, which is making important progress in the production of LVL made of European beech wood [12]. The plates used in these

experiments were made of 13 veneers, each with a thickness of about 3 mm (10 veneers in longitudinal direction and 3 veneers in the cross direction to ensure the dimensional stability) (Fig. 4.2). As shown in Fig. 4.1, the plates used in this experiments were slightly different than those contained in the European Technical Approval [3], but the number of longitudinal layers was the same. However, it was assumed that they had the same mechanical properties of the material tested by Van de Kuilen and Knorz [14], [15] in preparation of the approval (Tab. 2.1).

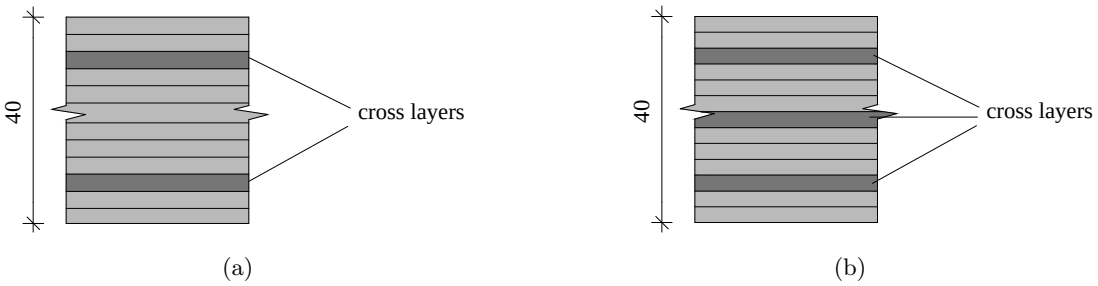

(a) (b)

Figure 4.1: (a) standard veneer configuration of the beech LVL produced by the company Pollmeier; (b) veneer configuration of the LVL plates used in the preliminary bending tests

The concrete tested belonged to the strength class C50/60 according to the Swiss Standard SIA 262 [66], and exhibited the mechanical properties summarised in Tab. 4.1. The concrete layer contained a shrinkage reduction admixture and a steel mesh to prevent shrinkage cracks. According to the models presented in Section 3.2, this mesh does not carry relevant forces. Fig. 4.3 illustrates the test setup and the most important measurements carried out in the four-point bending tests. This test setup included two hydraulic cylinders, two load distribution steel profiles (HEB 200), and two supports in a distance of 5.76 m.

Table 4.1: Preliminary bending tests: mechanical properties of concrete

	Elasticity modulus	Cylinder strength	Splitting tensile strength
	E_1 [N/mm^2]	$f_{c,1}$ [N/mm^2]	$f_{t,1}$ [N/mm^2]
Number of specimens	3	3	4
Mean value	37698	50.90	3.10
standard deviation	258	0.76	0.3

4.2.3 Test results

From the beginning of the tests, the lower part of the concrete cracked. Between the supports and the hydraulic cylinders, flexural-shear cracks grew starting from the load introduction points of the notches. In contrast, between the two hydraulic cylinders, bending cracks dominated. Tab. 4.2 summarises the failure loads and the failure modes of the specimens.

In the two experiments with rectangular notches, distinct brittle failure modes were observed. The first specimen (1A) failed due to a combined bending and tensile failure in the

Table 4.2: Preliminary bending tests: test results (* = the specimen was tested with a modified setup to prevent gap opening)

Specimen	Notch geometry	Failure mode	Failure load F_u [kN]	Equivalent distributed load $q_u \approx g + 2F_u/(bl)$ [kN/m^2]
1A	Rectangular notches	Combined bending-tensile failure in LVL plate (brittle)	55	34
1B	Rectangular notches	Shear failure in concrete cross section (brittle)	50	31
2A	2 waves	Horizontal shear failure in concrete along the waves (brittle)	31	21
2B	2 waves *	Horizontal shear failure in concrete along the waves (brittle)	47	29
3A	1 wave	Horizontal shearing-off failure in timber close to the support (brittle)	47	29
3B	1 wave	Horizontal shearing-off failure in timber close to the support (brittle)	47	29
4A	1 wave	Horizontal shearing-off failure in timber close to the support (brittle)	40	26
4B	1 wave *	Horizontal shearing-off failure in timber close to the support (brittle)	49	30

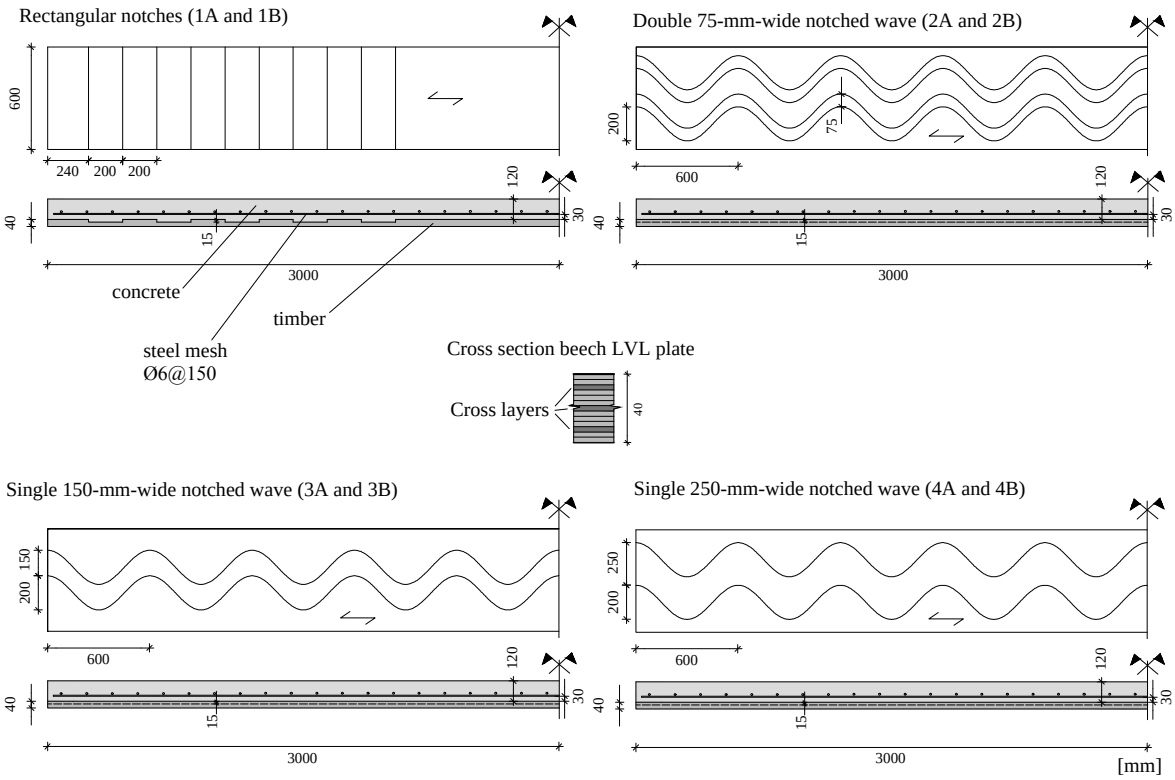

Figure 4.2: Preliminary bending tests: specimens

beech LVL plate at a force of 55 kN per jack. The failure occurred under the notch next to the left cylinder, at a distance of about 2 m from the support (Fig. 4.4, left). In contrast, in the second specimen (1B), a flexural-shear failure occurred in the concrete between the fixed support and the left HEB profile at a force of 50 kN per jack. This failure occurred suddenly and was characterised by the propagation of an existing flexural-shear crack (Fig. 4.4, right).

In the specimens with notched waves, two different brittle failure modes were observed (Fig. 4.5). In the specimens with double notched wave, a horizontal shear failure in the concrete occurred along the waves. In contrast, the specimens with a single notched wave exhibited a combined failure mode. First, a horizontal shearing-off failure occurred in the timber plate close to the fixed support. The failure occurred rapidly, and led to an abrupt and large opening of the gap between timber and concrete. After that, a failure in the concrete between the support and the cylinder occurred, as a consequence of the loss of bond between the timber and concrete. At the end of the test, the LVL plate was still intact, apart from the shearing-off failure close to the support, with no observable bending or tensile failures in the LVL.

Fig. 4.6 compares the structural behaviour of a specimen with rectangular notches to the one with notched waves. Fig. 4.6(a) shows the measured, horizontal relative displacement between the beech LVL plate and the concrete at the supports, as a function of the load applied per cylinder. After each load cycle, a residual plastic deformation can be seen. Further, it can be observed that the connection system with the rectangular notches is stiffer than the connection system with a single notched wave. Fig. 4.6(b) illustrates the measured deflection at mid-span

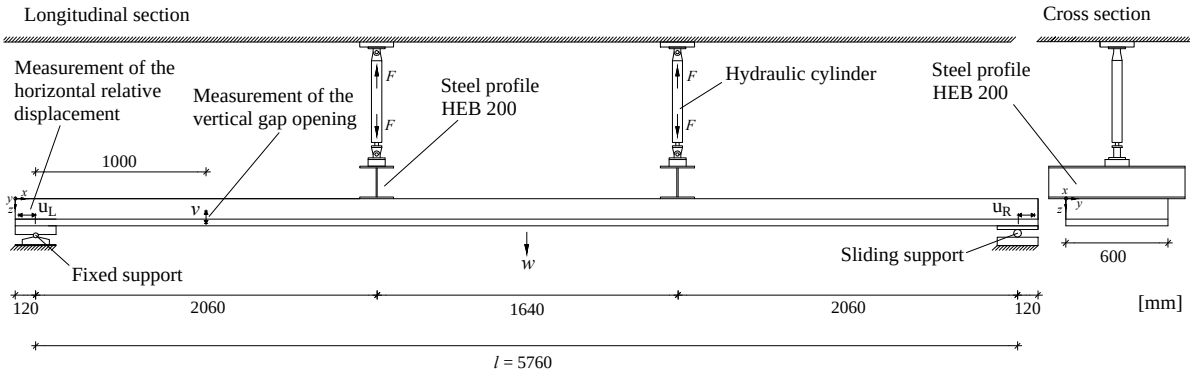

Figure 4.3: Preliminary bending tests: test setup

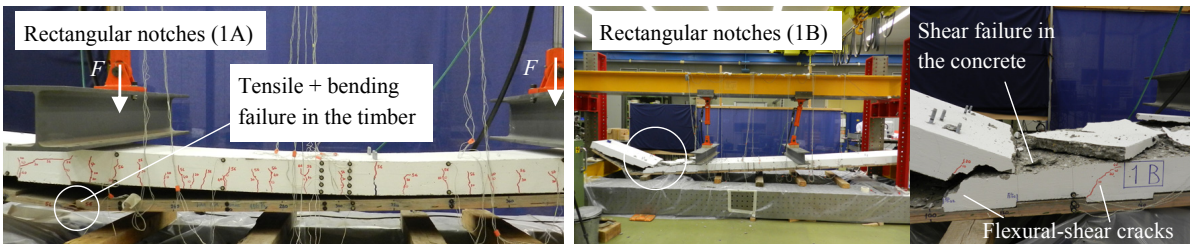

Figure 4.4: Preliminary bending tests: failure modes of the specimens with rectangular notches

as a function of the load applied per cylinder in a specimen with rectangular notches and in one with single notched wave. The specimen with rectangular notches shows slightly smaller deflections.

A phenomenon, which was observed during all tests, was a tendency to vertical gap opening between the timber and concrete starting from the first load levels. This gap opening occured between the hydraulic cylinders and the supports, whereas the area at mid span between the two cylinders did not show this tendency. Fig. 4.7(a) shows the vertical gap opening v measured between the fixed support and the left cylinder of specimen 3B as a function of the vertical load. The gap opening increased in a roughly linear way with increasing cylinder load, and the unloading-reloading cycles denoted a residual part. Fig. 4.7(b) shows a picture of specimen 3B at a load level of 30 kN per cylinder. The gap opening between the right cylinder and the support is clearly visible.

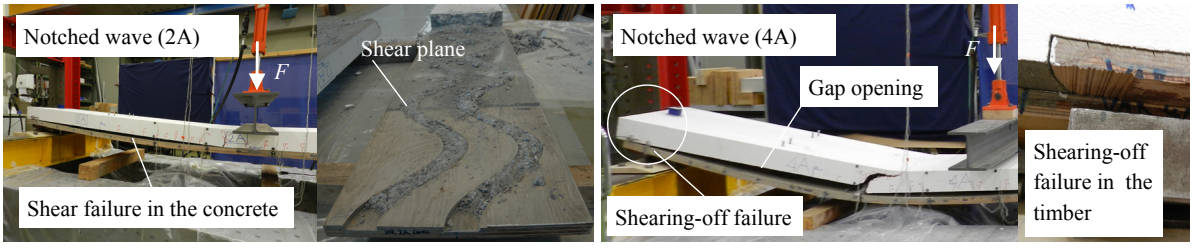

Figure 4.5: Preliminary bending tests: failure modes of the specimens with notched waves

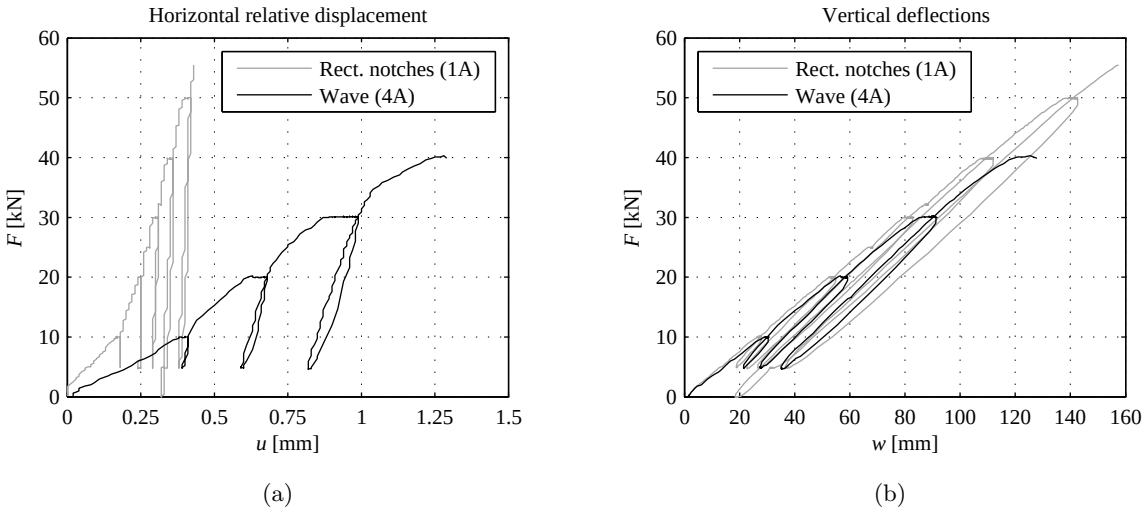

Figure 4.6: Results of the preliminary bending tests: (a) horizontal relative displacement; (b) deflection at mid-span

Two specimens with notched waves (2B and 4B) were tested with a modified test setup to investigate the influence of gap opening [91]. Six external reinforcements made of two steel profiles and two rods each were installed to prevent gap opening. Each reinforcement was provided with a load cell to measure the force which was necessary to keep the gap closed. It was found out that the vertical gap opening compromised the structural behaviour of these specimens. If the gap opening was prevented, the load-carrying capacity and the stiffness of the specimen increased, but the failure mode of the notched connection remained basically the same.

4.2.4 Comparison with the analytical model

First of all, it must be reminded that this test series had been performed before the model of Chapter 3 was developed. In the comparison of the test results with the analytical model, only the specimens with rectangular notches (1A and 1B) are considered. Since all notches were cut over the entire width of the specimens, it is assumed that the effective timber depth is 25 mm between the supports and the cylinders, and 40 mm between the two cylinders.

The elastic deflections are predicted according to Section 3.2 under the assumption that the concrete layer is cracked over the entire span. From the results of the shear tests described in Section 4.3, a connection stiffness of 650 kN/mm is assumed, which gives a γ-factor of round 0.95. Fig. 4.8(b) shows that the predicted elastic deflections are slightly smaller than the measured values.

The expected failure loads of the composite slabs represented in Fig. 4.8(a) are calculated according to the analytical model presented in Sections 3.2 and 3.3. First, the compressive strength of the concrete should be reached on top of the cross-section (1C,c). However, this could not be observed. The consequence would be a redistribution of the axial stresses within the compression zone by increasing strain. Afterwards, a combined bending-tensile failure in

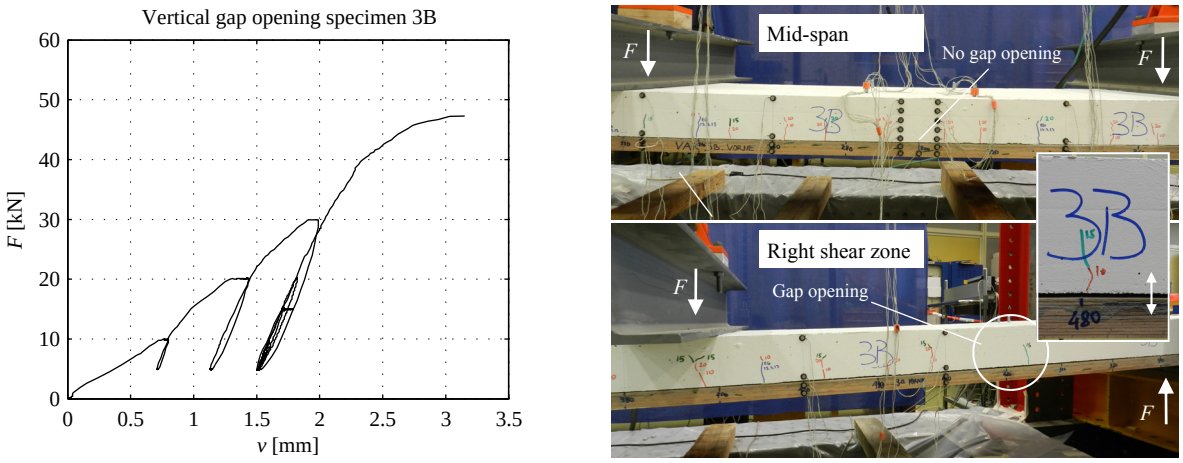

Figure 4.7: Gap opening in specimen 3B: (a) relationship between the cylinder load and the gap opening ; (b) gap opening at a load level of 30 kN

the timber (2BT) should occur at $F = 48$ kN per cylinder. This prediction corresponds approximately to the behaviour of specimen 1A, which failed due to a combination of tension and bending at a cylinder force of $F = 55$ kN. In specimen 1B, a flexural-shear failure in concrete occurred, although this failure was predicted at a cylinder load of about 100 kN. This shows evidence that the aspect of the model with the highest uncertainty is the structural behaviour of the unreinforced concrete member in the cracked zone, as assessed in Section 3.3.8.

The main reason for this discrepancy is that, as explained in Section 3.3.8, there are several factors which cannot be taken into account by the cantilever model used to predict the flexural-shear failure. The effective height of the cantilever $h_{1F,eff}$ may be smaller than the value assumed by the model ($h_{1F,eff} < h_{1F} = 2l_N - h_{cr}$). Since this parameter governs the section modulus for the calculation of the tensile stress σ_{1z}, it has a big influence on the flexural-shear failure load $T_{R,1F,Ni}$ calculated with the modified Mohr-Coulomb failure criterion (Fig. 4.9(a)). Fig. 4.9(b) shows the influence of $h_{1F,eff}$ on the cylinder load F_{1F} which causes a flexural-shear failure. An increase $h_{1F,eff}$ from 200 to 300 mm duplicates the failure load. Another problem of the cantilever model is that it assumes an idealised crack geometry. The crack depth h_{cr} may be locally greater than assumed, thus causing an increase of the lever which causes the tensile stresses in the concrete, or reducing h_{1F}. This experimental result shows the difficulty to model a cracked concrete section. However, to perform a complete evaluation of the problem, it would be necessary to carry out more experiments.

According to the analytical model, the other types of failure (e.g. shearing-off failure of the timber or compressive failure of the timber parallel to the grain) should occur at higher load levels than the maximum loads reached in the tests. During the experiments, these failures were not observed.

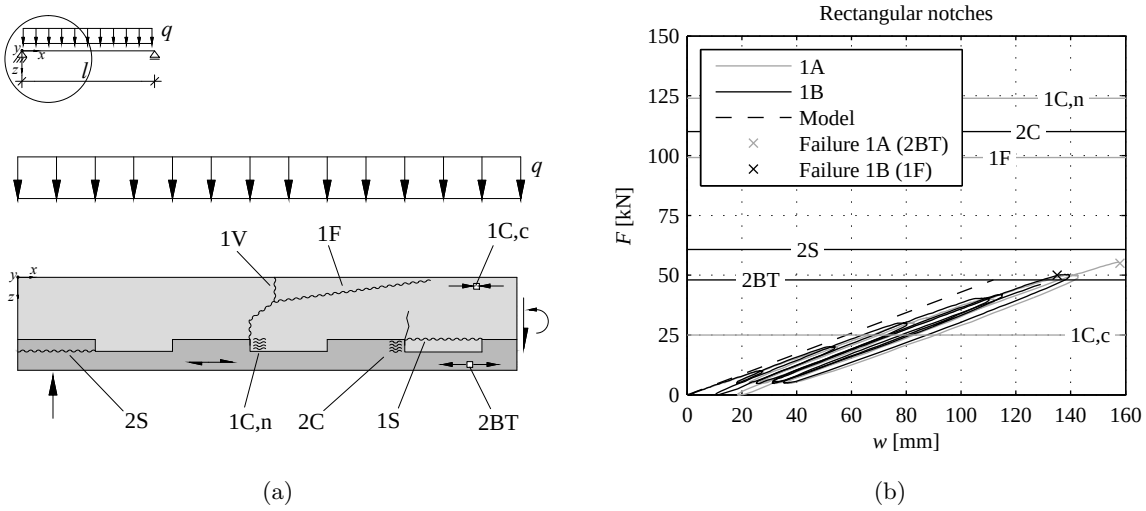

(a) (b)

Figure 4.8: Preliminary bending test of the specimens with rectangular notches: (a) failure modes calculated with the model; (b) comparison between test results and prediction

4.2.5 Discussion

Since these bending tests were performed at the beginning of the research project, the specimens were not designed according to the models of Sections 3.2 and 3.3. Indeed, brittle failures governed the tests and the structural behaviour was not optimal. Nevertheless, several conclusions can be drawn.

The first important outcome was that the bending tests demonstrated adequate load-carrying capacity of five of the six slabs assuming typical loads for office buildings (permanent load of 2.5 kN/m^2 and live load of 3 kN/m^2). The measured failure loads were higher than the design loads by factors of 2-3.

In all of the experiments, brittle failure was observed: bending and tensile failures in the timber, shear failures in the concrete, and shearing-off failures in the timber. This is an aspect of the structure that must be improved, because a brittle failure is not wanted. These experiments evidenced that, if the notch is located in a cracked concrete zone, the crack configuration can cause important structural problems like for instance flexural-shear failures which compromise the structural behaviour and are difficult to predict.

The first main difference between the connection systems tested is that the specimens with rectangular notches failed in the cross-section, whereas those with notched waves failed in the area of the waves and, as consequence, carried less load. Horizontal shearing-off failure in the wave could be caused by insufficient amplitude, thus causing excessive stress concentration.

All the notched connections tested were stiff, with rectangular notches being stiffer than the notched waves. The horizontal slip measured in the specimens with notched waves was higher than in those with rectangular notches. One possible reason for are the dimensions of the area for the force transfer. In the specimens with rectangular notches, the force is transferred along the full width of the specimen (600 mm), while in the wave notch specimens, the force is concentrated

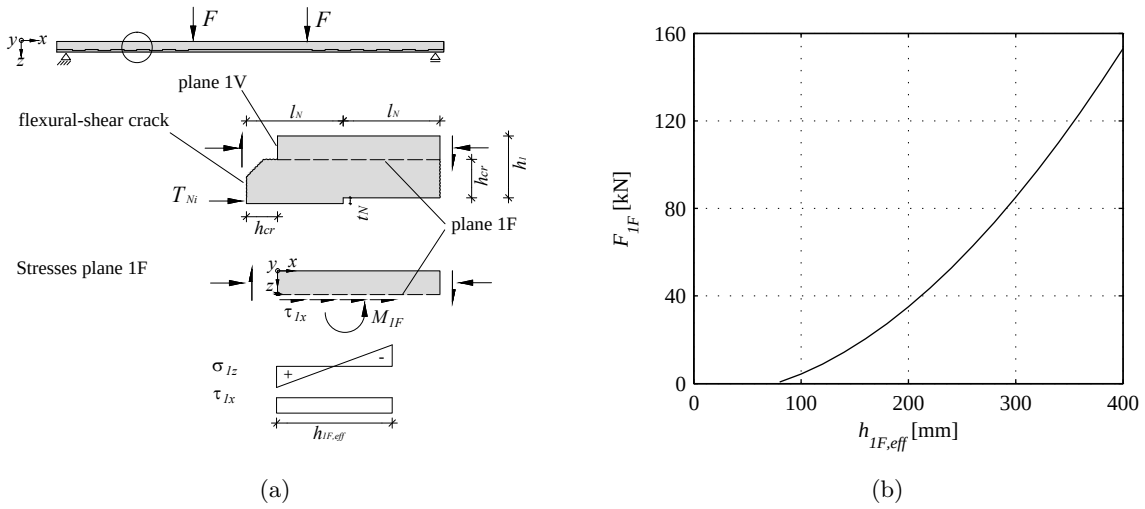

Figure 4.9: Preliminary bending test of the specimens with rectangular notches: (a) model for the prediction of flexural-shear failures; (b) relationship between the effective height of the failure plane 1F and the vertical cylinder load which causes a flexural-shear failure in the concrete

in limited zones smaller than 600 mm. Consequently, the specimens with rectangular notches showed a stiffer load-deflection behaviour because of the higher connection stiffness.

The causes of the gap opening observed between the supports and the loads are difficult to identify. Since this phenomenon occurred in the sectors where shear forces were transferred between the two parts of the composite member, a reason is probably the eccentricity between the action point of the axial forces and the interface. As explained in Section 3.3.13, this can generate different curvatures of the parts, causing gap opening during elastic behaviour. In the contact areas of the notches, the contact forces mobilise friction between the timber and concrete, which opposes to gap opening. However, as assessed in Section 3.3.13, these phenomena are difficult to quantify.

An aspect with potential of improvement is the configuration of the cross layers of the beech LVL plate. The cross layer at mid-height of the LVL plate coincides approximately with the bottom of the notches and thus lowers the resistance against shearing-off failure of the timber close to the notch.

Although the specimens with rectangular notches showed the best results, the exploitation of beech LVL was not optimal, because all notches were cut over the full width of the specimens. This means that, in the area with the maximal bending moment, the effective depth of the timber cross-section was 25 mm instead of 40 mm. Consequently, the resistance against a combined bending-tensile failure of the timber markedly decreased. This makes it more difficult to achieve a ductile failure.

In conclusion, these preliminary experiments showed that timber-concrete composite slabs made of beech LVL have a significant potential and put in evidence several issues of the notched connections. The results helped to develop models and constituted a starting point for the following research steps.

4.3 Connection shear tests

4.3.1 Introduction

The structural behaviour of notched connections for timber-concrete composite slabs made of beech LVL was studied with a series of shear tests. The influence of different notch geometries and material properties was investigated, and the test results allowed an evaluation of the load-carrying capacity and an estimation of the stiffness and the ductility of the connections tested. Furthermore, the test results were compared to the analytical models presented in Section 3.3.

4.3.2 Materials and methods

Test concept

The test-setup depicted in Fig. 4.10 was chosen because it simulated the forces acting on the notch close to the support of a timber-concrete composite member with positive bending moment. Because of equilibrium conditions, a shear test to study the behaviour of the other notches would be much more difficult to develop. Therefore, the test setup shown in Fig. 4.10 was not able to reproduce all aspects of the structural behaviour of the remaining notches between the support and the mid-span. First, the other notches do not face the influence of vertical compression due to the force transfer to the support. Secondly, in the notch close to the support, the load is transferred from the concrete to the timber in a direct way with a compression strut, whereas, in the other notches, tensile and shear stresses occur as shown in Section 3.3.8.

In the test concept shown in Fig. 4.10, in contrast to many current test methods, the timber part is pulled. Also in reality, the timber part of a composite slab with positive bending moment is subjected to tension. As discussed by Gehri [92], in the case of shear tests on connections, the fact that the load is introduced by pushing or by pulling the members influences the results. Similar issues were discussed by Steurer [63] (Section 2.7).

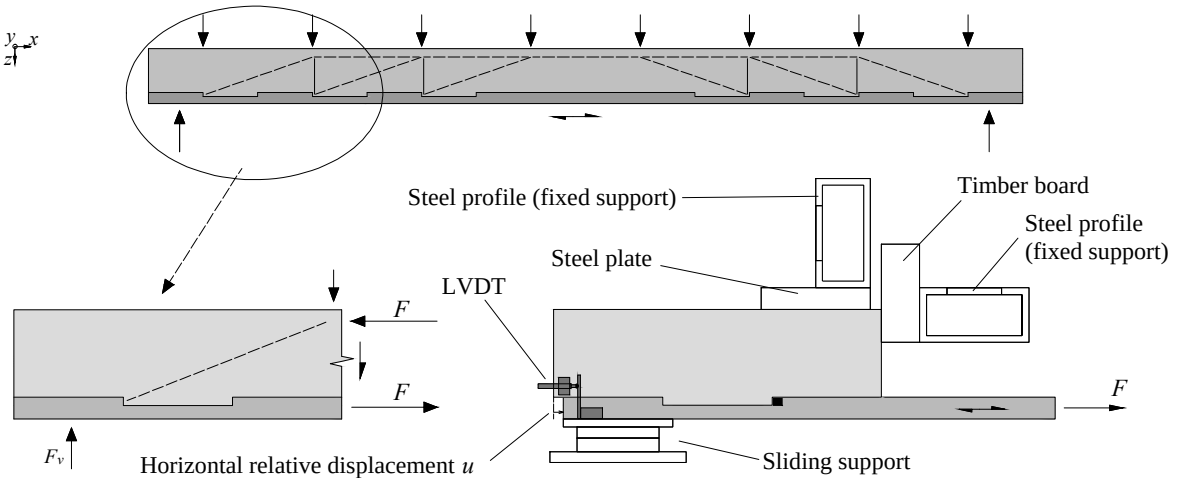

Figure 4.10: Connection shear tests: test concept

Test setup

The test setup described in Fig. 4.10 consisted of a tensile testing machine, which clamped and pulled the beech LVL plate, and a steel construction which carried the reaction forces necessary to ensure equilibrium of the system. The measurement setup was composed of six sensors: four linear voltage displacement transducers (LVDTs) to measure the relative displacements between the timber and concrete (Fig. 4.10) and two load cells to detect the vertical reaction force in the support F_v. The horizontal load F was directly measured by a load cell in the tensile testing machine.

Specimens

In the course of the experiments, the structural behaviour of 28 timber-concrete composite specimens with notched connections was investigated. Fig. 4.11 illustrates the geometry of the specimens and the configuration of the veneers in the beech LVL plates. In this experimental series, the beech LVL plates produced by the company Pollmeier were equal to those used in the preliminary bending tests (Section 4.2). The LVL material was not tested because it was assumed that the mechanical properties corresponded to those tested by Van de Kuilen and Knorz [14], [15] and summarised in Tab. 2.1. The differences between the approved material and the material used in these experiments are discussed in Section 4.2.

Tab. 4.3 illustrates an overview of the characteristics of the specimens tested, and Tab. 4.4 shows the mechanical properties of the concrete.

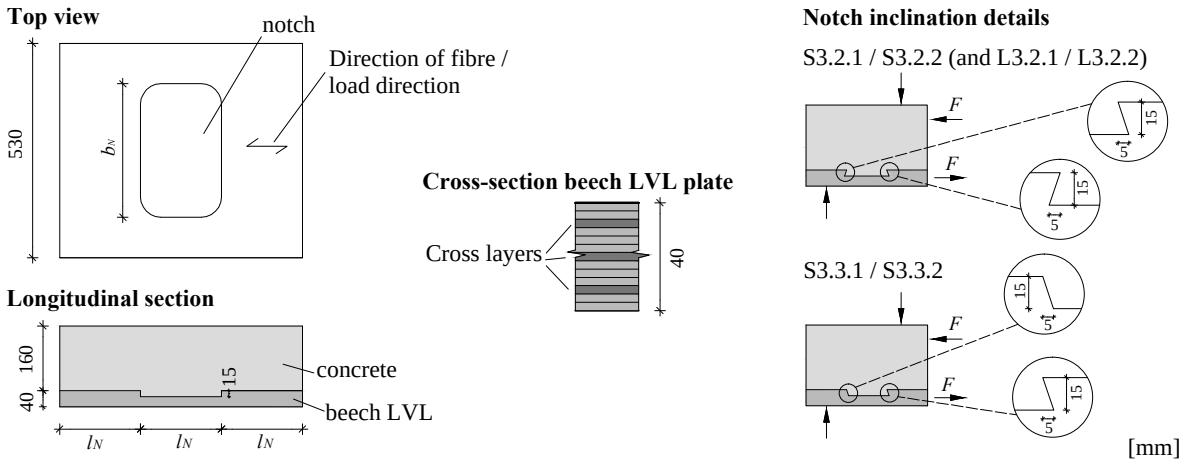

Figure 4.11: Connection shear tests: specimens

The specimens were 530 mm wide and were made of beech LVL plates with a thickness of 40 mm (Fig. 4.11). A 160 mm thick concrete layer was poured on the beech LVL plates. The connection between the timber and concrete was realised with 15 mm deep rectangular notches cut into the beech LVL plate. As shown in Tab. 4.3, two groups of timber-concrete composite specimens were tested: specimens with long notches (L) and specimens with short notches (S). In the specimens with long notches, the length of the concrete notch, the length of the timber over the support and the concrete length behind the notch were 200 mm each. As a result, the

Table 4.3: Connection shear tests: specimens

Specimen	Notch length l_N [mm]	Notch width b_N	Notch edge inclination	Concrete
L3.1	200	530	no	Concrete C50/60 + steel mat
L3.2	200	530	yes	Concrete C50/60 + steel mat
L3.1.f	200	530	no	Steel fibre reinforced concrete C35/45
L3.4	200	330	no	Concrete C50/60 + steel mat
S3.1	100	530	no	Concrete C50/60 + steel mat
S3.2	100	530	yes	Concrete C50/60 + steel mat
S3.3	100	530	yes	Concrete C50/60 + steel mat
S3.1.f	100	530	no	Steel fibre reinforced concrete C35/45
S3.4	100	330	no	Concrete C50/60 + steel mat

concrete layer poured on the timber had a total length of 600 mm. In the specimens with short notches, the length of the concrete notches, the length of the timber over the support and the concrete length behind the notch were 100 mm, and, consequently, the total concrete length was 300 mm.

The reference specimens of both groups (L3.1 and S 3.1) had a 530 mm wide notch with vertical edges (the notch edges were perpendicular to the horizontal surface of the beech LVL plate) and were made of a concrete C50/60 according to the Swiss Standard SIA 262 [66]. As done in the push-out tests on timber-concrete composite elements made of spruce LVL performed by Blass et al. [28], a thin reinforcing steel mat (diameter 6 mm and spacing 150 mm) was used to prevent unfavourable consequences of concrete shrinkage. Furthermore, the concrete C50/60 contained a liquid admixture to reduce drying shrinkage. For each group of specimens, the influence of several parameters was investigated. First, different inclinations of the notch edges were tested. In addition to the notches with vertical edges, the structural behaviour of notches with inclined edges was investigated. In these specimens (L3.2, S3.2 and S3.3), the edges were inclined by about 70° in positive and negative directions (Fig. 4.11). Secondly, the influence of the notch width was studied. Two specimens per group were constructed with beech LVL plates with 330 mm wide notches, instead of 550 mm (L3.4 and S3.4). In a third step, the variation in concrete mixture was investigated. In contrast to the specimens made of concrete C50/60 with reinforcing steel mat, two specimens per group were made of a steel fiber reinforced concrete C35/45 without reinforcing bars.

4.3.3 Test results

In this experimental series, three different failure modes were observed:

- a brittle shearing-off failure in the timber, which occurred mostly in the middle cross layer located close to the bottom of the notch (Fig. 4.12(a))

Table 4.4: Connection shear tests: concrete properties

Property		Concrete C50/60	Steel fibre reinforced concrete C35/45
Modulus of elasticity E_1	[N/mm^2]	36800	32900
Cylinder strength $f_{c,1}$	[N/mm^2]	44.4	47.5
Splitting tensile strength $f_{t,1}$	[N/mm^2]	3.3	3.7
Density	[kg/m^3]	2439	2389
Steel fibres content	[kg/m^3]	0	25
Diameter of the reinforcing bars	[mm]	6	-
Spacing of the reinforcing bars	[mm]	150	-
Maximum aggregate diameter	[mm]	16	16
Additives		Shrinkage reducing admixture	-

- a ductile compressive failure of the timber (Fig. 4.12(b))

- a brittle concrete failure (Fig. 4.12(c))

After the experiments, it was observed that some specimens showed a diagonal crack in the concrete irrespective of their failure mode (Fig. 4.12(d)). Some tests were interrupted when a horizontal load of 400 kN was reached because this load was critical for the test-setup.

Tab. 4.5 summarises the failure modes of all specimens, the maximum loads F_u, and the shear stiffness of the notch at service level K_{ser} obtained from the horizontal relative displacement measured between the timber and concrete as described in Section 2.3.3.

The relationship between the load F and the horizontal relative displacement u between the timber and concrete is illustrated in Figs. 4.13 and 4.14. In general, before the failure, if the diagram is enlarged, the curves are not completely elastic but denote a non-linearity, which causes a decrease in stiffness. This effect can be observed by comparing, for instance, Fig. 4.13(a) with Fig. 4.13(b), and Fig. 4.14(a) with Fig. 4.14(b). In Fig. 4.13(d), and Fig. 4.14(d), it can be seen that the stiffness of the specimens with reduced notch width is smaller. The diagrams of some specimens show a plateau. It is important to note that this plateau is related to a ductile failure only in the case of the specimens which failed due to a compressive failure in the timber (e.g. L3.1.f.1). In the other specimens, the plateau developed in less seconds and was related to the formation of cracks or to the initiation of brittle failures. For instance, in the case of the specimens with diagonal cracks (Fig. 4.12(d)), the plateau coincided with the crack opening process. As shown in Fig. 4.13(d), the plastic phase of specimens L3.4.1 and L3.4.2 denoted a slight hardening. In specimen L3.4.2, the hardening induced a shearing-off failure of the timber after the plastic deformation.

4.3.4 Comparison with the analytical model

In this section, the failure loads measured during the tests are compared to the estimation calculated with the analytical model for the structural behaviour of notched connections presented in Section 3.3. However, since the tests reproduce the notches over the supports, some particularities have to be taken into account. The horizontal component of the diagonal compression strut goes through the notch into the timber part of the composite member and the vertical component is transferred to the support. The load has many possibilities to be transferred, and, in reality, follows the most direct and efficient way. Since the concrete part does not contain reinforcing bars, the exact load-carrying mechanism is difficult to determine. Fig. 4.15 shows two possible load-carrying mechanisms in the concrete. It can be seen that, depending on the mechanism, tension occurs in the concrete. Furthermore, in the notch close to the support, the stress configuration in the concrete is different than in the other notches. Indeed, the remaining notches can be modelled like a series of cantilevers fixed in the compression zone, and are subjected to tension and shear stresses. Therefore, several issues of concrete notches could not be investigated in this test series.

In order to predict the type of failure according to the analytical models described in Section 3.3, some simplifications must be done. Fig. 4.16 illustrates the simplified models assumed to calculate the failure loads. It is assumed that three failure modes can occur: a shearing-off failure in the timber (2S), a compressive failure in the timber (2C) and a compressive failure in the concrete (1C,n). Tab 4.6 summarises the methods used to determine the critical stresses and the applied failure criteria. The theoretical failure loads of the specimens tested are calculated using the concrete properties listed in Tab. 4.4 and the timber properties listed in Tab. 2.1.

For the prediction of the concrete failure (1C,n), it is assumed that the force is concentrated in a diagonal strut. To predict the failure load, the compressive stress is calculated in the smallest section of the strut which corresponds to the projection of the notch edge, and a uni-axial strength criterion is applied.

Failure in the timber is predicted by considering the timber part as a plain stress state and by calculating the interaction between the stresses σ_z, σ_x and τ, generated by F and F_v, using the Tensor Polynomial theory. To achieve a rough estimation of the failure load, the Tensor Polynomial theory is applied with the interaction term F_{12} set to zero as shown in Section 2.4.1.

The main difficulty in predicting the timber failures 2C and 2S is the quantification of the vertical stress σ_z. As explained in Sections 3.3.5 and 3.3.6, this stress results from the superposition of the stresses due to the eccentricity of F in respect of the shear plane and the vertical compressive stresses due to the transfer of F_v to the support. Whereas the first component can be analytically estimated (Eq. 3.127), the distribution of the vertical compressive stress is unknown. For the following calculations, it is assumed that the vertical compressive stress is uniformly distributed over the notch length and the notch width (Tab. 4.6). With this assumption, the resulting vertical stress σ_z is always a compressive stress.

To predict the shearing-off failure (2S) according to the analytical models set up in Section 3.3.6, a critical shear plane must be identified. Since, as shown in Fig. 4.11, a cross layer is located slightly below the bottom of the notch, it is assumed that this layer corresponds to

Table 4.5: Results of the connection shear tests: shear stiffness K_{ser}, maximum load F_u, and failure

Specimen	K_{ser} [kN/mm]	F_u [kN]	Cause of interruption of test	Failure type
L3.1.1	690	386	Rolling shearing-off failure of the middle cross layer (2S)	Brittle
L3.1.2	617	400	The test was interrupted. After that, a diagonal crack in the concrete was observed.	[-]
L3.2.1	756	400	The test was interrupted. After that, a diagonal crack in the concrete was observed.	[-]
L3.2.2	835	393	Compressive failure in timber (2C)	Ductile
L3.1.f.1	797	388	”	”
L3.1.f.2	747	356	”	”
L3.4.1	220	311	Compressive failure in the timber (2C). After that, the concrete layer slid out of the notch	Ductile deformation, then sliding out
L3.4.2	200	310	Compressive failure in the timber (2C). Then, shearing-off failure of the timber	Ductile deformation, then brittle failure
S3.1.1	569	295	Rolling shearing-off failure of the middle cross layer (2S)	Brittle
S3.1.2	1010	366	”	”
S3.2.1	999	348	Shearing-off failure of the timber (2S) (90% rolling shear failure, 10% shear failure parallel to the grain)	”
S3.2.2	1213	385	Rolling shearing-off failure of the middle cross layer (2S)	”
S3.3.1	1403	397	The test was interrupted. The specimen did not show damages.	[-]
S3.3.2	821	341	Rolling shearing-off failure of the middle cross layer (2S)	Brittle
S3.1.f.1	928	382	Shearing-off failure of the timber (2S) (50% rolling shear failure, 50% shear failure parallel to the grain)	”
S3.1.f.2	591	355	Shearing-off failure of the timber (2S) (90% rolling shear failure, 10% shear failure parallel to the grain)	”
S3.4.1	159	318	Shearing-off failure of the timber (2S)	”
S3.4.2	213	319	Brittle concrete failure	”

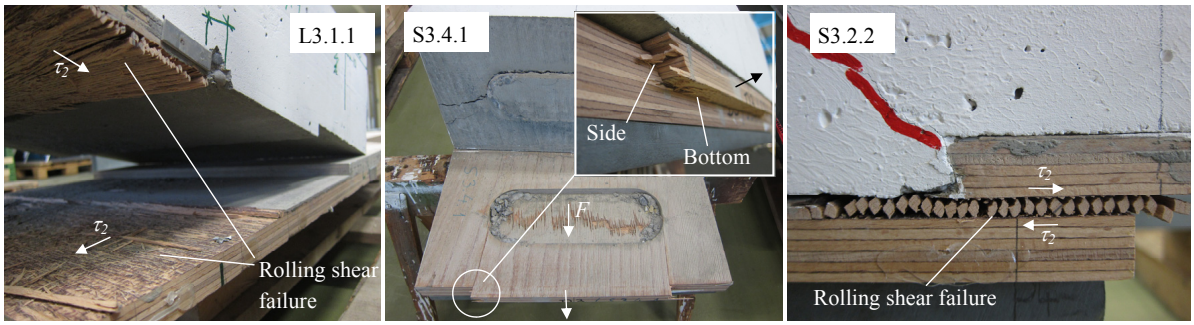

(a)

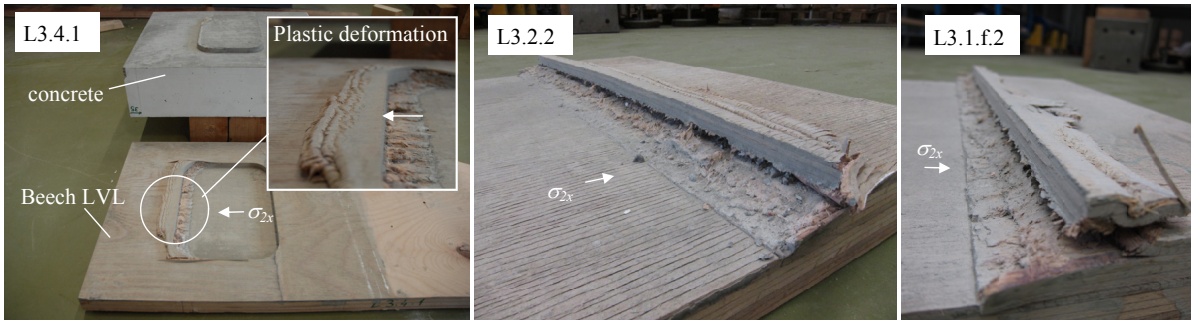

(b)

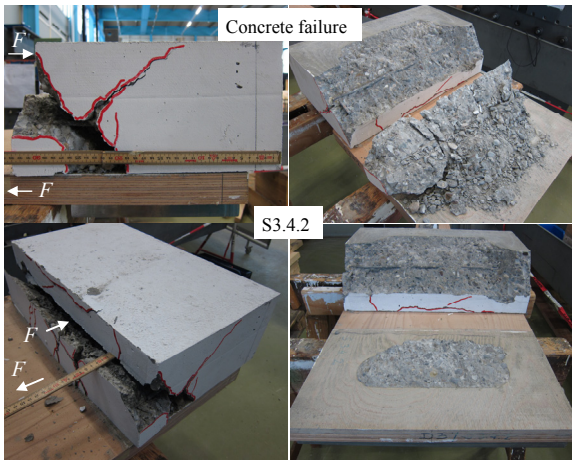

(c)

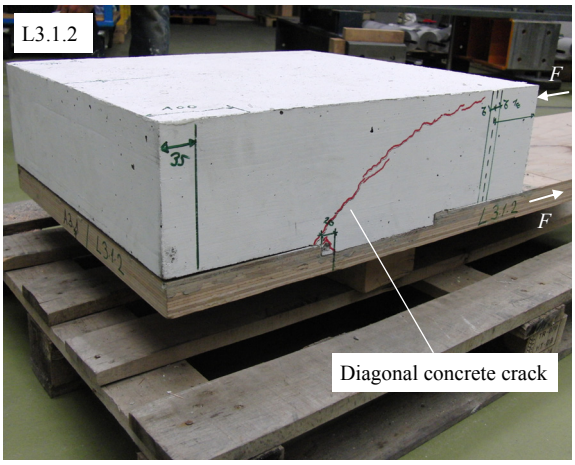

(d)

Figure 4.12: Connection shear tests: (a) shearing-off failure of the timber (2S); (b) compressive failure of the timber (2C); (c) concrete failure; (d) diagonal crack in the concrete

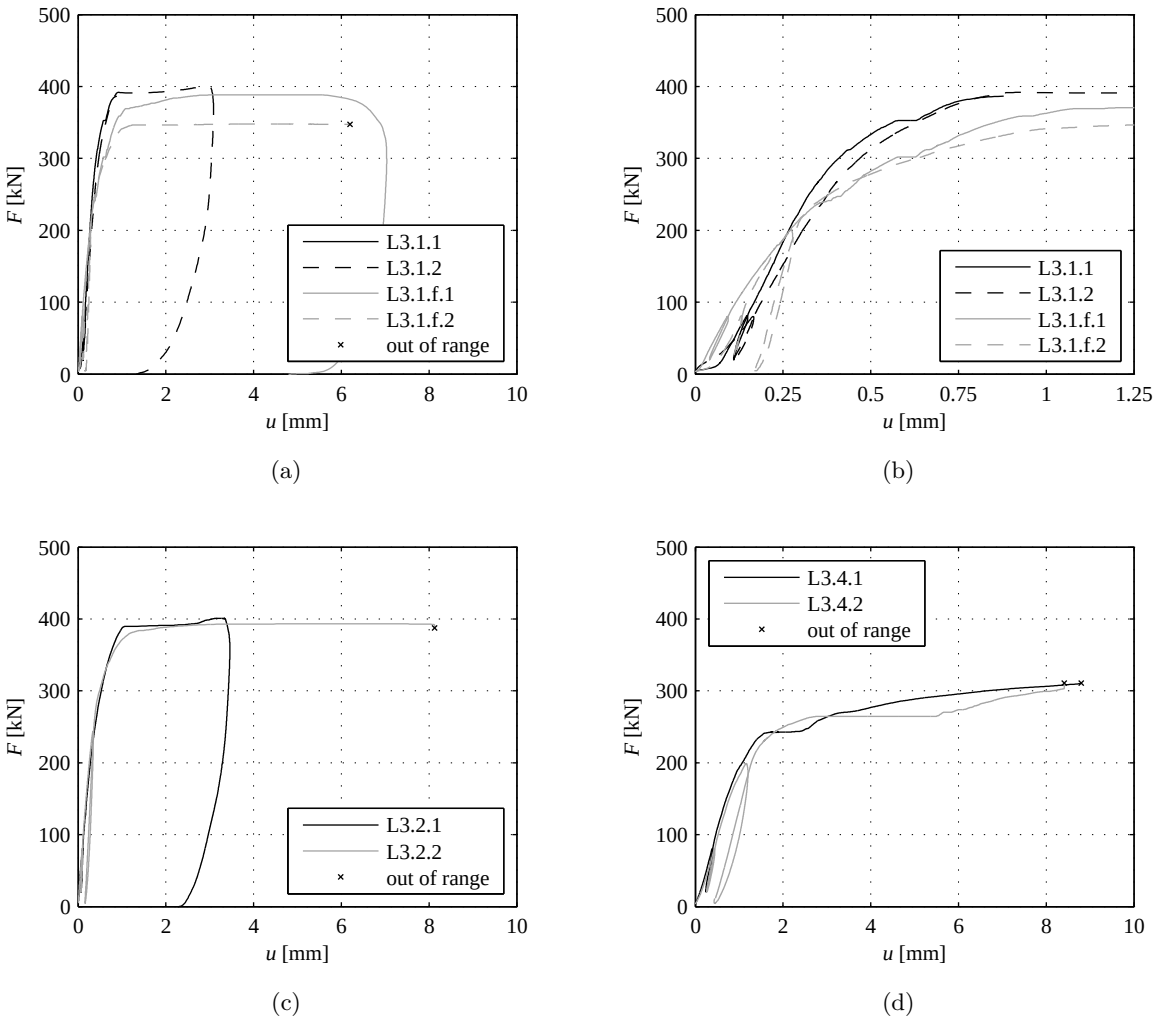

Figure 4.13: Results of the shear tests on the specimens with long notches (L): (a) specimens with $b_N = 530$ mm and notch edges perpendicuar to the interface; (b) magnification of (a); (c) specimens with $b_N = 530$ mm and inclined notch edges; (d) specimens with reduced notch width ($b_N = 330$ mm) and notch edges perpendicular to the interface

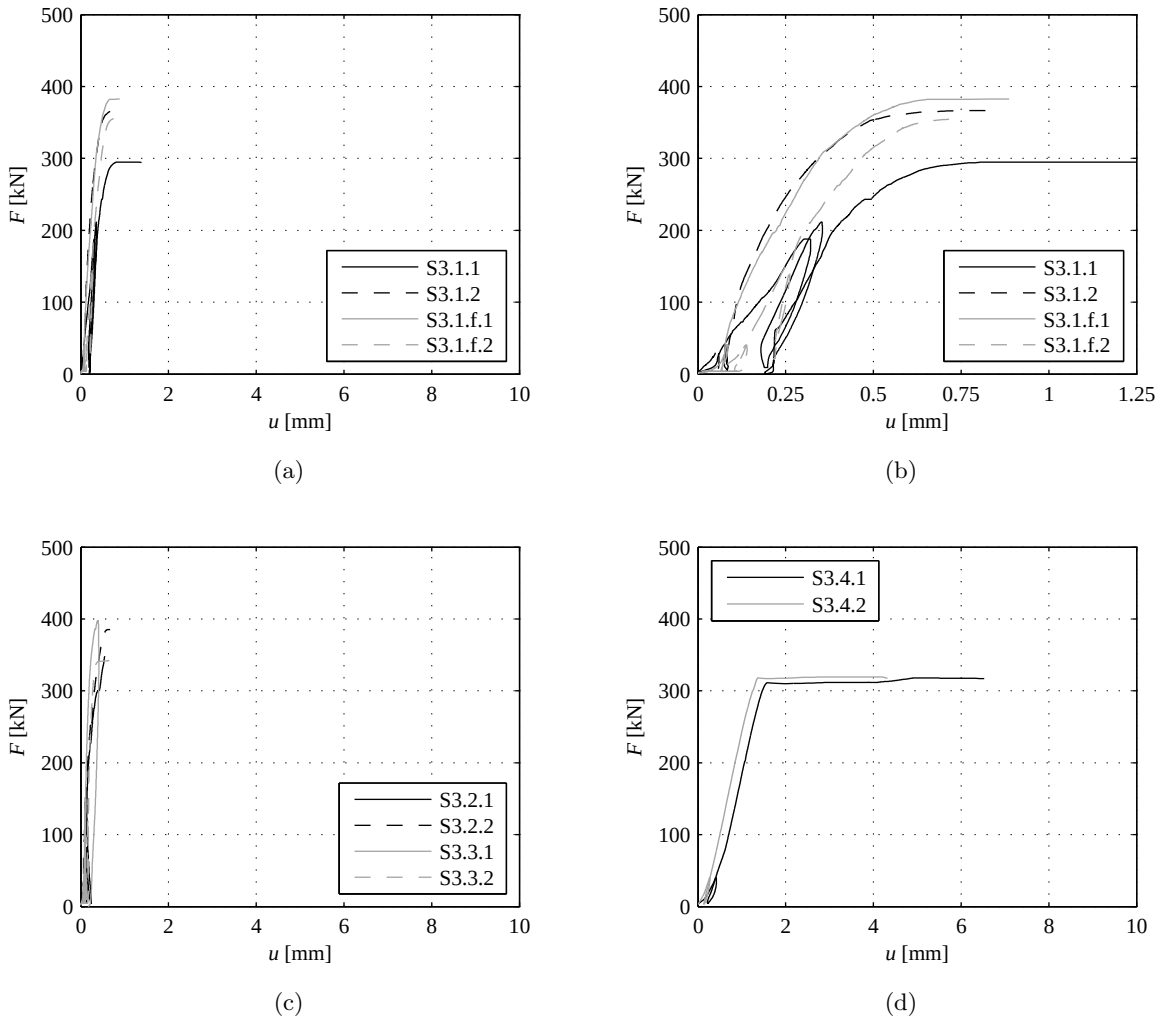

Figure 4.14: Results of the shear tests of the specimens with short notches (S): (a) specimens with $b_N = 530$ mm and notch edges perpendicuar to the interface; (b) magnification of (a); (c) specimens with $b_N = 530$ mm and inclined notch edges; (d) specimens with reduced notch width ($b_N = 330$ mm) and notch edges perpendicular to the interface

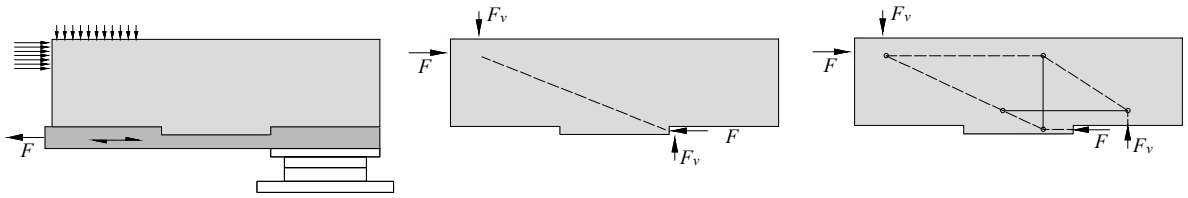

Figure 4.15: Connection shear tests: possible load-carrying mechanisms in the concrete part of the composite member

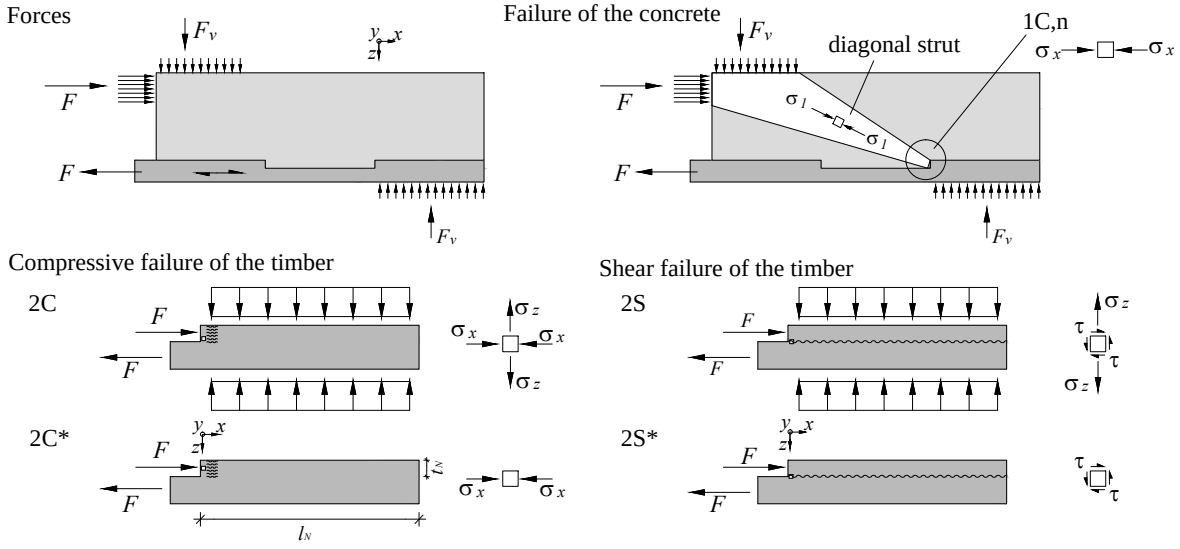

Figure 4.16: Connection shear tests: model to predict different types of failure

the shear failure surface. Therefore, the failure criterion obtained from the Tensor Polynomial theory (Eq. 3.163) is applied by taking into account the rolling shear strength of beech LVL $f_{Rv,2}$.

As illustrated in Tab. 4.6, since the distribution of the shear stress over $8t_N$ used in the analytical model is a rough estimation, a failure force $F_{2S,sup}$ is calculated assuming that the shear stress is distributed over the entire notch length l_N.

In the case of the specimens with reduced notch width, it is assumed that the notch sides contribute to the shear resistance of the specimen. The amount of shear force carried by the notch sides is estimated as follows:

$$F_{2s,sides} = 2 \cdot f_{v,2} \cdot l_N \cdot t_N \tag{4.1}$$

As discussed in Sections 3.3.5 and 3.3.6, the influence of the stress perpendicular to the interface σ_z on the failure types 2S and 2C depends on the notch geometry, and in some cases can be neglected. In the comparison, the failure loads of the timber are also predicted without taking into account the vertical stresses. The resulting failure loads are named 2C* and 2S*.

The comparison between experimental results and predicted failure loads shows, in some cases, a good agreement, and, in other cases, several discrepancies (Fig. 4.17). The reason for lies mostly in the simplifications assumed in the models.

Regarding the timber failures, the main simplifications in the models are the distribution of the vertical pressure caused by the transfer of F_v to the supports, and the rectangular shear stress distribution. Also the linear distribution of the vertical tension generated by the eccentricity is strongly idealised. Furthermore, the amount of horizontal load transferred from the concrete to the timber by means of friction is difficult to quantify, and in the analytical calculations was neglected.

Nevertheless, by considering multi-axial stress states by means of the Tensor Polynomial theory, prediction accuracy is improved. Furthermore, this approach shows evidence of several differences between the specimens with long and short notches:

- In the specimens with long notches (L), the estimated vertical compressive stress is very small. Therefore, the consideration of the multi-axial stress state does not change the prediction significantly. The differences between 2S* and 2S, and between 2C* and 2C are small.

- In contrast, in the specimens with short notches (S), the consideration of the multi-axial stresses by means of the Tensor Polynomial theory markedly increases the predicted failure loads. In these specimens, since the area b_N x l_N is smaller and the ratio F_v/F_h is higher, the vertical stresses are higher than in the specimens with long notch. Therefore, if the vertical stress is taken into account, F_{2C} is significantly higher than F^*_{2C}. This could explain the fact that, in the specimens with short notches, a compressive failure of the timber did not occur.

The model used to predict the compressive concrete failure in the notch (1C,n) is strongly simplified. Probably, in reality, the stresses in the concrete distribute in a different way than via the single compression strut of Fig. 4.15. A brittle concrete failure was observed only in one specimen with short notches (S3.4.2). As shown in Fig. 4.17, the model underestimated this failure load. In contrast, as shown in Fig. 4.17, the measured curves of all specimens except S3.4.1 and S3.4.2 slightly exceed the predicted failure force of concrete.

The diagonal crack observed in some specimens after the test (Fig. 4.12(d)) could be caused by tension in the concrete layer generated by the transfer of the force to the support as shown in Fig. 4.15.

4.3.5 Discussion

This analysis concentrated on the last notch close to the support. Although several conclusions are valid for every notch, it has to be taken into account that this test was not able to reproduce the structural behaviour of the remaining notches between the support and the mid-span, which do not benefit from the positive influence of vertical compression and have to carry a combination of shear and tension stresses in the concrete.

Table 4.6: Connection shear tests: stresses and failure criteria used to predict the failures

Type of failure		Stresses in the critical point	Failure criterion	
Shearing-off failure in the timber	2S	$\tau = \frac{F}{b_N \cdot 8t_N}$ $\sigma_z = \frac{3t_N F}{b_N l_N^2} - \frac{F_v}{b_N l_N}$	Tensor Polynomial theory	Eq. 3.163
	2S,sup	$\tau = \frac{F}{b_N \cdot l_N}$ $\sigma_z = \frac{3t_N F}{b_N l_N^2} - \frac{F_v}{b_N l_N}$	Tensor Polynomial theory	Eq. 3.163
	2S*	$\tau = \frac{F}{b_N \cdot 8t_N}$	$\tau = f_{Rv,2}$	
Compressive failure in the timber	2C	$\sigma_x = \frac{F}{b_N t_N}$ $\sigma_z = \frac{3t_N F}{b_N l_N^2} - \frac{F_v}{b_N l_N}$	Tensor Polynomial theory	Eq. 3.130
	2C*	$\sigma_x = \frac{F}{b_N t_N}$	$\sigma_x = f_{c,0,2}$	
Compressive failure in the concrete	1C,n	$\sigma_x = \frac{F}{b_N t_N}$	$\sigma_x = f_{c,1}$	

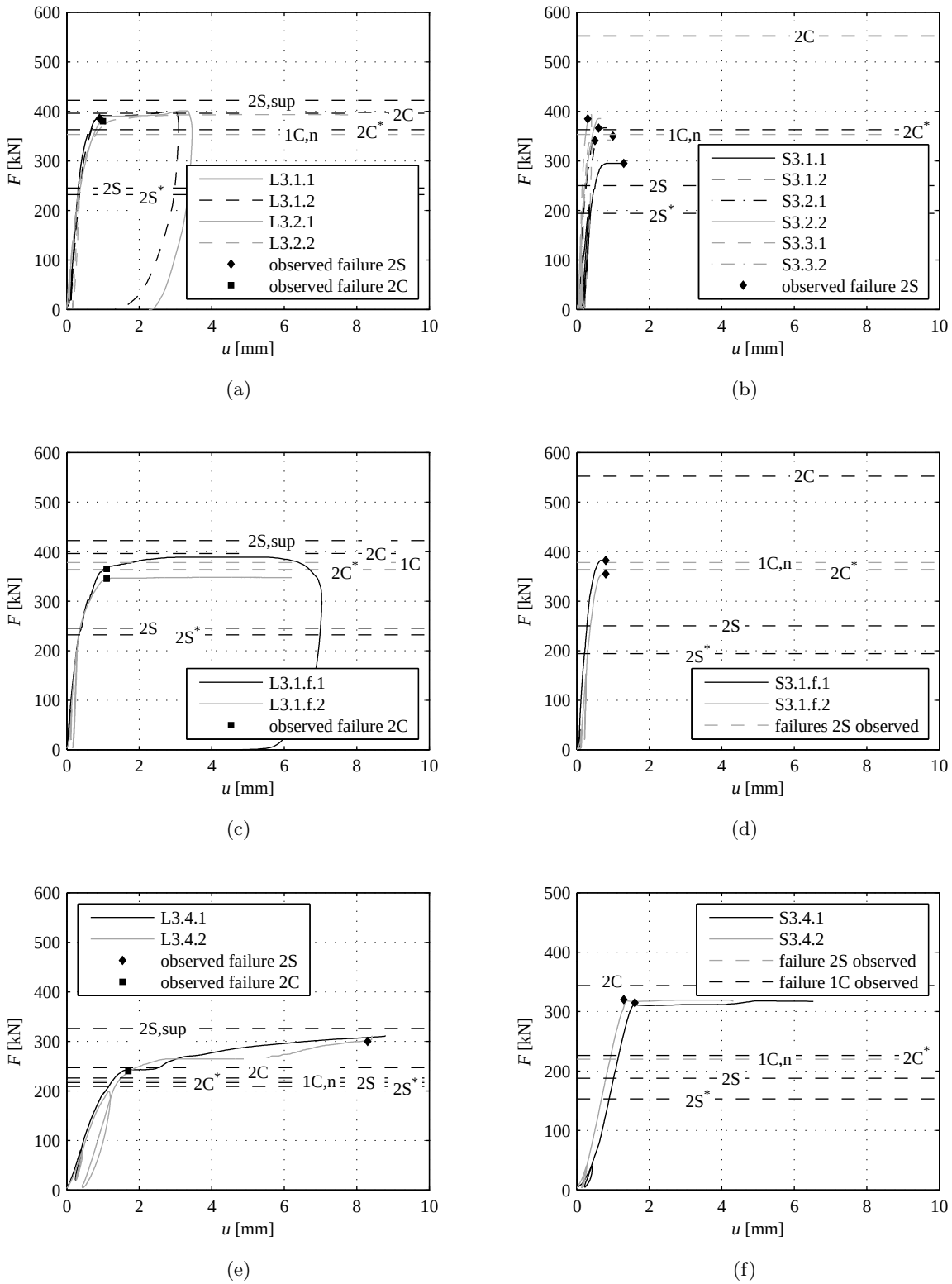

Figure 4.17: Connection shear tests: comparison between test results and analytical model

Non-linearity of the curves

Irrespective of the failure mode, all F-u curves denoted a non-linearity, which increased with increasing load. This progressive loss of shear stiffness could be a possible sign of stress redistributions in the timber and concrete.

Notch length

The notch length was set to 100 or 200 mm. The load which caused a rolling shear failure in the timber (2S) was not significantly different between long (200 mm) and short (100 mm) notches. In other words, the shear failure load of the timber was not directly proportional to the length of the timber next to the notch. There are several factors which probably contributed to this result.

- Firstly, this could be caused by the fact that there is a limit for the effective shear length. The model takes this into account by setting a maximal effective length of $8t_N$.
- Secondly, the vertical reaction measured in the tests with short notches was about three times higher than in the tests with long notches. Consequently, the specimens with short notches probably benefited from the positive effect of the vertical compressive stresses in the timber.

These factors were taken into account in the analytical model. However, because of several unknown aspects and assumptions, the prediction shows some discrepancies in comparison to the results.

Ductile compressive failures in the timber (2C) were observed only in specimens with long notches. For instance, specimen L3.4.1 (long notch with reduced width) failed in a ductile way due to a compressive failure in the timber at a horizontal load of 225 kN. In contrast, S3.4.1 (short notch with reduced width) exhibited a brittle shear failure in the timber at a horizontal load of 318 kN. A possible explanation is the influence of the vertical compressive stresses on the compressive failure in the timber. Since this compressive stress was significantly higher in the specimens with short notches, the compressive failure in the timber could not occur at the same load level as in the long notches. The calculation model takes this effect into account by superposition of the acting stresses according to the Tensor Polynomial theory.

At least, the test results showed that the long and short notches had about the same stiffness. As a consequence of these results, the notches with a length of 200 mm showed a better structural performance than the 100 mm long notches.

Steel fibres

The influence of steel fibres in the concrete instead of a steel mesh was studied experimentally with specimens L3.1.f.1, L3.1.f.2, S3.1.f.1 and S3.1.f.2. In comparison to the specimens with a concrete C50/60 and a steel mesh, no specimens with steel fibres exhibited concrete cracks at the end of the test. In contrast, the stiffness was in the same range as it was with the specimens with concrete C50/60 and steel mesh.

Notch inclination

The push-out tests performed did not allow evaluating the influence of the notch edge inclination on the load-displacement behaviour.

Notch width

In four specimens, the notch was cut with a reduced width ($l_N = 330$ mm). If the notch length was 200 mm, these specimens always showed a ductile compressive failure in the timber parallel to the grain with maximum plastic deformations of about 8 mm. A reduction of the notch width increased the concentration of the contact force between the timber and concrete, and allowed mobilizing the resistance of three shear planes instead of one. On the other hand, this reduction of the width caused an increase of the measured relative displacements between the timber and concrete.

Cross layers

In this test series, the veneer configuration was not varied. The beech LVL plates tested were made of 10 longitudinal veneers and 3 cross layers. This configuration was critical, because the cross layer at mid height of the cross section of the beech LVL plate coincided with the critical shear plane of the notch. This means that the shear strength in this plane corresponded to the rolling shear strength of a beech veneer, which is less than half of the shear strength parallel to the grain. If a beech LVL plate without the middle cross layer was used, shear failures in the timber would occur at higher load levels. However, at least two other cross layers must be there to ensure the dimensional stability of the plates.

Load-carrying capacity and stiffness

The load-carrying capacity of the notched connections tested satisfied the requirements for the design of slabs for office or residential buildings. The maximum loads carried by the specimens were between 310 kN and 400 kN in case of specimens with long notches, and between 295 kN and 397 kN for specimens with short notches. The estimated design horizontal load in the notch close to the support for a 6 m long and 0.53 m wide slab is between about 50 and 100 kN.

The stiffness of the specimens was calculated by considering the measured relative displacement at 40% of the failure load. For the specimens with long notches, the connection stiffness was between 617 and 835 kN/mm if the notch was cut over the entire width of the specimen ($b_N = 530$ mm), and between 195 and 216 kN/mm if the notch had a reduced width ($b_N = 330$ mm). For the specimens with short notches, the connection stiffness was between 569 and 1403 kN/mm if the notch was cut over the entire width of the specimen, and between 159 and 213 kN/mm if the notch had a reduced width. The corresponding γ-factors calculated for the elastic-cracked state of the composite member according to Section 3.2.3 were between 0.8 and 1 and were located in the asymptotic part of the mathematical relationship between K and γ. This means that the notched connections tested are able to ensure an almost full composite action in the elastic phase. However, it has to be taken into account that the clamping of the

beech plate by the tensile testing machine always caused small torsions of the specimens. This fact, added to the small inaccuracies by fixing the sensors, contributed to create variations of the resulting stiffness.

4.3.6 Conclusions

In conclusion, this test series showed that, depending on the design, notches as connection system for timber-concrete composite members made of beech LVL are able to fulfil the three most important requirements on connections mentioned in Section 2.3.3: load-carrying capacity, stiffness and ductility. The latter property is achieved by means of a ductile compressive failure of the timber parallel to the grain. This means that ductility comes from the timber part itself and not from additional mechanical fasteners.

4.4 Bending tests with distributed load

4.4.1 Introduction

A series of bending tests with distributed load was performed in the laboratory of the Institute of Structural Engineering (IBK) at ETH Zurich. The timber-concrete composite members with notched connection were made of beech LVL and the notch geometry was designed according to the analytical models described in Chapter 3. The purpose of the design was that a ductile failure (compressive failure of the timber in the notch) should govern the structural behaviour of the composite member. The most important examined parameter was the vertical reinforcement, and the test results were analysed and compared to the results of calculations applying the analytical models.

4.4.2 Materials and methods

In this experimental series, 11 composite specimens with 15 mm deep notches were tested. The layout of the specimens is illustrated in Figs. 4.19 and 4.20. Tables 4.7 and 4.9 summarise the construction details. The specimens were 6 m long, 530 mm wide and 200 mm deep. Each beech LVL plate was 40 mm deep with a 160 mm thick concrete layer. The notch dimensions were chosen according to Chapter 3 so that a compressive failure in the timber should govern the structural behaviour.

The beech LVL plates were produced by the company Pollmeier. In contrast to 40 mm thick LVL plates tested by Van de Kuilen and Knorz [14], [15] and considered by the European Technical Approval [3], the longitudinal layers were 12 instead of 10 (Fig. 4.18). In contrast, the number of cross layers was the same. Totally, the plate consisted of 14 veneers instead of 12. In contrast to the preliminary bending tests and the shear tests, to prevent rolling shearing-off failures, the beech LVL plates in this test series did not contain a cross layer in the middle. The higher number of longitudinal veneers influences the tensile, the compressive and the bending strength parallel to the grain. However, in the model calculations, this impact was neglected, and the values found by Van de Kuilen and Knorz [14], [15] were assumed (Tab. 2.1).

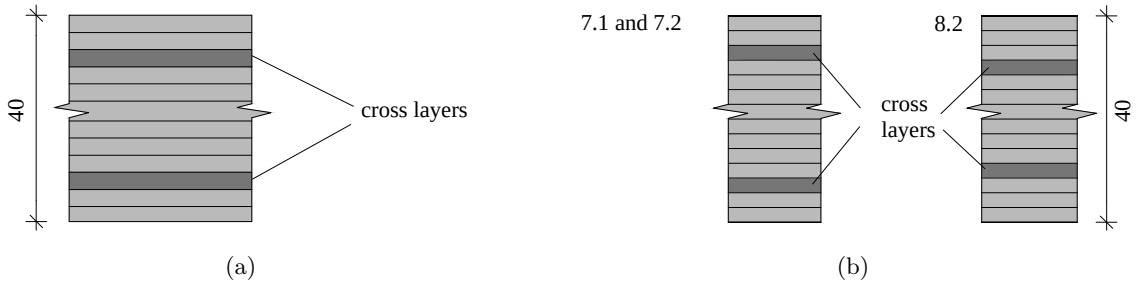

Figure 4.18: (a) Standard veneer configuration of the beech LVL produced by the company Pollmeier; (b) veneer configuration of the LVL plates used in the bending tests

The concrete that was tested had the strength class C50/60 according to the Swiss Standard SIA 262 [66], a maximum aggregate diameter of 16 mm, and contained a liquid admixture to reduce the impact of drying shrinkage and a steel mesh to prevent shrinkage cracks. According to the models presented in Section 3.2, this mesh does not carry relevant forces. The mechanical properties of the concrete tested are summarised in Tab. 4.8.

Table 4.7: Bending tests with distributed load: fixed dimensions [mm]

Specimen length		6000
Span	l	5660
Notch length	l_N	250
Specimen width	b	530
Notch depth	t_N	15
Timber thickness	h_2	40
Concrete thickness	h_1	160
Diameter of the shrinkage reinforcement		6
Spacing of the shrinkage reinforcement		150

Specimen 1 had notches with a constant width, whereas in all other specimens the notch width was designed proportional to the shear force generated by a uniformly distributed vertical load according to Section 3.3.4 (Fig. 4.19). The reference specimen was specimen 2.1, which had notches proportional to the shear force distribution and no vertical reinforcement. Specimen 3 was identical to specimen 2.1 but had inclined notch edges.

As shown in Fig. 4.19, Fig. 4.20 and Tab. 4.9, several types of vertical reinforcement were tested.

Firstly, the effect of vertical reinforcement within the concrete layer such as the distance baskets made of reinforcing steel fixed in specimen 4 and the punching steel dowels installed in specimen 5 was examined. Secondly, the influence of end-to-end reinforcement (with or without tolerance) which connected the timber and concrete vertically (specimens 2.2, 6, 7.1, 7.2 and 8.2) was studied.

The steel rods of specimen 6 had no tolerance. The reason is that they were fixed in the LVL plate before pouring the concrete. Specimen 2.2 was produced in the same way as specimen

Table 4.8: Bending tests: concrete properties

		Modulus of elasticity	Cylinder strength	Splitting tensile strength
Specimens 1 to 6				
Number of specimens	[-]	3	3	4
Mean value	[N/mm^2]	38800	52.6	3.4
Standard deviation	[N/mm^2]	500	5.1	0.4
Specimens 7.1 to 8.2				
Number of specimens	[-]	3	4	4
Mean value	[N/mm^2]	37011	56.9	3.4
Standard deviation	[N/mm^2]	229	0.65	0.62

2.1, but, before the test, round holes with a diameter of 16 mm were drilled. Then, in each hole, a 10.9 steel rod with a diameter of 6 mm designed according to Sections 3.3.10 and 3.3.11 was inserted to prevent concrete crack opening and gap opening. These rods had a tolerance in respect to horizontal relative displacements between the timber and concrete and should help to fulfil the model requirements discussed in Section 3.3.12. Before the test, the nuts of the rods of specimen 2.2 were turned by hand until they stopped moving. Then, they were turned by 360° using a fork wrench.

Specimens 7.1 to 8.2 (Fig. 4.20) were based on the same concept as specimen 2.2, but were produced subsequently. The reinforcement of these specimens was designed to fulfil the model requirements described in Section 3.3.12 as good as possible. It is unthinkable to use this reinforcement in practice. Since the behaviour of specimen 2.2 was governed by a failure of the rods caused by too small dimensions of the holes, specimens 7.1, 7.2, and 8.2 were produced with longer holes which were realised with wedges fixed before concreting. The rods were of strength class 8.8 and 10.9 depending on the position. Since the holes were 80 mm long, high plastic horizontal relative displacements could develop without causing a failure of the rods. The washers of the rods were placed on lubricated steel plates to prevent that the rods carried forces parallel to the interface between the timber and concrete. Furthermore, as shown in Fig. 4.20, 5-mm-thick polystyrene elements were fixed on the timber plates close to the notches to minimise hardening effects due to the vertical reinforcement discussed in Section 3.3.12, which are difficult to quantify. Since the model assumes that the connection is elastic and ideal-plastic, this measure allows a better comparison between the model and the test results. The difference between specimens 7 and 8 was that the beech LVL plates of specimens 7.1 and 7.2 were identical to specimens 1 to 6, whereas the LVL plate of specimen 8.2 came from another production series and showed a small difference in the veneer configuration (Fig. 4.20). The cross layers were slightly closer to the mid height, but were not below the notch bottom. This means that the shear stresses occurring due to shear transfer through the notch are not carried by cross layers. A variation of the position of the cross layers by constant number of veneers influences the

bending strength of the plate. However, this impact is neglected, and it is assumed that all plates have the mechanical properties determined by Van de Kuilen and Knorz [14], [15].

Before the tests, the rods of specimens 7.1, 7.2 and 8.2 were fixed with the procedure used with specimen 2.2.

Fig. 4.21 illustrates the test setup and the most important measurement points. The test setup should reproduce a distributed load. This included four hydraulic cylinders, four load distribution steel profiles (HEB 140) oriented in longitudinal direction, and eight steel plates which transferred the load from the steel profiles HEB 140 to the specimen. The supports were in a distance of 5.66 m. The vertical deflections were measured at mid-span (w_2) and at quarter-span (w_1 and w_3). The horizontal relative displacement between timber and concrete was measured close to each notch by means of LVDTs (u1 to u10). The cylinder load was calculated from the measured oil pressure.

Table 4.9: Bending tests with distributed load: description of the specimens

Specimen	Notch width	Vertical reinforcement	reinforcement type	Tolerance
1	Constant	[-]	[-]	[-]
2.1	Proportional to shear force	[-]	[-]	[-]
2.2	”	24 rods with ⊘ = 6 mm, strength class 10.9	End-to-end	Yes
3	”	[-]	[-]	[-]
4	”	120 steel bars with ⊘ = 5 mm built in distance baskets	Internal concrete reinforcement	No
5	”	21 punching dowels diameter ⊘ = 14 mm	Internal concrete reinforcement	No
6	”	30 steel rods ⊘ = 20 mm, strength class 4.5	End-to-end	No
7.1, 7.2, and 8.2	”	24 rods with ⊘ = 6 mm and strength class 8.8, and 16 rods with ⊘ = 6 mm and strength class 10.9	End-to-end	Yes

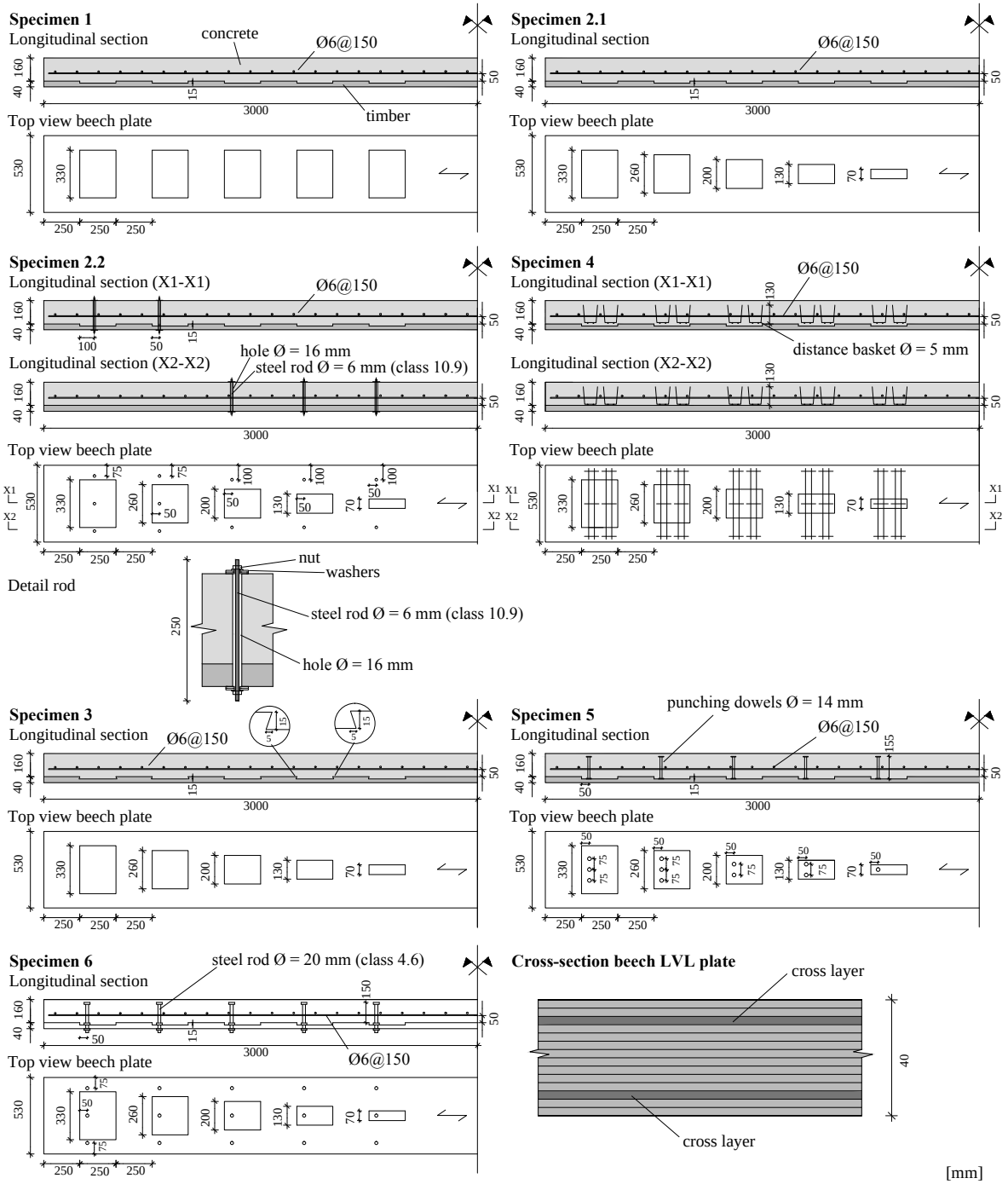

Figure 4.19: Bending tests with distributed load: specimens 1 to 6

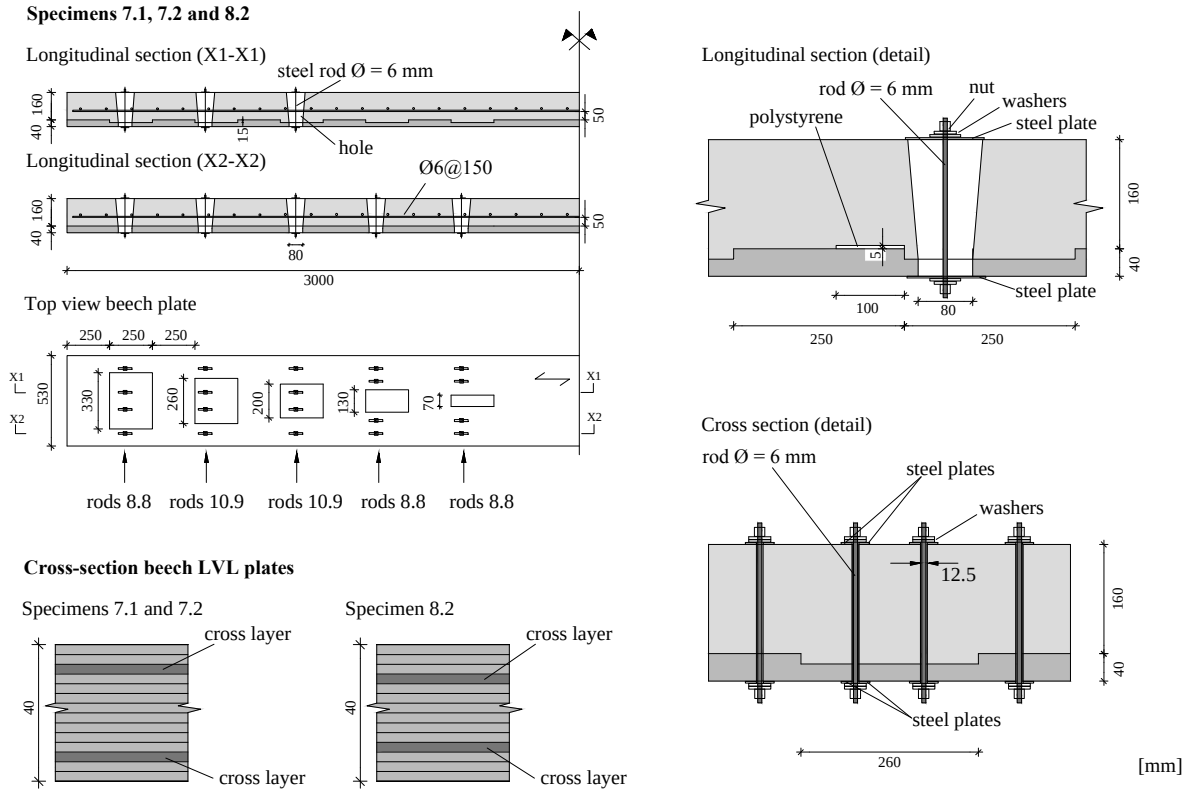

Figure 4.20: Bending tests with distributed load: specimens 7.1, 7.2 and 8.2

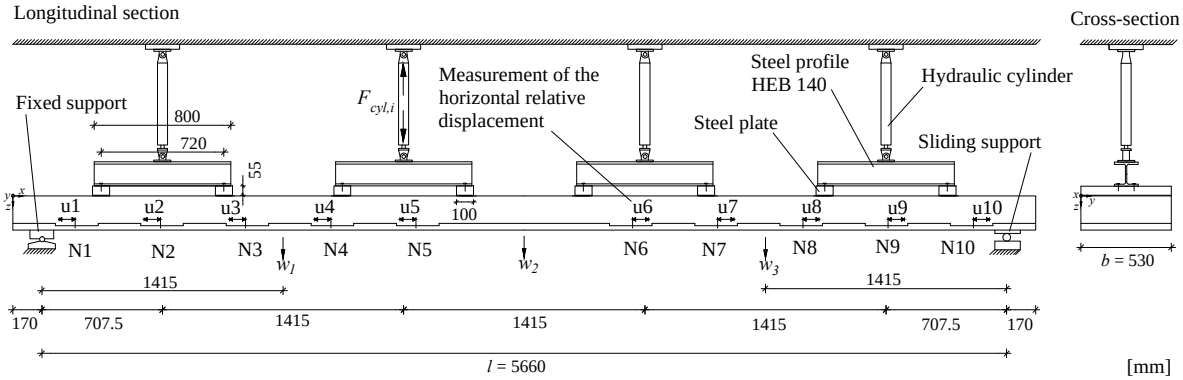

Figure 4.21: Bending tests with distributed load: test setup

4.4.3 Test results

Tab. 4.10 summarises the failure loads (including self-weight) and the failure modes of the specimens, and Fig. 4.22 illustrates the relationships between the vertical loads applied during the tests and the vertical deflections at mid-span. In Fig. 4.22, the specimens are regrouped depending on the type of vertical reinforcement. The uniformly distributed load q represented in Fig. 4.22 is calculated as the sum of the cylinder loads applied during the test divided by the surface of the specimen:

$$q = \frac{\sum_{i=1}^{4} F_{cyl,i}}{l \cdot b} \tag{4.2}$$

The load q_u is the maximum load reached during the test. The value q_u^* includes the self weight of the specimen and represents the effective load-carrying capacity.

In general, as predicted by means of the analytical model, all specimens except specimen 6 reached the compressive failure in the timber (2C). This failure mode is the primary objective of the design strategy presented in Section 3.3.12. Nevertheless, although the compressive failure in the timber was governing, only specimens 2.2, 7.1, 7.2 and 8.2 showed a satisfying ductile behaviour. As exposed in Tab. 4.10, the problem of specimens 2.1, 3, 4 and 5 was that, after the compressive timber failure, the gap between the timber and concrete opened, and the existing concrete cracks enlarged. these two phenomena compromised the structural behaviour. As shown in Fig. 4.22(d), end-to-end vertical reinforcement with tolerance solved this problem. Specimens 2.2, 7.1, 7.2 and 8.2 showed an elastic and a plastic phase, and the plastic amount of the deflection was more than 100 mm. The ductility of specimen 2.2 was limited by a failure of the rods due to the dimensions of the holes, whereas specimens 7.1, 7.2 and 8.2 failed due to a compressive failure in the concrete on top of the cross-section followed by a tensile-bending failure of the timber. Fig. 4.22 shows that the bending stiffness of the specimens tested lied in the same range.

Specimen 1: constant notches without vertical reinforcement

As shown in Fig. 4.22(a), the load-deflection behaviour of specimen 1 was marked by an elastic phase, a short plastic phase with load oscillations, and a ultimate brittle failure. During the elastic state, several flexural-shear cracks appeared close to the load transfer points of the notches. These cracks were stable and did not propagate. Then, a ductile compressive failure of the timber parallel to the grain occurred mainly in the notches close to the supports (N1 and N10). As shown in Fig. 4.23(a) and 4.23(b), the notches N1 and N10 were subjected to great plastic deformations, whereas the notches N2 and N9 showed comparatively small plastic deformations. The notches N7 and N8 did not exhibit plastic deformations. As illustrated in Fig. 4.23(c), because of the difference between the horizontal relative displacement of N10 and N9 and between N1 and N2, the flexural-shear cracks close to N9 and N2 enlarged. After that, a brittle tensile-bending failure of the timber occurred between N9 and N10 (Fig. 4.23(c)).

Table 4.10: Test results

Specimen	Maximal load q_u^* [kN/m^2]	Governing failure mode	Behaviour after failure	Ultimate failure
1	54.7	Compressive failure of the LVL in the notches close to the supports	Plastic deformations of the notches close to the supports; crack opening in concrete	Brittle tensile-bending failure of the LVL close to notch N9
2.1	46.3	Compressive failure of the LVL in most of the notches	Limited plastic deformations	Gap opening; crack opening in the concrete
2.2	72	”	Elevated plastic deformations with hardening	Failure of the rods
3	54.9	”	Limited plastic deformations	Gap opening; crack opening in the concrete; brittle failure in the concrete
4	45.5	”	”	Gap opening
5	56.5	”	”	Gap opening; crack opening in the concrete; brittle concrete failure
6	88.2	Brittle tensile-bending failure of the LVL	[-]	[-]
7.1	63.9	Compressive failure of the LVL in most of the notches	Elevated plastic deformations with hardening	Compressive failure of the concrete (cross-section); bending-tensile failure of the LVL
7.2	64.3	”	”	”
8.2	62.8	”	”	”

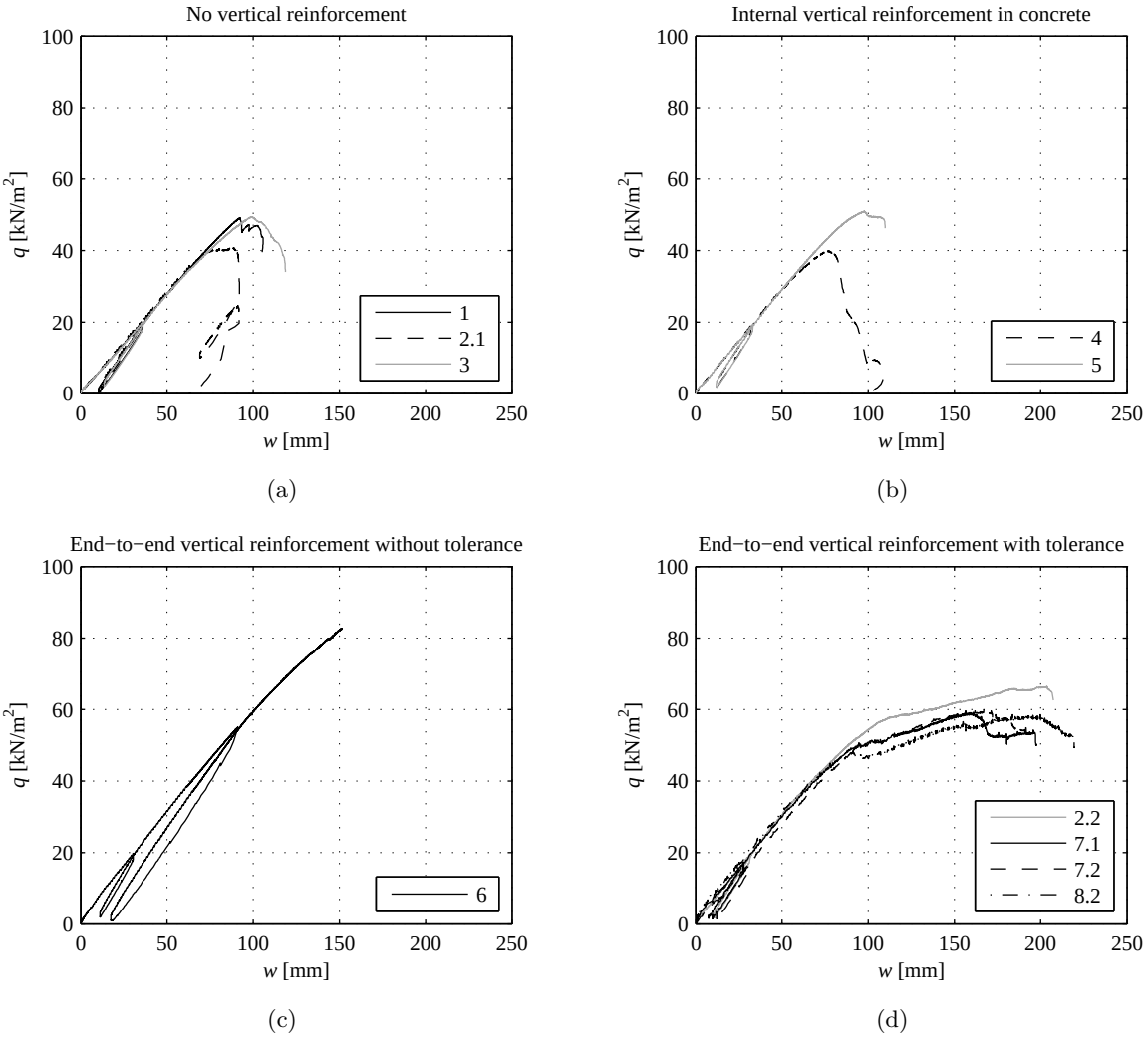

Figure 4.22: Relationship between the vertical load and the deflection at mid-span measured during the bending tests: (a) composite members without vertical reinforcement (specimens 1, 2.1 and 3) ; (b) composite members with internal vertical reinforcement in concrete (specimens 4 and 5); (c) composite member with end-to-end vertical reinforcement without tolerance (specimen 6); (d) composite members with end-to-end vertical reinforcement with tolerance (specimens 2.2, 7.1, 7.2 and 8.2)

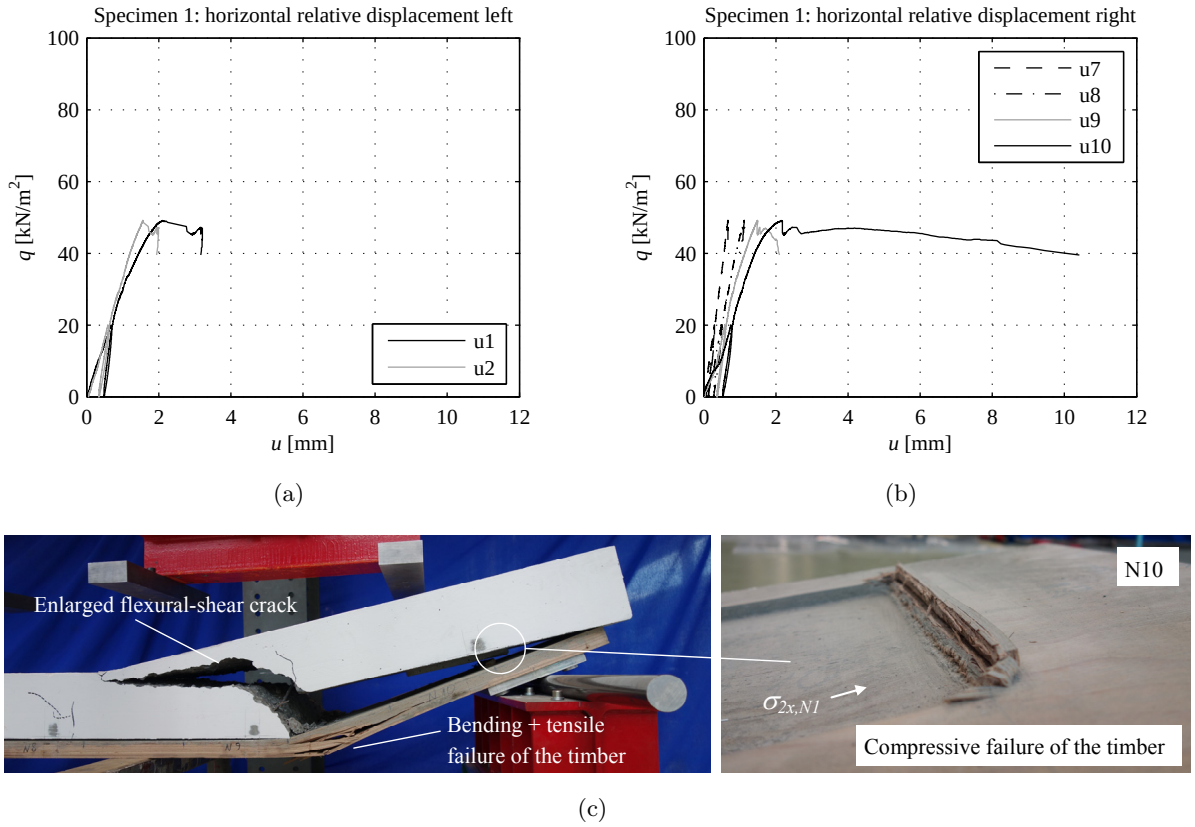

Figure 4.23: Specimen 1: (a) horizontal relative displacements measured between the fixed support and the mid-span; (b) horizontal relative displacements measured between the mid-span and the sliding support; (c) failure mode

Specimens 2.1 and 3: progressive notches without vertical reinforcement

As shown in Fig. 4.22(a), the load-deflection behaviour of specimen 2.1 was marked by an elastic phase and a short plastic plateau followed by a fast decrease of the load. During the elastic state, bending cracks at mid-span and flexural-shear cracks close to the notches appeared, and no gap opening was observed. Then, a ductile timber compressive failure occurred in most of the notches as measured in Fig. 4.24(a) and Fig. 4.24(b). In several notches, the plastic deformations of the timber were possible to observe after the separation of the two parts of the composite member as shown in Fig. 4.24(c). The measured horizontal relative displacements described in Fig. 4.24(a) and Fig. 4.24(b) denote some differences between the plastic deformations of the notches. For instance, N8, N9 and N10 deformed more than N7. This phenomenon probably caused the enlargement of the flexural-shear crack close to N7 shown in Fig. 4.24(d) . Furthermore, during the plastic phase, the gap between timber and concrete opened between the enlarged cracks and the supports. This coincided with the beginning of the load decrease.

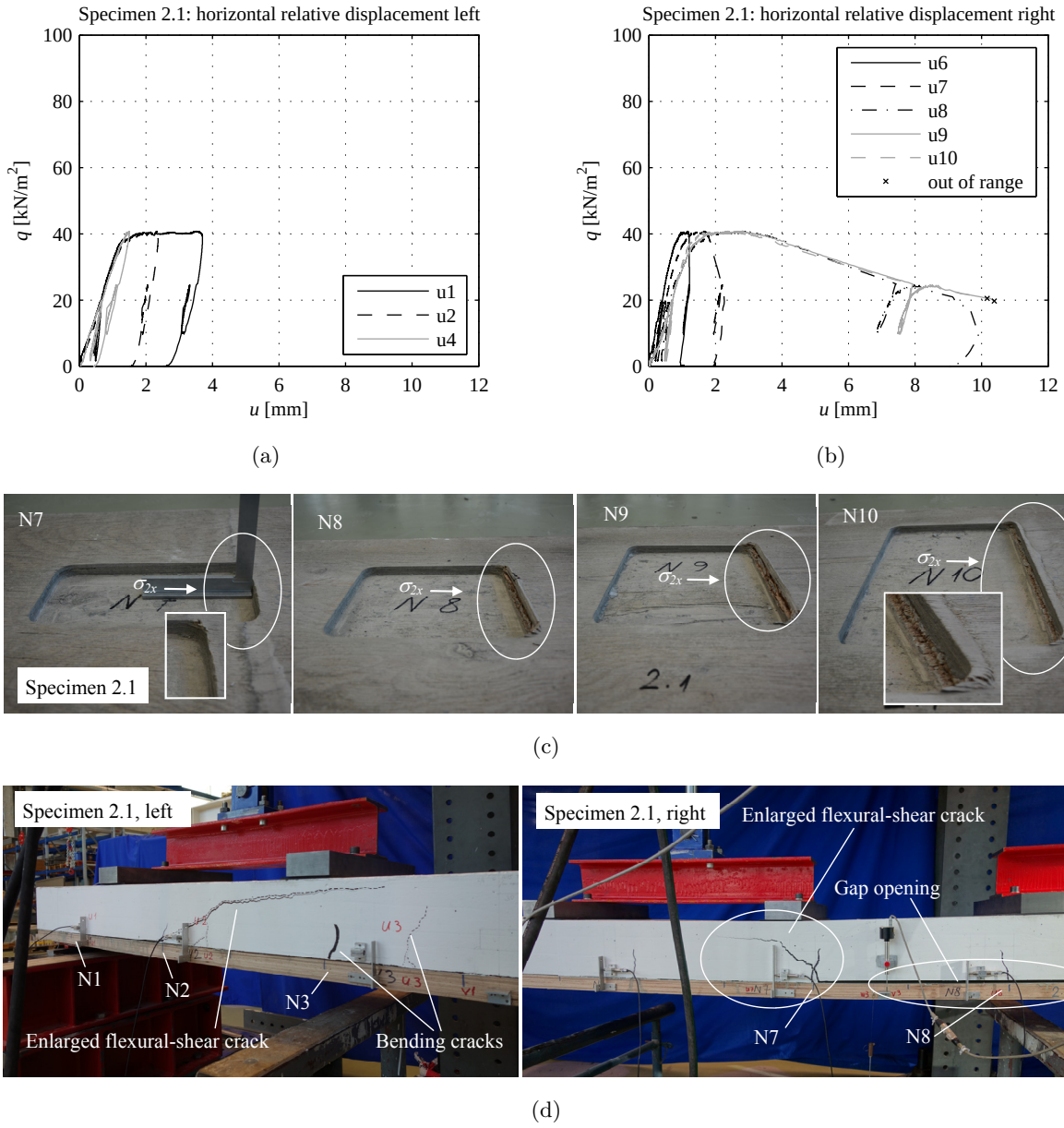

Figure 4.24: Specimen 2.1: (a) horizontal relative displacements measured between the fixed support and the mid-span; (b) horizontal relative displacements measured between the mid-span and the sliding support; (c) compressive failure of timber in notches N7 to N10; (d) crack opening and gap opening occurred during yielding of the notches

Specimen 3 was the same as specimen 2.1, but the notches were cut with inclined edges according to Fig. 4.19. The structural behaviour of specimen 3 was similar to specimen 2.1. Despite the compressive failure of the timber was reached in most of the notches, crack and gap opening governed the structural behaviour, and the final plastic deformations were small. The enlarged crack close to N7 caused a brittle concrete failure. In this test, it was not possible to evaluate the influence of the inclined edges.

Specimens 4 and 5: progressive notches with vertical reinforcement in concrete

The internal concrete reinforcement tested during this experimental series did not improve the structural behaviour in a relevant way. During the experiments 4 and 5, in opposition to the experiments 2.1 and 3, no flexural-shear cracks in the concrete were observed. However, the structural behaviour was similar to the composite members without reinforcement (specimens 2.1 and 3). The structural behaviour of specimen 4 was governed by gap opening between the left support and notch N5, which occurred after compressive failure of the notches. In specimen 5, after the compressive timber failure, the gap opened between the left support and the notch N4, and the bending crack close to N4 enlarged. The ultimate failure of specimen 5 was a brittle failure in the concrete close to this crack. Fig. 4.25 illustrates the relationship between the load and the horizontal relative displacement measured between the timber and concrete in specimens 5.

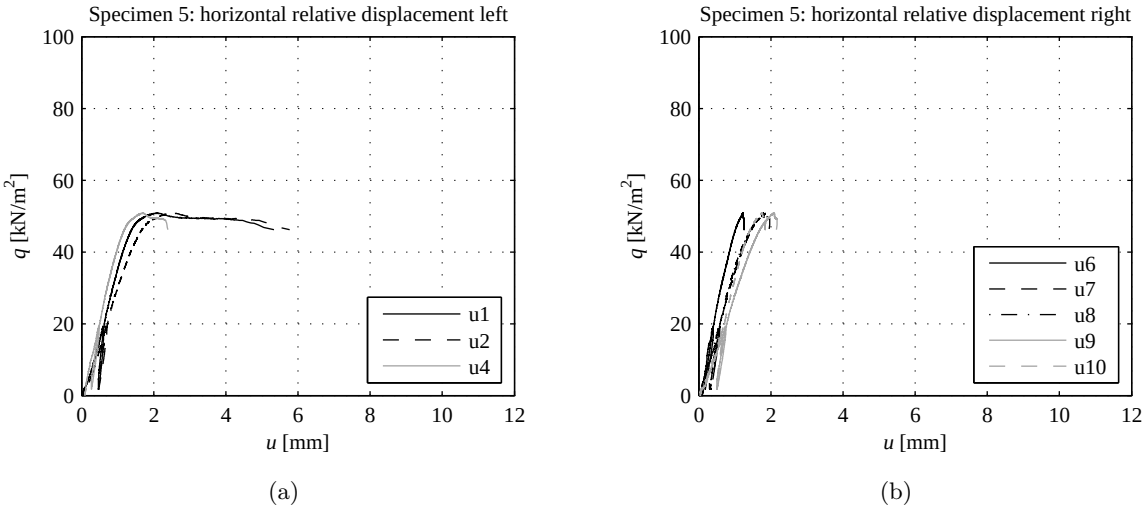

Figure 4.25: Specimen 5: relationship between the horizontal relative displacement and the load: (a) measurement points between the fixed support and the mid-span; (b) measurement points between the mid-span and the sliding support

Specimen 6: progressive notches with end-to-end reinforcement without tolerance

Specimen 6 was reinforced by means of thick end-to-end rods without tolerance. As shown in Fig. 4.22(c), the bending stiffness of specimen 6 was in the same range as it was with the other specimens tested, and the load-displacement curve was almost linear-elastic until the brittle tensile-bending failure. The measurement of the horizontal relative displacement between the timber and concrete shown in Figs. 4.26(a) and 4.26(c) does not give evidence to relevant plastic deformations in the notches. However, the magnifications shown in Figs. 4.26(b) and 4.26(d) exhibit a slight non-linearity of the connection behaviour: the connection stiffness tends to decrease with increasing load.

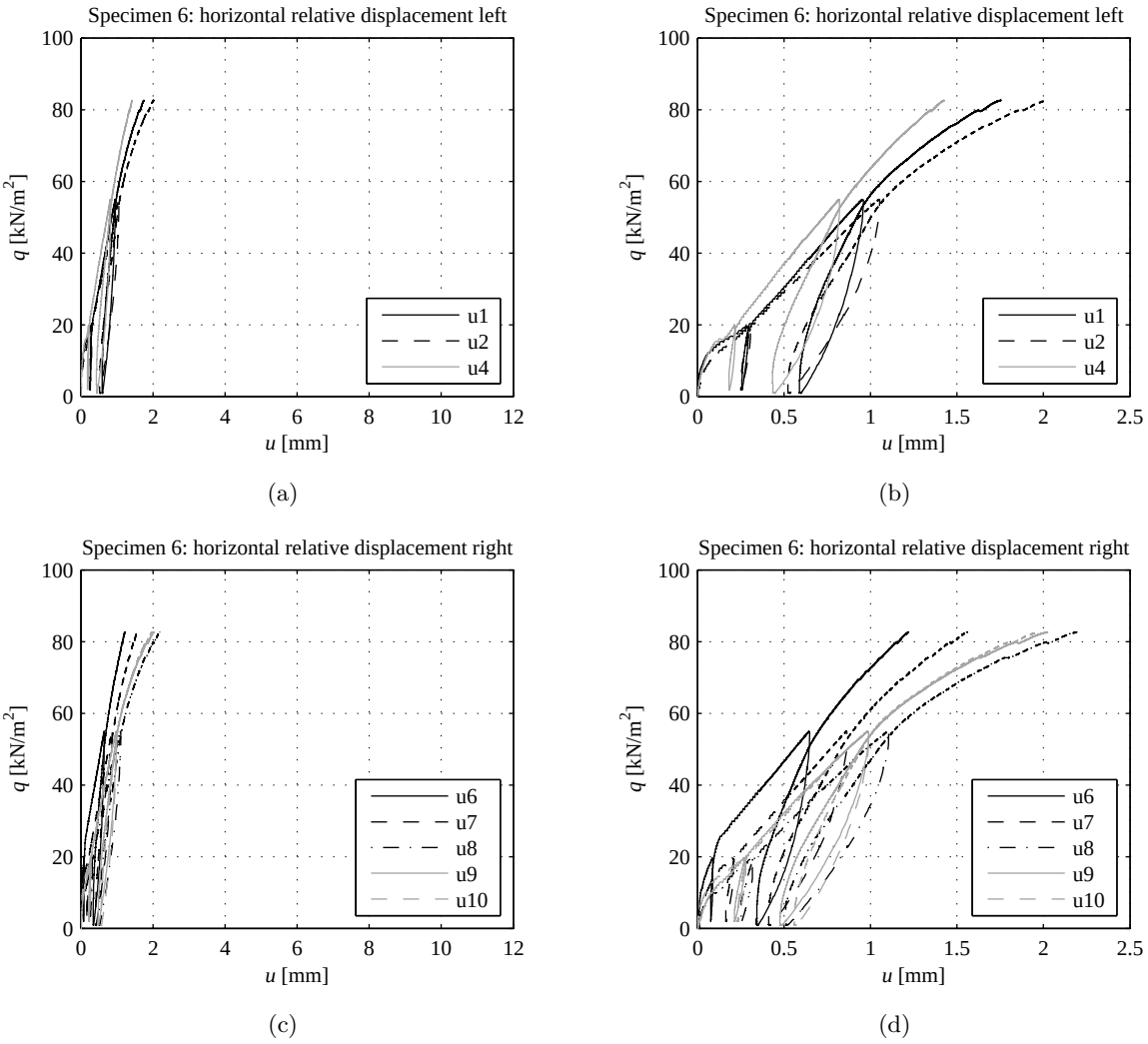

Figure 4.26: Specimen 6: relationship between the horizontal relative displacement and the load: (a) measurement points between the fixed support and the mid-span; (b) magnification of (a) ; (c) measurement points between the mid-span and the sliding support; (d) magnification of (c)

Specimen 2.2: progressive notches with end-to-end reinforcement with limited tolerance

Specimen 2.2 contained end-to-end steel rods with tolerance. The rods had a diameter of 6 mm and were inserted in round holes with a diameter of 16 mm. As shown in Fig. 4.22(d), the elastic phase of specimen 2.2 was similar to the one of the specimens shown in Figs. 4.22(a) and (b), but a higher ductility was achieved.

As illustrated in Fig. 4.29, the structural behaviour of specimen 2.2 was governed by compressive failure of the timber, and the ductility was limited by the rods. During notch yielding, the load-deflection behaviour described in Fig. 4.29(b) showed a relevant ductility and a hardening. As shown in Fig. 4.27, all notches provided with sensors, except N6, yielded causing relevant plastic deformations. Fig. 4.29(c) illustrates the compressive failure of the timber visible after the experiment. It can be seen that in some notches the damage is more

evident than in others. Furthermore, up to failure, no gap opening was observed. During the test, several flexural-shear cracks grew starting from the load-transfer points of the notches, but did not enlarge thanks to the rods (Fig. 4.28). In contrast, at mid-span, bending cracks predominated.

The specimen failed due to a brittle failure of the rods between the left support and notch N3, as shown in Fig. 4.29(d). This caused a sudden opening of the interface between the fixed support and notch N3, and a concrete failure close to notch N3. The failure of the rods was located close to the interface between the timber and concrete. This suggests that the rods were at limit stop because of the elevated plastic relative displacement between the timber and concrete.

Specimens 7.1, 7.2, 8.2: progressive notches with end-to-end reinforcement with elevated tolerance

In contrast to specimen 2.2, in specimens 7.1, 7.2 and 8.2, the holes were 12.5 mm wide and 80 mm long to prevent the failure of the rods observed in specimen 2.2. Furthermore, the specimens were provided with polystyrene elements to prevent hardening due to the compressive failure of the timber. As summarised in Fig. 4.22(d), specimens 7.1, 7.2 and 8.2 showed large ductility similar to specimen 2.2, but slightly smaller failure loads. In contrast to specimen 2.2, thanks to longer holes, the structural behaviour was not governed by failure of the rods. Thus, the entire failure mechanism could be investigated.

The structural behaviour of specimens 7.1, 7.2 and 8.2 was governed by a compressive failure of the LVL in the notches. Fig. 4.30 illustrates the failure process of specimen 8.2 as an example. Ductility of the composite member was induced by yielding of the notches (Fig. 4.30(c)), and was limited by the development of a compressive failure of the concrete at the top of the cross-section (Fig. 4.30 (d)), followed by a bending-tensile failure of the LVL (Fig. 4.30 (e)).

These three experiments were characterised by large plastic deformations in most of the notches. After a linear-elastic phase, the sensors, which measured the horizontal relative displacements close to the interface, detected significant plastic deformations at loads of $45 - 50$ kN/m^2 (Fig. 4.31). Fig. 4.30(c) illustrates the plastic deformations of two notches of specimen 8.2 after the end of the test. The compressive failure of the LVL in the notches was marked by a compressive deformation in longitudinal direction and an expansion in vertical direction. As illustrated in Section 4.4.2, before pouring the concrete, polystyrene elements were fixed to the top edge of the LVL part of the composite member (Fig. 4.33(a)). After the specimens were opened, it was observed that the polystyrene was compressed where the LVL had expanded in volume vertically (Figs. 4.33(b) and 4.33(c)).

However, a compressive failure of the LVL did not occur in all notches exactly at the same time. In general, the notches close to the supports began to yield first. As shown in Fig. 4.31, most of the notches showed large plastic deformations. The notches with the smallest plastic deformations were N5 and N6. Furthermore, during the experiments, it was observed that the plastic notch deformations on the left and on the right sides of the specimens always showed some

differences. This can be seen in Fig. 4.32(e), where the difference between the horizontal relative displacements measured near the two notches close the left and the right supports (u_1 and u_{10}) is plotted as a function of the deflection at mid-span. During the elastic phase, u_1 and u_{10} showed more or less the same displacements. As soon as the notches yielded, differences between u_1 and u_{10} arose. Then, the differences decreased progressively, and increased again before the ultimate failure. The reason for this difference in plastic notch deformation is discussed in Section 4.4.4.

As soon as the curves of the horizontal relative displacements, illustrated in Fig. 4.31, began to become flat, the vertical deflections began to increase, causing the marked non-linearity shown in Fig. 4.30(b). The load-deflection behaviour measured during yielding of the notches was characterized by four phases. First, the deflection showed a short plateau. Then, the load slowly increased with increasing deflection. After that, the deflection continued to increase, but the load reached a maximum and remained constant for awhile. Finally, the load decreased due to a compressive failure of the concrete at the top of the cross-section, which always occurred close to the holes where the rods were fixed (4.30 (d)). The concrete failure induced a progressive delamination, which was accompanied by creaking. In the three composite members tested, the failure of the concrete never occurred in the same place. In specimen 7.1, this failure was observed close to notch N7, in specimen 7.2 close to N3, and in specimen 8.2 next to N8. Since the hydraulic pump was regulated by hand, it was possible to observe the velocity of the failures. The ductile failure of the composite members tested can be described as a slow process. From the compressive failure of the LVL to the ultimate failure, a total time of $20 - 35$ min was needed. Yielding of the LVL subjected to compression was particularly slow. Then, as soon as the concrete began to fail due to compression, the velocity of the plastic deformation increased.

The development of the concrete cracks, observed in specimens 7.2, 7.2 and 8.2, was similar to specimen 2.2. Between the notches N5 and N6, the concrete cracks were generally perpendicular to the interface. In contrast, between the fixed support and N5 and between N6 and the sliding support, flexural-shear cracks occurred and remained closed and stable, thanks to the rods (Fig. 4.33(d)). After the LVL plate was separated from the concrete, it was possible to see a plan view of the flexural-shear cracks. All cracks started close to the areas where the shear forces were transferred from the timber to the concrete, and propagated more or less in a diagonal way in the direction of the mid-span (Fig. 4.33(e)).

The compressive failure of the concrete always developed in a small sector (Fig. 4.30 (d)). Starting from the moment in which this failure occurred, the bending line of the composite member was no longer parabolic, but tended to follow an angular form, which depended on the position of the concrete failure. This tendency was detected in all specimens tested. As shown in Figs. 4.32(a) and 4.32(b), immediately before the ultimate load limit, the bending lines were asymmetric and showed higher deflections close to the points where the concrete failed. Fig. 4.32(c) shows a picture of specimen 7.2 a short time before the end of the test as an example. Fig. 4.32(d) illustrates the relationship between the asymmetry of the bending line, calculated by means of the difference between the deflections at quarter-spans w_1 and w_3, and the deflection at mid-span. At the end of the elastic behaviour, the sensors w_1 and w_3 showed nearly the same value. After the notches began to yield, the curves represented in Fig. 4.32(d) followed a similar

trend, as can be seen in Fig. 4.32(e). Then, as soon as the concrete failed, the difference between w_1 and w_3 increased markedly.

The ultimate failure of the composite member was determined by a brittle tensile-bending failure of the timber cross-section, which always occurred before the compressive failure of the concrete (e.g. Fig. 4.30(e)). This failure was marked by timber creaking and local constriction of the timber cross-section, and occurred suddenly.

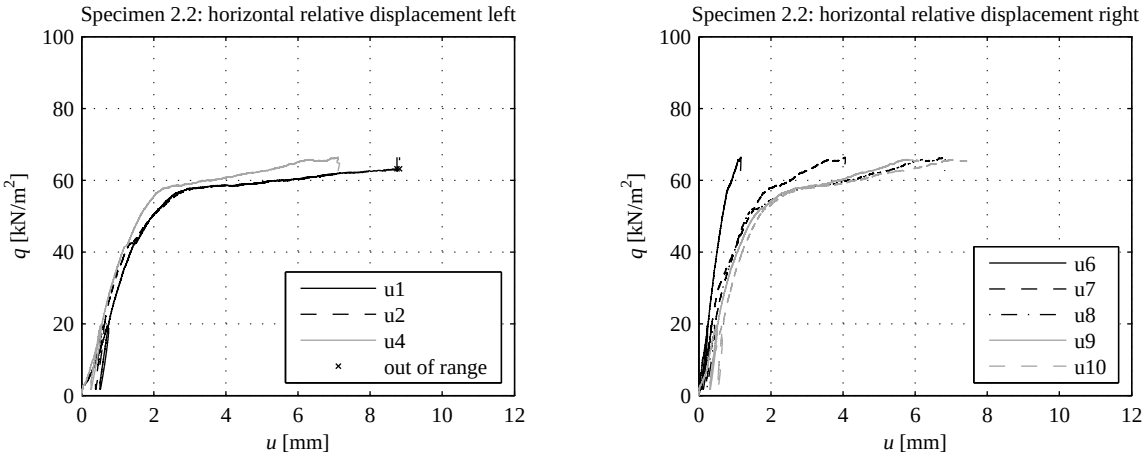

Figure 4.27: Specimen 2.2: relationship between the horizontal relative displacement and the load: (a) measurement points between the fixed support and the mid-span; (b) measurement points between the mid-span and the sliding support

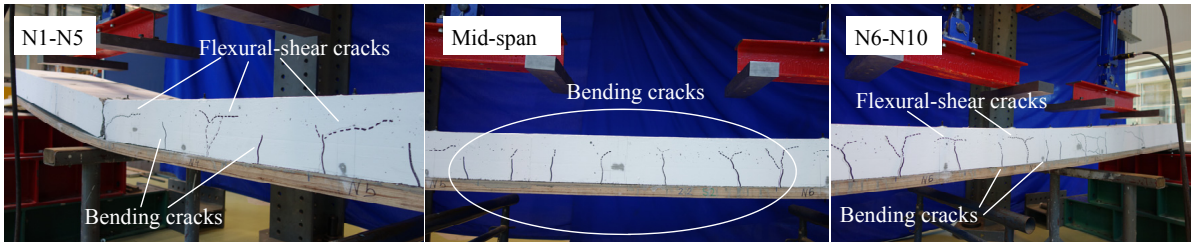

Figure 4.28: Specimen 2.2: concrete cracks after the end of the test

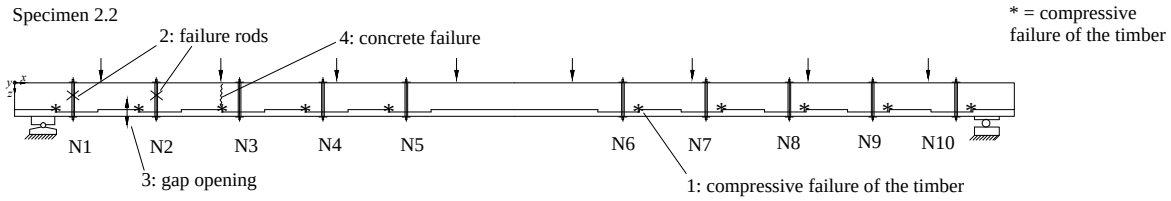

(a)

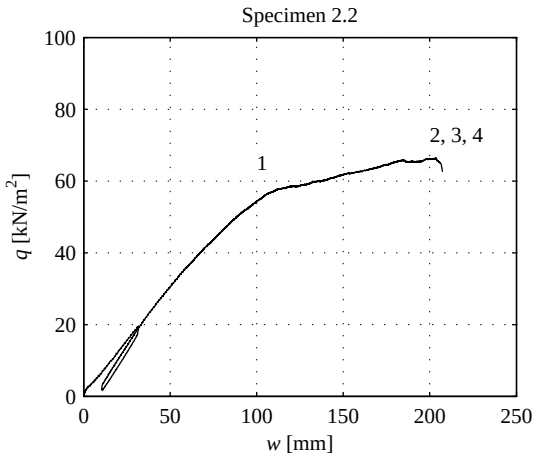

(b)

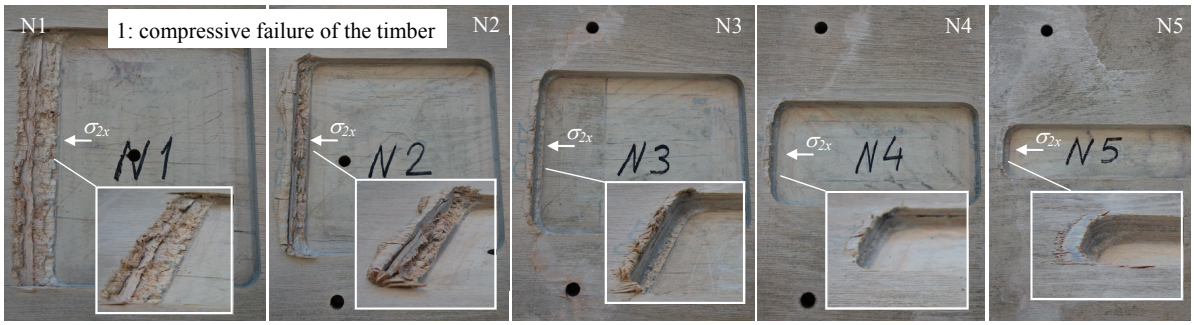

(c)

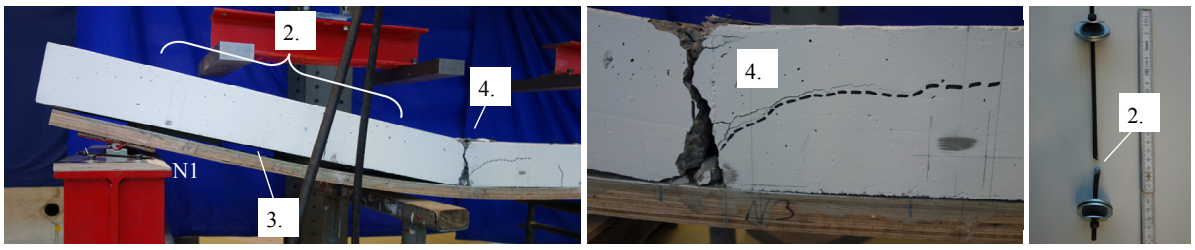

(d)

Figure 4.29: Specimen 2.2: (a) failure process; (b) relationship between the vertical load and the deflection at mid-span; (c) compressive failure of the timber in the notches between the fixed support and the mid-span (N1 to N5); (d) Failure of the rods (2.), gap opening (3.) and concrete failure (4.)

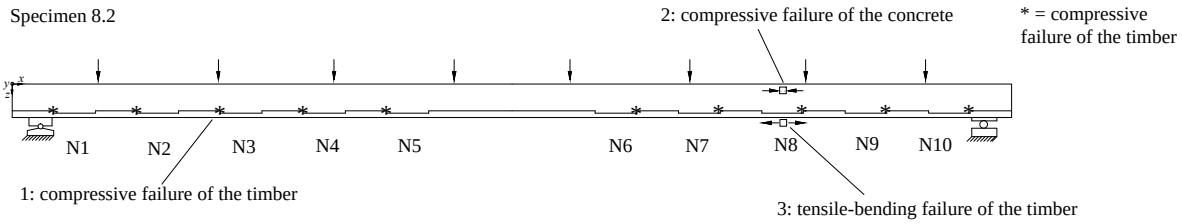

(a)

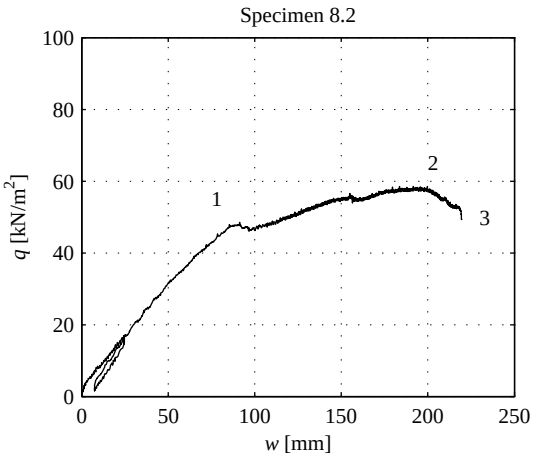

(b)

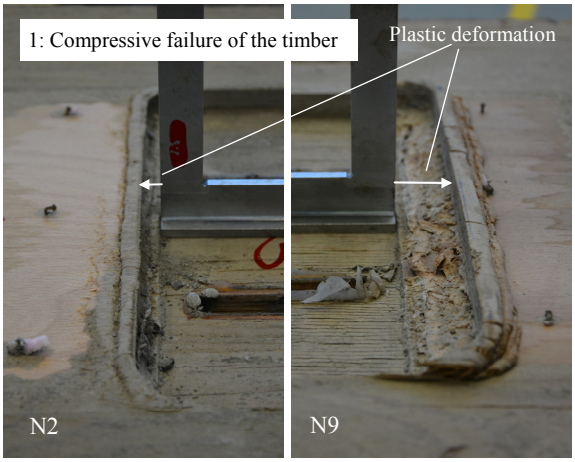

(c)

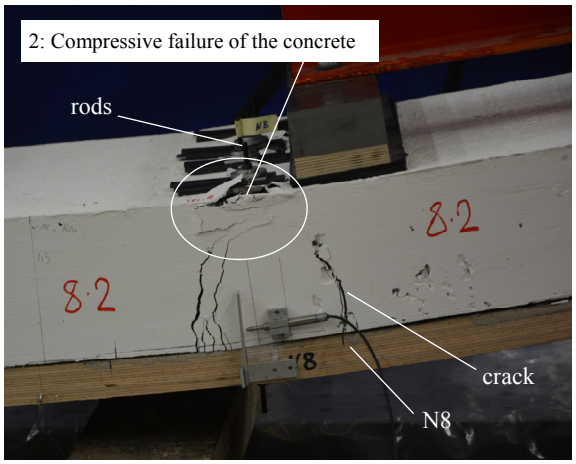

(d)

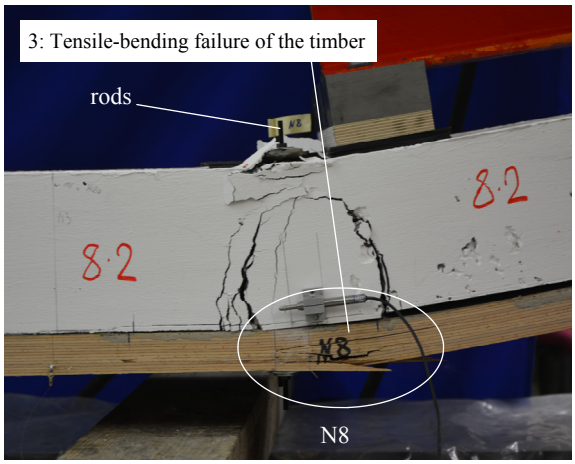

(e)

Figure 4.30: Specimen 8.2; (a) failure process; (b) relationship between the vertical load and the deflection at mid-span; (c) compressive failure of the timber; (d) compressive failure of the concrete; (e) tensile-bending failure of the timber

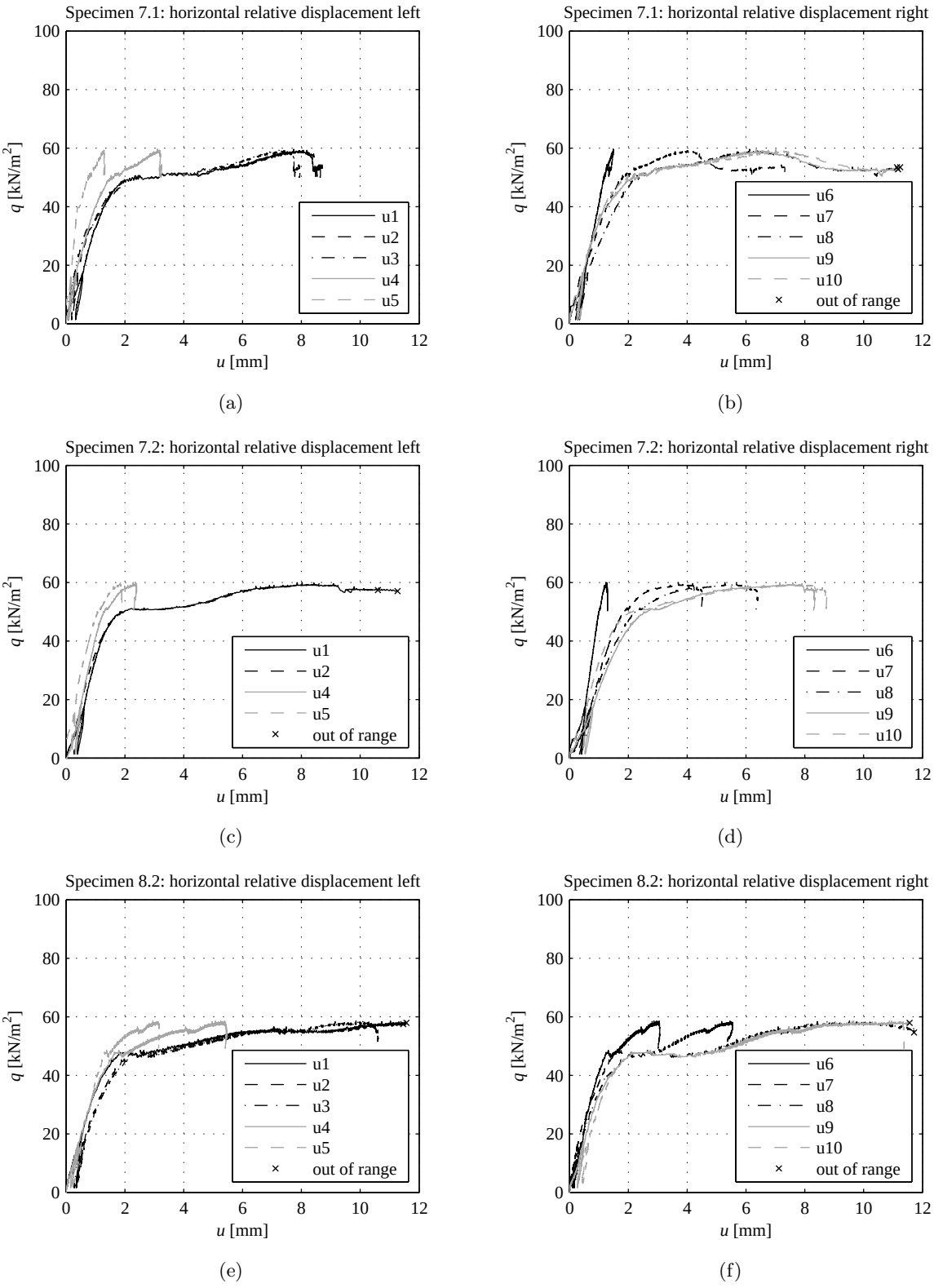

Figure 4.31: Specimens 7.1, 7.2 and 8.2: relationship between the horizontal relative displacement between the LVL and the concrete detected according to Fig. 4.21 and the load: (a) and (b) specimen 7.1; (c) and (d) specimen 7.2; (e) and (f) specimen 8.2

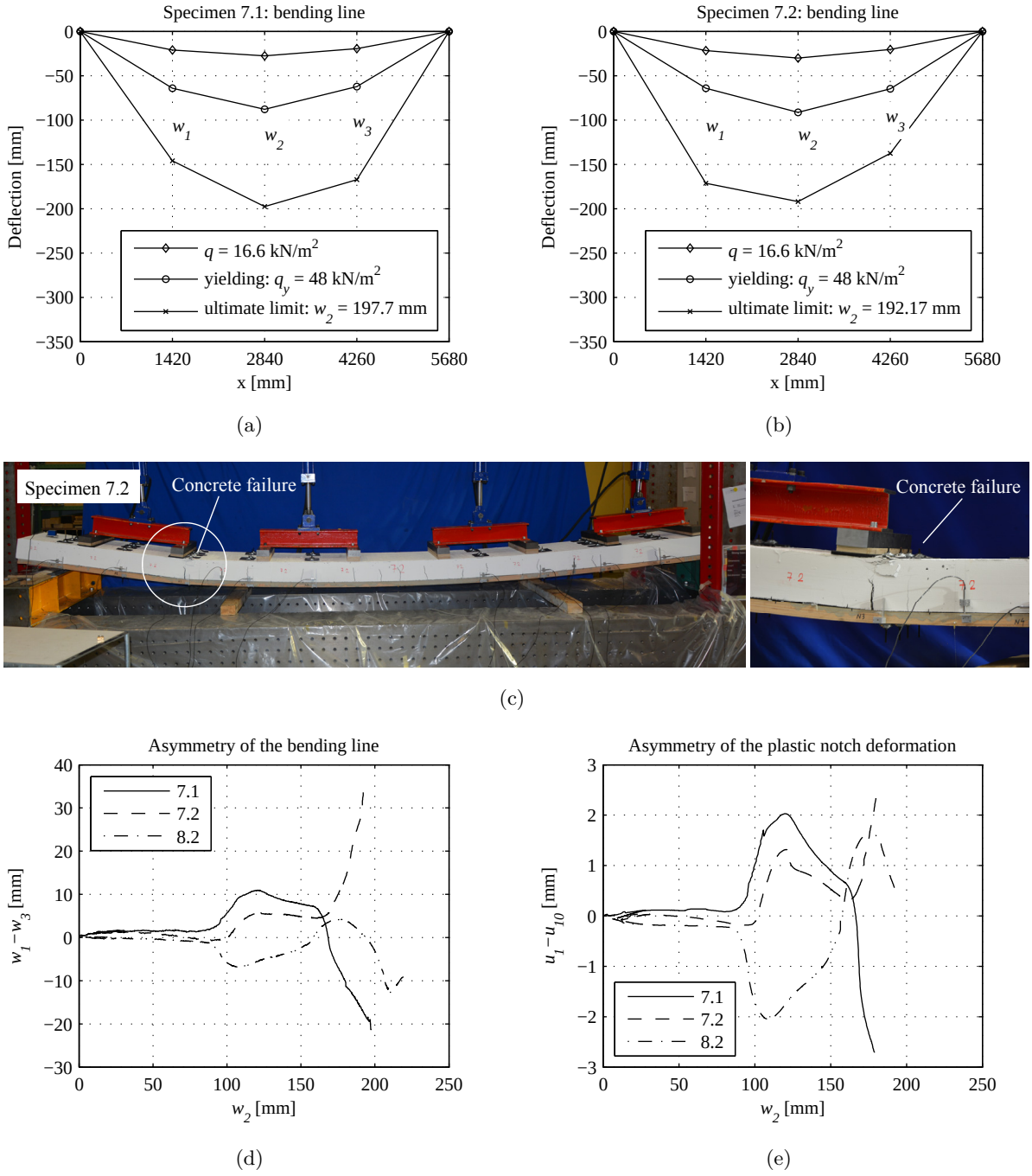

Figure 4.32: (a) Vertical deflections of specimen 7.1; (b) vertical deflections of specimen 7.2; (c) deformation of specimen 7.2 a short time before the ultimate failure; (d) difference between the deflections at quarter-spans w_1 and w_3 as a function of the vertical deflection at mid-span w_2; (e) difference between the horizontal relative displacements measured close to the supports as a function of the deflection at the mid-span

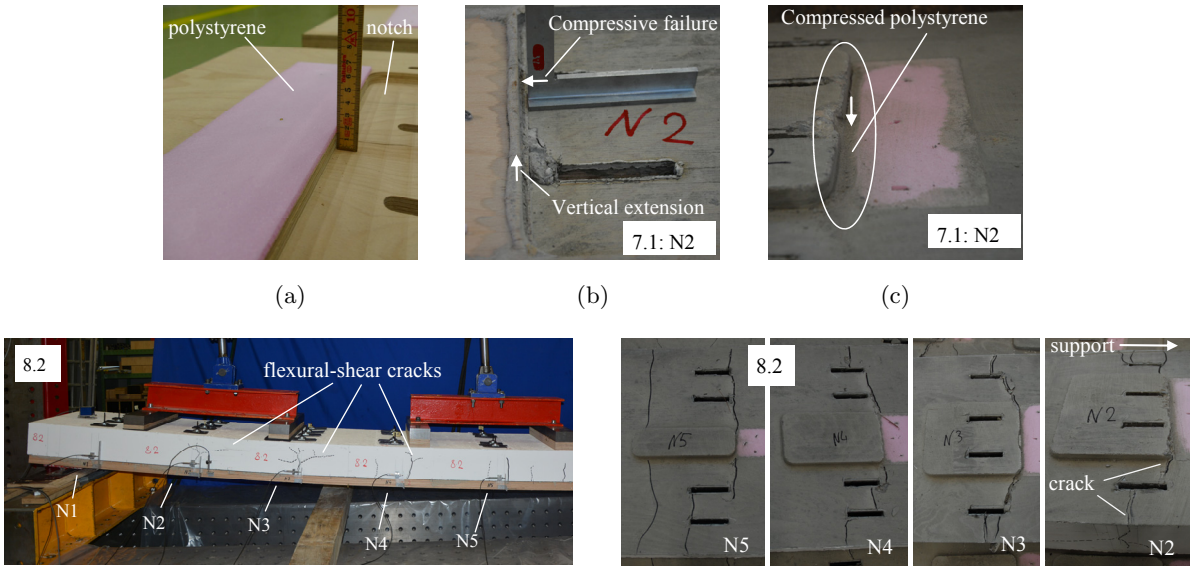

Figure 4.33: (a) Polystyrene elements fixed to the LVL part before concreting; (b) compressive failure of the LVL in notch N2 of specimen 7.1; (c) the polystyrene element close to notch N2 of specimen 7.1 was compressed by the timber, which expanded in the vertical direction due to a compressive failure in the longitudinal direction; (d) flexural-shear cracks between the fixed support and notch N5 of specimen 8.2 photographed at the end of the test; (e) bottom view of the flexural-shear cracks of specimen 8.2 photographed after the concrete part was separated from the timber part

4.4.4 Comparison with the analytical model

This section presents a comparison between the structural behaviour estimated by means of the analytical model described in Chapter 3 and the results of the tests on specimens 7.1, 7.2 and 8.2. The reason for the choice of these specimens is that the length of the holes and the presence of the polystyrene elements allowed observation of the entire structural behaviour. The failures modes and the failure loads were predicted according to Chapter 3 using the mean values of the mechanical properties reported in Tab. 2.1 and Tab. 4.8. Fig. 4.34(a) summarises the failure modes considered by the model. The steel rods were designed according to Sections 3.3.10 and 3.3.11 to carry approximately double the predicted ultimate load. Thus, they were able to prevent concrete crack opening and gap opening during the tests with high reliability.

As previously assessed, there were small differences between the plastic deformations of the notches. According to the model, if the load is uniformly distributed, all notches should yield simultaneously and should develop approximately the same deformation. During the experiments, the load was not perfectly evenly distributed but was introduced at eight points. Furthermore, the crack pattern influences the load-carrying mechanism. The crack patterns observed during the tests were not always the same.

In Figs. 4.34(b) and 4.34(c), the structural behaviour of specimens 7.1, 7.2 and 8.2 is plotted and compared to the prediction made with the analytical model according to Section 3.2. In Figs. 4.34(b) and 4.34(c), the load starts from the self-weight of the specimens, and the deflection measured is added to the expected deflection due to self-weight.

According to Figs. 4.34(b) and 4.34(c), during the elastic state, until about half of the yielding load, the predicted deflections correspond to the measurements. With increasing load, the deflections measured show a slight decrease of the bending stiffness and tend away from the prediction.

In general, the succession of the failures, the loads and the deformations correspond to the prediction. The failure mode which determined the end of the elastic behaviour and the beginning of connection yielding was the compressive failure of the LVL predicted by the model (2C). The three composite members yielded at about the same load level, and the measured yielding load corresponded to the prediction. A reason for this correspondence is that the variability of the compressive strength of beech LVL is small. Then, starting from the yielding point, although the LVL parts were provided with the polystyrene elements mentioned previously, the experiments showed a slightly larger hardening phase than the model. The principal reason for this discrepancy is that the model assumes an ideal-plastic behaviour of the LVL under compression. In reality, as observed during the shear tests described in Section 4.3, the compressive failure of the LVL generates hardening by nature. This phenomenon must be taken into account when the results of the bending tests are compared to the model calculations. Since the notch width was proportional to the shear forces generated by a uniformly distributed vertical load, the notches yielded at approximately the same load level as simplified by the model. Small differences in the behaviour of the notches, or the fact that not all notches yielded exactly at the same time, can be explained by the fact that the load was not perfectly evenly distributed like in theory, and that the crack depth was not constant over the length of the specimens.

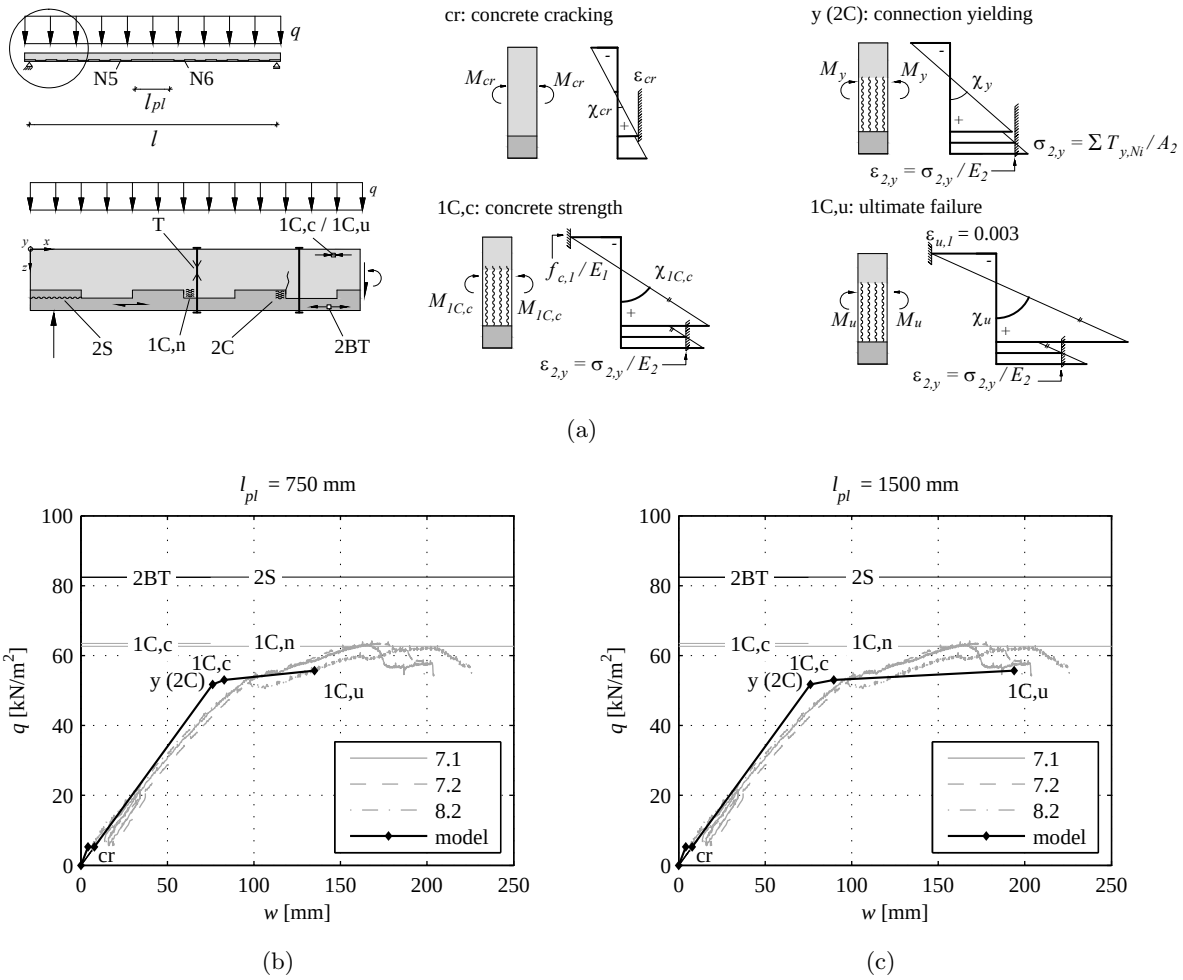

Figure 4.34: Comparison between the analytical model presented in Chapter 3 and the structural behaviour of specimens 7.1, 7.2 and 8.2: (a) failure modes considered by the analytical model; (b) comparison between the test results and the prediction made under the assumption of a localised plastic zone with a length of 750 mm; (c) comparison between the test results and the prediction made under the assumption of a localised plastic zone with a length of 1500 mm

According to the model, after the compressive failure of the LVL, the compressive strength of the concrete should be reached at the top of the cross-section (1C,c). Starting from this point, the compressive zone should begin to redistribute the stresses and to deform in a plastic way. However, during the tests, it was not possible to determine the specific moment in which the compressive strength of concrete was reached.

In the model, it is assumed that the zone of the composite member, where the cross-section develops plastic rotations, should be at mid-span and should have a length of at most the distance between the notches N5 and N6. According to the model, the rotation of the cross-section in the plastic zone should cause a failure of the compression zone of the concrete (1C,u), which is calculated with the assumption that the ultimate compressive strain of the concrete is about $\varepsilon_{u,1} \approx 0.003$. Then, the load should decrease and the deformation should continue.

As predicted by the model, the load began to decrease at the same time as local delamination of the concrete part on top edge of the cross-section occurred. This means that the concrete part locally reached the maximum compressive strain. However, during the tests, the exact dimensions of the plastic zones could not be determined. The difference with the model is that, during the experiments, the compressive failures of the concrete never occurred at mid-span, but always close to the holes where the rods were fixed. The reason for this difference is that the model does not take the holes into account. Close to the holes, the cross-section is weakened, and so failure is more likely to occur there. Furthermore, the place where the compressive failure of the concrete occurred was different in each specimen. It was observed that, during the plastic phase, the bending line was no longer parabolic, but the specimens tended to bend in an angled way. This tendency confirms the fact that a plastic zone exists where the rotation concentrates.

According to the model, a further increase of the curvature of the cross-section after the beginning of the compressive failure of the concrete should cause a combined tensile-bending failure of the LVL part of the composite member. The reason is that, with constant tensile stress at the centroid of the LVL cross-section, the curvature which causes a tensile-bending failure of the LVL (Eq. 3.77) is not much larger than the curvature corresponding to the concrete compressive failure (Eq. 3.78):

$$\frac{\chi_{2u}}{\chi_{1u}} = \frac{2 \cdot f_{m,2}}{h_2 \cdot E_2} \cdot \left(1 - \frac{\sigma_{2,y}}{f_{t,0,2}}\right) \cdot \frac{x_{IV}}{0.003} = 1.13 \tag{4.3}$$

During the tests, starting from the delamination of the compressive zone, the deflection continued to increase, and the load slowly decreased. After that, as predicted by the model, a combined tensile-bending failure of the LVL occurred below the concrete delamination. The differences between the maximum vertical deflections reached by the specimens is probably due to the fact that the plastic zone never developed at the same place.

The fact that the model for the prediction of the deflection increment due to rotation of the plastic zone is strongly simplified is the reason for the discrepancies between the predicted and the measured ultimate deflections. First, the dimensions of the plastic zones were determined with simplified assumptions. Second, the position of the ductile compressive failure of the concrete was never at mid-span, as assumed in the model. Furthermore, the model assumes that all notches yield at the same time and develop the same plastic deformations. The measured horizontal relative displacements indicated that the notches close to the supports developed larger plastic deformations. This influences the length of the zone where the cross-section experiences plastic rotations, causing differences with the model predictions. However, as shown in Figs. 4.34(b) and 4.34(c), if realistic dimensions of the plastic zone are assumed, the prediction lies approximately in the range of the experimental results.

One important requirement for the rods was that they should carry only vertical forces. Therefore, as shown in Fig. 4.20, the washers of the rods were placed on lubricated steel plates. Nevertheless, it is difficult to say if the rods effectively did not carry forces parallel to the interface. Most likely, since the horizontal LVDTs at the interface began to measure plastic deformations at approximately the predicted load level, the rods did not carry relevant horizontal forces.

Finally, the bottom view of the concrete part of the composite member, reported in Fig. 4.33, shows that the cracks initiated close to the notch edges. This agrees with the theory adopted in Section 3.3.10 for the design of the vertical reinforcement.

Since the reinforcement was designed according to the models described in Sections 3.3.10 and 3.3.11 with a high margin of safety, these bending tests did not allow for testing the load-carrying capacity of the reinforcement. Therefore, it was not possible to provide a complete validation of these models.

4.4.5 Discussion

This test series included several types of notches and vertical reinforcement. Specimens 7.1, 7.2 and 8.2 validated the analytical model for ductile and reliable design of timber-concrete composite members with notched connections, presented in Chapter 3.

The tests with progressive notches and without vertical reinforcement (specimens 2.1 and 3) showed that reaching ductile failure of the timber was not a problem, and, until this failure occurred, no gap opening and no other types of failure were observed. The difficulty was to achieve a relevant ductility after this failure. As theoretically explained in Section 3.3.9, during yielding of the notches, the interaction between the two materials causes notable problems. It was observed that a combination of enlargement of the existing concrete cracks and gap opening governed the load-displacement behaviour. As a consequence, although most of the notches reached a ductile compressive failure of the timber, only some of these notches developed relevant plastic deformations. In these cases, then the load decreased, and brittle failures of the concrete could occur. By observing the tests, it can be concluded that these phenomena are probably related. Furthermore, these mechanisms are unstable and difficult to predict. Thus, if no vertical reinforcement is designed, it is not possible to obtain a satisfying ductile behaviour. During these tests, no flexural-shear failure of the concrete part of the composite member occurred. Nevertheless, as explained in Section 3.3, it is critical to design notched connections without tensile reinforcement because of several factors which are difficult to quantify.

In contrast to specimen 2.1, the notches of specimen 1 were of constant width. As assessed in Section 3.3.4, since the composite member was subjected to a uniformly distributed vertical load, the compressive stress in the contact area between the LVL and the concrete was different in every notch. The notch close to the support should be subjected to the highest vertical compressive stresses, and the notch close to the mid-span to the smallest. Indeed, in specimen 1, the notches close to the supports developed larger plastic deformations than the other notches, and, consequently, the existing cracks enlarged. This crack enlargement probably interrupted the stress transfer through the concrete part of the composite member, and the vertical reactions were transferred to the timber part, causing the tensile-bending failure observed.

Specimens 4 and 5 showed that internal vertical reinforcement in the concrete does not improve the structural behaviour in a satisfying way. This means that it is necessary to prevent gap opening by using end-to-end reinforcement.

Specimen 6 is an example of end-to-end reinforcement designed in the wrong way. Since this reinforcement was too stiff, it carried a relevant amount of the horizontal shear forces.

Furthermore, the ductile load-carrying capacity of the rods, which could be activated, was too high. When the notches began to yield, the shear forces were redistributed to the rods, which had a significant reserve in load-carrying capacity. Furthermore, the rods introduced vertical internal forces which caused hardening of the notches. Therefore, this specimen failed due to a combination of tension and bending in the timber at mid-span. The slight non-linearity of the horizontal relative displacement shown in Fig. 4.26 has several possible explanations. A possible cause is an exceedance of the compressive strength of the timber and a consequent redistribution of the horizontal shear forces to the rods. Another cause of this non-linear connection behaviour could be that plastic hinges developed in the rods.

Specimen 2.2 showed that end-to-end reinforcement, designed according to Sections 3.3.10 and 3.3.11, is able to prevent the problems that occurred in specimens 2.1, 3, 4, 5 and 6. Almost all of the notches yielded, causing large plastic deformations. The rods with tolerance in specimen 2.2 carried the vertical tensile stresses in the concrete, prevented opening of the flexural-shear cracks, prevented gap opening, and allowed yielding of the notches. However, the tolerance of the holes was too small and the rods failed, probably due to a combination of tension and shear forces.

In contrast to specimen 2.2, specimens 7.1, 7.2 and 8.2 were constructed with longer holes to prevent failure of the rods, and were provided with polystyrene elements to reduce hardening in the timber compressive behaviour. The outcome was positive because these tests allowed for documentation of the entire structural behaviour of the composite members and for validation of the analytical model presented in Section 3.2. These specimens achieved very good structural behaviour with large ductility because a tensile-bending failure of the timber occurred very late. The governing failure mode was a ductile compressive failure of the timber, followed by a compressive failure of the concrete, which can also be classified as ductile. Only the third failure mode, which determined the end of the test, was a brittle bending-tensile failure of the timber. This ultimate failure represents the limit in the load-carrying capacity of the composite members studied. Indeed, in contrast to conventional reinforced concrete structures, the rotational capacity of the timber part limits the rotation of the cross-section in the plastic zone. Nevertheless, since the system failure was preceded by 10 compressive failures of the LVL material, with consistent mechanical properties, followed by a compressive failure of the concrete, a highly predictable structural system was able to develop. Indeed, after large plastic deformations, the maximum load reached during the tests was about the same in all specimens.

Although the amount of vertical reinforcement in specimens 7.1, 7.2 and 8.2 was small in comparison to that in conventional reinforced concrete members, the rods fulfilled the requirements for minimal reinforcement. This can be concluded because the flexural-shear cracks remained closed. Otherwise, the cracks would have propagated and brittle failure would have occurred. As illustrated in Section 3.3.10, before the reinforcement activates, the vertical tension is carried by the concrete by means of cantilever action. Then, as soon as flexural-shear cracks occur, the vertical tension is carried by the reinforcement, and a bracing mechanism (truss model) develops.

The fact that the yielding load and the failure load, determined for specimen 2.2, were higher than those for specimens 7.1, 7.2 and 8.2 suggests that the polystyrene elements, which were fixed to the timber plate, likely reduced the hardening phenomena. As shown in Fig. 4.33(e), the timber part of the composite member was able to expand in vertical direction after reaching the compressive strength. Thus, restraints caused by the vertical reinforcement were likely reduced. This modification to the specimens allowed for better verification of the analytical model, which assumes that the connection yielding is ideal plastic.

In conclusion, the tests 7.1, 7.2 and 8.2 demonstrated that the design approach and construction of the slab, presented in Section 3.3.12, ensures a ductile behaviour of the timber-concrete composite slabs made of beech LVL with notched connections. The use of notches as shear connections has two basic advantages. On one hand, the stiffness of the notch in elastic conditions minimises the deformations at service level. On the other hand, the notch is able to fail in a ductile way, resulting in good ductility at the failure level. Thus, the ductility of the composite member is generated by the timber, and the steel reinforcement should carry only vertical forces. In parallel, the reinforcement should allow plastic deformations in the timber. In tests 7.1 to 8.2, this requirement was achieved by fixing the rods in long holes. Furthermore, the composite member should be designed so that the maximum compressive strain of the concrete is reached before a combined tensile-bending failure of the timber occurs.

Specimens 2.2, 7.1, 7.2 and 8.2 were designed in a special way to validate the analytical model and to observe the failure mechanism as clearly as possible. Therefore, they are not yet suitable to be employed in practice. Indeed, it does not make sense to construct slabs, provided with such reinforcement. The next step will be to develop an economic and easily attachable reinforcement, which is able to achieve the structural requirements mentioned above.

4.5 Conclusion

The experimental analyses performed demonstrated that notches cut in beech LVL allow for a ductile compressive failure of the timber, and that a ductile failure mode together with a ductile design procedure is essential to achieve predictable behaviour of the composite member. This can be confirmed by comparing the first bending tests with the last series of tests. The specimens in the first bending test series were not designed according to the models presented in Chapter 3, and thus, showed several brittle failure modes. In contrast, several composite members tested in the last series were designed according to the models developed. Consequently, they exhibited a ductile and consistent behaviour and validated the analytical model.

Chapter 5

Conclusions

This thesis studied the structural behaviour of timber-concrete composite members made of beech LVL with notched connections. The research included theoretical and experimental analyses and was focused on the possibility to achieve a ductile failure mechanisms of the composite members.

In this work, a series of analytical models to describe the structural behaviour of notched timber-concrete connections were developed. During shear and bending tests, several failure modes of the notches were observed. Regarding the notches, the following conclusions can be drawn:

- Notched connections induce tensile and shear stresses in the timber and concrete. The stress configuration in the concrete can become particularly critical and difficult to predict. In this thesis, the behaviour of the unreinforced concrete layer was idealised by means of a console model. However, several parameters, such as the crack pattern, the stress distributions, the influence of internal stresses and the impact of timber deformations in the notches are challenging to estimate, and can cause significant deviations from reality. Therefore, to prevent a brittle failure of the concrete, it is necessary to provide the concrete part of the composite member with vertical reinforcement.

- A structural advantage of using notches to make the timber-concrete connection is the high stiffness at the service level.

- With an appropriate design, the structural behaviour of the notch can be governed by a compressive failure of the timber, which is ductile and thus desirable. The use of LVL materials instead of solid wood or glued laminated timber markedly improves the prediction accuracy of ductile compression failures of the timber parallel to the grain. Thus, a ductile notch design becomes feasible.

A timber-concrete composite member with a notched connection, subjected to bending, achieves ductility if the governing failure mode is yielding of the timber-concrete connection. In this thesis, an analytical model to describe the structural behaviour of timber-concrete composite members with ductile notched connections was developed and validated by means of bending

tests on timber-concrete composite members with notched connections made of beech LVL. Although this model focuses on notched connections, parts of it can be applied to study other ductile connection types. From this model, a ductile design method for LVL-concrete composite members with notched connections was derived (Fig. 5.1). Regarding the structural behaviour of timber-concrete composite members made of LVL with notched connections, subjected to bending, the following conclusions can be formulated:

- If the composite member is not provided with end-to-end vertical reinforcement, as soon as the notches yield, concrete crack enlargement and gap opening compromise the structural behaviour, and no ductility can be achieved.
- The ductility predicted by the analytical model can be reached if the composite member is provided with end-to-end vertical reinforcement. This reinforcement should hold the LVL and the concrete together, keep the concrete cracks closed, and carry vertical tension stresses within the concrete. Furthermore, it should allow for plastic longitudinal deformations of the LVL.
- Due to yielding of the notches, the curvature of the cross-section increases. The composite member should be designed so that the failure develops further into a ductile compressive failure of the concrete in the upper part of the composite member. If this is the case, the composite member will exhibit a consistent and highly-predictable structural performance because the system failure will be composed of several ductile failures of the LVL in the notches and a ductile compressive failure of the concrete.
- In general, the plastic deformations of the composite member are limited by the rotational capacity of the LVL part. If the bending stress becomes critical, its combination with the tension stresses causes a brittle failure of the LVL. This failure should occur as late as possible.

In conclusion, in this thesis, a clear analytical model to understand the structural behaviour of timber-concrete composite members with notched connections was developed. This model also supports for a ductile design of the composite member. Furthermore, this work showed that the use of beech LVL plates as the tensile reinforcement of the timber-concrete composite members ensures a ductile and highly-predictable structural behaviour, provided that the composite members are suitably designed.

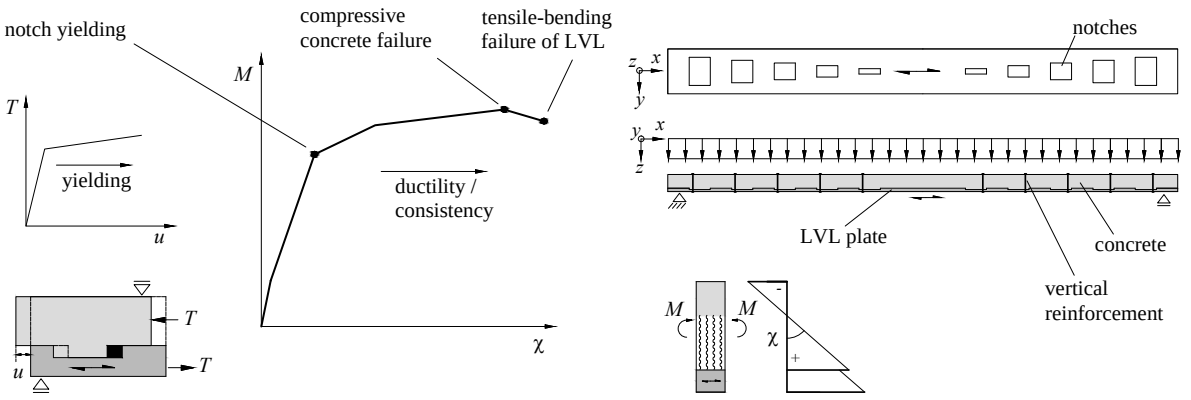

Figure 5.1: Timber-concrete composite member with a notched connection made of LVL, designed to achieve ductility

Chapter 6

Outlook

In this thesis, all experiments were performed with 40 mm thick beech LVL plates. However, the parametric studies show that a moderate increase of the LVL thickness does not compromise the structural behaviour of the composite member. An increase of the thickness of the LVL plate may be advantageous to meet other requirements for the slab, such as fire resistance and an improved construction process. The optimal thicknesses of the LVL and the concrete will be the result of a compromise between all requirements for the slab.

The last bending tests validated the analytical model for ductile design because the vertical reinforcement reached the theoretical requirements as closely as possible. The ductile composite members were provided with end-to-end reinforcement, placed in long holes. The washers of the rods could glide on the steel plates, placed at the borders of each hole. Thus, in theory, the reinforcement carried only vertical forces and was not able to prevent the plastic deformations of the LVL (Fig. 6.1(a)). The evaluation of the test results concluded that this special layout of the reinforcement prevented dowel action, and thus, the reinforcement behaved as desired. However, in practice, such a connection system is not possible because it needs a series of holes in the structure. Therefore, a new reinforcement system should be developed, meeting the following requirements:

- it carries the vertical tension stresses which develop within the concrete
- it prevents enlargement of flexural-shear cracks in the concrete
- it carries the tensile force, which is necessary to hold the LVL and the concrete together vertically and hence, it prevents gap opening between the LVL and the concrete
- it allows for plastic LVL deformations in the notches although the reinforcement is subjected to tension forces

Slabs in office and residential buildings are often designed as continuous beams to improve several aspects, among which is the reduction of the vertical deformations. Reinforced concrete and steel-concrete composite continuous beams exhibit ductility and redistribute bending moments away from the internal supports, when the cross-sections are able to generate plastic

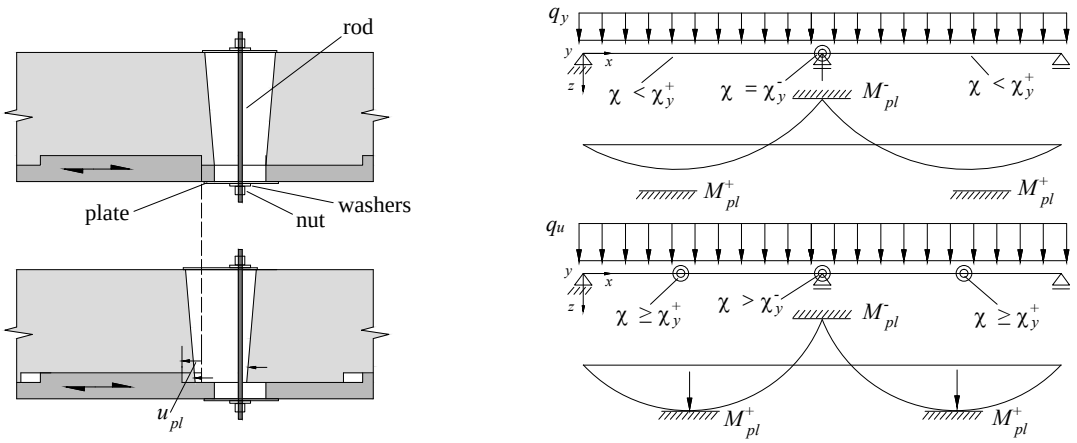

(a) (b)

Figure 6.1: (a) End-to-end reinforcement fixed in the specimens which validated the analytical model; (b) ductile behaviour of a two-span beam

hinges which have sufficient rotation capacity (Fig. 6.1(b)). In this case, a ductile design approach can be applied. Since the composite member developed in this thesis is able to carry exclusively positive bending moments, it must be installed as a single-span beam. A continuous beam can be realised if longitudinal reinforcing bars are installed over the internal supports to carry the tension due to negative bending moments. If the governing failure mode is the formation of plastic hinges over the internal supports, initiated by plastic extensions of the reinforcing bars, the bending moments can be redistributed away from the internal supports, until yielding of the notches and ductile failure of the compression zone are achieved. Further theoretical and experimental investigations are needed to achieve this progression of failure modes.

The choice of the configuration of the veneers allows for developing a composite slab which carries the vertical load in two directions. This is one additional possibility to optimise the structure. However, due to the presence of cross layers, several types of timber failures, e.g. the shearing-off failure, become more critical. Furthermore, a system to connect the LVL plates is necessary. Thus, detailed studies about this issue should be conducted.

In general, most of the model elements presented in Chapter 3 were validated by means of experiments. However, the model contains some assumptions based on theoretic considerations, which could not be completely validated:

- The estimation of the maximum plastic deflection of a composite member subjected to bending is based on the assumption of a plastic length (Section 3.2.6). This theory allows for a simple calculation of the range of the expected values. Further research is needed to predict deflection in a more accurate way.

- The models used to design the vertical reinforcement are based on truss models and simple equilibrium considerations. They enabled designing the specimens for the bending tests

so that the reinforcement did not fail (Sections 3.3.10 and 3.3.11). However, these models need additional theoretical and experimental studies to be completely verified.

- In the bending tests with the vertical reinforcement designed according to the analytical model, the reinforcement carried the vertical tension after opening of the concrete cracks. This means that the amount of reinforcement was sufficient to prevent brittle concrete failure. However, a reliable method to determine the minimum amount of vertical reinforcement should be developed.

- To prevent a shearing-off failure of the timber close to the notch, simplified stress distributions were assumed, and the influence of the most important parameters was studied (Section 3.3.6). In the bending tests performed, this failure never occurred. Nevertheless, this failure mechanism should be studied in further detail.

- As discussed in Sections 3.3.9 and 3.3.13, the gap opening in timber-concrete composite members with a notched connection is a complex problem, and may compromise the load-carrying mechanism of the composite member. Gap opening in elastic conditions can result from, for instance, different bending deflections of the layers, different deflections due to shear and eccentricity between the interface and the centroid of the effective area of the cross-sections. Plastic compressive timber deformations in the notches, compressive deformations of the concrete at the top of the cross-section and concrete cracks may worsen this problem. In this thesis, the gap opening was studied with simplified models, which represent a starting point to improve the knowledge about this problem.

Some issues related to the composite members developed in this thesis can be studied in greater detail and form the basis for further research:

- In the model to describe the structural behaviour of timber-concrete composite members with ductile connections (3.2), it is assumed that all connections yield simultaneously and are elastic-ideal plastic. The model can be extended to the general case.

- The shearing-off failure of the timber in front of the notch is brittle and implies a sudden collapse of the composite member. To prevent this failure, a reliable design model is needed. In this thesis, a widely used equation for the design of step joints, which assumes a rectangular shear stress distribution, is applied (2.38). This method could be justified by means of fracture mechanics theory. However, since this failure is brittle and must be prevented, further research is needed to study the real stress distributions and the failure mechanism. It would be useful to measure the shear strains in the timber in experiments.

- In this thesis, the structural behaviour of the notched connection was studied by means of analytical models to calculate the stresses and by means of failure criteria to estimate the failure loads (e.g. Mohr-Coulomb [5], Tsai and Wu [51]). An in-depth study on notches from the point of view of fracture mechanics would be useful.

- The moisture transfer between the concrete and the beech LVL was not studied in detail. After the test specimens were concreted (Chapter 4), it was observed that the LVL plates did not exhibit relevant deformations due to the moisture change. This is most likely prevented by the cross layers. Blass et al. [28] produced LVL-concrete composite specimens without cross layers and observed that the LVL plates bent during concrete hardening. After the experiments performed in the frame of this thesis, the composite specimens were opened, and it was observed that the first 1-2 veneers showed delamination (i.e. cracks in the longitudinal direction). In contrast, the other veneers did not exhibit cracks or colour changes, probably because they were protected from moisture by the glue layers. Due to the importance of this topic in practice, it should be studied in greater detail.

- The influence of the load duration and of the concrete shrinkage on the structural behaviour of LVL-concrete composite members with notched connections has yet to be studied.

- All experiments were performed with composite members made of European beech LVL, produced by the company Pollmeier [12] and concrete C50/60 [66]. The compressive strength of the concrete is determined following the assumption that a compressive failure of the LVL in the area of the notch edges should govern the structural behaviour. LVL products made of other wood species should also be usable. If the LVL layer has a smaller compressive strength parallel to the grain than beech LVL, concrete with a smaller compressive strength than C50/60 should be used.

- The parametric studies and the predictions of the test results were performed with mean values of the mechanical properties of the LVL and concrete, and the influence of the variation of the mechanical properties on the structural behaviour of the composite member was not studied. In order to develop a reliable design method for LVL-concrete composite members with notched connections, the influence of material property variation should be quantified.

- The failure criteria of Hoffman [50] and Tsai and Wu [51] were applied to the LVL because a failure function, which could take into account different stresses and strengths, was needed. However, in this thesis, these criteria were not studied in greater detail. It would be useful to examine the applicability of such criteria to wood and wood-based materials in depth. Some authors (e.g. [44]) already discussed several issues related to the application of phenomenological failure criteria to wood.

- This thesis focused on the failure process of the composite member. Several additional aspects, such as fire resistance, vibrations and sound insulation have yet to be studied.

Nomenclature

Abbreviations

1	Concrete
1C,c	Exceedance of the compressive strength of concrete $f_{c,1}$ on top of the cross section
1C,n	Compressive failure of concrete in the contact area A_N of the notch
1C,u	Exceedance of the maximum compressive strain of concrete $\varepsilon_{u,1}$ on top of the cross section
1F	Flexural-shear failure of concrete
1S	Horizontal shear failure of concrete close to the notch at a depth of $z = h_1$
1V	Vertical shear failure of concrete
2	Timber
2BT	Combined tensile-bending failure of timber
2C	Compressive failure of timber in the contact area A_N of the notch
2R	Rolling shear failure of timber
2S	Horizontal shearing-off failure of timber close to the notch, at a depth of $z = h_1 + t_N$
2S*	Horizontal shearing-off failure of timber close to the notch, at a depth of $z = h_1 + t_N$, calculated by taking into account the entire length of timber before the notch
2V	Shear failure of timber
1F,inf	Lower bound of the failure 1F, calculated with $b_{1F,inf}$
1F,sup	Upper bound of the failure 1F, calculated with $b_{1F,sup}$
1V,inf	Lower bound of the failure 1V, calculated with $b_{1V,inf}$
1V,sup	Upper bound of the failure 1V, calculated with $b_{1V,sup}$
eff	Effective

int	Interface
L	Long notch
LEFM	Linear elastic fracture mechanics
LVDT	Linear voltage displacement transducer
LVL	Laminated veneer lumber
S	Short notch
T	Tensile failure of the vertical reinforcement

Upper-case roman letters

$A_{...}$	Effective surface of the composite cross section
$A_{i,...}$	Cross section area of part i of the composite member
A_{inf}	Cross section area of the lower sector of the timber part, used to estimate the elastic shear stress distribution
A_N	Contact area of the notch
$A_{s,min}$	Minimal cross section area of the vertical steel reinforcement
$A_{s,T,Ni}$	Cross section area of the vertical steel reinforcement which is necessary to carry the vertical tensile force T_i close to the notch Ni calculated by means of a truss model
$A_{s,v}$	Cross section area of the vertical steel reinforcement which is necessary to prevent gap opening at ultimate limit state
A_{sup}	Cross section area of the upper sector of the timber part, used to estimate the elastic shear stress distribution
A_s	Total cross section area of the vertical steel reinforcement
C_i	Coefficient
C_i	Compression force in concrete
D	Connection ductility index
D_i	Diagonal of a truss model
E_0	Modulus of elasticity without long term effects
E_∞	Modulus of elasticity with long term effects
$E_{i,...}$	Modulus of elasticity of part i of the composite member
E_{inf}	Modulus of elasticity of the lower sector of timber
E_{sup}	Modulus of elasticity of the upper sector of timber
$EI_{...}$	Bending stiffness

F	External force
$F_{2S,sides}$	Amount of shear force carried by the notch sides
$F_{cyl,i}$	Load of the hydraulic cylinder i
$F_{F,...}$	Failure function calculated with the Tensor Polynomial theory
F_{ij}	Coefficient of the failure criterion according to the Tensor Polynomial theory
F_i	Coefficient of the failure criterion according to the Tensor Polynomial theory
F_u	External force which causes a failure
F_v	External vertical force
F_x	Force in x-direction
F_y	Force in y-direction
$G_{0,...}$	Shear modulus of timber parallel to the grain
G_i	Shear modulus of part i of the composite member
$G_{R,...}$	Shear modulus of timber perpendicular to the grain (rolling shear)
$I_{...}$	Effective moment of inertia of the composite cross section
I_i	Moment of inertia of part i of the composite member
K_{ser}	Shear stiffness of a timber-concrete connection at service level
$M_{...}$	Bending moment
M_{1F}	Moment in y-direction due to the distance in z-direction between T_{Ni} and plane 1F
M_{1S}	Moment in y-direction due to the distance between T_{Ni} and plane 1S
M_{ecc}	Eccentricity moment acting in a timber notch
M_i	Bending moment in part i of the composite member
M_{pl}^{+}	Positive plastic resisting moment of a cross section
M_{pl}^{-}	Negative plastic resisting moment of a cross section
$M_{R,...}$	Bending moment which causes a failure
N	Axial force
$N_{inf}(x)$	Axial force in the lower sector of timber
$N_{sup}(x)$	Axial force in the upper sector of timber
S	Shear strength
$S_{i,i+1,...}$	Effective static moment for the calculation of the theoretic elastic shear stress in the interface between the parts i and $i+1$ of the composite member
T	Connection shear force

T_i	Tension tie in a truss model
T_{Ni}	Horizontal shear force introduced in the notch Ni
$T_{R,...,Ni}$	Failure load of notch Ni
$T_{R,...}$	Failure load of a timber-concrete connection
$T^*_{R,2C,Ni}$	Force which causes a compressive failure of timber in notch Ni, calculated neglecting the stresses in z-direction
$T^*_{R,2S,Ni}$	Force which causes a shearing-off failure of timber close to notch Ni, calculated neglecting the stresses in z-direction
$T_{R,dowels,Ni}$	Force parallel to the interface carried by the mechanical fasteners fixed close to notch Ni
$T_{y,Ni}$	Yielding shear force of notch Ni
V	Shear force
V_i	Shear force in part i of the composite member
V_{Ni}	Shear force acting on the composite cross section close to notch Ni
$V_{R,...}$	Shear force which causes a failure
$W_{i,b...}$	Section modulus at the bottom of part i of the composite member
$W_{i,t...}$	Section modulus at the top of part i of the composite member
$W_{i...}$	Section modulus at the centroid of part i of the composite member
W_{notch}	Minimal section modulus of the shear plane of a timber notch
X	Strength in x-direction
X_c	Compressive strength in x-direction
X_t	Tensile strength in x-direction
Y	Strength in y-direction
Y	Yielding function (Mohr-Coulomb failure criterion)
Y_c	Compressive strength in y-direction
Y_t	Tensile strength in y-direction

Lower-case roman letters

a	Distance in the axial direction of the slab
$b_{1F,inf}$	Lower bound of the effective width of plane 1F (in y-direction)
$b_{1F,sup}$	Upper bound of the effective width of plane 1F (in y-direction)
b_{1S}	Width of plane 1S (in y direction)

$b_{1V,inf}$	Lower bound of the effective width of plane 1V (in y-direction)
$b_{1V,sup}$	Upper bound of the effective width of plane 1V (in y-direction)
$b_{i,...}$	Width of part i of the composite member
b_{int}	Width of the interface
b_{Ni}	Width of notch Ni
c	Cohesion (parameter of the Mohr-Coulomb failure criterion)
e	Distance between the centroids of the parts of the composite member
$e_{i,...}$	Distance between the centroid of the composite member and the centroid of part i
$f_{c,0,...}$	Compressive strength of timber parallel to the grain
$f_{c,90,...}$	Compressive strength of timber perpendicular to the grain
$f_{c,cube}$	Cube compressive strength of concrete
$f_{c,i}$	Compressive strength of part i of the composite member
f_{ct}	Tensile strength of concrete
$f_{m,0,...}$	Bending strength of timber parallel to the grain
f_{model}	Correction factor
$f_{R,v,...}$	Rolling shear strength of timber
f_s	Tensile strength of steel reinforcement
$f_{t,0,...}$	Tensile strength of timber parallel to the grain
$f_{t,90,...}$	Tensile strength of timber perpendicular to the grain
$f_{t,i}$	Tensile strength of part i of the composite member
$f_{v,0,...}$	Shear strength of timber parallel to the grain
g	Self-weight
g_k	Characteristic value of self-weight
h	Total depth of the composite member
$h_{1F,eff}$	Effective height of plane 1F (in x-direction)
h_{1F}	Height of plane 1F (in x-direction)
h_{1S}	Height of plane 1S (in x-direction)
h_{1V}	Height of plane 1V (in z-direction)
h_{cr}	Concrete crack depth in z-direction
$h_{i,...}$	Height of part i of the composite member

h_{inf}	Thickness of the lower sector of the timber part, used to estimate the elastic shear stress distribution
h_i^*	Distance in z-direction between the action point of the axial force N acting on the part i of the composite member and the connection force T_{Ni}
$h_{s,0}$	Sector of h_s loaded parallel to the grain
$h_{s,R}$	Sector of h_s loaded perpendicular to the grain
h_{sup}	Thickness of the upper sector of the timber part, used to estimate the elastic shear stress distribution
h_s	Thickness of the timber sector subjected to shear close to the notch, used to estimate the elastic shear stress distribution
$k_{...}$	Shear stiffness
k_s	Connection modulus
k_t	Uplift modulus
l	Length/span
l_A	Distance between the support and the timber-concrete connection next to it
l_{eff}	Distance between the supports of a single-span beam
l_{Ni}	Length of notch Ni
l_{pl}	Length of the plastic zone
m	Number of connections
$n_{bars\varnothing 6}$	Number of vertical reinforcement bars with a diameter of 6 mm
n_{bars}	Number of vertical reinforcement bars
n_i	Ratio between the modulus of elasticity of part i and the reference modulus of elasticity of the composite member
$p(x)$	Shear force in timber per length unit, caused by the load transfer in the notched connection
$q(v_u)$	Uniformly distributed force which is necessary to close the gap at ultimate limit state
$q_{...}$	Vertical distributed load
q_{Ak}	Characteristic value of the permanent load
$q_{d,est}$	Design value of the uniformly distributed load for the control of the aesthetics
$q_{d,ULS}$	Design value of the uniformly distributed load for the ultimate limit state analysis
q_i	Vertical uniformly distributed load acting on part i of the composite member

q_{Nk}	Characteristic value of the live load
$q_{R,...}$	Vertical uniformly distributed load which causes a failure
$q^*_{R,2C}$	Vertical uniformly distributed load which causes a compressive failure of timber in notch Ni, calculated neglecting the stresses in z-direction
$q^*_{R,2S}$	Vertical uniformly distributed load which causes a shearing-off failure of timber, calculated neglecting the stresses in z-direction
r	Stress perpendicular to the interface between two parts of a composite structure
s	Distance between two connections
t	Horizontal shear force per length unit acting in the interface of a composite member
t_{Ni}	Depth of notch Ni
t_N	Depth of all notches
u	Horizontal relative displacement at the interface between the components of a composite member
$u_{inf}(x)$	Displacement of the lower sector of timber
u_i	Horizontal relative displacement between timber and concrete close to notch Ni
$u_{pl,i}$	Plastic deformation of notch Ni
$u_{sup}(x)$	Displacement of the upper sector of timber
v	Gap opening
v_u	Gap opening at ultimate limit state
$w_{...}$	Deflection
$w_{1,u}$	Vertical deflection of the concrete part at quarter-span at ultimate limit state
w_1	Vertical deflection measured at quarter-span
$w_{2,u}$	Vertical deflection of the timber part at quarter-span at ultimate limit state
w_2	Vertical deflection measured at mid-span
w_3	Vertical deflection measured at quarter-span
x	Coordinate of the cross section (in longitudinal direction)
$x_{...}$	Neutral axis depth
y	Coordinate of the cross section (in direction of the cross section width)
z	Coordinate of the cross section (in direction of the cross section height)
$z_{s,...}$	z-coordinate of the centroid of the composite member
$z_{si,...}$	z-coordinate of the centroid of part i of the composite member

ui	Horizontal relative displacement measured close to the notch Ni
uL	Horizontal relative displacement between timber and concrete measured close to the left support
uR	Horizontal relative displacement between timber and concrete measured close to the right support

Upper-case greek letters

$\Delta l_{pl,i}$	Plastic deformation of a reinforcing bar of a reinforced concrete member
ΔM	Moment increase from the connection yielding (y) to the ultimate failure (u)
Δw_{III}	Increment of the vertical deflection at mid-span during state III
Δw_{IV}	Increment of the vertical deflection at mid-span during state IV
Δx	Transverse displacement in x-direction
Δx_0	Transverse displacement in x-direction due to shear parallel to the grain
Δx_R	Transverse displacement in x-direction due to rolling shear

Lower-case greek letters

α	Angle
$\alpha_{1,u}$	Angle of the concrete deformation at ultimate limit state
β	Angle
β_h	Factor to take the hardening into account
$\chi_{...}$	Cross section curvature
$\chi_{u,1}$	Cross section curvature, when the compressive strain on top of the concrete part reaches $\varepsilon_{u,1}$
$\chi_{u,2}$	Cross section curvature, when a combined tensile-bending failure (2BT) occurs in the timber part
$\delta(x)$	Internal shear deformation in timber
γ	Angle of the shear strain
γ_0	Angle of the shear strain due to shear stress parallel to the grain
γ_G	Load factor for permanent action
γ_i	γ-factor of part i of the composite member
γ_Q	Load factor for variable action
γ_R	Angle of the shear strain due to shear stress perpendicular to the grain

ψ_2	Reduction factor for quasi-permanent value of variable action
σ	Axial stress
$\sigma_{2x,Ni}$	Compressive contact stress between timber and concrete in x-direction in the notch Ni
$\sigma_{2z,Ni}$	Stress in z-direction in timber close to the notch Ni
σ_{90}	Stress perpendicular to the grain
$\sigma_{i,...}$	Axial stress in part i of the composite member
$\sigma_{i,m...}$	Bending stress in part i of the composite member
$\sigma_{i,t/b}$	Axial stress on top/bottom of part i of the composite member
$\sigma_{i,u}$	Axial stress in the centroid of part i at ultimate limit state
$\sigma_{i,y}$	Tensile stress in the centroid of part i when the connections are yielding
σ_{iz}	Axial stress in part i of the composite member in z-direction
$\sigma_i(z)$	Axial stress in part i as a function of the depth
σ_j	Axial stress in point j
$\sigma_{m,y}$	Bending stress due to a moment around the y-axis
$\sigma_{t,0}$	Tensile stress parallel to the grain
σ_x	Stress in x-direction
σ_y	Stress in y-direction
τ	Shear stress
$\tau_{1,x}$	Shear stress in concrete in x-direction close to the notch
$\tau_{1,z}$	Shear stress in concrete in z-direction close to the notch
$\tau_{12,Ni}$	Theoretic elastic shear stress in the interface between timber and concrete close to notch Ni
$\tau_{2,Ni}$	Horizontal shear stress in timber close to notch Ni
$\tau_{i,i+1}$	Shear stress in the interface between parts i and $i+1$ of the composite member
$\tau_{R,c}$	Shear strength of concrete
τ_{xy}	Shear stress in the x-y-plane
$\theta_{...}$	Rotation angle
ε	Strain
ε_{cu}	Maximum compressive deformation of concrete
$\varepsilon_{i,...}$	Axial strain in the centroid of part i of the composite member
$\varepsilon_{i,b,...}$	Axial strain at the bottom of part i of the composite member

$\varepsilon_{i,m,...}$	Bending strain in part i of the composite member
$\varepsilon_{i,t,...}$	Axial strain at the top of part i of the composite member
$\varepsilon_{u,1}$	Maximum compressive deformation of concrete
φ	Angle of internal friction (Mohr-Coulomb failure criterion)
φ	Creep factor

Indexes

b	Bottom
cr	Cracking
I	State I: connection elastic; concrete uncracked and elastic
II	State II: connection elastic; concrete cracked and elastic
III	State III: connection plastic; concrete cracked and elastic
IV	State IV: connection plastic; concrete cracked and plastic
m	Bending
Ni	Connection i/ notch i
t	Top
u	Ultimate limit state
y	Yielding

Other symbols

$\leftharpoondown\!\!\rightharpoonup$	Grain direction in timber
$\oslash$	Diameter
$\oslash_{bars}$	Diameter of the vertical reinforcement

Bibliography

[1] Swiss Standards Association, "SIA 261 - actions on structures", *Swiss Society of Engineers and Architects, Zurich, Switzerland*, 2003.

[2] A. Frangi and M. Fontana, "Elasto-plastic model for timber-concrete composite beams with ductile connection", *Structural Engineering International*, vol. 13, no. 1, pp. 47–57, 2003.

[3] Zulassungsstelle für Bauprodukte und Bauarten, "Z-9.1-838: Furnierschichtholz aus Buche zur Ausbildung stabförmiger unf flächiger Tragwerke", *Deutsches Institut für Bautechnik*, 2013.

[4] P. Marti, "Zur plastischen Berechnung von Stahlbeton", ETHZ, Report 104, 1980.

[5] ——, *BAUSTATIK: GRUNDLAGEN, STABTRAGWERKE, FLÄCHENTRAGWERKE*. John Wiley and Sons, 2012.

[6] L. Boccadoro and A. Frangi, "Experimental investigations on timber-concrete composite slabs made of beech laminated veneer lumber with notched connection", Institute of Structural Engineering ETH Zurich, test report, 2016.

[7] H. Kolb, "Biegeversuche und Prüfung des Brandverhaltens an Trägern aus verleimten Buchenschälfurnieren", *Holz als Roh-und Werkstoff*, vol. 26, no. 8, pp. 277–283, 1968.

[8] J. Ehlbeck and F. Colling, "Scherfestigkeit rechtwinklig zur Plattenebene und Schubmodul von Bau-Furniersperrholz aus Buche", *Holz als Roh-und Werkstoff*, vol. 43, no. 4, pp. 143–147, 1985.

[9] N. Krackler and P. Niemz, "Schwierigkeiten und Chancen in der Laubholzverarbeitung, Teil 1: Bestandssituation, Eigenschaften und Verarbeitung von Laubholz am Beispiel der Schweiz", *Holztechnologie*, vol. 52, no. 2, pp. 5–11, 2011.

[10] ——, "Schwierigkeiten und Chancen in der Laubholzverarbeitung, Teil 2: Verwendungsmöglichkeiten von sägefähigem Laubholz", *Holztechnologie*, vol. 52, no. 3, pp. 5–10, 2011.

[11] E. Gehri, *HOLZWERKSTOFFE AUF FURNIERBASIS*. Das Grafik Werk, 1993.

[12] J. Hassan and M. Eisele, "BauBuche–Der nachhaltige Hochleistungswerkstoff", *Bautechnik*, vol. 92, no. 1, pp. 40–45, 2015.

[13] H. J. Blass and J. Streib, "Baubuche Buchenfurnierschichtholz – Bemessungshilfe für Entwurf und Berechnung nach Eurocode 5", Pollmeier Massivholz GmbH und Co.KG, Tech. Rep., 2014.

[14] J.-W. van de Kuilen and M. Knorz, "Ergebnisse der Zulassungsversuche für eine allgemeine bauaufsichtliche Zulassung (abZ) von Furnierschichtholz aus Buche", Technische Universität München, Prüfbericht Nr. 10511, 2012.

[15] ——, "Ergebnisse der Zulassungsversuche für eine allgemeine bauaufsichtliche Zulassung (abZ) von Furnierschichtholz aus Buche", Technische Universität München, Prüfbericht Nr. 11513, 2013.

[16] A. Ceccotti, "Timber-concrete composite structures, Timber Engineering, Step 2", Centrum Hout, The Netherlands, Tech. Rep., 1995.

[17] J. Natterer, J. Hamm, and P. Favre, "Composite wood-concrete floors for multi-story buildings", *Proceedings of the International Wood Engineering Conference*, vol. 3, 1996.

[18] D. Yeoh, M. Fragiacomo, M. De Franceschi, and K. H. Boon, "State of the art on timber-concrete composite structures: Literature review", *Journal of Structural Engineering*, vol. 137, no. 10, pp. 1085–1095, 2011.

[19] A. Adekola, "Partial interaction between elastically connected elements of a composite beam", *International Journal of Solids and Structures*, vol. 4, no. 11, pp. 1125–1135, 1968.

[20] F. Stüssi, "Beiträge zur Berechnung und Ausbildung zusammengesetzter Vollwandträger", *Schweizerische Bauzeitung*, vol. 121, 1943.

[21] ——, "Zusammengesetzte Vollwandträger", *IVBH*, 1947.

[22] B. Heimeshoff, "Nachweis der Tragsicherheit und Gebrauchstauglichkeit von Einfeldträgern, die aus nachgiebig miteinander verbundenen Querschnittsteilen bestehen, im Ingenieurholzbau", *Holz als Roh-und Werkstoff*, vol. 49, no. 6, pp. 243–249, 1991.

[23] R. Pischl, "Die praktische Berechnung zusammengesetzter hölzerner Biegeträger mit Hilfstafeln zur Berechnung der Abminderungsfaktoren", *Bauingenieur*, vol. 44, pp. 181–185, 1969.

[24] J. Natterer and M. Hoeft, "Zum Tragverhalten von Holz-Beton-Verbundkonstruktionen", IBOIS, École Polytechnique Fédérale de Lausanne, Tech. Rep. Forschungsbericht CERS Nr. 1345, 1987.

[25] A. Frangi, "Brandverhalten von Holz-Beton-Verbunddecken", PhD thesis, ETH Zurich, 2001.

[26] K. Richter, R. Steiger, A. Frangi, and C. Sigrist, "Dokumentation D0235 Holzbau - Ergänzende Festlegungen-Norm SIA 265/1, Bauteile aus Holzwerkstoffen, Bemessungskonzept und Beispiele", *Swiss Society of Engineers and Architects, Zurich, Switzerland*, 2010.

[27] K. Möhler, "Über das Tragverhalten von Biegeträgern und mit zusammengesetztem Querschnitt und nachgiebigen Verbindungsmitteln", Habilitation, TH Karlsruhe, 1956.

[28] H. J. Blass, J. Ehlbeck, M. van der Linden, and M. Schlager, "Trag- und Verformungsverhalten von Holz-Beton-Verbundkonstruktionen", Versuchsanstalt für Stahl, Holz und Steine, Abteilung Ingenieurholzbau Universität Fridericiana Karlsruhe, Tech. Rep., 1995.

[29] Swiss Standards Association, "SIA 265 - timber structures", *Swiss Society of Engineers and Architects, Zurich, Switzerland*, 2012.

[30] H. Blass and M. Schlager, "Connections for timber-concrete-composite structures", *Proceedings of the Int. Conference on Composite Construction – Conventional and Innovative, Innsbruck, Austria*, 1997.

[31] P. Gelfi, E. Giuriani, and A. Marini, "Stud shear connection design for composite concrete slab and wood beams", *Journal of Structural Engineering*, vol. 128, no. 12, pp. 1544–1550, 2002.

[32] R. M. Gutkowski, K. Brown, A. Shigidi, and J. Natterer, "Investigation of notched composite wood-concrete connections", *Journal of Structural Engineering*, vol. 130, no. 10, pp. 1553–1561, 2004.

[33] B. C. Michelfelder, "Trag-und Verformungsverhalten von Kerven bei Brettstapel-Beton-Verbunddecken", PhD thesis, University of Stuttgart, 2006.

[34] A. Dias, S. Lopes, J. G. Van de Kuilen, and H. Cruz, "Load-carrying capacity of timber–concrete joints with dowel-type fasteners", *Journal of Structural Engineering*, vol. 133, no. 5, pp. 720–727, 2007.

[35] D. Yeoh, M. Fragiacomo, M. De Franceschi, and A. H. Buchanan, "Experimental tests of notched and plate connectors for LVL-concrete composite beams", *Journal of Structural Engineering*, vol. 137, no. 2, pp. 261–269, 2011.

[36] D. Yeoh, M. Fragiacomo, and B. Deam, "Experimental behaviour of LVL–concrete composite floor beams at strength limit state", *Engineering Structures*, vol. 33, no. 9, pp. 2697–2707, 2011.

[37] E. Lukaszewska, M. Fragiacomo, and H. Johnsson, "Laboratory tests and numerical analyses of prefabricated timber-concrete composite floors", *Journal of Structural Engineering*, vol. 136, no. 1, pp. 46–55, 2009.

[38] A. M. P. G. Dias, "Mechanical behaviour of timber-concrete joints", PhD thesis, TU Delft, 2005.

[39] A. Ceccotti, "Composite concrete – timber structures", *Progress in Structural Engineering and Materials*, vol. 4, no. 3, pp. 264–275, 2002.

[40] P. Clouston, L. A. Bathon, and A. Schreyer, "Shear and bending performance of a novel wood–concrete composite system", *Journal of Structural Engineering*, vol. 131, no. 9, pp. 1404–1412, 2005.

[41] A. M. Dias and L. F. Jorge, "The effect of ductile connectors on the behaviour of timber–concrete composite beams", *Engineering Structures*, vol. 33, no. 11, pp. 3033–3042, 2011.

[42] M. L. R. Van der Linden, "Timber-concrete composite beams", *HERON*, vol. 44, no. 3, 1999.

[43] J. Chapman, "Composite construction in steel and concrete – the behaviour of composite beams", *The Structural Engineer*, vol. 42, no. 4, pp. 115–125, 1964.

[44] B. Kasal and R. J. Leichti, "State of the art in multiaxial phenomenological failure criteria for wood members", *Progress in Structural Engineering and Materials*, vol. 7, no. 1, pp. 3–13, 2005.

[45] I. Smith, E. Landis, and M. Gong, *Fracture and fatigue in wood.* John Wiley and Sons, 2003.

[46] R. Jockwer, "Structural behaviour of glued laminated timber beams with unreinforced and reinforced notches", PhD thesis, ETH Zürich, 2014.

[47] R. V. von Mises, "Mechanik der festen Körper im plastisch-deformablen Zustand", *Nachrichten von der Gesellschaft der Wissenschaften zu Göttingen, Mathematisch-Physikalische Klasse*, vol. 1913, pp. 582–592, 1913.

[48] R. Hill, *The mathematical theroy of plasticity.* Oxford, Clarendon Press, 1950.

[49] C. B. Norris, "Strength of orthotropic materials subjected to combined stresses", *Report. United States Forest Products Laboratory*, no. 1816, 1950.

[50] O. Hoffman, "The brittle strength of orthotropic materials", *Journal of Composite Materials*, vol. 1, no. 2, pp. 200–206, 1967.

[51] S. W. Tsai and E. M. Wu, "A general theory of strength for anisotropic materials", *Journal of Composite Materials*, vol. 5, no. 1, pp. 58–80, 1971.

[52] R. Narayanaswami and H. M. Adelman, "Evaluation of the tensor polynomial and Hoffman strength theories for composite materials", *Journal of Composite Materials*, vol. 11, no. 4, pp. 366–377, 1977.

[53] R. Steiger and E. Gehri, "Interaction of shear stresses and stresses perpendicular to the grain", *International council for research and innovation in building and construction. Working commission W18-Timber structures, Meeting forty-four, Alghero, Italy*, 2011.

[54] S. Vasic, "Applications of fracture mechanics to wood", PhD thesis, University of New Brunswick, Faculty of Forestry and Environmental Management, 2000.

[55] M. Grosse, "Zur numerischen Simulation des physikalisch nichtlinearen Kurzzeittragverhaltens von Nadelholz am Beispiel von Holz-Beton-Verbundkonstruktionen", PhD thesis, Bauhaus–Universität Weimar, 2005.

[56] F. Schönborn, "Holz-Beton-Fertigteilelemente", PhD thesis, Leopold-Franzens-Universität Innsbruck, 2006.

[57] DIN, "DIN 1052: Holzbauwerke. Entwurf, Berechnung und Bemessung von Holzbauwerken", *DIN Deutsches Institut für Normung e. V., Berlin, Germany*, 2004.

[58] H. Kaiser, *WIND-ERTÜCHTIGUNG STATISCH AUSGENUTZTER HOLZDÄCHER ZUR AUFNAHME ANGESTELLTER SOLARPANEELE MITTELS IN SCHLITZE GEKLEBTER CFK-LAMELLEN.* epubli, 2010.

[59] F. Colling, *HOLZBAU-GRUNDLAGEN UND BEMESSUNGSHILFEN. 2. AUFLAGE.* Vieweg + Teubner, 2008.

[60] R. Stephan, "Beitrag zur Spannungsermittlung beim Versatzanschluss im Holzbau", PhD thesis, TH Hannover, 1950.

[61] F. Fonrobert, *GRUNDZÜGE DES HOLZBAUES IM HOCHBAU, 7. AUFLAGE*. Verlag von Wilhelm Ernst und Sohn, Berlin, 1960.

[62] B. Heimeshoff and N. Köhler, "Untersuchung über das Tragverhalten von Zimmermannsmässigen Holzverbindungen: Forschungsbericht", Lehrstuhl für Baukonstruktion und Holzbau Technische Universität München, Tech. Rep., 1989.

[63] A. Steurer, *GRUNDZÜGE DES HOLZBAUS – AUTOGRAPHIE ZUR VORLESUNG HOLZBAU*. ETH Zürich Institut für Baustatik und Konstruktion, Professur für Stahl-, Holz- und Verbundbau, 2004.

[64] H. Bachmann, *STAHLBETON I, GRUNDZÜGE DES STAHLBETONS UND DES VORGESPANNTEN BETONS, ZWEITER TEIL*. Eidgenössische Technische Hochschule Zürich, Abteilung für Bauingenieurwesen, 1991.

[65] A. Kenel, "Biegetragverhalten und Mindestbewehrung von Stahlbetonbauteilen", PhD thesis, ETH Zürich, 2002.

[66] Swiss Standards Association, "SIA 262 - Concrete Structures", *Swiss Society of Engineers and Architects, Zurich, Switzerland*, 2003.

[67] W. Kaufmann. (2015). Vorlesungsunterlagen Stahlbeton I – Kapitel 3.2 Stabtragwerke – Biegung. German, ETH Zurich – Institute of Structural Engineering, [Online]. Available: `www.kaufmann.ibk.ethz.ch`.

[68] A. Muttoni and M. F. Ruiz, "Shear strength of members without transverse reinforcement as function of critical shear crack width", *ACI Structural Journal*, vol. 105, no. 2, pp. 163–172, 2008.

[69] F. Leonhardt and R. Walther, "Shear tests on beams with and without shear reinforcement", *Deutscher Ausschuss für Stahlbeton*, no. 151, 1962.

[70] A. Muttoni and B. Thürlimann, "Shear tests on beams and slabs without shear reinforcement", ETH Institut für Baustatik und Konstruktion, Zürich, Switzerland, Tech. Rep., 1986.

[71] R. C. Fenwick and T. Pauley, "Mechanism of shear resistance of concrete beams", *Journal of the Structural Division*, vol. 94, no. 10, pp. 2325–2350, 1968.

[72] A. Muttoni and J. Schwartz, "Behavior of beams and punching in slabs without shear reinforcement", *IABSE colloquium*, IABSE, vol. 62, 1991, pp. 703–708.

[73] G. N. J. Kani, "The riddle of shear failure and its solution", *ACI - Journal*, vol. 61, no. 4, pp. 441–468, 1964.

[74] K. Zilch and G. Zehetmaier, *BEMESSUNG IM KONSTRUKTIVEN BETONBAU: NACH DIN 1045-1 (FASSUNG 2008) UND EN 1992-1-1 (EUROCODE 2)*. Springer-Verlag, 2010.

[75] M. P. Nielsen and L. C. Hoang, *Limit analysis and concrete plasticity*. CRC press, 2016.

[76] A. Muttoni, J. Schwartz, and B. Thürlimann, *Design of concrete structures with stress fields*. Springer Science & Business Media, 1997.

[77] P. Marti, "How to treat shear in structural concrete", *ACI Structural Journal*, vol. 96, no. 3, pp. 408–415, 1999.

[78] W. Kaufmann. (2015). Vorlesungsunterlagen Stahlbeton I – Kapitel 3.4 Stabtragwerke – Querkraft. German, ETH Zurich – Institute of Structural Engineering, [Online]. Available: `www.kaufmann.ibk.ethz.ch`.

[79] C. Zapfe, "Trag-und Verformungsverhalten von Verbundträgern mit Betondübeln zur Übertragung der Längsschubkräfte", PhD thesis, Universtät der Bundeswehr Müchen, 2001.

[80] K. W. Johansen, "Theory of timber connections", *International Association of Bridge and Structural Engineering*, vol. 9, 1949, pp. 249–262.

[81] S. Zöllig, "Holz-Beton-Verbund mit vorgefertigten Brettstapel-Modulen", *SAH-KURS 1999, TRAGENDE VERBUNDKONSTRUKTIONEN MIT HOLZ, SCHWEIZERISCHE ARBEITSGEMEINSCHAFT FÜR HOLZFORSCHUNG*, 1999.

[82] U. Kuhlmann and P. Aldi, "Simulation of grooved connections in timber–concrete composite beams considering the distribution of the material properties", *10th World Conference on Timber Engineering WCTE 2008, Miyazak; Japan*, 2008.

[83] Metsä Wood. (2014). Kerto manual: Mechanical properties. English, Metsä Wood, [Online]. Available: `www.metsawood.com`.

[84] P. Marti, M. Alvarez, W. Kaufmann, and V. Sigrist, *Tragverhalten von Stahlbeton*. Institut für Baustatik und Konstruktion, ETH Zürich, 1999.

[85] H. Bachmann, "Zur plastizitätstheoretischen Berechnung statisch unbestimmter Stahlbetonbalken", ETH, Eidgenössische Technische Hochschule Zürich, Institut für Baustatik IBK, Tech. Rep. 13, 1967.

[86] K. Timmermann and U. A. Meierhofer, "Holz/Beton-Verbundkonstruktionen: Untersuchungen und Entwicklungen zum mechanischen Verbund von Holz und Beton", EMPA, Report 115/30, 1993.

[87] L. Boccadoro and A. Frangi, "Experimentelle Untersuchungen zum Tragverhalten von Holz-Beton-Verbunddecken aus Buche", *Bautechnik*, vol. 92, no. 11, pp. 783–789, 2015.

[88] F. Leonhardt and E. Mönnig, *VORLESUNGEN ÜBER MASSIVBAU – TEIL 1: GRUNDLAGEN ZUR BEMESSUNG IM STAHLBETONBAU*. Springer, 1984.

[89] L. Boccadoro and A. Frangi, "Experimental analysis on the structural behavior of timber-concrete composite slabs made of beech-laminated veneer lumber", *Journal of Performance of Constructed Facilities*, vol. 28, no. 6, 2014.

[90] Swiss Standards Association, "SIA 260 - Basis of structural design", *Swiss Society of Engineers and Architects, Zurich, Switzerland*, 2003.

[91] L. Boccadoro and A. Frangi, "Timber-concrete composite slabs made of beech", *Proceedings Doktorandenkolloquium Stuttgart, Universität Stuttgart, Institut für Konstruktion und Entwurf*, 2014, pp. 11–18.

[92] E. Gehri, "Leistungsfähige Verbindungen: Kriterien und Konzepte", *Proceedings SAH-Fortbildungskurs Weinfelden*, 2000, pp. 13–25.